3.3.2

Number of research papers per teachers in the Journals notified on UGC website during the year 2023-24:

0.85

List of research publication

Year		2023-24	
Number of research papers		**23**	
2023-24			

Sr. No	Name of Teacher	Dept.	Title of the paper	Name of the journal	Page No
1.	P. M. Makode	Zoology	Analyzing the Bivalve Species of Genus Parreysia Along with Water Quality of Kuadhas and Pangoli Rivers from Gondia Maharashtra, India.	Bioscience Biotechnology Research Communication	01
2.	A. O. Dhore	Maths	Analysis of Marder's Space-Time Tsallis Holographic Dark Energy	East European Journal of Physics	05
3.	T. R. Tatte	Physics	Structural and Morphological Properties of Spinel Type Magnesium Aluminate Thick Films	Iconic Research And Engineering Journal	17
4.	T. R. Tatte	Physics	A Review on Spinel Ferrite Nanoparticles: Synthesis Methods and Applications	International Journal of Science and Research	21
5.	T. R. Tatte	Physics	Study of Microwave Dielectric Properties of FeCl3-doped Polyvinyl Acetate Based Thin Films	International Journal of Research Publication and Reviews	25
6.	T. R. Tatte	Physics	Preparation of Zinc doped Magnesium Ferrite Nanoparticles by Sol-Gel Method	The Rubrics Journal Of Interdisciplinary Studies	30
7.	T. R. Tatte	Physics	An Overview on Nanocrystalline Pervoskite (ABO_3): A Potential Material for Solid State Gas Sensor and its Applications	The Rubrics Journal Of Interdisciplinary Studies	38
8.	S. K. Shah	Marathi	Dalit kavitetil Nakar, vidroh ani atmshodh	Research Journal of India	43
9.	V. V. Kapile	Sports	A Study Of Football Players Of Akola City And Akola District On The Levels Of Theirphysical Fitness	International Research Journal of Physical Education And Sports Sciences	50

10.	S. S. Kawar	Physics	Effect of Zinc Nitrate on Morphology and Particle Size of Nano-sized Zinc Oxide	Tuijin Jishu/Journal of Propulsion Technology	54
11.	D. B. Dupare	Chemistry	Photodegration and sensing Applicability of Synthesized of Polyanailine Sn –NPs Aloe Bicomposites	High Technology letter	55
12.	D. B. Dupare	Chemistry	Comparative Study of Electrochemical Properties of Synthesized PANI-and PANI-Ni-NPs Aloe –Vera thin films Bicomposites	Journal of Emerging Technology and Innovative Research	68
13.	D. B. Dupare	Chemistry	Effect of different metal salts Dopant on Electrochemical Behaviour of PANI-Aleo-Vera Bicomposites	IDEAL International Multidisciplinary Half yearly Journal	75
14.	S. V. Deshmukh	Chemistry	Synthesis of 2-amino-4H-chromene derivative via three component reaction using sodium benzoate as a green catalyst	Heterocyclic Letters	84
15.	A. S. Nimkar	Maths	Kantowski Sachs Macroscopic Body Cosmological Models in Scalar Tensor Theories of Gravitation	Journal of Dynamical System & Geometric Theories	89
16.	A. S. Nimkar	Maths	Stability of Axially Symmetric Cosmological Model in Lyra's Geometry	Journal of Scientific research	91
17.	A. S. Nimkar	Maths	Anisotropic dark matter distribution in Saez –Ballester theory of gravitation	Indian J phys	101
18.	A. S. Nimkar	Maths	Stability of Macroscopic Body Cosmological Model in Ruban's Background	Jnanabha	102
19.	R. P. Shirsat	Botany	Current scenario of Wild Edible plants (WEPs) their importance, Possible threats, and conservation: A mini-review	Journal of Agriculture and Ecology Research International	111
20.	R. P. Shirsat	Botany	Fluorescent study, preliminary phytochemistry and HPTLC profiling of Salvinia molesta D. S. mitchell	International Journal of Botany Studies	121
21.	S. S. Dhande	Zoology	Study of Local Fish Availability and Fish Marketing System of Murtijapur, Akola District (Maharashtra)	Vidyabharati International Interdisciplinary Research Journal	125
22.	S. S. Dhande	Zoology	Study of Some Spiders From Family Araneidae in and around Daryapur Tehsil, District Amravati	International Journal of Scientific Research	129
23.	M. Mujahid	Chemistry	An efficient synthesis of optically active herbicide (S)-metolachlor via reductive ring opening of 2-methoxymethylaziridine	Arkivoc	131

Analyzing the Bivalve Species of Genus Parreysia Along with Water Quality of Kuadhas and Pangoli Rivers from Gondia Maharashtra, India.

G. V. Ade[1] and P. M. Makode[2]

[1]Department of Zoology, Shankarlal Agrawal Science College Salekasa,

District Gondia, Maharashtra, India

[2]Department of Zoology, Shri. Dr. R. G. Rathod Arts and Science College

Murtizapur District Akola, Maharashtra, India

ABSTRACT

Aquatic environments benefit greatly from the contribution of freshwater bivalves. They are crucial for ancient remedies, and a variety of industrial uses, primarily the manufacturing of pearls, slacked lime, and use as a food source in various regions Malacofauna was assessed from Kuadhas river and Pangoli river of Gondia Maharashtra for six months. The physicochemical parameters comprising pH, turbidity, color, nitrate, sulfate, phosphate, silica, free carbon dioxide, alkalinity, dissolved oxygen, and total hardness were evaluated since aquatic body water quality has an impact on the occurrence and survival of flora and fauna. This paper deals particularly with different species and varieties from the genus *Parreysia* among freshwater bivalves. From study sites genus Parreysia represents total 8 species as *Parreysia favidens, Parreysia favidens marcens, Parreysia corrugata, Parreysia corrugata nagpoorensis, Parreysia cylindrica, Parreysia Radiatula shurtleffiana, Parreysia (Radiatula) khadakvaslaensis, Parreysia Radiatula caerulea gaudichaudi.* Bivalve occurrence peaked in the post-monsoon season and declined during the monsoon. *Parreysia favidens and Parreysia corrugata* are widely distributed in the Kuadhas River. The two major species in the *Pangoli River are Parreysia (Radiatula) khadakvaslaensis* and *Parreysia favidens.* In both rivers *Parreysia favidens marcens, Parreysia corrugata nagpoorensis*, and *Parreysia Radiatula shurtleffiana* are listed as being rarer species.

KEY WORDS: PFRESHWATER BIVALVES, GONDIA DISTRICT, MAHARASHTRA, MALACOFAUNA, PHYSICOCHEMICAL PARAMETERS.

INTRODUCTION

Freshwater mollusks contribute significantly to the biogeochemical cycle and are an essential component of the aquatic ecosystem (Dey, 2007). Among molluscs, bivalves don't have head like that of gastropods. Externally structure consisting of two valves made up of calcium carbonate and joined together by soft ligament at a hinge. Inside the shell have mantle secreted by shell enclosing visceral mass, two pairs of gills and foot (Rao, 1989). In rivers and lakes, freshwater bivalves serve as filters. Numerous species can be found in dense clusters and filter out a lot of silt, bacteria, diatoms, blue-green algae, and other microscopic organisms as well as heavy metals and big organic compounds. Genus *Parreysia* of class Bivalvia, comes under subclass Palaeoheterodonta and family Unionidae of phylum Mollusca (Rao, 1989).

Some species of *Parreysia* are used as food sources such as *Parreysia favidens*, P*arreysia caerulea*. Soup made from *Parreysia favidens*, intended to treat blood pressure and heart issues also shell lime water is used to cure intestinal parasites (Tripathy and Mukhopadhayay, 2015). Molluscs distribution and abundance in water bodies are influenced by physicochemical parameters and the vegetation of the water body (Choubisa, 1992). Bad water quality and other human activities, leading to habitat destruction, effects on survival and diminishing diversity of sensitive malacofauna.

In India molluscan diversity and relation to physicochemical properties studied recently by number of researchers including, Chutia and Kardong (2021), Kumar et al., (2019), Padghane et al., (2017), Kamble (2018). Sarwade et al., (2015). Gondia situated north-eastern site of Maharashtra

141

state most of the land of district is covered with forest and lakes and rivers. It is in the northeastern region of Maharashtra state, and most of the district's territory is covered in rivers, lakes, and forests. In this area little or no work is done on malacofaunal diversity hence This paper particularly enlists species of genus *Parreysia* from Kuadhas and Pangoli rivers of Gondia Maharashtra along with information on some physicochemical parameters of these water bodies.

Figure 1: Location of study area Kuadhas river (A) and Pangoli river (B)
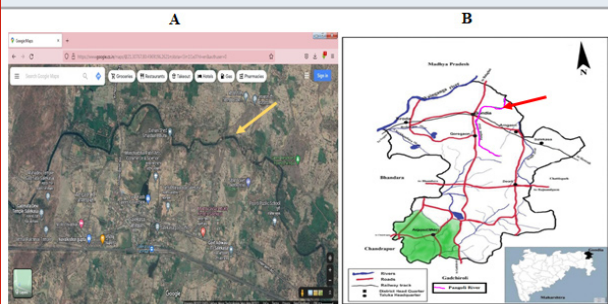
MATERIAL AND METHOS

Gondia district in the Indian state of Maharashtra. It is located between latitudes 20.39 and 21.38 North and 79.27 and 80.42 East. As most of the territory is covered by forests, the Gondia district of Maharashtra is home to a wide variety of plants and animals. Kuadhas river originates from Darekasa hills of the district and is a sub-tributary of Bagh River of the region. Pangoli river has it's beginning from Tumsar hills of the district and is tributary of Bagh River (Figure 1).

Kuadhas and Pangoli rivers were visited from November 2022 to April 2023. The quadrate sampling method was used to perform the quantification (Christian and Harris 2005). Samples were collected from bank of rivers by hand picking and with the help of hand net and scoop net. (Rao et al., 1989). (Only molluscan shells are used for study and no live molluscs were brought to laboratory for analysis). After being transported to the lab, the shells were cleaned with a soft bristle brush to avoid breaking the shells and to properly clean the mud for shell character identification. Identification of malacofauna was done by following keys by Rao (1989), Ramkrishna and Dey (2005).

Table 1. Physicochemical analysis of Kuadhas river and Pangoli river in Gondia district Maharashtra, India

Study Sites → Water Parameters	Kuadhas River		Pangoli River	
	Minima	Maxima	Minima	Maxima
Temperature (^{0}C)	24	31	23.6	32
pH	7.0	7.52	7.33	7.67
Color (Hazen)	------	BQL	BQL	3
Turbidity (NTU)	1.5	2.61	3.8	23.1
Phosphate (mg/L)	BQL	0.29	BQL	4.43
Sulphate (mg/L)	8.73	10.38	2.94	17.26
Nitrate (mg/L)	1.14	3.86	1.50	16.16
Total Dissolved Solids (mg/L)	82	224	106	322
Alkalinity (mg/L)	42	104	55	124
Total Hardness (mg/L)	45	130	55	130
Dissolved Oxygen (mg/L)	5.50	6.80	5.8	6.7
Silica (mg/L)	BQL	4.24	0.31	4.12
Free CO_2 (mg/L)	3.17	7.4	3.0	5.28

Water samples were collected from both rivers at the same time and analysed for thirteen water parameters as temperature, pH, color, turbidity, total dissolved solids, total hardness, alkalinity, free carbon dioxide, dissolved oxygen, silica, phosphate, sulphate and nitrate of water sample. The physicochemical analysis of water was performed as per standard methods, (APHA, 1998; Trivedi and Goel 1984).

RESULTS AND DISCUSSION

The studied physicochemical parameters of water samples from Kuadhas river and Pangoli river have been given

in Table 1. The physicochemical parameters of Kuadhas river were recorded as: water temperature (24 - 31^0 C), pH (7.0-7.52), Color (BQL), Turbidity (1.5- 2.61 NTU), Phosphate (BQL- 0.29 mg/L), Sulphate (8.73-10.38 mg/L), Nitrate (1.14- 3.86 mg/L), Total Dissolved Solids (82- 224 mg/L), Alkalinity (42-104 mg/L), Total Hardness (45-130 mg/L), Dissolved Oxygen (5.50-6.80 mg/L), Silica (BQL – 4.24mg/L), Free CO_2 (3.17-7.4 mg/L).

As compared to Kuadhas river, the upper and lower limits of water parameters of Pangoli river had higher: temperature (23.6 - 32^0 C), pH (7.33-7.67), Color (BQL-3 Hazen), Turbidity (3.8- 23.1 NTU), Phosphate (BQL- 4.43

2

mg/L), Sulphate (2.94-17.26 mg/L), Nitrate (1.5- 16.16 mg/L), Total Dissolved Solids (106-322 mg/L), Alkalinity (55-124mg/L) Total Hardness (55-130 mg/L), Dissolved Oxygen (5.8-6.7 mg/L), except Silica (0.31 – 4.12mg/L) and Free CO_2 (3.0-5.28 mg/L). Positive correlation between molluscan population and total hardness, alkalinity, chlorides, phosphates, nitrate- nitrogen by many researchers (Garg et al 2009; Dorlikar et al., 2014; Sarwade et al., 2015).

In the present work, we have reported species from genus Parreysia of family Unionidae of bivalves from Kuadhas and Pangoli rivers of Gondia district Maharashtra India (Figure 2). All eight species of Genus Parreysia were found at Kuadhas river from November 2022 to April 2023 includes,

Figure 2: Collected and identified Parreysia species from Kuadhas river and Pangoli river of Gondia district Maharashtra, India
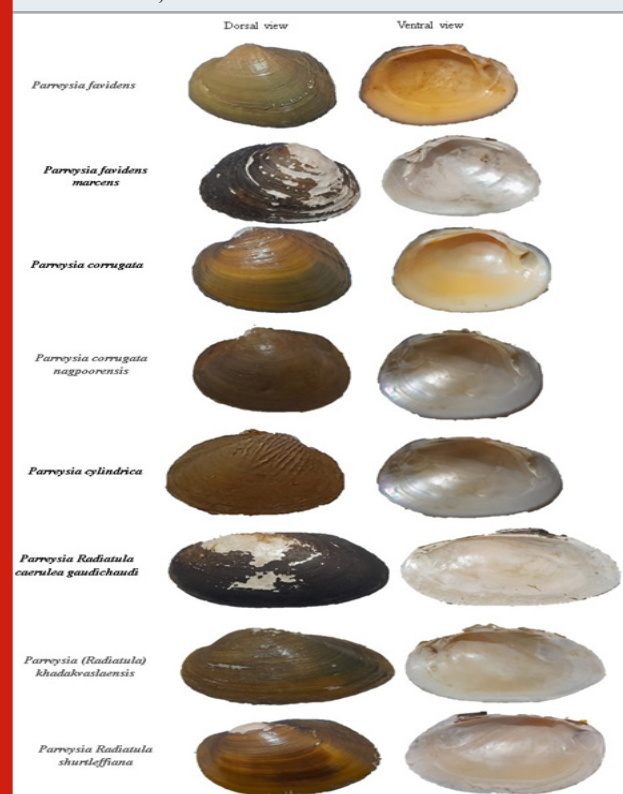
Parreysia favidens, Parreysia favidens marcens, Parreysia corrugata, Parreysia corrugata nagpoorensis, Parreysia cylindrica, Parreysia Radiatula shurtleffiana, Parreysia (Radiatula) khadakvaslaensis, Parreysia Radiatula caerulea gaudichaudi. Parreysia favidens followed by Parreysia corrugata are most abundant species found at Kuadhas river and Pangoli river. Parreysia corrugata nagpoorensis and Parreysia favidens marcens as rare species at study area. Only four species of Parreysia were reported from Pangoli river includes Parreysia favidens, Parreysia corrugata, Parreysia (Radiatula) khadakvaslaensis and Parreysia cylindrica (Figure 3 and 4).

Kuadhas river showed maximum diversity of molluscs due to present of phytoplankton vegetation serve as food for molluscs, less anthropogenic activity found at this river. Least diversity and molluscan assemblage found at Pangoli river due to habitat destruction as number of small dams built across the river and other anthropogenic activities.

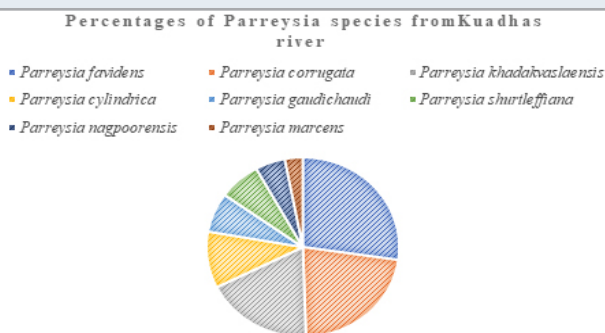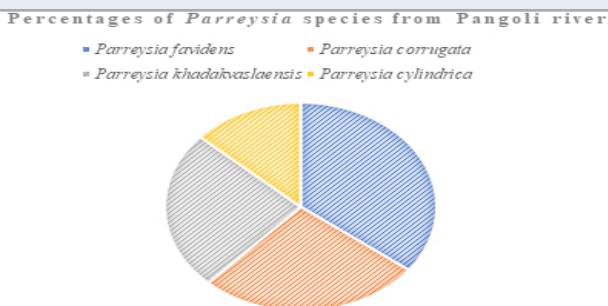Figure 3: Percentages of Parreysia species from Kuadhas river.

Figure 4: Percentage of Parreysia species from Pangoli river

CONCLUSION

Eight species of genus *Parreysia were* recorded from two rivers Kuadhas and Pangoli rivers from Gondia district Maharashtra during six months of the survey. This is the first attempt to study malacofauna in this region and will help to explore malacofauna and development of conservation policies to protect the species in the near future. Further study will be continued for a longer period and from different water bodies of the region to enlist molluscan diversity and their seasonal variations.

REFERENCES

APHA (1998). Standard methods for examinations of water and waste water, 20th Editions Washington, DC. 169 pp.

Choubisa, S.L., 1992. Molluscs as bio-indicators for the trophic stages of lakes and lotic environments. Bulletin of Pure and Applied Science, 11, pp.35-40.

Christian, A.D. and Harris, J.L., 2005. Development and assessment of a sampling design for mussel assemblages in large streams. The American midland naturalist, 153(2), pp.284-292.

Chutia, J. and Kardong, D., 2021. Current status and

3

seasonal distribution of malacofaunal assemblage in Poba Reserve Forest in relation to certain physico-chemical parameters. Asian Journal of Biological and Life Sciences, 10(1), pp.93-100.

Dey, A., 2007. Handbook on Indian freshwater molluscs. AICOPTAX--Mollusca, Zoological Survey of India.

Dorlikar, A.V., Mohite, A.S. and Charde, P.N., 2014. Correlation of molluscan diversity with physicochemical characteristics of water of Gorewada reservoir, Nagpur, India. International Journal of Life Sciences, Special Issue A, 2, pp.197-201.

Garg, R.K., Rao, R.J. and Saksena, D.N., 2009. Correlation of molluscan diversity with physico-chemical characteristics of water of Ramsagar reservoir, India. International Journal of Biodiversity and Conservation, 1(6), pp.202-207.

Gondia Gazetteer (2021). Database of Gondia District redirected from official website of Gondia District (M.S.), India, www.gondia.nic.in.

Kamble, V.S., 2018. Study of diversity of freshwater molluscs from drought prone region Sangola, district Solapur (MS), India. J Emerg Technol Innov Res, 5(8).

Kumar, R. and Maansi, W.M., 2019. Molluscan Biodiversity and its seasonal fluctuations in Teekar Taal, Haryana. Indian International Journal of Research-Granthalayah, 7(1), pp.169-178.

Padghane, S., Chavan, S., Dudhmal, D. and Walke, D., 2017. Mollusc diversity and its role as a food for crabs and water birds in Godavari River Basin Nanded (MS), India. International Journal of Advanced Scientific and Technical Research, 7, pp.149-161.

Rao S N.V., 1989. Handbook, freshwater molluscs of India.

Sarwade, A.B., Pati, S.K. and Kamble, N.A., 2015. Diversity of molluscan fauna from freshwater bodies of Sangli district: A comprehensive study in relation to environmental variables. International Journal of Pharmaceutical Sciences and Research, 6(8), p.3563.

Tripathy, B. and Mukhopadhayay, A., 2015. Freshwater molluscs of India: an insight of into their diversity, distribution and conservation. Aquatic Ecosystem: Biodiversity, Ecology and Conservation, pp.163-195.

Trivedy, R.K. and Goel, P.K., 1984. Chemical and biological methods for water pollution studies. Environmental publications.

4

ANALYSIS OF MARDER'S SPACE-TIME TSALLIS HOLOGRAPHIC DARK ENERGY COSMOLOGICAL MODEL IN $f(R,T)$ THEORY OF GRAVITY

 Abhijeet Ompratap Dhore[a*], **Mohini Ramrao Ugale**[b]

^{a}Department of Mathematics, Shri. Dr. R.G. Rathod Arts and Science College,
Murtizapur, Dist.-Akola 444 107, Maharashtra, India
^{b}Department of Science and Humanities, Sipna College of Engineering and Technology,
Amravati 444 701, Maharshtra, India
*Corresponding Author e-mail: drabhijeetdhore@gmail.com

In this paper, the investigation explores an anisotropic cosmological model based on Marder's space-time Tsallis holographic dark energy (THDE) within the framework of $f(R,T)$ theory of gravity, where R represents the Ricci scalar and T signifies the trace of the stress energy-momentum tensor. field equation have solved for class of $f(R,T)$ gravity i.e. $f(R,T) = R + f(T)$. To obtain the precise solution, we employed the density of the THDE model along with the volumetric expansion laws, namely the power law and exponential law. Also explores the physical and geometrical aspects of the model.

Keywords: *f(R,T) gravity; Marder's space-time; THDE; Volumetric expansion*

PACS: 04.50.kd, 04.20.-q, 98.80.-k

1. INTRODUCTION

Based on the latest observations in astrophysics, there is strong evidence indicating that the universe is presently expanding at an accelerated rate, presenting intriguing opportunities for advancements in modern cosmological theories [1, 2, 3, 4]. The observed accelerated expansion of the universe is thought to be propelled by dark energy (DE). DE constitutes the dominant portion of the universe, making up 68% of the total energy in the observable universe at present. In contrast, dark matter (DM) and ordinary matter (baryonic matter) contribute 26% and 5% respectively [5]. The specific traits of DE continue to elude understanding, leading to the formulation of various theories and explanations. Indeed, within various theories and models, the cosmological constant model is often regarded as the most straightforward choice for DE, characterized by an equation of state (EoS) parameter $\omega = -1$. However, it is not without its challenges, including issues such as cosmic coincidence and fine-tuning problems [6, 7]. To address these challenges, the scientific literature has proposed various DE models, including quintessence, phantom, k-essence, tachyon, holographic dark energy (HDE), and others. In contemporary times, the exploration of HDE models has become a promising pathway for comprehending cosmic expansion, operating within the framework of the holographic principle (HP) [8]. The HP posits that the limit on the vacuum energy Λ of a system with size L should not surpass the threshold of the black hole mass with an equivalent size. This limitation arises from the potential formation of a black hole in the quantum field in a vacuum, and the infrared (IR) and ultraviolet cutoffs [10]. The energy density of HDE is defined as $\rho_{HDE} = 3d^2 m_p^2 L^{-2}$, where m_p is the reduced Plank mass and L represents the IR cutoff, describing the size of the universe in the context of the HP [11].

In recent times, various HDE models, including the Modified Ricci (MRHDE), THDE, Rényi HDE (RHDE), and Sharma-Mittal HDE (SMHDE), have been proposed and introduced. Certainly, within these models, RHDE stands out as it is founded on the absence of interactions between cosmic sectors. Notably, this model exhibits greater stability on its own [12]. M. Tavayef et al. [13] explored the Tsallis and Cirto entropy expressions while incorporating the HDE hypothesis. Their investigation led to the formulation of a novel type of DE called THDE. The study further delved into the dynamics of this THDE within the framework of a non-interacting flat Friedmann-Robertson-Walker (FRW) universe, examining the evolutionary aspects of the system. In the scenario of non-interacting cosmos, SMHDE is acknowledged for its classical stability [13, 14, 15]. M. Abdollahi Zadeh et al. [16] have delved into the repercussions of introducing various IR cutoffs, including the particle horizon, the Ricci horizon, and the Granda-Oliveros (GD) cutoffs, on the properties of the THDE. Spyros Basilakos et al. [17] demonstrated how Tsallis cosmology can effectively address both the Hubble constant (H_0) and the matter density fluctuation amplitude (σ_8) tensions simultaneously. This modified cosmological scenario is achieved by applying the gravity-thermodynamics conjecture with the use of non-additive Tsallis entropy instead of the standard Bekenstein-Hawking entropy. A. Mohammadi et al. [18] conducted a study exploring

the application of the HP within the framework of Bianchi type-III space-time. A. Pradhan and A. Dixit [20] explored a THDE model within a flat FRW space-time, considering the higher derivative theory of gravity. A. Al. Manon et al. [21] have investigated a cosmological scenario illustrating the ongoing acceleration of the universe, featuring the coexistence of DM and THDE. M. Vijaya Santhi and Y. Sobhanbabu [22] have explored the dynamics of THDE, utilizing the Hubble radius as the IR cutoff, in a homogenous and anisotropic Bianchi type-III universe. This investigation was conducted within the context of the Saez-Ballester (SB) theory of gravitation and by solving the field equations associated with SB theory they have developed both interacting and non-interacting DE models. Y. Sobhanbabu and M. Vijaya Santhi [23] have dedicated their efforts to examining THDE, incorporating the Hubble radius as the IR cutoff, within a homogenous and anisotropic Kantowski-Sachs universe. This investigation unfolds within the framework of SB theory of gravitation. They have formulated both non-interacting and interacting models for THDE by solving the field equations and employing the connection between the metric potentials. B. D. Pandey et al. [24] have developed HDE model incorporating Tsallis entropy, a one parameter extension of Boltzmann-Gibbs entropy. R. Saleem et al. [25] have investigated the dynamics of warm inflation within a modified cosmological framework in the context of Rastall gravity. Within this scenario, they altered the standard Friedmann equations by incorporating recently proposed Tsallis and Barrow HDE entropies. M. Vijaya Santhi and Y. Sobhanbabu [26] have formulated both interacting and non-interacting models for THDE in an anisotropic and homogenous Bianchi type-VI_0 space-time. This was accomplished within the context of a scalar-tensor theory proposed by SB. To achieve this, they employed the relationship between the metric potentials of the model and a varying deceleration parameter, resolving the SB field equations. M. Sharif and S. Saba [27] have explored the reconstruction paradigm for the THDE model by incorporating the generalized Tsallis entropy conjecture with the Hubble horizon. This investigation took place within the framework of $f(G,T)$ gravity. M. Zubir and L. Rukh Durrani [28] have investigated THDE in a flat FRW model, utilizing the framework of $f(R,T)$ gravity. Ayman A. Aly [29] has developed a novel $f(T)$ modified gravity model, incorporating a THDE model and a Hubble cutoff. A. Pradhan et al. [30] have explored the Tsallis holographic quintessence, k-essence, and tachyon models of DE within the context of modified $f(R,T)$ gravity, employing the GO cutoff. S. H. Shekh et al. [31] analyzed THDE, transitioning into HDE through a specific selection of the positive non-additivity parameter δ. This study was carried out within the framework of modified $f(T,B)$ gravity, examining the validity of thermodynamics and energy conditions for a homogenous and isotropic FRW universe.

Expanding on the constructive discussions and favorable results emphasized earlier, this article explores the THDE model within the context of $f(R,T)$ gravity. The inquiry focuses on validating both the power law and exponential law components of the model.

2. TSALLIS HOLOGRAPHIC DARK ENERGY

It is essential to remember that the establishment and derivation of the conventional HDE density ($\rho_{HDE} = 3d^2m_p^2L^{-2}$) are contingent upon the entropy area relationship $S \sim A \sim L^2$ of black holes, where $A = 4\pi L^2$ represents the area of the horizon [9]. Nevertheless, the definition of HDE can be adjusted or revised in light of quantum considerations [32, 33]. Tsallis and Cirto illustrated that the horizon entropy of a black hole could potentially be modified according to mathematical expression of the form

$$S_\delta = \gamma A^\delta \tag{1}$$

where, γ is an unknown constant and δ dentoes the non-additivity parameter [14]. It is evident that the Bekestein entropy is registered when the appropiate limit of $\delta = 1$ and $\delta = (4G)^{-1}$. Certainly, at this limit, the power law distribution of probability becomes ineffective, and the system can be described by the conventional probabitilty distribution [14].

Following the HP, which asserts that the number of degrees of freedom of a physical system should scale with its bounding area rather than its volume [34]. Cohen et al. [9] suggested that system entropy (S) should be constrained by an IR (L) cutoff, leading to proposed relation involving the IR cutoff and UV (Λ) as

$$L^3\Lambda^3 \leq (S)^{3/4} \tag{2}$$

which combining with eqn. (1) leads to [9]

$$\Lambda^4 \leq (\gamma(4\pi)^\delta)L^{2\delta-4} \tag{3}$$

where, Λ^4 denotes the vacuum energy density. Employing the aforementioned inequality, we can suggest the THDE density as follows

$$\rho_t = BL^{2\delta-4} \tag{4}$$

where B is unknown parameter [35, 36, 37] and IR cutoff is taken as Hubble radius which leads to $L = H^{-1}$, where H is hubble parameter [10]. The density of THDE model along with its derivative by using eqn. (4) becomes

$$\rho_t = BH^{4-2\delta} \tag{5}$$

6

$$\dot{\rho}_t = B(4 - 2\delta)H^{3-2\delta}\dot{H} \tag{6}$$

where, $\dot{H}$ is the derivative of Hubble parameter w.r.t t [10].

3. METRIC AND FIELD EQUATIONS

We consider the Marder's space-time in the form [38]

$$ds^2 = M_1^2(dx^2 - dt^2) + M_2^2 dy^2 + M_3^2 dz^2 \tag{7}$$

where, M_1^2, M_2^2, M_3^2 are functions of cosmic time t. In recent years, M. Vijaya Santhi et al. [39] have conducted research on the dynamics of a Marder's space-time cosmological model, which is grounded in the concept of bulk viscous strings within the framework of $f(R)$ gravity. Sezgin AYGÜN [40] has explored a homogenous and anisotropic Marder space-time model within the framework of (R,T) gravity, where the space-time is filled with a bulk viscous string matter distribution. D. D. Pawar and S. P. Shahre [38] have explored Marder's space-time within the framework of (R,T) gravity, integrating a perfect fluid under a titled congruence.

In this work we study the Marder's space-time in (R,T) gravity with THDE. Here, the energy-momentum tensor for matter (T'_{ij}) and THDE $(\overline{T}_{ij})$ are given as follows:

$$T'_{ij} = diag[1, 0, 0, 0]\rho_m \tag{8}$$

$$\overline{T}_{ij} = diag[1, -\omega_t, -\omega_t, -\omega_t]\rho_t \tag{9}$$

it can be parameterized as

$$\overline{T}_{ij} = diag[1, -\omega_t, -\omega_t, -(\omega_t + \alpha)]\rho_t \tag{10}$$

where ρ_t and ρ_m are energy densities of THDE, and matter respectively and p_t and $_m$ is pressure of THDE and matter respectively. $\omega_t = \frac{p_t}{\rho_t}$ is an EoS parameter. Here, α the deviation from the EoS parameter in the z-direction, commonly referred to as the skewness parameter. We have an energy conservation equation as

$$(T'_{ij} + \overline{T}_{ij})_{;j} = 0 \tag{11}$$

The exploration of diverse cosmological models within the framework of (R,T) theory of gravity depends on the characteristics of the matter source under consideration. Harko et al. [41] introduced following class of $f(R,T)$ gravity:

$$f(R,T) = \begin{cases} R + 2f(T) \\ f_1(R) + f_2(T) \\ f_1(R) + f_2(R)f_3(T) \end{cases} \tag{12}$$

In this study, we have adopted a specific functional form, expressed as $f(R,T) = R + 2f(T)$. Here, $f(T)$ is a function of the trace of the energy-momentum tensor. By using this functional, the field equation can be rewritten as

$$R_{ij} - \frac{1}{2}Rg_{ij} = (T'_{ij} + \overline{T}_{ij})_{;j} + 2f_T(T'_{ij} + \overline{T}_{ij})_{;j} + [f(T) + 2pf_T]g_{ij} \tag{13}$$

where f_T is a partial derivative of f w.r.t T. We designate the function $f(T)$ to be contingent upon the trace of the energy-momentum tensor of matter, specifically as

$$f(T) = \lambda T \tag{14}$$

where λ is arbitrary constant. So $f_T = \lambda$. In metric (7), the Ricci scalar R can be represented in terms of metric potentials as [38]

$$R = -2\left(\frac{\ddot{M}_1}{M_1^3} + \frac{\ddot{M}_2}{M_1^2 M_2} + \frac{\ddot{M}_3}{M_1^2 M_3} - \frac{\dot{M}_1^2}{M_1^4} + \frac{\dot{M}_2 \dot{M}_3}{M_1^2 M_2 M_3}\right) \tag{15}$$

In this analysis, we investigate the cosmological implications of the arbitrary function suggested by Harko et al. [41], which is represented by the expression

$$f(R,T) = R + 2f(T) \tag{16}$$

where R is the Ricci scalar and T is the trace of the energy-momentum tensor.

The field eqn. (13) for the metric (7), utilizing eqns. (8), (10), and (14) from modified $f(R,T)$ gravity, results in the following system of eqns:

$$\frac{1}{M_1^2}\left(\frac{\ddot{M}_2}{M_2} + \frac{\ddot{M}_3}{M_3} + \frac{\dot{M}_2\dot{M}_3}{M_2M_3} - \frac{\dot{M}_1\dot{M}_2}{M_1M_2} - \frac{\dot{M}_1\dot{M}_3}{M_1M_3}\right) = -(8\pi + 2\lambda)(\omega_t + \alpha)\rho_t + [2p_t - 3\omega_t\rho_t - \alpha\rho_t + \rho_m + \rho_t]\alpha \quad (17)$$

$$\frac{1}{M_1^2}\left(\frac{\ddot{M}_1}{M_1} + \frac{\ddot{M}_3}{M_3} - \frac{\dot{M}_1^2}{M_1^2}\right) = -(8\pi + 2\lambda)\omega_t\rho_t + [2p_t - 3\omega_t\rho_t - \alpha\rho_t + \rho_m + \rho_t]\alpha \quad (18)$$

$$\frac{1}{M_1^2}\left(\frac{\ddot{M}_1}{M_1} + \frac{\ddot{M}_2}{M_2} - \frac{\dot{M}_1^2}{M_1^2}\right) = -(8\pi + 2\lambda)\omega_t\rho_t + [2p_t - 3\omega_t\rho_t - \alpha\rho_t + \rho_m + \rho_t]\alpha \quad (19)$$

$$\frac{1}{M_1^2}\left(\frac{\dot{M}_1\dot{M}_2}{M_1M_2} + \frac{\dot{M}_1\dot{M}_3}{M_1M_3} + \frac{\dot{M}_2\dot{M}_3}{M_2M_3}\right) = -(8\pi + 2\lambda)(\rho_m + \rho_t) + [2p_t - 3\omega_t\rho_t - \alpha\rho_t + \rho_m + \rho_t]\alpha \quad (20)$$

We express the energy conservation eqn. (11) for both matter and THDE as follows,

$$(\dot{\rho}_m + \dot{\rho}_t) + \left(\frac{\dot{M}_1}{M_1} + \frac{\dot{M}_2}{M_2} + \frac{\dot{M}_3}{M_3}\right)[\rho_m + (1 + \omega_t)\rho_t] + \frac{\dot{M}_1}{M_1}\alpha\rho_t = 0 \quad (21)$$

where overhead (.) denotes for ordinary differentiation w.r.t t.

4. SOLUTION OF FIELD EQUATIONS AND COSMOLOGICAL MODELS

The set of field eqns. (17)-(20) represents a set of four independent eqns. with seven unknowns $M_1, M_2, M_3, \rho_m, \rho_t, \omega_t, \alpha$. From eqns. (18) and (19), we get

$$\frac{\dot{M}_2}{M_2} - \frac{\dot{M}_3}{M_3} = 0 \quad (22)$$

on integration gives,

$$\frac{M_2}{M_3} = c_2\exp(c_1\int dt) \quad (23)$$

To simplify matters, we decide that $M_1 = M_2$. The dynamical parameters for Marder's space-time cosmological model are delineated as follows: The spatial volume of the metric is

$$V = a^3(t) = M_2^2M_3 \quad (24)$$

The directional Hubble parameters

$$H_x = H_y = \frac{\dot{M}_2}{M_2},$$
$$H_z = \frac{\dot{M}_3}{M_3} \quad (25)$$

The generalized mean Hubble's parameter H is expressed as

$$H = \frac{1}{3}(H_x + H_y + H_z) = \frac{1}{3}\left(\frac{2\dot{M}_2}{M_2} + \frac{\dot{M}_3}{M_3}\right) \quad (26)$$

The expansion scalar

$$\theta = 3H = 2\frac{\dot{M}_2}{M_2} + \frac{\dot{M}_3}{M_3} \quad (27)$$

The mean anisotropic parameter

$$A_m = \frac{1}{3}\sum_{i=1}^{4}\left(\frac{H_i - H}{H}\right)^2 \quad (28)$$

The Shear scalar

$$\sigma^2 = \frac{3}{2}A_mH^2 \quad (29)$$

The deceleration parameter

$$q = -1 + \frac{d}{dt}\left(\frac{1}{H}\right) \tag{30}$$

From eqns. (23) and (24), we get

$$M_2 = V^{1/3}c_2^{1/3}\exp\left(\frac{c_1}{3}t\right) \tag{31}$$

$$M_3 = V^{1/3}c_2^{-2/3}\exp\left(-\frac{2}{3}c_1 t\right) \tag{32}$$

where c_1 and c_2 are integrating constants. From eqns. (31) and (32), metric (7) becomes

$$ds^2 = \left[V^{1/3}c_2^{1/3}\exp\left(\frac{c_1}{3}t\right)\right]^2 (dx^2 + dy^2 - dt^2) + \left[V^{1/3}c_2^{-2/3}\exp\left(-\frac{2}{3}c_1 t\right)\right]^2 dz^2 \tag{33}$$

To obtain the complete solution, we require two different volumetric expansion laws, both the power law expansion and exponential law expansion i.e. $V = t^m$ and $V = e^{4H_0 t}$ respectively [42].

5. MODEL FOR POWER LAW EXPANSION

We are contemplating a volumetric expansion by a power law relation as

$$V = t^m \tag{34}$$

where m is a positive constant. The positive value of the exponent m aligns with observational evidence that anticipates the universe.

The metric potentials (31) and (32) becomes

$$M_2 = t^{m/3}c_2^{1/3}\exp\left(\frac{c_1}{3}t\right) \tag{35}$$

$$M_3 = t^{m/3}c_2^{-2/3}\exp\left(-\frac{2}{3}c_1 t\right) \tag{36}$$

As the time t approaches zero, the analysis suggests that metric potentials (35) and (36) tend toward zero. Consequently, the model exhibits an initial singularity. Eqn. (33) with the help of eqns. (35) and (36) can be written as

$$ds^2 = \left[t^{m/3}c_2^{1/3}\exp\left(\frac{c_1}{3}t\right)\right]^2 (dx^2 + dy^2 - dt^2) + \left[t^{m/3}c_2^{-2/3}\exp\left(-\frac{2}{3}c_1 t\right)\right]^2 dz^2 \tag{37}$$

From eqns. (25), (35), and (36), the directional Hubble parameters are

$$H_x = H_y = \frac{m}{3t} + \frac{c_1}{3} \tag{38}$$

$$H_z = \frac{m}{3t} - \frac{2c_1}{3} \tag{39}$$

From eqns. (26), (35), and (36), the mean Hubble parameter is given by

$$H = \frac{m}{3t} \tag{40}$$

From eqns. (27) and (40), the expansion scalar is given by

$$\theta = \frac{m}{t} \tag{41}$$

From eqns. (28), (38), (39), and (40), the mean anisotropic parameter is given by

$$A_m = \frac{2c_1^2 t^2}{m^2} \tag{42}$$

From eqns. (29), (40), and (42), the Shear scalar is

$$\sigma^2 = \frac{c_1^2}{3} \tag{43}$$

From eqns. (30) and (40), the deceleration parameter is

$$q = \frac{3}{m} - 1 \tag{44}$$

The energy conservation eqn. (21) results in the derivation of the subsequent separate conservation eqn. as

$$\dot{\rho}_m + 3H\rho_m = 0 \tag{45}$$

$$\dot{\rho}_t + 3H(1 + \omega_t)\rho_t + \frac{\dot{M}_2}{M_2}\alpha\rho_t = 0 \tag{46}$$

On integrating eqn. (45), we get matter density as

$$\rho_m = \frac{c_3}{t^m} \tag{47}$$

where c_3 is an integrating constant.

The DM is pressure less [29] i.e.

$$p_m = 0 \tag{48}$$

From eqns. (5), (6), and (40), the density of THDE is given as

$$\rho_t = B\left(\frac{m}{3t}\right)^{4-2\delta} \tag{49}$$

$$\dot{\rho}_t = -B(4 - 2\delta)\left(\frac{m}{3t}\right)^{3-2\delta}\left(\frac{m}{3t^2}\right) \tag{50}$$

For Λ-CDM model, the DE EoS is

$$\omega_t = -1 \tag{51}$$

we get THDE pressure as

$$p_t = -B\left(\frac{m}{3t}\right)^{4-2\delta} \tag{52}$$

From eqns. (40), (46), (49), (50), and (51), the skewness parameter is given as

$$\alpha = \left(\frac{4-2\delta}{t}\right)\left(\frac{m}{3t} + \frac{c_1}{3}\right)^{-1} \tag{53}$$

The density parameter for THDE and the energy density parameter for matter are defined and calculated as follows:

$$\Omega_t = B\left(\frac{m}{3t}\right)^{4-2\delta}\left(\frac{m^2}{3t^2}\right)^{-1} \tag{54}$$

$$\Omega_m = \left(\frac{c_3}{t^m}\right)\left(\frac{m^2}{3t^2}\right)^{-1} \tag{55}$$

Hence,

$$\Omega_t + \Omega_m = \left[B\left(\frac{m}{3t}\right)^{4-2\delta} + \frac{c_3}{t^m}\right]\left(\frac{m^2}{3t^2}\right)^{-1} \tag{56}$$

6. MODEL FOR EXPONENTIAL LAW EXPANSION

The exponential law expansion is

$$V = e^{4H_0 t} \tag{57}$$

Typically, this results in a universe resembling de Sitter space-time. In this scenario, H_0 represents the Hubble Parameter during the current epoch. We have delved into the dynamics of the universe within the framework of the $f(R,T)$ gravity, specifically emphasizing exponential law. This exploration is aimed at offering a thorough grasp of the dynamics of the model and contrasting it with those observed in the power law model.

The metric potentials (31) and (32) becomes

$$M_2 = \left(e^{4H_0 t}\right)^{1/3} c_2^{1/3} \exp\left(\frac{c_1}{3}t\right) \tag{58}$$

$$M_3 = \left(e^{4H_0 t}\right)^{1/3} c_2^{-2/3} \exp\left(-\frac{2c_1}{3}t\right) \tag{59}$$

Eqn. (33) with the help of eqns. (58) and (59) can be written as

$$ds^2 = \left[\left(e^{4H_0 t}\right)^{1/3} c_2^{1/3} \exp\left(\frac{c_1}{3}t\right)\right]^2 (dx^2 + dy^2 - dt^2) + \left[\left(e^{4H_0 t}\right)^{1/3} c_2^{-2/3} \exp\left(-\frac{2c_1}{3}t\right)\right]^2 dz^2 \tag{60}$$

From eqns. (25), (58), and (59), the directional Hubble parameters are

$$H_x = H_y = \frac{4}{3}H_0 + \frac{c_1}{3} \tag{61}$$

$$H_z = \frac{4}{3}H_0 - \frac{2c_1}{3} \tag{62}$$

From eqns. (26), (58) and (59), the mean Hubble parameter is given by

$$H = \frac{4}{3}H_0 \tag{63}$$

From eqns. (27) and (63), the expansion scalar is given by

$$\theta = 4H_0 \tag{64}$$

From eqns. (28), (61), (62) and (63), the mean anisotropic parameter is given by

$$A_m = \frac{c_1^2}{8} \tag{65}$$

From eqns. (29), (64) and (65), the Shear scalar is

$$\sigma^2 = \frac{c_1^2 H_0^2}{3} \tag{66}$$

From eqns. (30) and (63), the deceleration parameter is

$$q = -1 \tag{67}$$

On integrating eqn. (45), we get the matter density for the model as

$$\rho_m = -c_4 e^{-4H_0 t} \tag{68}$$

where c_4 is an integrating constant. The DM is pressure less [29] i.e.

$$p_m = 0 \tag{69}$$

From eqns. (5), (6), and (63), the density of THDE is given as

$$\rho_t = B\left(\frac{4}{3}H_0\right)^{4-2\delta} \tag{70}$$

$$\dot{\rho}_t = 0 \tag{71}$$

For Λ-CDM model, we get THDE pressure as

$$p_t = -B\left(\frac{4}{3}H_0\right)^{4-2\delta} \tag{72}$$

From eqns. (46), (63), (70) and (71), skewness parameter is becomes

$$\alpha = 0 \tag{73}$$

The density parameter for THDE and the energy density parameter for matter are defined and calculated as follows:

$$\Omega_t = B\left(\frac{4}{3}H_0\right)^{4-2\delta}\left(\frac{16}{9}H_0^2\right)^{-1} \tag{74}$$

$$\Omega_m = \left(-c_4 e^{-4H_0 t}\right)\left(\frac{16}{9}H_0^2\right)^{-1} \tag{75}$$

Hence,

$$\Omega_t + \Omega_m = \left[B\left(\frac{4}{3}H_0\right)^{4-2\delta} + \left(-c_4 e^{-4H_0 t}\right)\right]\left(\frac{16}{9}H_0^2\right)^{-1} \tag{76}$$

7. DISCUSSION

In the preceding section, we endeavored to unravel the precise solution of the THDE cosmological model within Marder's space-time framework. To do so, we postulated both a power law expansion and an exponential expansion law as plausible scenarios for the evolution of the universe. We have discovered that,

In section 5, for power law model.

- From Figure 1, both the Hubble parameter and the expansion scalar are approaching infinity as $t = 0$ signifies that at the inception of the universe, it was characterized by an infinitely dense and hot state. This characteristic behavior aligns with the concept of the Big Bang singularity, marking the beginning of cosmic expansion. As time progresses, both the Hubble parameter and the expansion scalar show a decrease. This pattern implies a diminishing rate of universal expansion over time. Despite the ongoing expansion, the momentum of this process gradually diminishes over time. As the cosmic time approaches infinity, both the Hubble parameter and the expansion scalar tend toward zero. This suggests that the rate of expansion of the universe is approaching a constant value. Such a scenario hints at a future phase where the rate of expansion of the universe becomes nearly constant, known as the de Sitter phase.

- Item From Figure 1, as cosmic time increases, the anisotropic parameter grows at an increasing rate. From eqn. (42), it is evident that the behavior of the anisotropic parameter is contingent upon the constants c_1 and m. Under this circumstance, the anisotropic parameter escalates as cosmic time t increases, yet diminishes with higher values of m.

- From eqn. (44),
    1. If $m = 3$ the deceleration parameter becomes zero. It indicates that the expansion of the universe is neither accerlerating, but rather proceeding at a constant rate. This scenario is consistent with a universe in which the gravitational effects of matter and energy are exactly balanced by the expansion itself.
    2. If $m > 3$ then the deceleration parameter is positive ($q > 0$), it indicates that the expansion of the universe is decelerating. In this scenario, the gravitational forces exerted by matter and energy within the universe are sufficiently strong to slow down the rate of expansion over time.
    3. If $m < 3$ then the deceleration parameter is negative ($q < 0$), it indicates that the expansion of the universe is accelerating. In this scenario, the gravitational effects of matter and energy are not sufficient to counteract the expansion, causing it to accelerate over time.

- From Figure 2(a), at the beginning of cosmic time $t = 0$ the density of THDE is significantly high, implying a phase of rapid expansion similar to cosmic inflation. As cosmic time progresses, the density of THDE decreases, indicating a corresponding reduction in the rate of expansion of the universe over time.

- From Figure 2(b), at the beginning of cosmic time ($t = 0$) the density goes to zero, which signifies a crucial epoch.
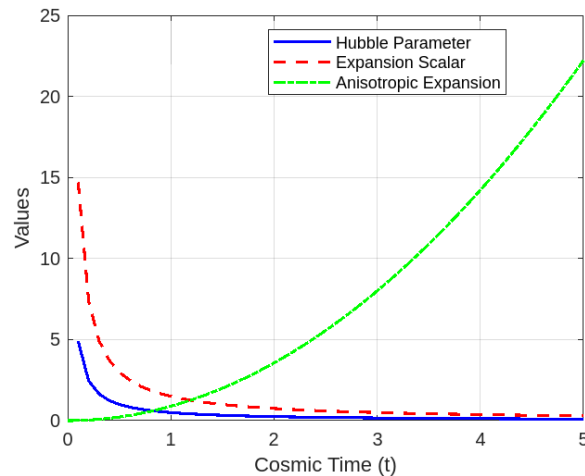

Figure 1. Hubble parameter, expansion scalar and anisotropic parameter versus cosmic time (t) for the particular choice of constants $c_1 = 1, m = 1.5$ in power law model
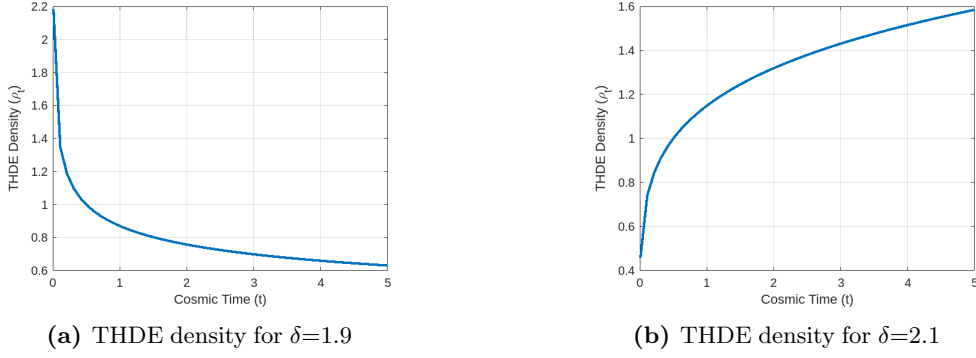
(a) THDE density for δ=1.9   **(b)** THDE density for δ=2.1

Figure 2. THDE density versus cosmic time (t) for the particular choice of constant $m = 1.5$ in power law model

(a) THDE pressure for δ=1.9   **(b)** THDE pressure for δ=2.1
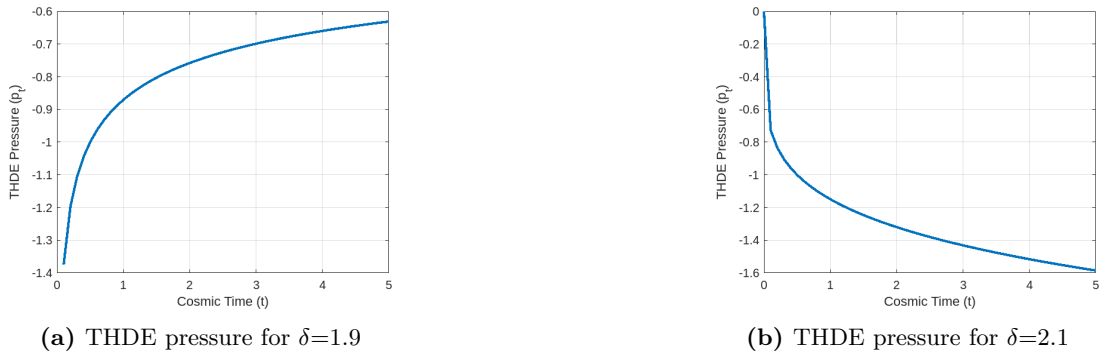
Figure 3. THDE pressure versus cosmic time (t) for the particular choice of constant $m = 1.5$ in power law model

- From Figure 2(a) (with $\delta = 1.9$), as cosmic time extends towards infinity the THDE density appears to stabilize at a fixed value. This suggests a scenario where, in the distant future, THDE could potentially dominate the energy density of the universe.

- From Figure 2(b) (with $\delta = 2.1$), as the cosmic time approaches infinity, the THDE density asymptotically approaches a non-zero value. In this case, the THDE density does not diminish to zero but approaches a finite value.

  In section 6, for the exponential law model.

- The deceleration parameter $q = -1$ for this model signifies that the universe undergoes an accelerated expansion [42]. The expansion scalar maintains a constant value indicating that the rate of expansion of the universe remains constant over time [43]. The anisotropic parameter is constant, it implies that the universe exhibits isotropy.

- We found that the Hubble parameter, density, and pressure are constant.

8. CONCLUSION

We investigated Marder's space-time model incorporating THDE within the framework of $f(R,T)$ gravity. The volumetric expansion law is utilized to derive precise solutions for field equations. Both the power law model and exponential law model yield the following conclusions. We analyzed 2D graph of the parameter by using MATLAB.

In the power law model, many fascinating findings emerge from our investigation. When the Hubble parameter is positive (t), we observe a universe is expanding. As time progresses towards infinity, the expansion gradually decelerates and eventually approaches zero. Interestingly, we have obtained the value of the deceleration parameter that depends on constant ($m = [2, 4]$), i.e. whether the universe accelerating or decelerating. From Figure 2(a) and 2(b), ($\delta < 2, \delta > 2$) the behavior of the universe suggests an evolving state where THDE plays a significant role in the expansion dynamics, potentially leading to an indefinite expansion. However, slight variations in the value of δ may influence the specific details of the expansion dynamics. Additionally, our examination highlights the existence of negative pressure, as depicted in eqn. (52). This negative pressure

13

is a distinctive attribute of DE. The inclusion of DE within the model provides evidence supporting the idea that DE plays a crucial role in influencing the dynamics of our universe.

In the exponential law model, we have obtained all dynamics parameters such as Hubble parameter (H), expansion scalar (θ), Shear scalar (σ^2), anisotropic parameter (A_m) are constant. Hence, as the universe evolves over time, this model demonstrates behavior similar to that of a cosmological constant model in its later stages. Additionally, the negative sign of the deceleration parameter signifies the expansion of the universe is accelerating. The ratio of the Shear scalar to the expansion scalar is non-zero, indicating that the universe is anisotropic.

Our findings indicate that the universe exhibits anisotropy during its early stages, yet as time progresses, the anisotropic behavior diminishes, leading to an isotropic present day universe. This conclusion aligns with various observational data. The models proposed in this paper offer a suitable description of the evolutionary trajectory of the universe.

ORCID

Abhijeet Ompratap Dhore, https://orcid.org/0009-0003-9970-3960; **Mohini Ramrao Ugale**, https://orcid.org/0000-0002-4795-1052

REFERENCES

[1] A.G.Riess, A.V. Filippenko, P. Challis, A. Clocchiatti, A. Diercks, P.M. Garnavich, et al., "Observational evidence from supernovae for an accelerating universe and a cosmological constant," The astronomical journal, **116**(3), 1009 (1998). https://doi.org/10.1086/300499.

[2] S. Perlmutter, G. Aldering, M.D. Valle, S. Deustua, R.S. Ellis, S. Fabbro, "Discovery of a supernova explosion at half the age of the Universe," Nature, **391**(6662),51-54 (1998). https://doi.org/10.1038/34124.

[3] C.L. Bennett, R.S. Hill, G. Hinshaw, M.R. Nolta, N. Odegard, et al., "First-year wilkinson microwave anisotropy probe (wmap)* observations: foreground emission," The Astrophysical Journal Supplement Series, **148**(1), 97 (2003). https://doi.org/10.1086/377252.

[4] M. Tegmark, M.A. Strauss, M.R. Blanton, K. Abazajian, S. Dodelson, H. Sandvik, et al., "Cosmological parameters from SDSS and WMAP," Physical review D, **69**(10), 103501 (2004). https://doi.org/10.1103/PhysRevD.69.103501.

[5] P.A. Ade, N. Aghanim, M.I.R. Alves, C. Armitage-Caplan, M. Arnaud, M. Ashdown, et al., "Planck 2013 results, I. Overview of products and scientific results," Astronomy and Astrophysics, **571**, A1 (2014). https://doi.org/10.1051/0004-6361/201321529.

[6] S. Weinberg, "The cosmological constant problem," Reviews of modern physics, **61**(1), 1 (1989). https://doi.org/10.1103/RevModPhys.61.1.

[7] J.M. Overduin, and F.I. Cooperstock, "Evolution of the scale factor with a variable cosmological term," Physical Review D, **58**(4), 043506 (1998). https://doi.org/10.1103/PhysRevD.58.043506.

[8] A.Y. Shaikh, "Diagnosing renyi and tsallis holographic dark energy models with hubble's horizon cutoff," Indian Journal of Physics, **98**, 1155–1162 (2023). https://doi.org/10.1007/s12648-023-02844-3.

[9] A.G. Cohen, D.B. Kaplan, and A.E. Nelson, "Effective field theory, black holes, and the cosmological constant," Physical Review Letters, 82(25), 4971 (1999). https://doi.org/10.1103/PhysRevLett.82.4971.

[10] M. Younas, A. Jawad, S. Qummer, H. Moradpour, and S. Rani, "Cosmological implications of the generalized entropy based holographic dark energy models in dynamical Chern-Simons modified gravity," Advances in High Energy Physics, **2019**, 1287932 (2019). https://doi.org/10.1155/2019/1287932.

[11] Y. Aditya, S. Mandal, P.K. Sahoo, and D.R.K. Reddy, "Observational constraint on interacting Tsallis holographic dark energy in logarithmic Brans–Dicke theory," The European Physical Journal C, **79**(12), 1020 (2019). https://doi.org/10.1140/epjc/s10052-019-7534-5.

[12] H. Moradpour, S.A. Moosavi, I.P. Lobo, J.M. Graça, A. Jawad, and I.G. Salako, "Thermodynamic approach to holographic dark energy and the Rényi entropy," The European Physical Journal C, **78**, 1-6 (2018). https://doi.org/10.1140/epjc/s10052-018-6309-8.

[13] M. Tavayef, A. Sheykhi, K. Bamba, and H. Moradpour, "Tsallis holographic dark energy," Physics Letters B, **781**, 195-200 (2018). https://doi.org/10.1016/j.physletb.2018.04.001.

[14] C. Tsallis, and L.J. Cirto, "Black hole thermodynamical entropy," The European Physical Journal C, **73**, 1-7 (2013). https://doi.org/10.1140/epjc/s10052-013-2487-6.

[15] A.S. Jahromi, S.A. Moosavi, H. Moradpour, J.M. Graça, I.P. Lobo, I.G. Salako, and A. Jawad, "Generalized entropy formalism and a new holographic dark energy model," Physics Letters B, **780**, 21-24 (2018). https://doi.org/10.1016/j.physletb.2018.02.052.

[16] M.A. Zadeh, A. Sheykhi, H. Moradpour, and K. Bamba, "Note on Tsallis holographic dark energy," The European Physical Journal C, **78**, 1-11 (2018). https://doi.org/10.1140/epjc/s10052-018-6427-3.

[17] S. Basilakos, A. Lymperis, M. Petronikolou, and E.N. Saridakis, "Alleviating both H_0 and σ_8 tensions in Tsallis cosmology," The European Physical Journal C, **84**(3), 297 (2024). https://doi.org/10.1140/epjc/s10052-024-12573-4.

[18] A. Mohammadi, T. Golanbari, K. Bamba, and I.P. Lobo, "Tsallis holographic dark energy for inflation," Physical Review D, **103**(8), 083505 (2021). https://doi.org/10.1103/PhysRevD.103.083505.

[19] J. Bharali, and K. Das, "Modified Tsallis Holographic Dark Energy," Astrophysics, **66**(3), 366-382 (2023). https://doi.org/10.1007/s10511-023-09797-9.

[20] A. Pradhan, and A. Dixit, "Tsallis holographic dark energy model with observational constraints in the higher derivative theory of gravity," New Astronomy, **89**, 101636 (2021). https://doi.org/10.1016/j.newast.2021.101636.

[21] A.A. Mamon, A.H. Ziaie, and K. Bamba, "A generalized interacting Tsallis holographic dark energy model and its thermodynamic implications," The European Physical Journal C, **80**, 1-12 (2020). https://doi.org/10.1140/epjc/s10052-020-08546-y.

[22] M.V. Santhi, and Y. Sobhanbabu, "Bianchi type-III Tsallis holographic dark energy model in Saez–Ballester theory of gravitation," The European Physical Journal C, **80**(12), 1198 (2020). https://doi.org/10.1140/epjc/s10052-020-08743-9.

[23] Y. Sobhanbabu, and M.V. Santhi, "Kantowski–Sachs Tsallis holographic dark energy model with sign-changeable interaction," The European Physical Journal C, **81**(11), 1-10 (2021). https://doi.org/10.1140/epjc/s10052-021-09815-0.

[24] B.D. Pandey, P.S. Kumar, Pankaj, and U.K. Sharma, "New Tsallis holographic dark energy," The European Physical Journal C, **82**(3), 233 (2022). https://doi.org/10.1140/epjc/s10052-022-10171-w.

[25] R. Saleem, I. Shahid, and M. Sabir, "An exact solution approach to warm inflation using Tsallis and Barrow holographic dark energy entropy within Rastall gravity," The European Physical Journal Plus, **137**(2), 279 (2022). https://doi.org/10.1140/epjp/s13360-022-02494-0.

[26] M.V. Santhi, and Y. Sobhanbabu, "Tsallis holographic dark energy models in Bianchi type space time," New Astronomy, **89**, 101648 (2021). https://doi.org/10.1016/j.newast.2021.101648.

[27] M. Sharif, and S. Saba, "Tsallis holographic dark energy in f (G, T) gravity," Symmetry, **11**(1), 92 (2019). https://doi.org/10.3390/sym11010092.

[28] M. Zubair, and L.R. Durrani, "Exploring tsallis holographic dark energy scenario in f (R, T) gravity,' Chinese Journal of Physics, **69**, 153-171 (2021). https://doi.org/10.1016/j.cjph.2020.11.024.

[29] A.A. Aly, "Study of F (T) gravity in the framework of the Tsallis holographic dark energy model," The European Physical Journal Plus, **134**, 1-7 (2019). https://doi.org/10.1140/epjp/i2019-12698-6.

[30] A. Pradhan, G. Varshney, and U.K. Sharma, "The scalar field models of Tsallis holographic dark energy with Granda–Oliveros cutoff in modified gravity," Canadian Journal of Physics, **99**(10), 866-874 (2021). https://doi.org/10.1139/cjp-2020-0605.

[31] S.H. Shekh, V.R. Chirde, and P.K. Sahoo, "Energy conditions of the f (T, B) gravity dark energy model with the validity of thermodynamics," Communications in Theoretical Physics, **72**(8), 085402 (2020). https://doi.org/10.1088/1572-9494/ab95fd.

[32] S. Wang, Y. Wang, and M. Li, "Holographic dark energy," Physics reports, **696**, 1-57 (2017). https://doi.org/10.1016/j.physrep.2017.06.003.

[33] B. Wang, E. Abdalla, F. Atrio-Barandela, and D. Pavon, "Dark matter and dark energy interactions: theoretical challenges, cosmological implications and observational signatures," Reports on Progress in Physics, **79**(9), 096901 (2016). https://doi.org/10.1088/0034-4885/79/9/096901.

[34] G.T. Hooft, "Dimensional reduction in quantum gravity," (1993). https://doi.org/10.48550/arXiv.gr-qc/9310026.

[35] B. Guberina, R. Horvat, and H. Nikolić, "Non-saturated holographic dark energy," Journal of Cosmology and Astroparticle Physics, **2007**(01), 012 (2007). https://doi.org/10.1088/1475-7516/2007/01/012.

[36] S. Ghaffari, M.H. Dehghani, and A. Sheykhi, "Holographic dark energy in the DGP braneworld with Granda-Oliveros cutoff," Physical Review D, **89**(12), 123009 (2014). https://doi.org/10.1103/PhysRevD.89.123009.

[37] A.S. Jahromi, S.A. Moosavi, H. Moradpour, J.M. Graça, I.P. Lobo, I.G. Salako, and A. Jawad, "Generalized entropy formalism and a new holographic dark energy model," Physics Letters B, **780**, 21-24 (2018). https://doi.org/10.1016/j.physletb.2018.02.052.

[38] D.D. Pawar, and S.P. Shahare, "Anisotropic tilted cosmological model in f (R, T) theory of gravity," New Astronomy, **75**, 101318 (2020). https://doi.org/10.1016/j.newast.2019.101318.

[39] M.V. Santhi, A.S. Rao, T. Chinnappalanaidu, and S.S. Madhu, "Bulk viscous string cosmological model in a modified theory of gravity," Mathematical Statistician and Engineering Applications, **71**(3s2), 1056-1072 (2022). https://doi.org/10.1142/S0219887819500051.

[40] S. Aygün, "Marder type universe with bulk viscous string cosmological model in $f(R,T)$ gravity," Turkish Journal of Physics, **41**(5), 436-446 (2017). https://doi.org/10.3906/fiz-1704-14.

[41] T. Harko, F.S. Lobo, S.I. Nojiri, and S.D. Odintsov, "$f(R,T)$ gravity," Physical Review D, **84**(2), 024020 (2011). https://doi.org/10.1103/PhysRevD.84.024020.

[42] P.K. Sahoo, B. Mishra, and S.K. Tripathy, "Kaluza–Klein cosmological model in $f(R,T)$ gravity with $\Lambda(T)$," Indian Journal of Physics, **90**, 485-493 (2016). https://doi.org/10.1007/s12648-015-0759-8.

[43] V.R. Chirde, and S.H. Shekh, "Plane symmetric dark energy models in the form of wet dark fluid in f(R, T) gravity," Journal of Astrophysics and Astronomy, **37**, 1-16 (2016). https://doi.org/10.1007/s12036-016-9391-z.

АНАЛІЗ КОСМОЛОГІЧНОЇ МОДЕЛІ ГОЛОГРАФІЧНОЇ ТЕМНОЇ ЕНЕРГІЇ ЦАЛЛІСА У ПРОСТОРІ-ЧАСІ МАРДЕРА В $f(R,T)$ ТЕОРІЇ ГРАВІТАЦІЇ

Абхіджит Омпратап Доре[a], **Мохіні Рамрао Угале**[b]

[a]*Департамент математики, Shri. Dr. R.G. Коледж мистецтв і науки Ратод,*
Муртізапур, Округ Акола 444 107, Махарштра, Індія

[b]*Департамент науки та гуманітарних наук, Інженерно-технологічний коледж Сипна,*
Амраваті 444 701, Махарштра, Індія

У цій роботі досліджується анізотропна космологічна модель, заснована на просторово-часовій голографічній темній енергії Цалліса (THDE) Мардера в рамках $f(R,T)$ теорії гравітації, де R представляє скаляр Річчі, а T означає слід тензора енергії-імпульсу напруги. рівняння поля розв'язано для класу гравітації $f(R,T)$, тобто $f(R,T) = R + f(T)$. Щоб отримати точне рішення, ми використали щільність моделі THDE разом із законами об'ємного розширення, а саме степеневим і експоненціальним законом. Також досліджуються фізичні та геометричні аспекти моделі.

Ключові слова: $f(R,T)$ *гравітація; простір-час Мардера; THDE; Об'ємне розширення*

Structural and Morphological Properties of Spinel Type Magnesium Aluminate Thick Films

T.R.TATTE

Department of Physics, Shri. Dr. R. G. Rathod Arts and Science College, Murtizapur, Dist. Akola, Maharashtra State, India

Abstract-** **Magnesium aluminate($MgAl_2O_4$) powder sample was successfully prepared by co-precipitation method. The structural properties of the prepared material was investigated by X-ray diffraction (XRD) and Fourier transform infrared spectroscopy (FTIR). XRD study shows that the sample has the spinel structure and crystallite size of the prepared sample was 6.2 nm. FTIR spectrum explained the vibrational stretching frequencies of the material. Results of transmission electron microscopy with electron diffraction (TEM-ED) corroborates with XRD analysis. The morphology of the film and elemental composition of the sample was studied by using scanning electron microscopy with energy dispersive X-ray analysis (SEM-EDAX) and the result shows the prepared film contain highly porous structure.

Indexed Terms-** **Magnesium aluminate, XRD, FT-IR, SEM, TEM

I. INTRODUCTION

The environment contains a mixture of synthetically produced chemical components, toxic and explosive gases.Monitoring is needed so that effective measures can be taken to control and minimize the emission of hazardous gases to keep the environment safe and clean. At present, there are large number of gas detecting systems that have been used in process, for high performance gas sensors with high sensitivity and selectivity [1, 2]. Semiconductor gas sensor is chemiresistive type gas sensor. Chemiresistive gas sensors are based on SnO_2, TiO_2, WO_3, NiO, ZnO, Al_2O_3, CuO, In_2O_3, Cr_2O_3, etc. metal oxide material.

These materials can be utilized to detect combustible, reducing, or oxidizing gases with sensors which are based on the resistance change responses to the target gases [3]. The SMO sensor detecting harmful gases like CO, H_2S, H_2, NO_x and hydrocarbons (propane, butane etc.) low concentration level because of their high sensitivity, robustness and simple signal processing. Nanocrystalline structured gas sensing materials have been developed to enhance the sensitivity of a SMO sensor. The magnesium aluminate spinel possesses the properties such as high resistance to chemical attack, good mechanical strength from room temperature to high temperatures, low dielectric constant, excellent optical properties, low thermal expansion and good catalytic properties [4-8].

Moreover, there are different methods available to achieve nanocrystalline metal oxides with small particle size, such as combustion, hydrothermal route [9-13], citrated sol-gel method, Sono-chemical method, microwave heating, polymer solution route, solid state reaction method [14], co-precipitation [15,16] and self-heat sustained technique.

Among these methods, co-precipitation method is very easy and low cost method, which is operated at low temperature. Moreover, considering the importance of $MgAl_2O_4$ in various applications, it was decided to study magnesium aluminate prepared by co-precipitation method and to evaluate their structural properties.

II. EXPERIMENTAL

Magnesium aluminate ($MgAl_2O_4$) has been prepared by co-precipitation route. High purity precursors were used for the synthesis of the powder. As a result no further refinement was needed. Aluminum nitrate $[Al(NO_3)_3.9H_2O]$, magnesium nitrate $[Mg(NO_3)_2.6H_2O]$ and ammonia solution (25 wt. %) Sd fine GR grade chemical are used for the synthesis of nanoparticles.

In the beginning, the stoichiometric molar amounts of analytically pure $[Al(NO_3)_3.9H_2O]$ and

$[Mg(NO_3)_2.6H_2O]$ were weighed and dissolved in distilled water and subsequently stirred at 80^oC for 2 h to obtain a homogeneous and stable solution. Then aqueous ammonia (25 wt. %) was added drop wise at room temperature in the resulting liquid mixture under vigorous stirring till pH becomes 9. Here ratio of Mg/Al is 1:2. The collected precipitates comprising of hydroxides of metal ions and some water contents [17]. This precipitate was filtered-washed with ethanol and distilled water for number of times to remove excess of ammonia. In second stage, resulting precipitate was dried in oven for 22 h at 110^oC to evaporate the water content. Calcination was done at 800^oC for 4 h in furnace to obtain $MgAl_2O_4$. Taken solid phase sample wasgrinded in a mortar to make it powder.

The synthesized powder and a solution of ethyl cellulose (a temporary binder) were mixed together with butylcellulose, butyl carbitol acetate and turpineol in order to obtain the paste. Pastes incorporating mass percentage ratio of80:20, with $MgAl_2O_4$ and the binder respectively were ground in an agate pestle and mortar with for 1 h. This paste was screen printed onto glass substrate surface in desired patterns. This thick film was allowed to dry for 24 h at room temperature and heat treatment was given to the film at $500°C$ for 1 h.

III. RESULT AND DISCUSSIONS

3.1 XRD Analysis

Figure 1 depicts the XRD pattern of $MgAl_2O_4$ powder prepared by co-precipitation method. XRD pattern shows the spinel structure in accordance with JCPDS card. No other phases were detected in the calcinated sample. For $MgAl_2O_4$, the characteristic peaks for spinel structure were broad with maximum at 18.71, 30.89, 36.37, 44.51, 59.02, 64.99,77.05 and 82.41 which can be indexed as (1 1 1), (2 2 0), (3 1 1), (4 0 0), (5 1 1), (4 4 0), (5 3 3) and (4 4 4) diffraction planes, respectively. The crystallite size has been calculated from the XRD peaksusing Debye-Scherrer formula. Further, the lattice parameter of the prepared powder was calculated from the XRD peaks by indexing corresponding peaks in a cubic space group Fd-3m, using least square refinement. The XRD pattern show the formation of crystalline cubic structure.
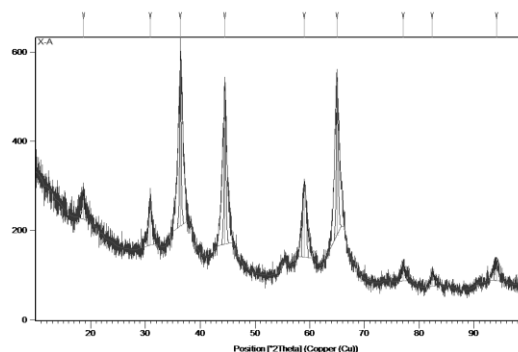

Figure1: X-ray diffraction pattern of $MgAl_2O_4$ powder calcinated at 800^oC.

3.2 FT- IR Analysis

Figure 2 shows the FT-IR spectrum of the $MgAl_2O_4$ nanoparticle. The peak position at 3457.05 cm^{-1} was attributed to the O-H stretching vibration and 1642.67 cm^{-1} which is due to the moisture adsorbed by the product [18-22]. FromFigure 2, it can be observed that the peak at 1518.25 cm^{-1} was attributed to Al-O stretching vibration [23]. The splitting of the high frequency band may be explained by the statement that a certain number of Al^{3+} ions occupy the tetrahedral site in the spinel structure [24]. The sample measurement of spectrum shows the bands which are in almost good conformity with ideal values of single crystals. The changes in the observed values are due to the formation of nanophase. The bands appeared at 527.98 assigned to the spinel formation of $MgAl_2O_4$.
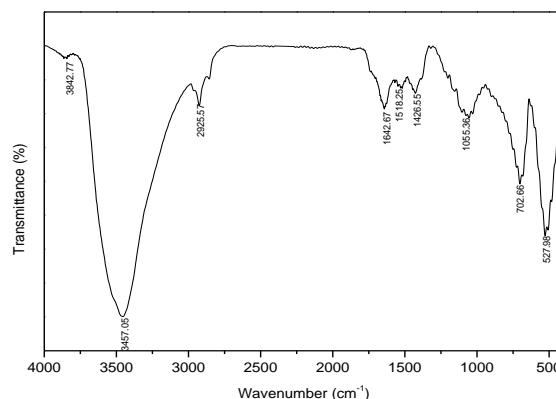

Figure 2: FT-IR spectrum of $MgAl_2O_4$ powder calcinated at 800^oC.

18

3.3 SEM Analysis

The surface morphology of thick film was analyzed by using scanning electron microscope (SEM). SEM image of $MgAl_2O_4$ thick film is shown in Figure 3. SEM image show a few particles are in the range 24-26 nm and some agglomerates are formed. The microstructure shows the homogeneous distribution of the particles in the sample. The film contains highly porous structure which has a large portion of atoms residing at surfaces and interfaces between the pores.
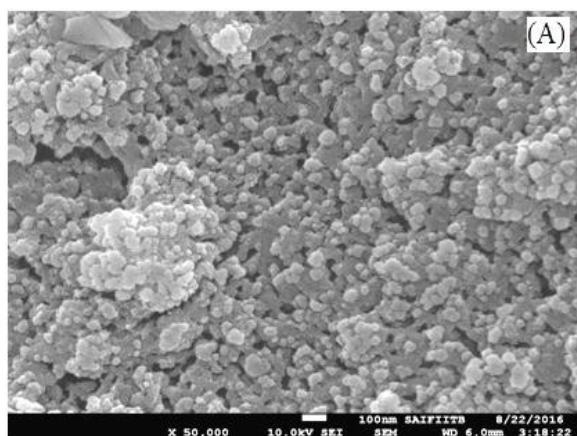

Figure 3: SEM image of nanocrystalline $MgAl_2O_4$

3.4 EDAX

Figure 4 shows the EDAX spectrum of $MgAl_2O_4$ thick film. The elemental analysis as obtained from EDAX is in close agreement with the starting composition used for the synthesis. Spectrum reveals presence of Mg, Al, and O elements.
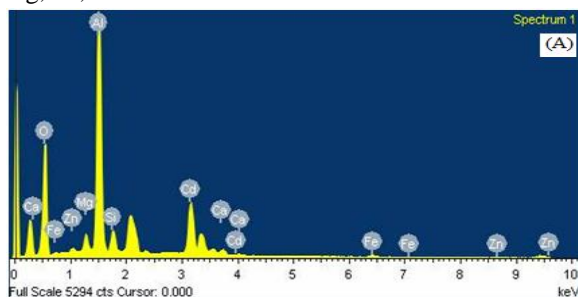

Figure 4: EDAX spectrum of $MgAl_2O_4$

3.5 TEM

Morphology of $MgAl_2O_4$ was characterized with Transmission Electron Microscopy (TEM). TEM image of $MgAl_2O_4$ powder annealed at $800^{\circ}C$ is shown in Figure 5. Figure exhibits the local distribution of the crystallite size can be revealed.

The average crystallite size calculated from the XRD data agrees with the TEM results. The small amount of agglomerations is observed in the micrograph.
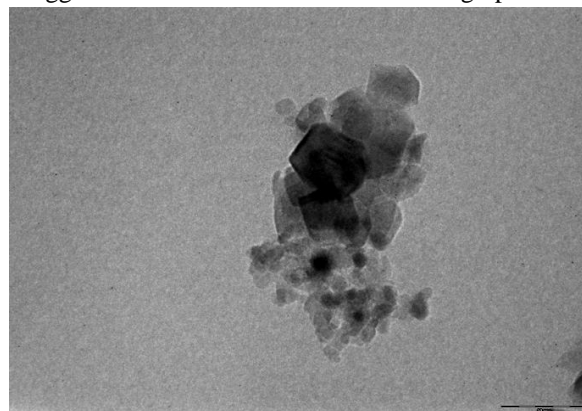

Figure 5: TEM photograph of $MgAl_2O_4$.

3.6 SAED

The selected area electron diffraction (SAED) pattern is presented in Figure 6. From figure 6, it can be seen that there is presence of continuous rings which deduced that the orientation of the crystallites is random within the field of view. It is observed that the spottype pattern which is indicative of the presence of single crystallite particles and no evidence was found for more than one pattern, suggesting the single-phase nature of the material.
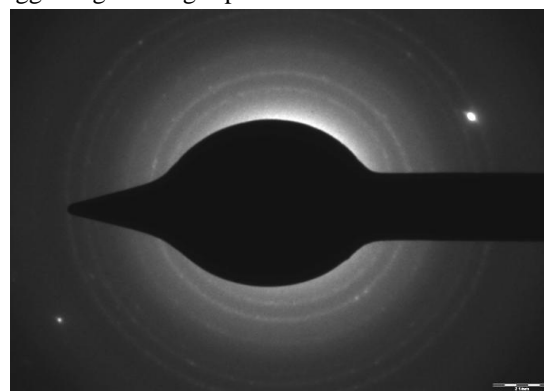

Figure 6: Selected area diffraction pattern of $MgAl_2O_4$ powder.

CONCLUSION

In the present study, $MgAl_2O_4$ powder sample was successfully prepared using less expensive, environment-friendly and low temperature co-precipitation route. XRD pattern reveals the formation of nanocrystalline cubic structure of prepared sample. The crystallite size is 6.2 nm. FT-IR

19

spectrum explained the vibrational stretching frequencies of the material. The decrease in intensity of the absorption band in FT-IR spectra suggested the occupation of ions at the octahedral B site. By using scanning electron microscopy with energy dispersive X-ray analysis (SEM-EDAX), the surface morphology and elemental composition of the sample was characterized. The average crystallite size of sample estimated from XRD analysis concurs with TEM investigation.

ACKNOWLEDGEMENT

REFERENCES

[1] S. Zampolli, I. Elmi, F. Ahmed, M. Passini, G. C. Cardinali, S. Nicoletti, L. Dori, Sens. and Actuat. B 101 (2004) 39-46.

[2] D. M. Bon, Ulbrich, I. M. Ulbrich, J. A. de Gouw, C. Warneke, W. C. Kuster, M. L. Alexander, A. Baker, A. J. Beyersdorf, D. Blake, R. Fall, Chem. Phys.11 (2011) 2399-2421.

[3] M. Batzill, U. Diebold, Prog. Surf. Sci.79 (2005) 147-154.

[4] G. B. Nuernberg, E. L. Foletto, C. Campos, H. Fajardob, N. Carreno, L. Probst, J. Power Sour. 208 (2012)409-414.

[5] F. Saito, W. Kim, Powder Technol. 113 (1999) 109-113.

[6] T. W. Dung, L.R. Ping, A. M. Azad, Mater. Res. Bull. 36 (2001) 1417-1430.

[7] A. D. Mazzoni, M. A. Sainz, A. Caballero, E. F. Aglietti, *Mater.Chem. Phys.78*(2002)*30-37.*

[8] S. A. Bocanegra, A. D. Ballarini, O. A. Scelza, S. R. Miguel, Mater. Chem. Phys. 111 (2008)534-541.

[9] D. Makovec, M. Drofenik, A. Znidarsic, J. Eur. Ceram. Soc. 21(2001) 1945-1949.

[10] J. A. Toledo, M. A. Valenzuela, P. Bosch, Appl. Catal. A. 198 (2000) 235-245.

[11] S. C. Goh, C. H. Chia, S. Zakaria, M. Yusoff, C. Y. Haw, Sh. Ahmadi, N. M. Huang, H. N. Lim, Mater. Chem. Phy. 120 (2010) 31-35.

[12] D. Zhao, X. Wu, H. Guan, E. Han, J. of Supercrit. Fluids 42 (2007) 226-233.

[13] Q. Liu, J. Sun, H. Long, X. Sun, X. Zhong, Z. Xu, Mater. Chem. Phy.108 (2008) 269-273.

[14] C. H. Yan, Z. G. Xu, F. X. Cheng, Solid State Commun. 111(1999) 287-291.

[15] S. Toshihiko, I. Shinichiro, K. Takayuki, Y. Goro, Int. J. Miner. Process. 62 (2001) 94-95.

[16] K. Kaneko, T. Katsura, Bull. Chem. Soc. Jpn. 52 (1979) 96-100.

[17] Z. Yue, W.Guo, J Zhou, Z. Gui, L. Li, J. Magn. Magn. Mater. 270 (2004) 216-233.

[18] K. Nakamoto, Organometallic, and Bioinorganic Chemistry, sixth ed., Wiley-Interscience, USA, 2009.

[19] M.Y. Nassar, A. S. Attia, K. A. Alfallous, M. F. El-Shahat, Inorg. Chim. Acta405 (2013) 362-367.

[20] M.Y. Nassar, Mater. Lett. 94 (2013) 112-115.

[21] M.Y. Nassar, I. S. Ahmed, Mater. Res. Bull. 47 (2012) 2638-2645.

[22] M.Y. Nassar, I. S. Ahmed, Polyhedron 30 (2011) 2431-2437.

[23] G. Korotcenkov, I. Boris, A. Cornet, J. Rodriguez, A. Cirera, V. Golovanov, Y.Lychkovsky, G. Karkotsky, Sens. and Actuat. B 120 (2007) 657-664.

[24] B. L. Patil, S. R. Sawant, S. A. Patil, J. Matter Sci. 29(1994) 175-178.

A Review on Spinel Ferrite Nanoparticles: Synthesis Methods and Applications

T. R. Tatte

Department of Physics, Shri. Dr. R. G. Rathod Arts and Science College, Murtizapur, Dist. Akola, Maharashtra State, India
Email: *truptitatte21[at]gmail.com*

Abstract: *Spinel ferrites are among the most promising soft magnetic materials due to their superior coercivity, tailored band gap, high saturation magnetization, and other physical, thermal, and electrical characteristics. Spinel ferrite nanomaterialsare gaining importance due to their diverse applications in biomedical, water treatment, and industrial electronic devices. Ferrite nanoparticles are utilized in electronic domains to create sensors, biosensors, transducers, and transformers. In this review, attention has been paid to the synthesis and applications of spinel ferrites across various fields.*

Keywords: Spinel ferrites; Nanoparticles; Synthesis methods, Applications

1. Introduction

Spinel ferrite nanoparticles are in the spotlight of current nanoscience due to immense application potential. Very interesting aspects of the spinel ferrite nanoparticles are their excellent electrical and magnetic properties often accompanied with other functional properties, such as catalytic activity. Spinel ferrite materials are metal oxides with spinel structures that have the general chemical formula AB_2O_4, where A and B represent various metal cations that are located at tetrahedral (A site) and octahedral (B site) positions, respectively. The types, quantities, and placements of the metal cations in the crystalline structure have a significant impact on the physicochemical properties of ferrites [1, 2].

Due to their unique and remarkable properties, nanocrystalline magnetic materials have attracted attention from various fields. Nanomaterials have particle size up to 100 nm and high surface - to - volume ratio, which altered or enhanced reactivity, thermal, mechanical, optical, electrical, and magnetic properties as compared to their bulk counterparts [3 - 6]. While the chemical composition of bulk materials is the main determinant of their qualities, the particle size, and morphology of nanomaterials, in addition to the chemical composition, dictate the majority of their features. The size and shape of spinel ferrite nanomaterial can be controlled by manipulating reaction variables such as properties is manipulated by changing the synthesis method, processing temperature and also substitution [7 - 9].

Spinel ferrite nanoparticles can be fabricated by various methods such as hydrothermal method, sol - gel method, chemical co - precipitation method, citrate precursor method, combustion method, solid state high temperature reactions etc. Nanoparticles of spinel ferrites are of growing interest for a wide range of applications like high density magnetic information storage, magnetic resonance imaging, targeted drug delivery etc. They also offer immense possibilities of tailoring its various properties for applications [10, 11]. Magnetic $CoFe_2O_4$, $MnFe_2O_4$, $CuFe_2O_4$, $ZnFe_2O_4$, and $NiFe_2O_4$ nanoparticles have received a great deal of attention owing to their thermal and chemical stability, as well as their distinctive structural, magnetic, optical, electrical, and dielectric properties, and their broad range of technological applications including photo catalysis, photoluminescence, biosensors, humidity - sensors, catalysis, magnetic refrigeration, permanent magnets, magnetic drug delivery, magnetic (hyperthermia) [12, 13].

The purpose of this review gives some general processing methods and applications on spinel ferrite nanomaterial which is found to be useful due to their electronic, optical, electrical, magnetic and catalytic properties.

2. Synthesis methods

Different synthesis methods can be utilized simultaneously to produce nanoparticles of various sizes. It is known that the synthesis process affects the physical and chemical behavior of nanoparticles. The development of new preparation techniques and application scenarios has been a key area of research since the discovery of magnetic nanoparticles. Among the various methods available for the synthesis of spinel ferrite materials, the most popular include physical, chemical and biosynthesis methods. Chemical synthesis is the most common approach for preparing NPs since it has a high capacity for producing nanoparticles in a reasonable time and at a low cost. Some few synthesis method such as sol - gel method [14, 15], chemical co - precipitation [16], Hydrothermal and Solvo - thermal synthesis [17], Self - propagating high temperature synthesis (SHS) technique [18], Micro – emulsion technique [19], citrate precursor method [20] etc. have been discussed.

2.1 Sol - Gel Method

The sol - gel process involves the transition of a solution of metal compounds from a liquid sol into a solid gel. In liquid, sol is a diffusion of the solid particles where only the Brownian motions suspend the particles and this sol is heated and then to form a homogenous gel which can achieved by the addition of base or acidic solutions. A gel is intermediate where both liquid and solid are dispersed in each other, which presents a solid network containing liquid components. Usually inorganic metal salts or metal organic compounds such as metal alkoxides are used as starting

precursors in the preparation of the sol. The purpose of this precursor is to a series of hydrolysis and polymerization reactions to form a colloidal suspension, or a sol. By elimination of water, the hydroxide molecules gets condensed and then formation of a metal hydroxide. When all metal hydroxides species are linked to one another in a network, and formation of dense porous gel is obtained. Further heating at higher temperature and then drying of the gel, the gel is converted into ultrafine powders of metal oxides.

2.2 Chemical Co - Precipitation

In the chemical co - precipitation method, an aqueous solution of suitable salts of iron, lithium, manganese and other desired, suitable materials is mixed under a fine control of pH by using a precipitating agent like NaOH or NH_4OH solutions which causes the precipitation of the other metals present in the solution. The precipitate represents a significantly uniform mixture of organic compounds of the ferrite metals on an atomic scale. In case of ferrite, it is important to prevent agglomeration; Ostwald ripening etc. Filtrated the precipitate and then dried. Then dried precipitate is heated at a high temperature to dehydrate the precipitate and to burn out carbonaceous matter leaving a residue of the oxides of the respective metals. After this, particles are sintered. The reaction and transport rates can be affected by the concentration of reactants, temperature, pH, the order in which the reagents are added to the solution and mixing. The particle structure and crystallinity can be influenced by reaction rates and impurities. This method doesn't work very well in cases where two reactants have very different solubilities in water and the reactants do not precipitate at the same rate. This method offers distinct advantages like simple, rapid preparation, easy control of particle size and composition.

2.3 Hydrothermal and solvothermal synthesis

To create crystalline nanoparticles, hydrothermal and solvothermal syntheses use a variety of wet - chemical processes. High purity and controllable morphology of nanoparticles can be produced by simple and effective hydrothermal and solvothermal procedures. A nonaqueous solution, such as methanol, ethanol, or ethylene glycol, is used in solvothermal synthesis to dissolve the metal precursors under high pressure and at a moderate temperature. Hydrothermal synthesis refers to the synthesis through chemical reactions in an aqueous solution above the boiling point of water.

2.4 Self - Propagating High Temperature Synthesis Technique

In this method, organic acid is taken as precursur in aqueous solution. This solution containing all necessary cations and combustible anions in the desired product. After dehydration, the precursor becomes dry gel and this dry gel is amorphous in nature. Moreover, when calcinating this dry gel directly yields the required materials in presence of air/oxygen. In case of this process, the starting materials are mixed in the atomic scale. The phase formation occurs at lower calcination temperature as compared to ceramic route

and giving ultrafine powder. The overall process completes within 5 minutes.

2.5 Micro – emulsion Technique

Micro - emulsions are clear, isotropic mixtures of water, oil, and a surfactant that are stable and clear. This method uses surfactants to aid in the coexistence of two immiscible liquids in a single phase. One of the micro - emulsion solvents is water/oil, which is used to prepare the solution by dispersing immiscible solvents. The nanoparticles precursor is typically dispersed as 1–100 nm Nano droplets in the aqueous phase. Surfactant molecules encircle water droplets, forming "micelles" that act as nanoreactors. This results in the formation of magnetic nanoparticles inside the micelles, which confines the particles and limits particle nucleation, development, and agglomeration.

2.6 Citrate Precursor Method

In this method, the starting materials such as nitrates are complexed in an aqueous solution with α−carboxylic acids such as citric acid. By adding ammonium hydroxide to the solution, the pH is controlled at 7. The solution is refluxed with continuous stirring using magnetic bar agitator and then dried. By the evaporation of the solution, a highly viscous mass is formed and resulting from metal nitrates and citric acid making a redox reaction to occur and then this metal nitrates react with water. The chelating agent citric acid is used for deprotonating with ammonium hydroxide and the metal hydroxide by removing protons. Then the formation of metal ions having a positive valency and carboxylic ions with negative valency together with water molecules. This co - ordinate bonds are used to form the metal and acid complex which is the ash - synthesized powder obtained. At last point auto - combustion process takes place. The powder is pressed into pellets and then given final sintering for densification.

3. Applications of Spinel Ferrites

The properties of ferrite, including its structure, particle size, and shape, can vary depending on the cation type and synthesis method employed, resulting in diverse applications.

3.1 Sensors

Sensors are electronic devices that detect changes in a given material in a specific environment. Ferrite nanoparticle - based sensors possess exceptional sensitivity, low detection limits, and high signal - to - noise ratios. The detection of variations in humidity is one of the most common uses of sensors. The monitoring of humidity is a widespread practice in both industrial and residential settings, as it helps to maintain human comfort, regulate storage conditions for various items, and ensure optimal operating conditions for industrial processes and devices. Typically, humidity sensing is primarily attributed to the surface effects of the interaction between water vapor and solids.

3.2 Photo luminescent applications

22

Mixed spinel nanostructures such as $CoFe_2O_4$, $NiFe_2O_4$, and $ZnFe_2O_4$ are known for their photoluminescence at room temperature, which is considered one of their most significant properties. The spectrum of photoluminescence offers insights into various characteristics such as surface oxygen vacancies, defects, charge carrier trapping, and transfer efficiency.

3.3 Magnetic applications

The variation of exchange contact between tetrahedral and octahedral sites causes the magnetization to be dependent on grain size. To minimize media noise in high - density magnetic recording, the magnetic particles utilized should have a nanoscale size to limit the exchange interactions occurring between adjacent grains. To achieve great storage density, the particles must also have high H_C values. The magnetic characteristics (M_R, M_S, and H_C) of spinel ferrites are affected by their composition, particle size, crystal structure, and cationic distribution between octahedral and tetrahedral sites.

3.4 Dielectric applications

The dielectric structure typically consists of grains that are good conductors separated by grain boundaries with low conductivity. The dielectric properties of spinel ferrites are influenced by factors such as structural homogeneity, cation distribution, particle size, density, and porosity.

Additionally, the dielectric properties can be significantly affected by synthesis techniques and thermal treatment parameters such as temperature, time, and heating/cooling rates.

3.5 Waste water treatment

Industrial wastewater management has become one of the most pressing issues in developed countries in recent years. Textile wastewaters contain a variety of non - biodegradable organic dyes, as well as other pollutants in varying concentrations. Untreated effluents harm not only humans and animals but also plants. RhB is a synthetic, highly poisonous, water - soluble organic dye that is commonly found in the wastewaters and is widely employed as a colorant in various industries. For the treatment of RhB - containing water, various procedures have been used, including ozonation, the electrochemical method, and the Fenton process. In recent years, magnetic NPs have attracted considerable attention due to their special magnetic properties, high adsorption capacities and surface area to volume ratio.

3.6 Catalytic applications

Spinel ferrites are commonly used as heterogeneous catalysts due to their ease of recovery from reaction mixtures by filtering or using an external magnetic field, making the process cost - effective and environmentally friendly through their multiple recyclings. To be economically valuable and ecologically friendly, heterogeneous catalytic nanoparticles play a key role in the selective protection of functional groups.

3.7 Photo catalytic applications

Photo catalysts are important materials that facilitate the use of solar energy in oxidation and reduction reactions, with numerous applications including removing water and air pollution, managing odors, deactivating bacteria, splitting water to generate hydrogen, inactivating cancer cells, and other areas. Currently, photo catalysis is a preferred method for removing dyes, as irradiation of light on a semiconductor can generate electron - hole pairs that can be utilized for oxidation and reduction processes. Dye degradation is caused by the generation of active radicals during the photo catalytic reaction.

3.8 Biomedical applications

For use in biomedical applications, magnetic nanoparticles need to have high magnetic saturation values and be biocompatible, while also being stable and non - agglomerated when dispersed in water. These nanoparticles can be used within individual cells to facilitate magnetic fluid hyperthermia, drug delivery, and stimulation of metabolic pathways through thermal excitation. $MnFe_2O_4$ nanoparticles have attracted significant interest in the field of biomedicine due to their desirable properties, including simple synthesis, controllable size, high magnetization value, super paramagnetic nature, ability to be monitored by an external magnetic field, and high biocompatibility.

4. Conclusions

Recently nanostructured spinel ferrite materials have received a lot of attention due to its unique features, including stability under mechanical, chemical, and thermal conditions and can be modified suitably and promising technological applications in different fields of life. Among all the reviewed synthesis strategies, the usefulness of spinel ferrite in many applications depends largely on the synthesis processes; efficient synthesis processes yield spinel ferrite that can function better and endure the conditions under which they are synthesized. Nevertheless, the cost - effective synthesis of large amounts of spinel ferrite with monodisperse size and shape for a biomedical purposes, however, needs more study and it is important to take into account and thoroughly examine the toxicity of specific spinel ferrite nanoparticles.

References

[1] D. H. K. Reddy, Y. S. Yun, Coord. Chem. Rev., 315 (2016) 90.
[2] K. K. Kefeni, B. B. Mamba, Sustainable materials and technologies., 23 (2020).
[3] S. Mokhosi, W. Mdlalose, S. Mngadi, M. Singh, T. Moyo, Journal of Physics: Conference Series. IOP Publishing; (2019).
[4] S. Chakrabarty, M. Pal, A. Dutta, Ceram. Int.44 (12) (2018) 14652.
[5] G. Asab, E. A. Zereffa, T. AbdoSeghne, International journal of biomaterials. (2020).
[6] M. Anand, J. Appl. Phys., 128 (2) (2020).
[7] B. K. Kuanr, P. Kishan, N. Kumar, S. L. N. Rao, P. K. Singh and G. P. Srivastava, J. Appl. Phys, 8 (1986) 63.

23

[8] H. B Im, D. G Wickham, IEEE Trans. onmagn., 8 (1972) 765.

[9] Z. Yue, Ji Zhou, X. Wang, Z. Gui and L. Li, J. European Cera. Soci., 23 (2003) 189.

[10] R. D. McMichael, R. D. ShuU, L. J. Swartzendruber and L. H. Bennett, J. Magn. Magn. Mater., III (1992) 29.

[11] D. G. Mitche, J. Magn. Reson. Imaging, 7 (1997) 1.

[12] V. Anjana, S. John, P. Prakash, A. M. Nair, A. R. Nair, S. Sambhudevan, B. Shankar, IOP Conference Series: Materials Science and Engineering. IOP Publishing; 2018.

[13] M. Ahmad, M. A. Khan, A. Mahmood, S. S. Liu, A. H. Chughtai, W. C. Cheong, B. Akram, G. Nasar, Ceram. Int., 44 (5) (2018) 5433.

[14] J. Azadmanjiri, S. A. SeyyedEbrahimi, H. K. Salehani, Ceramic International, 33 (2007) 1623.

[15] J. G. Lee, H. M. Lee, C. S. Kim, and Y. J. Oh, J. Magn. Magn. Mater., 177 (1998) 900.

[16] K. Maaz, A. Mumtaz, S. K. Hasanain, and A. Ceylan, J. Magn. Mater., 308 (2007) 289.

[17] T. N. Pham, T. Q. Huy, A. T. Le, RSC Adv.10 (52) (2020) 31622.

[18] W. B. Cross, L. Affleck, M. V. Kuznetsov, et al., J. Mater. Chem., 9 (1999) 2545.

[19] E. Meydan, S. Demirci, N. Aktas, N. Sahiner, O. F. Ozturk, Inorg. Chem. Commun., 126 (2021).

[20] Ibetombi. Soibam, S. Phanjoubam, C. Prakash, J. Alloys Compd., 475 (2009) 328.

24

Study of Microwave Dielectric Properties of FeCl₃-doped Polyvinyl Acetate Based Thin Films

T. R. Tatte [a]*

[a] Department of Physics, Shri. Dr. R. G. Rathod Arts and Science College, Murtizapur, Dist. Akola, Maharashtra State, Pin-444107, India.
Doi: https://doi.org/10.55248/gengpi.4.1223.123449

A B S T R A C T

Polyvinyl acetate films doped with Ferric chloride (FeCl3) have been prepared by sudden quenching technique from their aqueous solutions. In this paper, dielectric constant, dielectric loss and loss tangent of undoped and FeCl3 - doped poly vinyl acetate films of different thicknesses have been studied at 9.1 GHz microware frequency. The change in the dielectric constant and loss was observed with doping % of FeCl3. The maximum dielectric constant, dielectric loss and loss tangent was found at 1.96, 0.53, 0.27 FeCl3 mol.% resp. The variation of dielectric constant, dielectric loss and loss tangent showed an increasing trend with increasing dopant concentration. It has been concluded that, the dielectric constant, dielectric loss and loss tangent depend on dopant concentration.

Keywords: Microwave bench; Poly vinyl acetate; Fe – doping effect; Dielectric response.

1. Introduction

In the recent years, conjugated polymers have been the main focus of research throughout the world [1,2]. They have very diverse structure and applications ranging from domestic articles to sophisticated scientific and medical instruments. The modern era can definitely be called a polymer era as we wear these manmade materials sleep between them, build houses, pull switches, with their help. We can see and hear the sights remote from us. This polymers made revolutionary advancement in the field of medicine, with their help cripples could walk heart valves can be repaired and damage human organs could be replaced.

Now a day through proper selection of monomers and their combinations, catalysts and other additives and adopting appropriate polymerization conditions and techniques, experts are able to construct polymers molecules of almost any desired size, shape, complexity and of any desired chemical structure suited to almost any contemplated end use.

Polymers like Poly vinyl acetate is easily available in market. It has low cost and is easily soluble in organic solvents such as methanol. Poly vinyl acetate is mainly used for the manufacture of PVA, especially in the form of thin films. Poly vinyl acetate with other polymers and compounds, it is used in adhesives and for the large scale manufacture of gramophone records. The aim of present work is to prepare thin films of undoped and FeCl₃ doped Poly vinyl acetate having different thickness and to determine the dielectric constant and dielectric loss at microwave frequency.

2. Experimental

2.1 Preparation of Films

FeCl₃ – doped polyvinyl acetate thin films of varying thicknesses of different concentration, the size of rectangular waveguide in X-band microwave bench, were prepared in the laboratory by sudden quenching technique [3]. Powdered form of poly vinyl acetate and methanol were taken in test tube and then added FeCl₃ in proper proportion to this mixture by calculating weight percent formula. Weighing was done on monopan balance. This mixture was finely mixed for 1 hour to form a homogeneous mixture. Cleaned glass plate with acetone and poured some mixture on glass plate to form film of 0.1 concentration. The second film was prepared by adding some methanol to remaining mixture and poured on glass. Using the aforementioned method, five types films of different concentration 0.1, 0.2, 0.3, 0.4 and 0.5 were prepared. For each type of film concentration, five samples of varying thicknesses were also prepared.
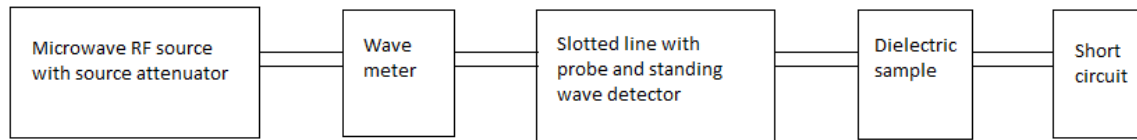
Fig.1: Experimental set up for measurement of the dielectric constant.

Dielectric constant measurement at microwave frequency

For accurate measurement of dielectric constant width at twice minima method was used [4]. Following steps were followed in this method.

1.   The frequency of source was determined by taking micrometer reading of cavity resonator.

2.   The guide wavelength λg, was measured by short circuiting waveguide section.

3.   The distance, ΔX shown in Fig.2 was measured by width at twice minima method.

4.   The position of minima without sample A was recorded Fig. 2.

5.   Dielectric sample (film) was then introduced in the waveguide touching the short – circuit end.

6.   The distance ΔXs, was measured.

7.   The position of minimum 'B' of standing wave pattern occurring with sample was recorded Fig. 2.

8.   Shift in minima Δl was calculated.

The dielectric constant was calculated by using the formula (1). The reading were noted at which beam voltage near about 150V and beam current at 25 mA and at room temperature.
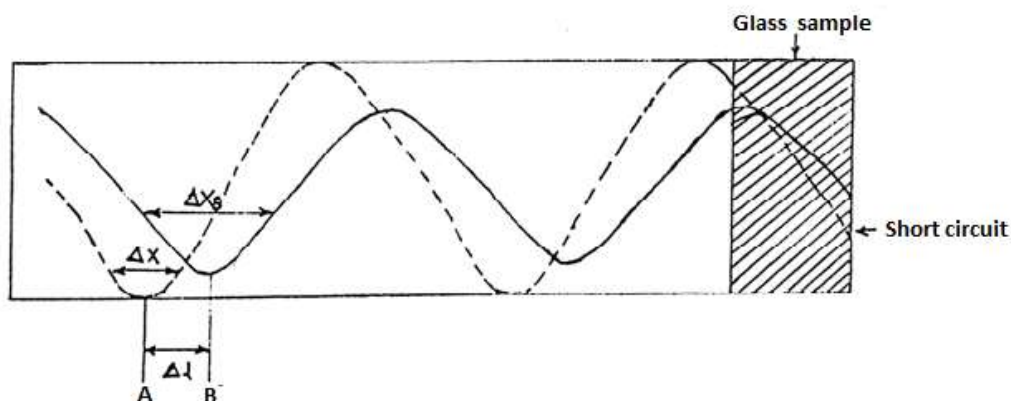
Fig. 2: Standing waves in the waveguide with and without sample.

3. Results and discussion

The dielectric constant, dielectric loss and loss tangent and $FeCl_3$ - doped polyvinyl acetate films of different thicknesses are studied at 9.1 GHz microwave frequency and at room temperature. The values of dielectric constant (ϵ') and dielectric loss (ϵ'') depicted in Table 1 are found to be reasonable to the films.

Table 1: Values of dielectric constant (ϵ'), dielectric loss (ϵ'') and loss tangent ($\tan\delta$) for different concentration at microwave frequency (9.1 GHz).

% of $FeCl_3$ doping	Dielectric constant (ϵ')	Dielectric loss (ϵ'')	Loss tangent ($\tan\delta$)
0.1	1.7670	0.1457	0.0824
0.2	1.8126	0.2370	0.1307
0.3	1.8159	0.2435	0.1340
0.4	1.8432	0.2980	0.1616
0.5	1.9602	0.5320	0.2714

Dielectric constant (ϵ') is given by the following formula [5]:

$$\epsilon' = \left(\frac{\lambda_0}{\lambda_c}\right)^2 + \left(\frac{\lambda_o}{\lambda_d}\right)^2 \left\{1 + \frac{\alpha_d \lambda_d}{2}\right\} \tag{1}$$

where, λ_0 - free space wavelength(= 3.29 cm); λ_c - cut off wavelength(= 4.5828cm); λ_d - wavelength of wave(= 3.03 cm).

α_d can be determined by following formula:

$$\alpha_d = \frac{\Delta x . 2\pi}{\lambda^2 g} \tag{2}$$

where, Δx - width at twice minima; λ_g - guide wavelength(= 4.72 cm).

Dielectric loss (ε") is determined from the following formula:

$$\varepsilon'' = 1/\Pi \ (\lambda_0/\lambda_d)^2 \alpha_d \lambda_d \tag{3}$$

Loss tangent (tanδ) was calculated using the formula [4]:

$$\tan\delta = \varepsilon''/\varepsilon' \tag{4}$$

Thickness, width (Δx) all values for different concentrations are included in Table 2. Fig. 3 shows the plot of dielectric constant (ϵ') versus % of FeCl$_3$ doping for different concentration of Fe - doped polyvinyl acetate films. The variation of dielectric constant increases with increasing dopant concentrations. The maximum dielectric constant was observed at 1.96 FeCl$_3$ mol%. It showed that for different composition of material, we get different dielectric constant.

Table 2: Values of width (Δx) for different concentrations and thicknesses at room temperature.

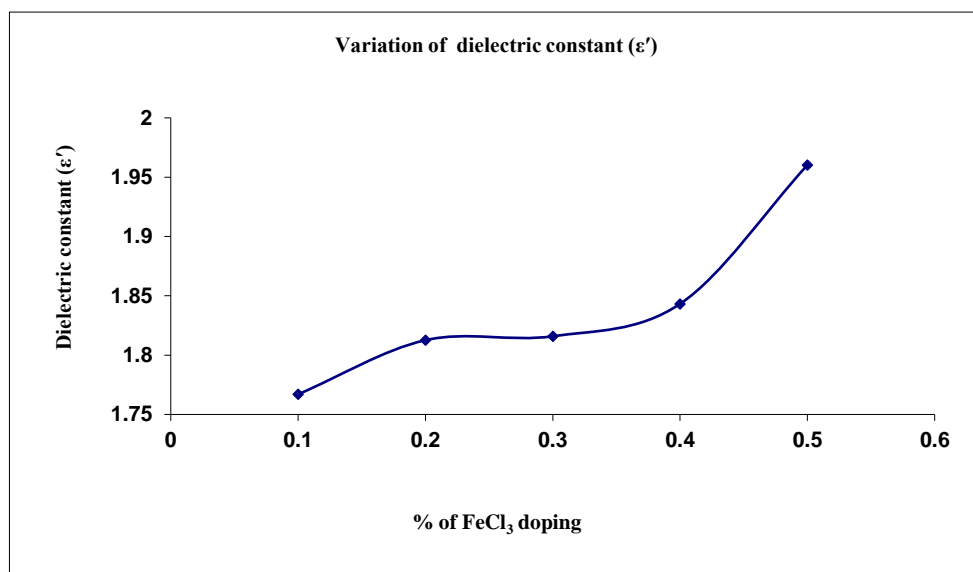| Sample concentration	Thicknesses (cm)	Position of twice minimum T.R. with sample Δx₁(cm)	Position of twice minimum T.R. without sample Δx₀ (cm)	Δx₁- Δx₀ (cm)	Mean Δx (cm)
0.1	0.0256	1.865	1.73	0.135	0.455
	0.0044	1.855		0.125	
	0.0055	1.800		0.070	
	0.0018	1.800		0.070	
	0.0032	1.785		0.055	
0.2	0.0047	1.860	1.73	0.130	0.740
	0.0038	1.920		0.190	
	0.0029	1.865		0.135	
	0.0023	1.905		0.175	
	0.0133	1.840		0.110	
0.3	0.0033	1.940	1.73	0.210	0.760
	0.0046	1.830		0.100	
	0.0327	1.940		0.210	
	0.0077	1.810		0.080	
	0.0025	1.890		0.160	
0.4	0.0346	1.840	1.73	0.110	0.930
	0.0047	1.960		0.230	
	0.0234	1.980		0.250	
	0.0070	1.905		0.175	
	0.0512	1.895		0.165	
0.5	0.0029	2.160	1.73	0.430	1.660
	0.0035	2.175		0.445	
	0.0073	2.195		0.465	
	0.0464	1.930		0.200	
	0.0858	1.850		0.120	

Fig. 3: Variation of dielectric constant ($\in'$) with % of $FeCl_3$ doping at room temperature.

The variation of dielectric loss ($\in''$) versus % of $FeCl_3$ doping at room temperature as shown in Fig. 4. From figure, it can be seen that, dielectric loss increases with increasing doping % of $FeCl_3$. The maximum dielectric loss is found to be 0.53. The variation of tangent loss (tan δ) with % of $FeCl_3$ doping as shown in Fig. 5. From figure, it is clear that, loss tangent for different concentration is different. The loss tangent increases with increasing doping % of $FeCl_3$. The maximum loss tangent is found to be 0.27.
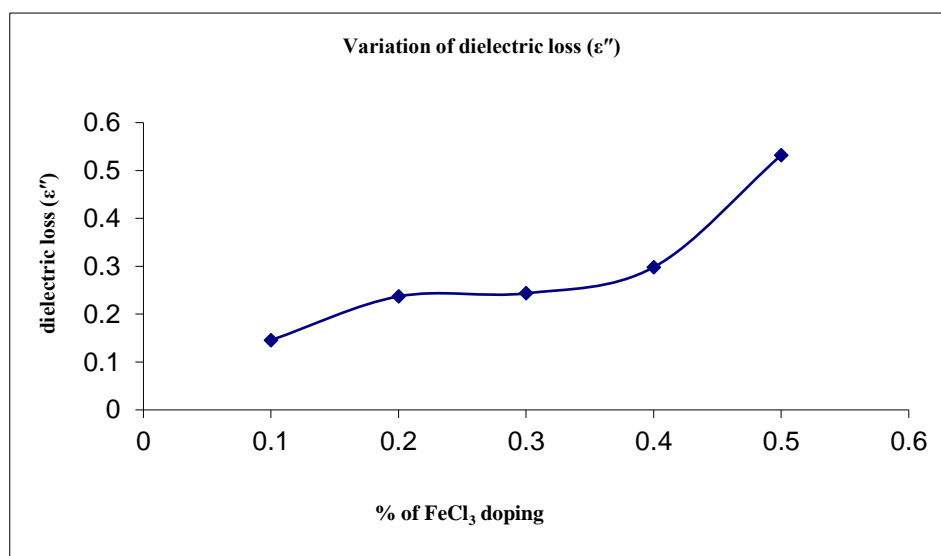
Fig. 4: Variation of Dielectric loss ($\in''$) with % of $FeCl_3$ doping at room temperature.

The origin of microwave dielectric loss in polymers are categorized as: (a) dipolar absorption dispersions in both crystalline and amorphous polymers; (b) dipolar losses due to impurities, additives or fillers in a polymer material; (c) microwave absorption in conducting polymers (poly acetylene and poly (sulphur nitride)) for which the current carriers are electrons; and (d) photon-phonon absorption spectra corresponding to the density of states in amorphous regions of a polymer material [6].
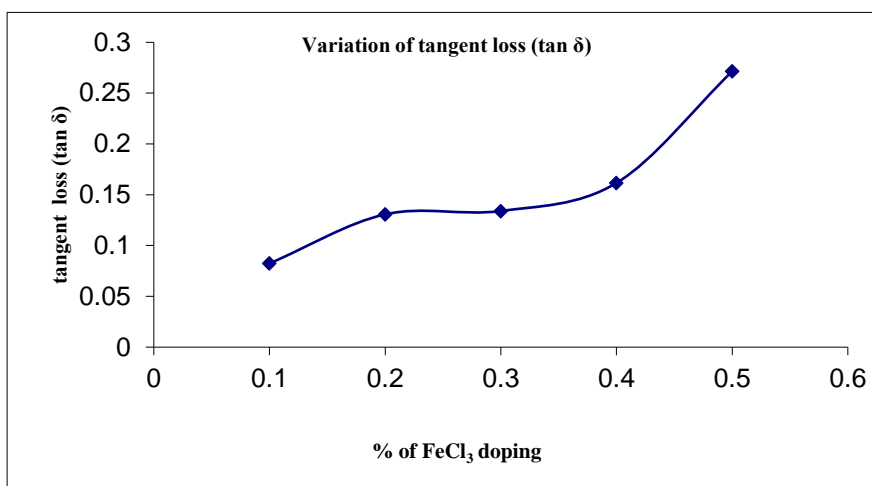
Fig. 5: Variation of tangent loss with % of $FeCl_3$ doping at room temperature.

When $FeCl_3$ doped in polyvinyl acetate, in this reaction the splitting of a chloride anion occurs forming the negatively charged macrocation, which is then transferred to the positively charged. The principal mechanics of microwave absorption in poly vinyl acetate and $FeCl_3$ is the reorientation of dipoles. Microwave processing is suitable to these materials, because it form strong dipoles. Permittivity and dielectric loss with increasing concentration and increase in temperature. The materials tend to be efficient absorbers of microwave radiation.

Polymer dielectric constant can vary during a processing cycle or if a phase change occurs as temperature varies, solvents is removed and the reaction proceeds changing the type and concentration of dipoles. The properties of amorphous region suggest the existence of many localized state and release the excited charge carriers in these states. Therefore, the dopant present in low concentration does not significantly affect the dielectric constant. But, when the dopant is present in large concentration it creates additional sites for trapping and thereby enhancing the dielectric constant.

4. Conclusions

In summary, the dielectric properties of $FeCl_3$ - doped polyvinyl acetate films of different thicknesses have been investigated at 9.1 GHz microwave frequency and at room temperature. The dielectric constant, dielectric loss and loss tangent are observed to depend on doping concentration of $FeCl_3$. A little variation in the dielectric constant is observed with doping % of $FeCl_3$ and also, dopant present in low concentration does not significantly affect the dielectric constant. But, when dopant is present in large concentration, it creates additional sites for trapping and thereby, enhancing the dielectric constants. In general, at microwave frequency the movement of network and modifying ions are held responsible for relative dielectric constant and the oscillations between them for losses.

References

Mohd Hamzah Harun, Elias Saion, Anuar Kassim, Ekramul Mahmud (2009). J. Advancement OF Science & Arts Dielectric Properties of Poly (vinyl alcohol)/Polypyrrole Composite, *Polymer Films* Vol. 1.

Biswas Dutta, P., S and De, S K (2002). Dielectric Relaxation in Polyaniline-Polyvinyl alcohol Composites, *Materials Research Bulletin* 37, 193-200.

Yawale S P, Pakade S V (1993*). J. Mater. Sci. (UK)* 20 5451.

Lance A L (1964). Introduction to microwave theory and measurements (New York: McGraw-Hill)

Von-Hippel R (1954) Dielectric materials and applications (NewYork: Wiley & Sons) pp 104–115.

Bur Anthony J (1985). Dielectric properties of polymers at microwave frequencies: a review, *J. Elsevier*, 26, 963–977.

Preparation of Zinc doped Magnesium Ferrite Nanoparticles by Sol-Gel Method

T. R. Tatte*, V. D. Kapse, M. S. Pande

Department of Physics, Shri. Dr. R. G. Rathod Arts and Science College, Murtizapur, 444107, Dist. Akola, Maharashtra State, India.

Department of Physics, Arts, Science and Commerce College, Chikhaldara, 444807, Maharashtra State, India.

Department of Physics, Gajanan Maharaj College of Engineering, Shegaon, 444203, Maharashtra State, India.

1. Introduction

During the last decade, the world has seen huge interest in developing and understanding the matter of nanometric scale. It has allowed the scientists to develop and characterize materials with prominent properties and nanometric sizes. Due to the note-worthy properties, exhibited by nonmaterial, they have become centre of attention in the scientific community. The fabrication of spinel-structured ferrite nanoparticles has been intensively investigated in recent years due to their unique physical and chemical properties, as well as technological applications in ferrofluids [1], high-density magnetic recording media [2], biomedicine [3] and radar-absorbent materials [4].

Spinel ferrites, MFe_2O_4 (M = Mg, Mn, Fe, Co, Ni, Zn, Cu, Cd, etc.) are a technologically important group of materials. Among different ferrites, magnesium ferrite ($MgFe_2O_4$) enjoys a special attention because of its vast applications in high density recording media, heterogeneous catalysis, adsorption, sensors and magnetic technologies. $MgFe_2O_4$ is a partially inverse spinel and its degree of inversion is sensitive to the thermal history of the sample, microstructure and preparative parameters. Nanoparticles of $MgFe_2O_4$ have good photo electrical properties [5-7]. To fabricate various types of nanoparticles, a large number of methods are used such as physical, chemical, biological and hybrid methods. The nanoparticles synthesized using each method exhibit particular properties. So, the synthesis of nanostructured materials has become a particularly important area of research.

There are several methods for synthesizing nanosized spinel ferrite particles such as hydrothermal, co-precipitation, combustion, sol–gel, precursor, spray drying and freeze drying, microemulsion and reverse micelle method [8–15]. To prepare nanoferrites with simple routes by using cheap, non-toxic and eco-friendly precursors are still the core issue, among other proven synthesis methods [16]. Among these methods, the nanoparticles prepared by sol-gel method have been studied, although this synthesis provides a quick and easy way to prepare nanoparticle, it usually produces sample with large size distribution and less defined crystal chemistry.

Herein, the purpose of this work is to prepare nanocrystalline Zn doped Mg spinel ferrite by a sol-gel method with a low calcination temperature involving low cost metal nitrates as raw materials and study of their structural properties.

2. Experimental

Preparation of nanocrystalline $Mg_{0.5}Zn_{0.5}Fe_2O_4$ powder was synthesized by the sol-gel technique. All chemicals were of analytical grade and were used without further purification. The stoichiometric molar amounts of Ferric nitrate $[Fe(NO_3)_3.9H_2O]$, Magnesium nitrate $[Mg(NO_3)_2.6H_2O]$, Zinc nitrate $[Zn(NO_3)_2.6H_2O]$ and Citric acid $[C_6H_8O_7.H_2O]$ were weighed separately with a ratio 0.5M:0.25M:0.5M. These reagents were mixed with distilled water and volume made up to 100 ml. The solution mixture was stirred and heated at 60^oC for 3 h and followed by 80^oC, until the mixture changed to gel form. The gel was then dried in an oven at 100^oC for 24 h. The obtained powder was then calcined in a muffle furnace at 700^oC for 2 h to improve the crystallinity of the prepared material. Finally, brown color powder was obtained. Taken solid phase sample was grinded in a mortar to make it powder for further analysis.

The phase confirmation was determined using XRD (Bruker, AXD D8-Discover using Cu Kα radiation with an accelerating voltage 40 kV). FT-IR image was recorded using 3000 Hyperion Microscope with Vertex 80 (Bruker, Germany) to provide information about the structural coordination in the powder sample. The TEM image was recorded using CM 200 (Philips) with an accelerating voltage of 20-200 kV.

Appropriate quantity of mixture of organic solvents such as butyl cellulose, butyl carbitol acetate and turpineol was added to the mixture of $Mg_{0.5}Zn_{0.5}Fe_2O_4$ and a solution of ethyl cellulose (a temporary binder). The mixture was then ground to form paste. The paste obtained was screen printed onto a glass substrate in desired patterns. The thick films so prepared were fired at 500°C for 1 h. Surface morphology of thick film was observed by using SEM (JSM-7600F microscope) with an accelerating voltage of 0.1 to 30 kV.

3. Result and discussions

3.1 XRD analysis

The X-ray diffraction pattern of $Mg_{0.5}Zn_{0.5}Fe_2O_4$ calcinated at 700^oC for 2 h was exhibited in Fig. 1. Main peaks were found at 2θ values = 29.90^o, 35.21^o, 56.58^o, 62.14^o and 73.48^o which were identified as corresponding to Miller index (220), (311), (400), (511) and (440) respectively (JCPDS card no. 73-2211). The XRD peaks and their positions with the calculated lattice parameter confirm that all the compositions exhibit single-phase cubic spinel structure with Fd3m space group. No peaks from other phases are detected, indicating high purity of the products.

The average crystallite size (D) was calculated from XRD peaks broadening using the Debye-Scherrer approximation, which is defined as

$$D = \frac{K\lambda}{\beta\cos\theta} \quad (1)$$

where, D is the average crystallite size, k is a constant equal to 0.9, λ is the X-ray wavelength and β is the peak full width at half maximum (FWHM) and θ is the angle of diffraction.

However, the lattice constant of as-synthesized ferrite powder was a= 8.421A°. A similar linear variation of lattice constant with Zn content has been observed by El-Sayed [17] and Kakatkar et al. [18] for M–Zn ferrites with M = Ni, Co, Cu, Mg. The average crystallite size was determined from the XRD powder pattern using Debye–Scherrer formula and was found to be 30 nm.
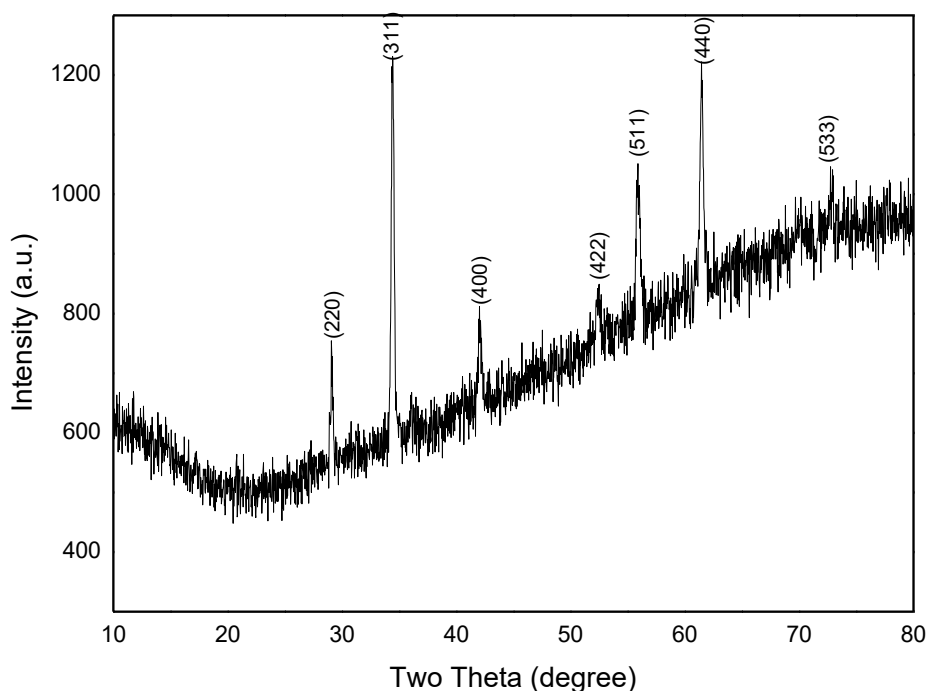
Fig. 1. XRD pattern of Mg$_{0.5}$Zn$_{0.5}$Fe$_2$O$_4$ calcined at 700°C.

3.2 FT-IR analysis

FT-IR spectrum of Mg$_{0.5}$Zn$_{0.5}$Fe$_2$O$_4$ nanoparticle was presented in Fig. 2. Vibrations of ions in the crystal lattice were usually observed in the range of 4000 - 400 cm^{-1} in IR analysis. Two main broad metal-oxygen bands were seen in the IR spectra relative to spinel ferrite compounds. Infrared spectrum shown in Fig. 2 had two absorption bands near about 400 cm^{-1} and 600 cm^{-1} for octahedral and tetrahedral sites

540

respectively. Waldron [19] attributed the higher absorption band position (600 cm^{-1}) to the intrinsic stretching vibrations of tetrahedral complexes and the lower absorption band position (400 cm^{-1}) to octahedral-metal stretching because of the difference in Fe^{3+}– O^{2-} distances for the octahedral and tetrahedral sites respectively. The Mg^{2+} ions occupy mainly the octahedral sites but fraction of these ions may be migrated into tetrahedral sites. This would explain the existence of a weak shoulder in the range of 690 –710 cm^{-1}. This confirms that the Mg ferrite has a partially inverse spinel structure.
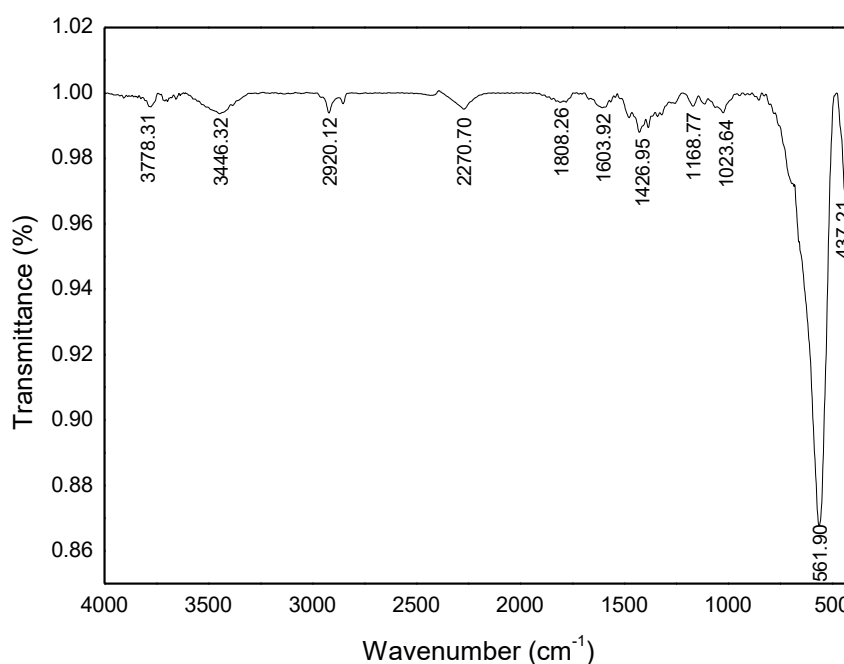
Fig. 2. FTIR spectrum of nanocrystalline Mg$_{0.5}$Zn$_{0.5}$Fe$_2$O$_4$.

3.3 TEM analysis

The size and morphology of the obtained Mg$_{0.5}$Zn$_{0.5}$Fe$_2$O$_4$ nanocrystal was characterized by TEM observation. Fig. 3(a) shows TEM image of Mg$_{0.5}$Zn$_{0.5}$Fe$_2$O$_4$ nanoparticle. The corresponding SAED pattern is shown in Fig. 3(b). As can be seen from Fig. 3(a) and (b), the prepared product consists of small sized nanocrystals with irregular shapes. It appears that a higher temperature reaction favors a particle with larger grain sizes, because a higher temperature enhanced the atomic mobility and caused the grain growth to result in a better crystallinity. As it can be seen that the result estimated from TEM micrograph was in good accordance with the XRD

analysis. The selected area aperture used in this study sufficed to reveal all the corresponding bright rings of the spinel structure. It was observed that the spot type pattern which is indicative of the presence of single crystallite particles and no evidence was found for more than one pattern, suggesting the singlephase nature of the material.
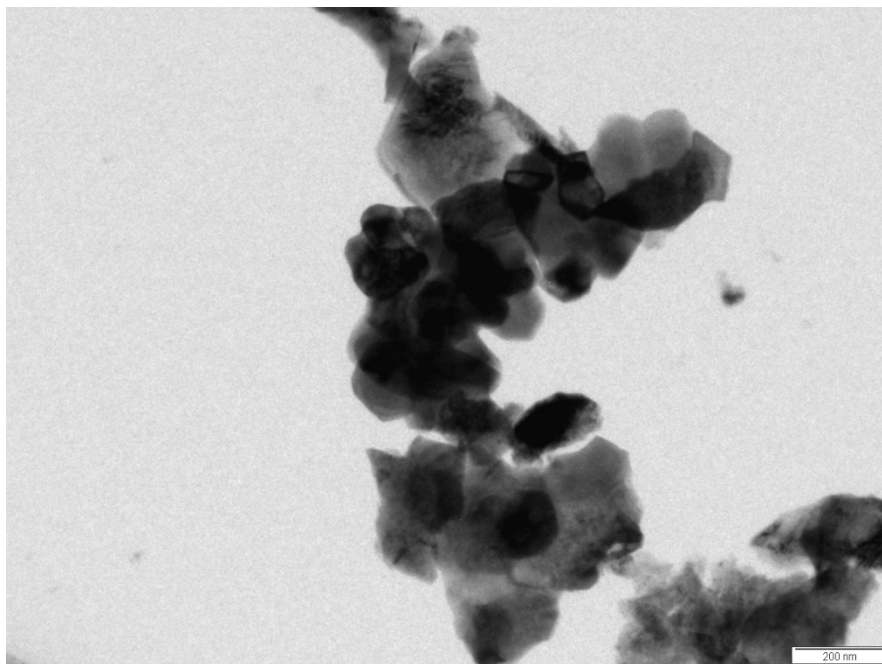

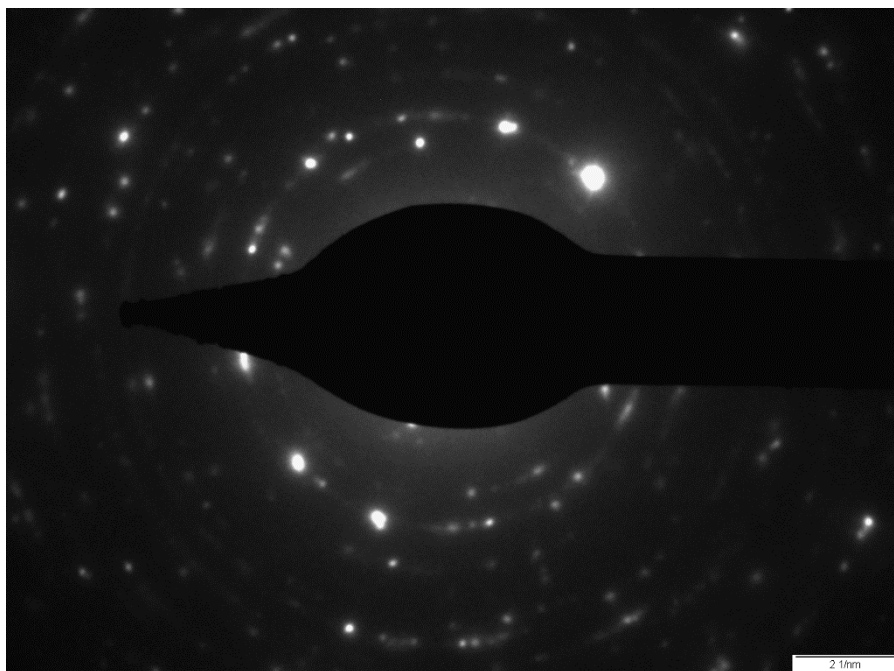**Fig. 3(a). TEM image of nanocrystalline Mg$_{0.5}$Zn$_{0.5}$Fe$_2$O$_4$.**

Fig. 3(b). SAED micrograph of nanocrystalline Mg$_{0.5}$Zn$_{0.5}$Fe$_2$O$_4$.

3.4 SEM analysis

SEM technique was employed for finding morphology of the thick film. Fig. 4 shows SEM image of the nanocrystalline spinel $Mg_{0.5}Zn_{0.5}Fe_2O_4$. The SEM technique was employed for finding morphology of the powder; it shows formation of the agglomerated particle. SEM image shows that the sample exhibit large grains structure having irregular morphology (polygons) with the presence of soft agglomerations.
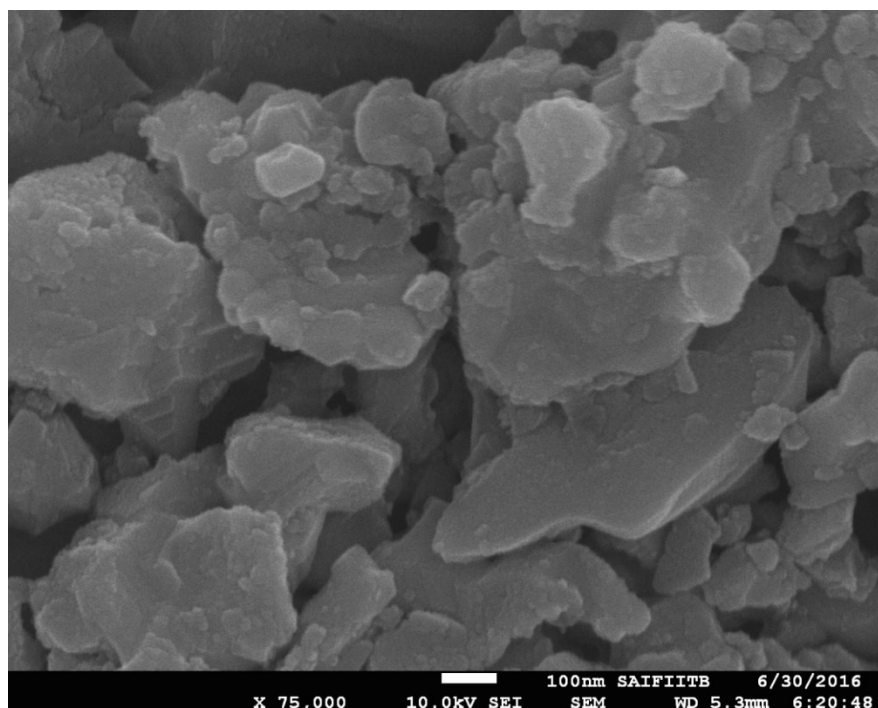
Fig. 4. SEM image of nanocrystalline $Mg_{0.5}Zn_{0.5}Fe_2O_4$.

3.5 Energy dispersion X-ray analysis

Energy dispersion X-ray analysis (EDX) was investigated the elemental composition of synthesized $Mg_{0.5}Zn_{0.5}Fe_2O_4$ thick film. EDX spectrum of the nanocrystalline $Mg_{0.5}Zn_{0.5}Fe_2O_4$ is as shown in Fig. 5. The EDX analysis exhibit the presence of Mg, Zn, Fe and O and EDX spectrum reveal almost the same ratio of Mg/Zn/Fe for the nanocrystalline $Mg_{0.5}Zn_{0.5}Fe_2O_4$ as they were actually added during synthesis process. Hence, confirms the purity of nanocrystalline $Mg_{0.5}Zn_{0.5}Fe_2O_4$.
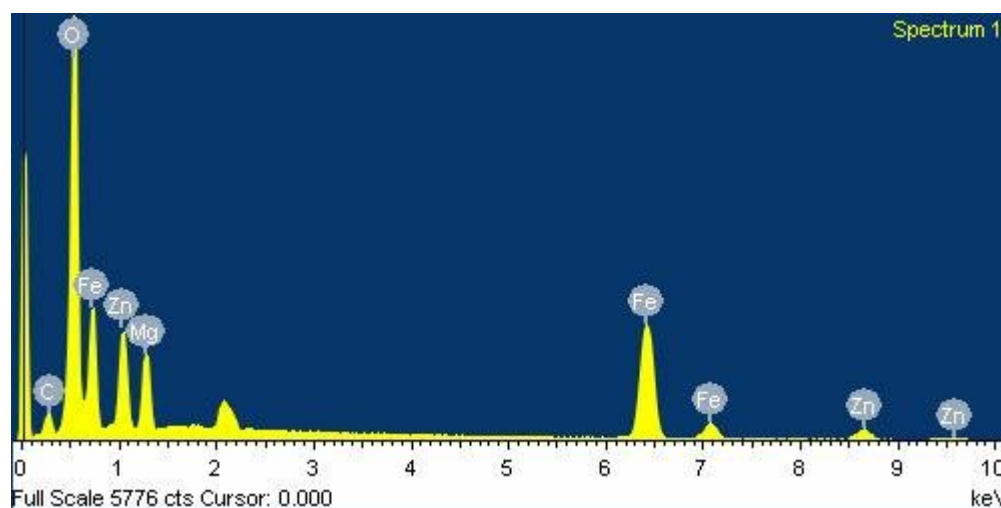
Fig. 5. EDX spectrum for nanocrystalline $Mg_{0.5}Zn_{0.5}Fe_2O_4$.

4. Conclusions

Zinc doped magnesium ferrite nanoparticles ($Mg_{0.5}Zn_{0.5}Fe_2O_4$) was prepared using less expensive, environment-friendly and low temperature sol-gel method using citric acid as anionic surfactant calcined at 700^oC. XRD pattern reveals that the synthesized ferrite consists of nano crystalline particle with average crystallite size 30 nm. The FT-IR spectrum exhibits main absorption bands around 561 cm^{-1} and 437 cm^{-1} corresponding to the vibration modes of the tetrahedral and octahedral sites respectively. The crystallite size from TEM analysis matches well with XRD results confirming the usefulness of sol-gel method for the synthesis of nanocrystalline $Mg_{0.5}Zn_{0.5}Fe_2O_4$. The morphological investigations from SEM showed the sample surface is fully covered by grains with irregular shape. The EDX confirmed the presence of Mg, Zn, Fe and O with values as per the initial precursor concentration.

Acknowledgements

References

[1] K. Raj, R. Moskowitz, J. Magn. Magn. Mater., 85 **(1990)** 233.

[2] A. Moser, K. Takano, D. T. Margulies, M. Albrecht, Y. Sonobe, Y. Ikeda, S. Sun, E. E. Fullerton, J. Phys. D: Appl. Phys., 35 **(2002)** R157.

[3] J. M. Bai, J. P. Wang, Appl. Phys. Lett., 87 **(2005)** 152502.

[4] R. C. Che, L. M. Peng, X. F. Duan, Q. Che, X. L. Liang, Adv. Mater., 16 **(2004)** 401.

[5] A. M. Duncan, H. D. Rouvaray, Microclusters, Sci. Am., 12 **(1989)** 110.

[6] A. Pradeep, P. Priyadharsini, G. Chandrasekaran., J. Magn. Mag. Mater., 320 **(2008)** 2779.

[7] Ü. Özgür, Y. Alivov, H. Morkoç, J. Mater. Sci.: Materials in Electronics, 1 **(2009)** 169.

[8] S. Komarneni, E. Fregeau, E. Breval, R. Roy, J. Am. Ceram. Soc., 71 **(1998)** C-26.

[9] Q. Chen, A. J. Rondinone, B. C. Chakoumakos, Z. J. Zhang, J. Magn. Magn. Mater., 194 **(1999)** 1.

[10] K. Suresh, N. R. S. Kumar, K. C. Patil, Adv. Mater., 3 **(1991)** 148.

[11] A. S. Albuquerque, J. D. Ardisson, W. A. A. Macedo, J. Magn. Magn. Mater., 192 **(1999)** 277.

[12] N. S. Gajbhiye, S. Prasad, G. Balaji, IEEE Trans. Magn., 35 **(1999)** 2155.

[13] H. F. Yu, A. M. Gadalla, J. Mater. Res., 11 **(1996)** 663.

[14] M. P. Pileni, N. Moumen, J. Phys. Chem., 100 **(1996)** 1867.

[15] C. Liu, B. Zou, A. J. Rondinone, Z. J. Zhang, J. Am. Chem. Soc., 122 **(2000)** 6263.

[16] B. B. Dora, S. Kumar, R. K. Kotnala, B. C. Raulo, M. C. Sahu, Int. J. Pharm Sci. Rev. Res., 30 **(2015)** 294.

[17] A. M. E1Sayed, Ceramic Inter., 28 **(2002)** 363.

[18] S. V. Kakatkar, S. S. Kakattkar, R. S. Patil, A. M. Sankpal, S. S. Suryavanshi, D. N. Bhosale, S. R. Sawant, Phy. Stat. Sol.(b), 198 **(1996)** 853.

[19] R. D.Waldron, Phys. Rev., 9 **(1955)** 1727.

An Overeview on Nanocrystalline perovskite (ABO₃): A potential material for solid state gas sensor and its applications

Dr. Manisha S. Pande [a*], Dr. V. D. Kapse [b],
Dr. P. M .Chandak[c], Dr. T. R. Tatte[d]

[a*] Department of Physics, Shri Sant Gajanan Maharaj College Of Engineering, Shegaon.
[b] Department of Physics, Arts, Science and Commerce College, Chikhaldara.
[c] Department of Physics, B.B. Arts,N.B.Commerce & P.Science College, Digras, Dist. Yavatmal.
[d] Department of Physics, Shri Dr. R. G. Rathod Arts & Science College,Murtizapur.

FULL PAPER

1. Introduction

In day today modern life detection of different gases play a vital role. The significant area of research towards gas sensing that leads to the fabrication of gas sensing devices which detect various harmful gases. Human body suffers from different diseases due to the emission of various toxic and hazardous gases. Solid-state sensors are among the most versatile of all sensors, as they detect a wide variety of gases, and can be used in many different applications. Among the unique attributes of the solid-state sensor are the abilities of the sensor to detect both low ppm levels of gases, as well as high combustible levels. Solid state gas sensors, are the excellent candidates to the fabrication of commercial gas sensors for a wide range of applications [1-5]. The development of high precision gas sensors is crucial for the monitoring of harmful (exhaust) gases in the environment. A variety of dangerous gases, such as CH_4, NO_2, LPG, NH_3, SO_2, CO, H_2S, NO_2, Acetone, H_2, ethanol, and methanol, are constantly released by industry, transportation, and agricultural activities. Many of these gases are hazardous to human health as well as the environment, even at levels measured in parts per million, or ppm. Some of these gases, like H_2, are naturally explosive when exposed to air.

In recent years, nanomaterials based on perovskite have been used in a variety of sustainable applications. Their structural properties enable researchers to investigate functionalities in a variety of directions, including solar cells, LEM devices, transistors and sensors, etc. Perovskite nano-materials have been shown to have

1078

remarkable sensing performance to a wide range of chemical and biological species, both in solids and solutions. In particular, they are able to detect small molecules (e.g., oxygen, nitrogen dioxide, carbon dioxide, etc.). In addition, Solid-state gas sensors are emerging as a viable substitute for the intended real-time functions in light of recent developments in the material sciences and advancements in processing and downsizing techniques. The greatest options for the development of commercial gas sensors for a broad range of such applications are solid state gas sensors, which are based on a variety of concepts and materials. [6-10].

2. Structure, Stability and Properties of Perovskites

Perovskite is the name given to the compounds that have the formula type ABX_3 with different sized 'A' and 'B' cations bonded to anion X [11]. ABO_3 Perovskites exhibit good thermal stability with an eV band gap of 3–4, which is why they were used in a lot of gas sensing studies [12]. Perovskite materials can be employed as sensors for gaseous species because their stability was significantly disrupted when exposed to gaseous environments, such as NO_2, CH_4, NH_3, C_2H_5OH, acetone, etc. [13]. The chemiresistive I–V, phosphorescence, and fluorescence responses of these perovskite materials can be used to record the sudden changes in them. However, in these sensing investigations, the opto-electronic characteristics of perovskites are crucial. Renowned contenders with remarkable attributes including electrical conductivity, ferroelectricity, superconductivity, catalytic activity, etc. are perovskite oxides. There are several ways to synthesis the naocrystalline perovskite material, including the hydrothermal, sol-gel, and chemical co-precipitation processes, etc. Because of the remarkable stability of the perovskite structure, structural flaws can be created when one or both of the cations in the A and B sites are partially substituted with other metals that have a different oxidation state.

3. Applications of Perovskite materials

The desirable characteristics of perovskites contributed to a significant development in research in recent years, indicating a genuine interest in the possible uses of these materials. They consist of, but are not confined to:

- Superconductivity

- Characteristics of catalysis

- The unique characteristics of optoelectronics.

Numerous companies are interested in using perovskites and are working to further the technology through research. Photovoltaics and optoelectronics are two companies that are particularly interested in perovskites:

1079

39

Solar energy

Since they are cheaper for production as well as greater flexible qualities than conventional silicon solar cells, perovskite materials present a possible substitute. Perovskite-based solar cells have demonstrated significant commercial promise in recent years, with their efficiency rising to above 25% in lab settings. The resilience and lifetime of these solar cells are presently being researched.

LED

LEDs have been around for many years, but the next generation of this technology will be offered by perovskite-based LEDs. Perovskite materials' optoelectronic qualities, which include their high photoluminescence quantum yield, tunability, and less expensive manufacture, have attracted the attention of numerous scientists and technological businesses.

4. Review of solid state gas sensor

Soil, water, and air pollution are the three categories into which environmental contamination falls. Of these three categories, air and water pollution are the main contributors to disasters since they spread quickly over a wide area in a short amount of time. Since industrial progress has dramatically expanded environmental pollution to such a level that public concern is now so great that it cannot be ignored any longer, environmental monitoring and management are absolutely necessary. Therefore, in order to address these environmental issues, thorough study has been done to quickly identify these contaminants and lower their levels to within the regulatory allowed concentrations. These factors have contributed to the advancement of solid-state gas sensor research and development in recent years. Gas sensors with metal oxides as the sensing medium have been widely used in gas detection applications. In fact, there is growing interest in gas sensing for nanocrystalline semiconducting metal oxides with regulated compositions, which also represent an intriguing new area of fundamental research [14]. Because of its oxide stability, high response, low production cost, and ability to respond to a wide spectrum of chemicals, semiconductor metal oxide nanostructures are the most preferred of all the solid state gas sensing materials. They respond quickly, are robust, dependable, and reasonably priced. Different types of solid state gas sensors are semiconductor gas sensor, optical gas sensor, electrochemical gas sensor, etc. Semiconductor gas sensors (SGS), known sometimes as chemoresistive gas sensors, are typically based on metal oxides (e.g. SnO_2, TiO_2, In_2O_3, WO_3, NiO, etc.). Recent applied research and product releases in this sector of gas sensors have revealed some noteworthy developments regarding the use of nanotechnologies and gas-sensing layers. In the sensing industry, optical gas sensors are crucial for measuring chemical and biological quantities. Changes in the absorption spectrum were used to measure the first optical chemical sensors. Chemical sensors and biosensors currently employ a wide range of optical techniques, such as

1080

40

ellipsometry, surface plasmon resonance (SPR), spectroscopy (luminescence, phosphorescence, fluorescence, Raman), interferometry (white light, modal, and optical waveguide structures), spectroscopy of guided modes in optical waveguide structures (grating coupler, resonant mirror), and interferometry (white light, phosphorescence, and fluorescence). Electrochemical gas sensors use an electrochemical cell, which is made up of two terminals (an anode and a cathode) of the same composition and a casing that holds a collection of chemical reactants (electrolytes or gels) in contact with the environment. A membrane on the top of the gas sensor enclosure allows the gas sample to pass through it. At the anode, oxidation happens, and at the cathode, reduction happens.

5. Conclusion

In this review study, the materials chosen for the construction of such gas sensors, and the sources of emission and regulatory standards of air pollutants are briefly reviewed. It has been addressed how advances in material science have led to the development of potential solid-state gas sensors, with the aim of comprehending the underlying technology and offering targeted functionality for a particular application. Perovskites are an extremely interesting and diverse class of materials which exhibit many useful characteristics that are determined by their composition. In the current research, we examine recent advancements in perovskite-based materials with excellent characteristics for application in optoelectronics and photovoltaics.

References

[1] P. T. Moseley, B. C. Tofield (eds.), Solid State Gas Sensors, Adam Hilger, Bristol and Philadelphia (1987).

[2] M. J. Madou, S. R. Morrison (eds.), Chemical Sensing with Solid State Devices, Academic Press, New York, 1989.

[3] A. Mandelis, C. Christofides (eds.), Physics, Chemistry and Technology of Solid State Gas Sensor Devices, Wiley (1993).

[4] P. T. Moseley, Meas. Sci. Technol. 8, 223 (1997).

[5] I. Lundström, Sensors and Actuators B 35-36, 11 (1996).

[6] P. T. Moseley, B. C. Tofield (eds.), Solid State Gas Sensors, Adam Hilger, Bristol and Philadelphia (1987).

[7] M. J. Madou, S. R. Morrison (eds.), Chemical Sensing with Solid State Devices, Academic Press, New York, 1989.

[8] A. Mandelis, C. Christofides (eds.), Physics, Chemistry and Technology of Solid State Gas Sensor Devices, Wiley (1993).

41

[9] P. T. Moseley, Meas. Sci. Technol. 8, 223 (1997).

[10] I. Lundström, Sensors and Actuators B 35-36, 11 (1996)

[11]. T.M., Fthenakis, V.M., Eds.; Academic Press: Cambridge, MA, USA, 2018; pp. 233–254.

[12]. Varignon, J.; Bibes, M.; Zunger, A. Origin of band gaps in 3d perovskite oxides. Nat. Commun. 2019, 10, 1658.

[13]. Zhu, Z.; Sun, Q.; Zhang, Z.; Dai, J.; Xing, G.; Li, S.; Huang, X.; Huang, W. Metal halide perovskites: Stability and sensing-ability. J. Mater. Chem. C **2018**, 6, 10121–10137.

[14]. N. Barsan, M. Schweizer-Berberich, W. Göpel, Fresenius J. Anal. Chem. 365, 287 (1999).

42

Chief Editor
Dr. Pavan Mandavkar
Principal, Indira Mahavidyalaya & Chairman, DBMRC
President, Sant Gadge Baba Amravati Vidyapeeth Marathi Pradhyapak Parishad, Amravati

Associate Editor
Dr. Veera Mandavkar
Director, Dr. Bhau Mandavkar Research Centre (DBMRC)

Index

दलित कवितेतील: नकार, विद्रोह आणि आत्मशोध

प्रा. डॉ. साजिद के. शाह

सहायक प्राध्यापक तथा मराठी विभाग प्रमुख,

श्री डॉ. आर. जी. राठोड कला व विज्ञान महाविद्यालय,

मूर्तिजापूर, जिल्हा- अकोला.

मो.न.९८५०३९४५७१, ८७८८६००८५६   Email: shahsajid7047@gmail.com

सारांश :-

दलित कविता १९६० नंतर उदयास आलेली असली तरी, तिची पाळेमुळे प्राचीन मराठी कवितेत दिसून येतात. याचा पहिला आविष्कार संत चोखामेळा यांच्या संतवाणीत आढळतो. जातिप्रथेचे, जातीहीनतेचे दुःख त्यांनी आपल्या रचनांमधून मांडले आहे. त्यांच्या रचनेत कोठेही आक्रस्ताळेपणा दिसत नाही. त्यांनी संयमित भाषेत आपले दुःख मांडलेले आहे. त्यानंतर महात्मा फुले यांचे दलित साहित्याला महत्त्वपूर्ण योगदान आहे. दलित साहित्य हा केवळ साहित्यातला एक प्रवाह राहिला नाही, तर समाजपरिवर्तनाची ही एक महत्त्वाची चळवळ ठरली. ही चळवळ आंबेडकरी विचारांनी दिलेल्या आत्मभानातून उभी राहिली. संपूर्ण दलित समाजाला या चळवळीने मोठी ताकद दिली, शब्द दिला. दलित कविता नकार, विद्रोह आणि आत्मशोध यावर आधारित आहे. " डॉ. बाबासाहेब आंबेडकर यांच्या व्यक्तिमत्वाचा, त्यांच्या कार्याचा, त्यांच्या विचारांचा परिणाम म्हणजे दलित साहित्य...'" दलित कविता, बाबासाहेब आंबेडकरांबद्दल कृतज्ञता व्यक्त करण्याबरोबरच त्यांच्या विचारांचा प्रचार-प्रसार करीत प्रवास करीत आलेली आहे. दलित साहित्य हा सामाजिक परिवर्तनाचा लढा आहे. माणसाला माणूस म्हणून अधिकार मागणारा हा संघर्ष आहे.

बीज शब्द:-	दलित साहित्य, स्वातंत्र्य, समता, बंधुता, नकार, विद्रोह, आत्मशोध इ.
उद्दिष्टे:-	दलित कवितेचे स्वरुप, नकार, विद्रोह, आत्मशोध इत्यादी समजून घेणे.
गृहितके:-	दलित कवितेतून दलित समाजाचा वास्तविक जीवनानुभव व्यक्त होतो. दलित कविता सामाजिक परिवर्तनाचा लढा आहे.
संशोधन आराखडा:-	प्रस्तुत शोधनिबंधासाठी द्वितीय तथ्य संकलन पद्धतीचा अवलंब करण्यात आला. त्यासाठी वर्णनात्मक विश्लेषण पद्धती वापरण्यात आली.
साहित्याचे पुनर्विलोकन:-	प्रस्तुत शोधनिबंधासाठी ग्रंथ, पुस्तके, दैनिक वृत्तपत्रे, मासिके, इंटरनेट इत्यादींचे पुनर्विलोकन करण्यात आले.

प्रस्तावना:-

' साहित्य' ही समग्र जीवनाला व्यापून टाकणारी अभिव्यक्ती आहे. जीवनासंबंधी एक मूल्ययुक्त दृष्टिकोण साहित्यात निर्माण होत असतो. साहित्यात मानवी जीवनाच्या वृत्ती-प्रवृत्तींचा आविष्कार होत असतो. साहित्य समग्र मानवी जीवनाला आविष्कृत करण्याचे प्रभावी माध्यम आहे. पृथ्वीतलावरील प्रत्येक मानवी समाज आपल्या भावभावना साहित्यातून व्यक्त करीत आलेला आहे. ज्याने जे भोगले, जे अनुभवले ते मौखिक व लिखित पद्धतीने व्यक्त झालेले आहे. भारतासारख्या विविधतेने नटलेल्या व विविध संस्कृतींचा समुच्चय असलेल्या, विविध समूहांचे प्रतिबिंब विविध भाषांमधून अभिव्यक्त होत आले आहे. त्यापैकीच मराठी भाषेतील साहित्य आहे. 'मराठी साहित्य' महाराष्ट्राच्या अस्मितेचा सर्वात महत्त्वपूर्ण घटक आहे. महाराष्ट्राच्या संस्कृतीला उज्वल ठेवणारा वारसा आहे. मराठी साहित्याच्या प्रवाहामधील 'दलित साहित्य' हा अविस्मरणीय साहित्यप्रवाह राहिलेला आहे. दलित साहित्याचा प्रवाह मराठीमध्ये १९६० च्या दशकात रूढ झाला. प्रस्थापित

45

साहित्यव्यवहाराला सर्वार्थाने छेद देणारा आणि दलित समाजाच्या सामाजिक दुःखाला अत्यंत सशक्तपणे मांडणाऱ्या या प्रवाहाने चाकोरीबद्ध अशा मराठी साहित्य विश्वात क्रांतिकारक बदल घडवून आणला. भारतरत्न डॉ. बाबासाहेब आंबेडकर यांच्या समग्र वैचारिक अधिष्ठानातून आकाराला आलेल्या या प्रवाहाने केवळ मराठीच नव्हे तर एकूणच हिंदुस्थानी साहित्यालाही एक नवे वळण दिले. हे वळण साहित्यक्षेत्रातील एखाद्या विशिष्ट वर्गातील पारंपरिक वर्चस्वाला छेद देणारे तर होतेच, पण त्याचबरोबर या प्रवाहाने संकेतबद्ध आणि संकुचित अशा वाड.मयीन सिद्धांताच्याही मर्यादा उघड केल्या. आक्रमक आणि जिवंत भाषेतून व्यक्त झालेल्या दलित साहित्याच्या अभिव्यक्तीने सामाजिक उद्वेगाला, अस्वस्थतेला समोर ठेवले. " व्यवस्थेविरुद्ध बंड झाले की, नवे संदर्भ, नवी मूल्य जीवनाला व त्याचबरोबर साहित्याला लाभत असतात. या बंडाची एक ऐतिहासिक कामगिरी दलित साहित्याने वा आंबेडकरी साहित्याने केली आहे."² असे अविनाश डोळस यांनी आपले मत व्यक्त केली आहे. ते यथार्थ वाटते.

जातीधर्मांच्या अहंकारात अडकलेल्या उच्चवर्णीयांना वास्तवाची जाणीव करून देत स्वातंत्र्य, समता व बंधुभाव या तत्त्वत्रयीचा आग्रह धरून नवसमाजनिर्मितीची आस बाळगणाऱ्या या प्रवाहाने मराठी साहित्याला कल्पकतेच्या कलावादी दालनातून बाहेर काढले. वैचारिकदृष्ट्या दूषित असलेल्या धर्मग्रंथांची चिकित्सा केली. या सगळ्या साहित्य व्यवहाराच्या मागे अर्थातच ज्ञाननिष्ठा आहे ती डॉ. बाबासाहेब आंबेडकर यांची. " विषम व्यवस्था आणि त्याविरुद्धचे असमाधान यामुळे समाजमनात वेदना आणि विद्रोहाने पेट घेतला. याचे स्वरूप म्हणजे स्वातंत्र्योत्तर काळातील वाड.मयीन प्रवाह होत."³ यातीलच एक प्रवाह म्हणजे दलित साहित्य आहे.

नकार, विद्रोह आणि आत्मशोध :-

दलित साहित्यात स्वातंत्र्य, समता आणि बंधुता या तत्त्वविचारातून विद्रोहाचा आविष्कार झाला. हा विद्रोह सामाजिक प्रतिष्ठेसाठी तर आहेच आहे, पण त्याचबरोबर परिवर्तनासाठीही महत्त्वाचा ठरला. " दलित साहित्य हे केवळ सौंदर्याच्या कुंजात रमणारे साहित्य नाही. त्यातील नकार, विद्रोह ह्यांच्या स्फोटक जाणिवांमुळे ज्वालाग्राही बनलेले आहे. ही ज्वालाग्राही जाणीव सर्वकष क्रांतीचे स्वप्न पाहणारी आहे."⁴ आत्मकथन, कविता आणि नाटकांनी दलित साहित्याला एक वेगळी ओळख दिली. कथा, कादंबऱ्या आणि समीक्षेनेही लक्ष वेधून घेतले. नवनिर्मितीचे असे आविष्कार खूप टोकदारपणे उमटत राहिले, परिणामी साठ-सत्तर ते नव्वदपर्यंतचा काळ हा दलित साहित्याच्या विद्रोहाने भारावलेला दिसतो. " कथा, कादंबऱ्यांहून कवितेची परिणामकारकता अधिक तीव्र असते."⁵ असे मत वसंत आबाजी डहाके यांनी व्यक्त केले आहे. याला दलित कविता अपवाद नाही.

दलित कवितेमधून व्यक्त झालेली अभिव्यक्ती सहज व तितकीच प्रखर होती. अशी जी अभिव्यक्ती झाली ती मराठी साहित्यासाठी सर्वार्थाने नवी होती. शतकानुशतके सामाजिक, आर्थिक परिस्थितीने जी अमानुष अवहेलना या समाजाच्या वाट्याला आलेली होती, या अमानुषतेविषयीचा एक स्वाभाविक प्रक्षोभ होता. नकार आणि विद्रोहातून आकाराला आलेला हा प्रक्षोभच दलित साहित्याचे वैशिष्ट्य ठरले.

जीवनवादी समाजाभिमुखता हे एक वैशिष्ट्य सांगता येईल आणि याचे मुख्य कारण म्हणजे सामाजिक चळवळी आणि साहित्य यांच्यातल्या एकत्वामुळे या प्रवाहाने अत्यंत सामर्थ्याने आपल्या जगण्याचे किंवा दलितत्वाचे दर्शन घडवले असे म्हणता येते. स्वातंत्र्योत्तर काळाच्या दोनेक दशकांनंतर जे सामाजिक परिवर्तनाचे पडसाद महाराष्ट्रात उमटायला लागले त्यामागे दलित साहित्यातील विद्रोह हा विशेष कारणीभूत ठरला. " दलित साहित्याच्या चळवळीची जाणीव मूल्यगर्भ जाणीव आहे. ती बाह्यजीवनातील व मनोजीवनातील विसंगतीचा प्रत्यय आणून देणारी आहे." ६ हा विद्रोह सामाजिक विधायकतेसाठी होता, आत्मसन्मानासाठी होता आणि सर्वात महत्त्वाचे म्हणजे नव्या युगजाणिवांचा होता. साहित्याच्या सर्वच प्रकारातून हा विद्रोह प्रकटला. विशेषतः कवितेतील अभिव्यक्ती अधिक टोकदार होती. मुळात हा विद्रोह व्यक्त करण्याची गरज दलित साहित्यिकांना का वाटली? याचा विचार करणे गरजेचे वाटते. निर्मिती कोणतीही असो, त्या निर्मितीच्या मुळाशी एक विशिष्ट प्रकारची मूल्यव्यवस्था असते. ही मूल्यव्यवस्था

46

समाजनियंत्रण करत असते. असे नियंत्रण मग समाजातल्या विविध संस्थांवर येऊ लागले की माणसाच्या स्वाभाविक जगण्यावर, त्याच्या नैसर्गिक हक्क आणि अधिकारावरही निर्बंध लादले जाऊ लागतात. असे घडू लागले की, 'विद्रोह' अपरिहार्य ठरतो. या विद्रोहातच संघर्षाची बीजे दडलेली असतात. फुले-शाहू-आंबेडकर यांच्या विचारांचा प्रभाव दलित जीवनावर व साहित्यावर पडलेला आहे. डॉ. बाबासाहेब आंबेडकर यांचे विचार आणि नेतृत्वामुळे एकूणच दलित समाजामध्ये आत्मभानाची जाणीव निर्माण झाली.

डॉ. आंबेडकरांनी दलित साहित्यिकांना आवाहन केले होते. याचा निर्देश करणे गरजेचे वाटते. ते म्हणाले होते, " मला साहित्यकारांना आवर्जून सांगायचे आहे की, उदात्त जीवनमूल्ये आपल्या साहित्यप्रकारातून आविष्कृत करा. आपले लक्ष आकुंचित, मर्यादित ठेवू नका. ते विशाल बनवा. आपली वाणी चार भिंतीपुरती राखू नका, तिचा विस्तार होऊ द्या. आपली लेखनी आपल्या प्रश्नापुरती बंदिस्त करु नका. तिचं तेज खेड्यापाड्यातील गडद अंधार दूर होईल असं प्रवर्तित करा. आपल्या देशात उपेक्षितांचं, दलितांचं, दुःखितांचं फार मोठं जग आहे, हे विसरु नका. त्यांचं दुःख, त्यांची व्यथा समजून घ्या आणि आपल्या साहित्याद्वारे त्यांचे जीवन उन्नत करण्यास झटा, त्यातच खरी मानवता आहे."[७]   डॉ. आंबेडकरांच्या या भूमिकेमुळे एकूणच दलित साहित्याला एक मोठे पाठबळ मिळाले. त्याशिवाय त्यांच्या सर्व राजकीय चळवळीमुळे-मग ती चळवळ धर्मांतराची असो की अन्य कोणतीही, दलित साहित्याचे रूप प्रखर बनत गेले. जुन्या जीवनमूल्यांशी केवळ वरवरचा संघर्षच केला नाही, तर या मूल्यांना नाकारण्याचीच भूमिका व्यक्त झाली. दलित साहित्यातील विद्रोह त्या अर्थाने खूप महत्त्वाचा आहे. नामवंत समीक्षक भालचंद्र फडके यांनी विद्रोहाचे केलेले विश्लेषण याद्ष्टीने पाहण्यासारखे आहे. दलित लेखकाला नवा माणूस अभिप्रेत असल्यामुळे त्याची भाषा विद्रोहाची आणि सम्यक क्रांतीची असल्याचे त्यांनी म्हटले आहे. विद्रोहाची भूमिका या लेखकांना का घ्यावी लागली, तर समाजव्यवस्थेने व्यक्तीविकासाला वाव दिला नव्हता. खरेतर महाराष्ट्रात अनेकदा या स्वरूपाचे विद्रोही स्वर उमटले होते, पण दलित साहित्यातला विद्रोह हा खूप वेगळा होता. फडक्यांनीच म्हटल्याप्रमाणे 'विद्रोह' हा मूल्यांच्या प्रतिष्ठापनेसाठी असतो. एक मूल्यसमूह नाकारुन नवा मूल्यसमूह अस्तित्वात यावा म्हणून विद्रोहाचा असतो. म्हणून मूल्यभाव नसेल तर विद्रोहाला काहीही अर्थ नसतो. याचाच अर्थ असा की, जिथे जिथे प्रतिगामी वृत्ती वाढत जाते, जिथे जिथे मानवतेची विटंबना होते; तिथे तिथे विद्रोह जन्माला येतो. दलित साहित्यातला हा विद्रोह 'स्वत्व' शोधासाठी आहे. 'गोलपिठा'त नामदेव ढसाळ म्हणतात,

"नंतर उरल्यासुरल्यांनी कुणालाही गुलाम करु नये.

लुटू नये, काळा गोरा म्हणू नये, तू ब्राह्मण, तू क्षत्रिय,

तू वैश्य, तू शुद्र असे हिणवू नये.

एक तीळ सर्वांनी कुरडून खावा, माणसावरच सूक्त रचावे, माणसाचेच गाणे गावे माणसाने."

तर यशवंत मनोहर 'भीमरावजी आंबेडकर' या कवितेत स्वातंत्र्यप्राप्तीनंतरही दलित, शोषितांवर होणारे अन्याय, अत्याचार पाहून म्हणतात,

"आमची लक्तरलेली आयुष्य शिवलीस, तो सुईदोरा कुठे ठेवलास?

अरे, या बेशरम अत्याचारांना फाडताना आम्ही विजयी होऊ, असे शस्त्रसाठे कुठे ठेवलेस?"

ज्योती लांजेवार आपल्या 'माया' कवितेत म्हणतात,

"देऊ केलेलं उष्टं अन्न स्वाभिमानानं नाकारताना

तू शिकून आंबेडकरावानी हो जो बापा."

दलित कविता डॉ. बाबासाहेब आंबेडकरांप्रती कृतज्ञता व्यक्त करणारी तर आहेच, पण त्याचबरोबर बाबासाहेबांचा संदेश घेऊन सामाजिक क्रांतीच्या लढ्यात रणशिंग फुंकणारी ही आहे. दलित कवितेला अधिक समर्थ करण्याचे काम बाबुराव बागुल यांनी केले. शोषित-पीडित माणूस त्यांच्या साहित्याचा केंद्रबिंदू होता. देश, देव, धर्म, संस्कृती यापेक्षा माणूस श्रेष्ठ आहे. माणसाचे महत्त्व आणि त्याचे मोठेपण व्यक्त करताना ते म्हणतात,

" वेदा आधी तू होतास

वेदाच्या परमेश्वरा आधी तू होतास

तूच सूर्याला सूर्य म्हटले

आणि सूर्य, सूर्य झाला

तूच चंद्राला चंद्र म्हटले

आणि चंद्र, चंद्र झाला

अवघ्या विश्वाचे नामकरण तू केलेस."

अशा व्यापक मानवतावादाच्या भुमिकेतून दलित जीवनाचे चित्रण यांच्या कवितेतून आलेले आहे. दलित साहित्याने सामान्यातल्या सामान्य माणसाला नायकत्व दिले. त्याला स्वाभिमानाने उभे केले. दलित कवितेतून दलित जीवनाचे अनेक पदर आविष्कृत झाले. भूक आणि अस्पृश्यतेसह विविध स्वरूपाच्या अन्याय आणि अत्याचाराची चर्चा पहिल्यांदाच दलित साहित्याने घडवून आणली. दलित साहित्य हे मुक्ती लढ्यातून उरलेले साहित्य आहे. यासंदर्भात फ.मुं. शिंदे म्हणतात, " मुक्तीलढ्यातून स्फुरलेले साहित्य किती अस्सल आहे, असतं हे दलित साहित्यात दिसून येते. विश्वात्मकता हा साहित्याचा धर्म मानला तरी दलित साहित्यातील विश्वात्मकता भारतीय साहित्यात सापडणार नाही."[८]

नामदेव ढसाळ, यशवंत मनोहर, राजा ढाले, अर्जुन डांगळे, दया पवार, वामन निंबाळकर, त्र्यंबक सपकाळे यांच्यासह अनेक कवींनी कवितेतून जी अभिव्यक्ती केली ती इथल्या संस्कृती आणि परंपरेच्या विरोधातील होती. " ज्या समाजव्यवस्थेने व ज्या विचारव्यवस्थेने आपले अस्तित्व नाकारले होते, आपल्याला नाकारले होते, आपली प्रतिमा विकृत करून ती प्रमाण मानली होती, ती नाकारने हा विद्रोहाचा आविष्कार आहे."[९] 'पंधरा ऑगस्ट एक संशयास्पद महाकाय भगोष्ट...' असे म्हणण्याचे धाडस या कवितेने केले. बंडाची ही एक अपरिहार्य ठिणगी होती. इतकी टोकदार अभिव्यक्ती मराठी कवितेने पूर्वी पाहिली नव्हती. एका मूक समूहाचा हा आक्रोश होता. हा विद्रोह अनेकांच्या पचनी पडण्यासारखा नव्हता हे खरे, पण तरीही प्रस्थापित मूल्यांचा निषेध करणाऱ्या या प्रवाहाचे जोरदार स्वागत झाले. कारण सामाजिक परिवर्तनासाठी आणि शोषणमुक्त समाजव्यवस्थेसाठी हा विद्रोह आवश्यकच होता. साठोत्तरी दलित कवितेतून व्यक्त झालेला हा विद्रोह अत्यंत प्रामाणिक आणि एका विशिष्ट भूमिकेतून आलेला होता. नामदेव ढसाळ ते प्रज्ञा पवार असा दलित कवितेचा जवळपास पाच दशकांचा प्रवास आपण पाहिला तर तो खूप वैशिष्ट्यपूर्ण असल्याचे दिसते. प्रत्येक दशकात या कवितेने नवे रूप धारण केले असले तरी 'विद्रोह' मात्र कायम राहिला आहे. आज खूप मोठ्या प्रमाणात कविता लिहिली जात आहे हे खरे, मात्र पूर्वसुरींचा प्रभाव टाळून व्यक्त होणारे कवी किती? असा प्रश्न आपल्यासमोर उपस्थित होतो. दलित साहित्यातील आत्मशोध महत्वाचा घटक आहे. "आत्मशोध म्हणजे लेखक आणि त्याच्या भोवतालचे वास्तव यामधील नातेसंबंध."[१०] अशी आत्मशोधाची व्याख्या दत्ता भगत यांनी केली आहे.

दलित लेखकांच्या पहिल्या दोन पिढ्यांनी अत्यंत सशक्तपणे लेखन केले. आज काळ बदलला आहे. शिक्षणासह सर्वच क्षेत्रात सामाजिकदृष्ट्या समानता आली असली तरी छुप्या स्वरूपात 'जात' अजूनही अस्तित्वात आहेच आणि जातीसह इतर प्रश्नही कायम आहेत. उलट आज सर्वच समाजात जातीय आणि धार्मिक अस्मिता अधिक टोकदार झाल्याचे चित्र आहे. अर्थात आता हे प्रश्न केवळ दलितांचेच आहेत असेही नाही. जागतिकीकरणोत्तर काळाने सर्वांपुढेच काही पेच निर्माण केले आहेत आणि त्याविषयीची प्रतिक्रिया उमटत आहे. मात्र जी ठळक ओळख साठ-सत्तरच्या दशकात दलित साहित्याने निर्माण केली होती ती मात्र आज काहीशी पुसट झाली आहे. बदलत्या काळाबरोबर विद्रोहाचे स्वरूपही बदलत आहे. कारण मुख्य प्रवाहाला आणि प्रस्थापित अभिरुचीला धक्का देण्याचे जे काम आधी झाले ते आज अपवादानेच होताना दिसते.

48

समारोप:-

मराठी साहित्यात महत्त्वाचा आणि स्वतंत्र प्रभाव टिकवून असलेला दलित साहित्य प्रवाह. फुले-आंबेडकरी विचारधारेने प्रेरित साठोतरी काळात साहित्य, समाज, संस्कृती, नकार, विद्रोह, आत्मभान, बांधिलकी या घटकांना कवेत घेत दलित कविता जोरकसपणे अवतरली. तिच्यातील मूल्याधिष्ठितेमुळे तिला एक वेगळे सौंदर्य प्राप्त झाले. साठोतरी काळात अवतरलेली फुले-शाहू-आंबेडकरी विचारधारेची ही कविता, तिच्या आगेमागेच कवितेतील प्रयोग आणि खेळ यालाच नवता आणि क्रांती मानणाऱ्या लघुअनियतकालिकांच्या चळवळीतून आकार घेत असलेल्या समाजविन्मुख, वाचकविन्मुख कवितेच्या पार्श्वभूमीवर, मराठी कवितेतील मुख्य प्रवाह ठरून, मराठी कवितेला समाजाभिमुख करण्यास पूरक ठरली. दलित वाङ्मयाचा उदय १९६० नंतर झाला. चीड आणि बंड ही चळवळीची दोन प्रमुख वैशिष्ट्ये होती; तर वेदना विद्रोह आणि नकार ही या साहित्यातील महत्त्वाची तत्त्वे होती. स्वातंत्र्य, समता, बंधुता, विज्ञाननिष्ठा, न्याय आणि लोकशाही ही मूल्य दलित साहित्याचा मूलाधार आहेत. उच्च जात व कनिष्ठ जात अशी विषमता असून 'दलितत्व' हे या विषमतेचे अपत्य आहे. दलितांवर या विषमतावादी समाजव्यवस्थेने पिढ्यांपिढ्या अन्याय केला. त्याला विरोध करण्यासाठी साहित्यकलेला दलितांनी त्यांच्याविरुद्ध लढण्याचे एक हत्यार बनविले आहे. त्यामुळे दलित लेखकांची जबाबदारी या विषमतेविरुद्ध लेखन करून लढा देणे ही आहे, असे हा साहित्यप्रवाह मानतो.

निष्कर्ष:-

१) दलित साहित्य १९६० नंतर निर्माण झालेला महत्वपूर्ण साहित्यप्रवाह आहे.

२) दलित कवितेवर शाहू-फुले-आंबेडकर विचारांचा प्रभाव आहे.

३) दलित कविता नकार, विद्रोह आणि आत्मशोध या त्रयीवर आधारित आहे.

४) दलित कविता स्वातंत्र्य-समता-बंधुता या मूल्यांचा पुरस्कार करणारी आहे.

५) दलित कवितेचे स्वरूप पारंपरिक कवितेपेक्षा पूर्णत: भिन्न आहे.

६) दलित कविता समष्टीचा आविष्कार आहे.

संदर्भग्रंथ सूची:-

१) कोतापल्ले नागनाथ, साहित्याचा अन्वयार्थ, पृष्ठ क्रमांक ५

२) डोळस अविनाश, आंबेडकरी विचार आणि साहित्य, पृष्ठ क्रमांक १८

३) लिंबाळे शरणकुमार, साठोतरी वाइ.मयातील प्रवाह, दिलीपराज प्रकाशन, पुणे. प्रथमावृत्ती २०९६, पृष्ठ क्रमांक ५

४) संपा. डॉ. कुंभार प्रकाश, दलित साहित्य: काही विचार काही दिशा. कैलाश पब्लिकेशन, औरंगाबाद. प्रथमावृत्ती २००२, पृष्ठ क्रमांक १६

५) डहाके वसंत बाबाजी, कवितेविषयी, स्वरूप प्रकाशन, औरंगाबाद. प्रथमावृत्ती १९९९, पृष्ठ क्रमांक २५१

६) मुक्तिबोध शरदचंद्र, दलित साहित्य एक अभ्यास, पृष्ठ क्रमांक १३४

७) डॉ.आंबेडकर बाबासाहेब, विदर्भ साहित्य संघ, नागपूर. १९५६ स्मरणिका पृष्ठ क्रमांक ८

८) शिंदे फ.मुं. संघर्षाचा धर्म, दलित साहित्य चर्चा व चिंतन- संपा. गंगाधर पानतावणे. पृष्ठ क्रमांक १६७

९) डॉ. पानतावणे गंगाधर, साहित्य प्रकृती आणि प्रवृती, पृष्ठ क्रमांक ४०

१०) भगत दता, दलित साहित्य, पृष्ठ क्रमांक ३९

❖❖❖

A STUDY OF FOOTBALL PLAYERS OF AKOLA CITY AND AKOLA DISTRICT ON THE LEVELS OF THEIRPHYSICAL FITNESS

Kapile V. V.[1]

[1]Director of Physical Education and Sports, Shri Dr. R.G. Arts and Science College Murtizapur, Akola (M.S)-INDIA.
E. Mail: kapile.vinod@rediffmail.com

ABSTRACT

The purpose of this study was to compare the physical fitness of Football players of Akola City and Akola District. The purpose of this study was to compare the rural and urban Football players and to find out which of these two categories is more physically fit in response to tests administered so as one can improve the standard and level of physical fitness in rural and urban Football players. A total of 100 Football players (Akola City 50, Akola District 50) were selected randomly from District Level Football competitions. The research was a descriptive comparative method. The criterion measures adopted for this study were muscular strength and Endurance, Flexibility and speed. The data collection tools used in the study was Sit Ups, sit & reach, 50 yard dash. Data of Physical Fitness Components between Akola city and District Football players was compared by using independent Sample t test. The level of significance was kept at 0.05 level of significant. The statistical analysis of physical components revealed that in the parameters such as sit-ups, sit and reach, and 50 m dash there was significant difference between Football players of Akola city and Akola district. The results also showed that all the physical fitness components the Muscular strength and Endurance, Flexibility and speed Akola district Football players were found to be better than Akola city Football players. Finally the researcher concluded that the Akola district Football players are more fitas compare to Akola city Football players.
Keywords: Physical fitness, Football players, Akola City & Akola District.

50

INTRODUCTION

Fitness concepts in elementary physical education centre on children's understanding of fitness as good health, and a working knowledge of activities that promote a healthy level of fitness. However, with increased leisure time, and changes in life styles wrought by the industrial revolution, which took a large proportion of the population away from farm life and into more urban areas, this definition is no longer considered comprehensive enough. The definition for physical fitness is now defined as the body's ability to function efficiently and effectively in work and leisure activities, not only at a set point in time, but at various ages and stages within a person's life cycle. The key is in finding optimum health within the limits of one's lifestyle, in order to be able to resist hypo kinetic diseases. General fitness implies the ability of a person to live most effectively with his/ her potentials, which depend upon the physical, mental, emotional, social and spiritual components of fitness which are highly interrelated. The purpose of this study was to compare the physical fitness of Football players of Akola City and Akola District. The purpose of this study was to compare the rural and urban Football players and to find out which of these two categories is more physically fit in response to tests administered so as one can improve the standard and level of physical fitness in rural and urban Football players.

DESIGN OF THE STUDY

A total of 100 Football players (Akola City 50, Akola District 50) were selected randomly from District Level Football competitions. The research was a descriptive comparative method. The criterion measures adopted for this study were muscular strength and Endurance, Flexibility and speed. The data collection tools used in the study were Sit Ups, sit & reach, 50 yard dash. Data of Physical Fitness Components between Akola city and District Football players was compared by using independent Sample t test. The level of significance was kept at 0.05 level of significant.

INDIA

TOGETHER WE REACH THE GOAL INDIA

UAE

GERMANY

51

Table No.1.1

Descriptive statistics of Sit-ups, Sit & reach and Speed between Football players of Akola city and Akola district

Variables	Akola City				Akola District			
	N	Mean	Standard Deviation	St. Error Mean	N	Mean	Standard Deviation	St. Error Mean
Sit-ups	50	25.22	4.42	0.62	50	29.54	7.08	1.00
Sit & reach	50	15.65	4.93	0.69	50	20.91	3.97	0.56
Speed	50	8.461	0.93	0.36	50	8.17	0.43	0.45

Table No.1.2

Independent sample't' test of Sit-ups, Sit & reach and speed

Physical fitness variables	't' value	Df	Sig. (2-tailed)	Mean Difference	Std. Error Difference
Sit-ups	3.659	98	0.001	4.32000	1.18063
Sit & reach	5.873	98	0.001	5.26000	0.89556
speed	1.987	98	0.049	0.28960	0.89556

DISCUSSION AND FINDINGS

The statistical analysis of physical components revealed that in the parameters such as sit-ups, sit and reach and 50 m dash there was significant difference between Football players of Akola city and Akola district. The results of descriptive statistics have indicated that the subjects mean scores in sit-ups, sit and reach and speed in case of Akola city Football players were found (25.2200 ± 4.42299, 15.6500 ± 4.93245, 8.461 ± 0.93respectively while in case of Akola District Football Players the mean scores in sit-

ups, sit and reach and speed were found (29.5400 $\pm$ 7.08033, 20.9100 $\pm$ 3.97144, 8.17$\pm$0.43) respectively.

CONCLUSION

In the present the results also showed that all the physical fitness components the Muscular strength and Endurance, Flexibility and speed Akola district Football players were found to be better than Akola city Football players. Finally the researcher concluded that the Akola district Football players were more fit as compare to Akola city Football players.

REFERENCES

1. Kansal, D. K. Textbook of of Applied Measurement Evaluation & sports selection. P.B
2. Berger and Paradis, John, Samuel (2010) Sports fitness & training, Rojet publication
3. New Delhi 110002(India), pp.1-2
4. ChoudhuriDipayan, choudhuri Soma, Kulkarni Vasant A. (2002). Physical fitness: A comparative study between students of residential (Sainik) and non-residential schools (aged 12-14 years). Indian journal of physiology and pharmacology, 96(3): 328-332
5. Patrick, C. R. (1975) The construction of motor a fitness test battery for girls in lower elementary grades." Dissertation Abstract international,33p.1250A.

INDIA

TOGETHER WE REACH THE GOAL   INDIA

UAE

GERMANY

Effect of Zinc Nitrate on Morphology and Particle Size of Nano-sized Zinc Oxide

V. S. Kalyamwar[1]*, S. D. Charpe[2], S. S. Kawar[3], R. B. Pedhekar[4] P.D. Shirbhate[5]

[1]* Department of Physics, Bharatiya Mahavidyalaya, Amravati, India

[2]Department of Physics, J. D. Patil Sangludkar Mahavidyalaya, Daryapur Dist. Amravati, India

[3] Department of Physics, Dr. R. G. Rathod Arts & Science College, Murtizapur Dist. Akola, India

[4]Mahatma Jyotiba Fule Commerce, Science & Vitthalrao Raut Arts College, Bhatkuli, Dist. Amravati, India.

[5] Department of Physics, Gopikabai Sitaram Gawande Mahavidyalaya, Umarkhed Dist. Yavatmal, India.

Abstract:

Zinc oxide nanostructures were synthesized by chemical route method. The XRD spectrum indicates that the sample is wurtezite (hexagonal) structured ZnO with lattice constants of a = 3.249A0, c = 5.206 A0. The crystallinity and structure of these ZnO nanostructures were studied by X-ray diffraction. The morphologies of these synthesized nanostructures were analyzed by transmission electron microscope. Effects of concentration of zinc nitrate during synthesis on the morphology and particle size of resultant product were investigated.

Keywords: Chemical route method, Zinc oxide

Introduction

Semiconductor nanostructures are a very important topic in the ongoing research activity across the world. As the semiconductor particles exhibit size dependent properties like scaling of the energy gas and corresponding change in the optical properties, they are considered as the front runners in the technologically important materials.

Zinc oxide is attracting tremendous attention due to its interesting properties like wide direct band gap of 3.37 eV at room temperatures and high exciton binding energy of 60 meV. Zinc oxide is promising materials for electronics or optoelectronics applications such as solar cells, gas sensors, liquid crystal displays, heat mirrors, surface acoustics wave devices etc [1-10].

A variety of techniques like spray pyrolysis, molecular beam epitaxy, chemical vapor deposition, hydrothermal method, pulsed laser deposition, sol-gel method, laser ablation [11-17] etc. have been widely used to synthesis ZnO nanostructures.

In the present study, ZnO nanostructures were synthesized by using chemical route method. The crystallinity and structure of these ZnO nanostructures were studied by X-ray diffraction. The morphologies of these synthesized nanostructures were analyzed by transmission electron microscope.

Experimental

All chemicals were of analytical grade and were used as purchased without further purification.

In typical process, 2.974 g Zn $(NO_3)_2 \cdot 6H_2O$ (Zinc nitrate hexahydrate) was dissolved in 100ml distilled water and 2.0 g of NaOH was dissolved in 100 ml distilled water. The zinc nitrate solution was added drop wise to the NaOH solution to form white solution. Then, white solution was subsequently kept at 75^0C For 12 hr. The

4835

Photodegration and Sensing Applicability of Synthesized of Polyaniline Sn-Nps Aloe Vera Biocomposites

R. E. Khadse[1], N. V. Rathod[2], M. S. More[2], D. B. Dupare *

1. Late Pundlikrao Gawali Arts and Science Mahavidyalaya Shirpur (Jain) Di-Washim

2. Department of Chemistry, R. A. Arts, Shri. M. K. Commerce and Shri. S. R. Rathi Science

   College Washim

3. Department of Chemistry, Shri R.G. Rathod Arts and Science College, Murtizapur,

 Di.Akola.

 *Corresponding Author:

 Dr. D. B. Dupare
Associate Professor
Department of Chemistry,
Shri R.G. Rathod Arts and Science College,
 Murtizapur, Di.Akola.

Abstract: The Greenway synthesis has proved more advantageous in creating Sn-NPs networks with demanding features for diverse applications than the standard chemical synthesis route because it is time-consuming, requires huge quantities of chemicals, and is poisonous. In this study, we synthesized Polyaniline-Sn-Nps biocomposites from Aloe Vera extract. The plant extracts of the Aloe Vera plant contain a number of phytochemicals that are employed as reducing and capping agents for Sn metal salt in the green synthesis process. It is environmentally beneficial for the production of polyaniline biocomposites. The produced thin film was dissolved in DMSO solvent for UV, FTIR, and XRD analysis, and the thin uniform morphology was studied using electron microscopy and scanning electron microscopy. The electrochemical conductivity of the synthesized films, as well as I-V characterization for voltage variations ranging from 0.5v to 12v, were investigated utilizing four probe instrumentation approaches. The synthesized film of PANI-SnNps Biocomposites was suitable for photocatalytic and ammonia gas sensing applications.

 Keywords: *Polyaniline, Aloe Vera, Sn-NPs,Green synthesis and Biocomposites*.

1. Introduction:

Green synthesis and sustainable research have emerged unexpectedly in the contemporary period as a result of the numerous applications of scientific research, medical science, catalysis, and optical, magnetic, and digital technologies. Green chemistry synthesis has been significantly kept because of its easy manufacturing method, ecologically friendly, reusable, cheap cost, and smooth isolation and separation [1-2]. The Pani is conductive, has extra stability, and $SnCl_4$ is selective and sensitive to ultraviolet light radiation due to the huge band gap (3.6eV), with the significantly greater electron-hole recombination, which is useful to employ for many purposes [3-4]. Sn-metal dopant has several oxidation states; Sn-doped has proven to be powerful [5]. Tin tetrachloride is employed as both a catalyst and a polymer stabilizer. It is widely used in the fabrication of SnO_2 coating for toughening glass in glass enhancement and manufacture [6]. Tin metal has been utilized as a catalyst, as well as in electroplating, textile dyeing, and printing. It is currently utilized as a reducing agent in metallurgical operations. The green synthesis approach for MNPs is simple because to their molecular armament and vast amounts of the key bioreactors and molecule suppliers for synthesis. Numerous metabolites found in plant leaves act as reducing agents, allowing nanoparticles to be synthesized. Aloe vera is a cactus-like plant that contains ninety percent water. The ultimate solid fabric has about 75 active substances, including water, lipids, soluble vitamins, minerals, enzymes, polysaccharides, and phenolic compounds [7-8]. The Plant extract was utilized in the manufacture of NPs, due to its cheap and secure to the environmentdue to the increasing reputation and popularity of organic capping agents [9].

In this study, Sn-doped PANI-SnNPs Aleovera plant extract biocomposites were designed with an optimal stoichiometric composition using a green synthesis strategy. The plant extract anticipated that the polysaccharide in the interior gel would reduce and stabilize SnNPs. The creation and unification of PANI-SnNPs hybrid biocomposites were investigated using UV, FTIR, XRD, and scanning electron microscopy structures. PANI-Sn NPs composites were used to investigate the photocatalytic degradation characteristics of methylene blue. Its thin film is used in studies on I-V characterisation. It is also employed for ammonia gas sensing characteristics, which were examined with this compound using four probe instrumentation approaches.

2. Materials and method

All the chemicals were of analytical grade and purchased from Merck (India), Quligen chem. Tin tetra chloride used as the precursor was purchased from Quligen chem. Aniline is 99%

pure and double distilled prior to use. The Aniline (AR grade) was purified and stored in a refrigerator prior to use. Ammonium peroxidisulphate (APS) oxidant was used.   The de-ionized water was employed for preparing all the solutions and reagents. The Aleovera leaves were collected locally from the botanical garden of college, at Murtizapur, Di Akola.

2.1. Preparation of aloe vera plant extract

The Aleovera extract was prepared by finely cutting the aloe vera leaf and removing the hard cover coat of leaf, then the inner gel-like semisolid material collected was grinded it mortal and pestle, then kept in ultra sonicator for 20 to 30 minutes to obtained uniform liquid gel near about 10gm was mixed with 50 mL of distilled water (1:5) and stirred at room temperature for 10 min. The mixture was cooled and filtered using vacuum filtration. Finally, the extract is stored in a refrigerator10 ^{0}C for further use.

2.2 Biosynthesis of SnNPs using aloe vera extract

To synthesize the Sn nanoparticles, dissolve 1.0 N of Stannous tetra Chloride (SnCl$_4$) in 100 ml of deionized water. The optimized stoichiometric ratio of stannous chloride in variable 1-10ml solution   in 50 ml beakers and added leaf extract drop wise under constant stirring to achieve 7PH in solution. The mixture was subjected to stirring for 1–2 hours continuously in an ultrasonicator. The optimized composition SnNPs formed during this processis collected and centrifugation (2,000 rpm) ultra -centrifuge instruments and after centrifugation the sample is collected and washes it with deionized water repeatedly washed to remove the by-product. The nanoparticles were dried at 110°C in a microwave oven for 30 minutes for calcination at 150°C for one hour because we needed a secondary polysaccharide binder and stabilizer.

2.3. Synthesis of Biocomposites of PANI- SnNPs

The PANI- SnNPs composites were prepared by optimized concentration of 10 ml aniline 0.1.,0.2.,0.3., 0.4.,0.5.,0.6.,0.7.,0.8.,0.9.and 1M with 1M hydrochloric solution in 50 ml of beaker we add 0.1,0.2.,0.3.0.4., and 0.5M SnNPs dopant then inserted glass substrate then oxides with 0.5M of APS then this beaker kept in Ultrasonicator for half an hour then beaker kept in refrigerator 24 hours. A thin glass films were formed to wash the films with tap water and dry it. The precipitate remained in a beaker washed with deionized water and the precipitate was collected for future chaterization techniques. Fig 2.1 shows the all experimental setup for synthesis of PANI-NPs Aleovera Biocomposites.
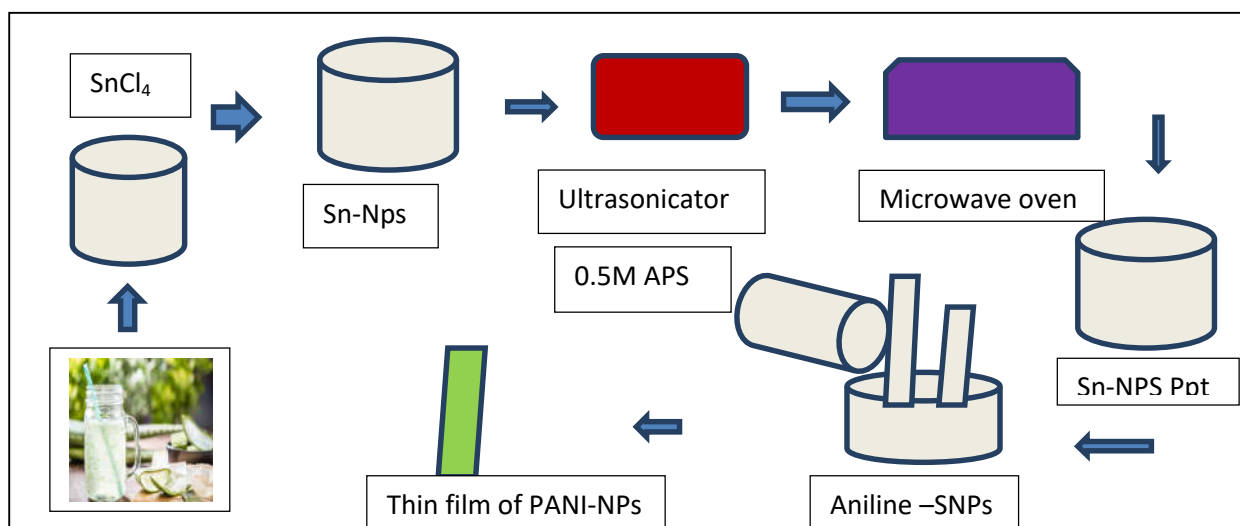
Fig 2.1Systematic synthesis of PANI-NPs Aleovera Biocomposites

2.4 Chaterization Technique:

These synthesized composites were characterized by U.V.-Visible spectroscopy recorded on UV- VIS Spectrophotometer Carry Agilent Tech. The functional group stressing and bending were presented by FTIR Spectroscopy and IR spectra were recorded on Bunker Alpha-T FT IR Spectrometer. The Olympus electron microscope is used for thin surface morphology and observation of stability as well as granular or tubular sized nanoparticles of PANI/SnNPs /Aloe-Vera at the Department of Botany. XRD Spectroscopy carried out by determining was nanoparticle tin metal was present and Size of metal, the XRD Studied at Department of Physic Pune University. The conductivity and I-V characterization were carried out using four probe instruments. The photodegration chaterization carried out for energy storage application. The gas sensing applicablity that was observed was for indigenously computer control instrumentation at the department of physics at BAMU University.

3 Results and Discussion
3.1. UV-Visible absorption

The Synthesized composite of PANI-SnNPs was characterized by U.V. Visible spectroscopy recorded on UV- VIS Spectrophotometer, the PANI, PANI-Aleovera and PANI-SnNPs dissolved in DMSO solvent individual to observe the U.V. absorption peak as shown in fig 3.1.
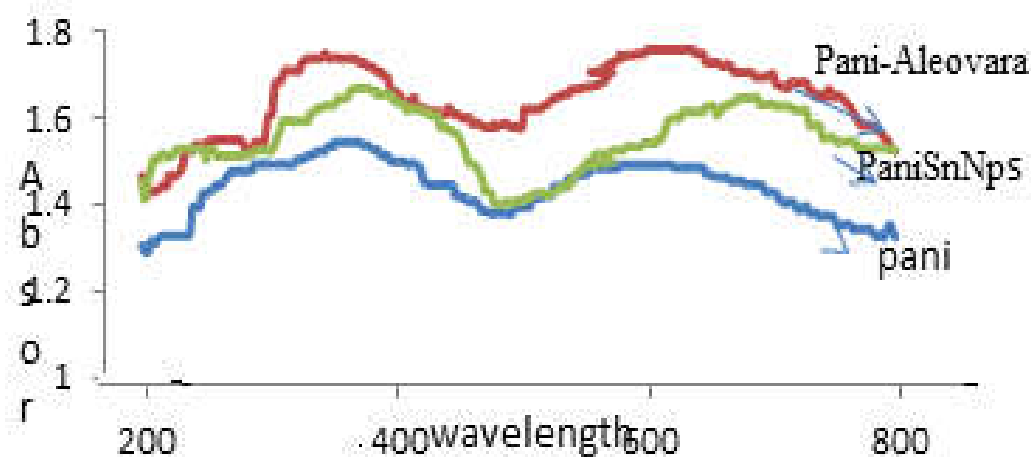
Fig 3.1. U.V-Visible absorption Synthesized films

Fig.3.1, could be the distinctive peak of polyaniline observed that the characteristic band. The band observed at 262-270 nm samples corresponds to the π-π* transition of Polyaniline films. The bands that appear at 334 nm are due to n-π* due to a lone pair on nitrogen in the Polyaniline ring, which is an inter charge transfer band associated with the benzenoid to quinoid ring. The transitions of 597 nm quinone-imine groups, together with the extending tail at 800nm. The conducting emeraldine salt (ES) phase in the polymer is identified.

  The PANI Aleovera plant extra biocomposites material shows absorption peaks at variable distinctive peaks that, at 282 – 312 nm at higher and broad range peaks due to Pani and bio-polyphenol transition peaks, the broad peak of Aleovera due to secondary metabolites are present 556 nm, 622 nm in nature at high absorption and quinoid ring tail at 712-799 nm .
The PANI-Sn NPs Biocomposites an intensive peak at 222-242nm then shifted to the polyaniline π-π* transition. The 382-422nm   peak absorbance in the shift spectrum and the broadness size, which they settle to mixed with polyaniline and Aleovera plant extract mixed with the required Sn - nanoparticles. The characteristic wavelength, at which the absorption coefficient is maximum, is observed to be around 495 nm. The values of the same are ~646 nm, and ~758 nm. The intensity of the absorption peak is related to the color concentration of the solution formation PANI-Sn-NPs.

3.2. FTIR Analysis

The Synthesized composite of PANI-SnNPs. was characterized by FTIR spectroscopy recorded on FTIR Spectrophotometer shown in fig 3. 2.
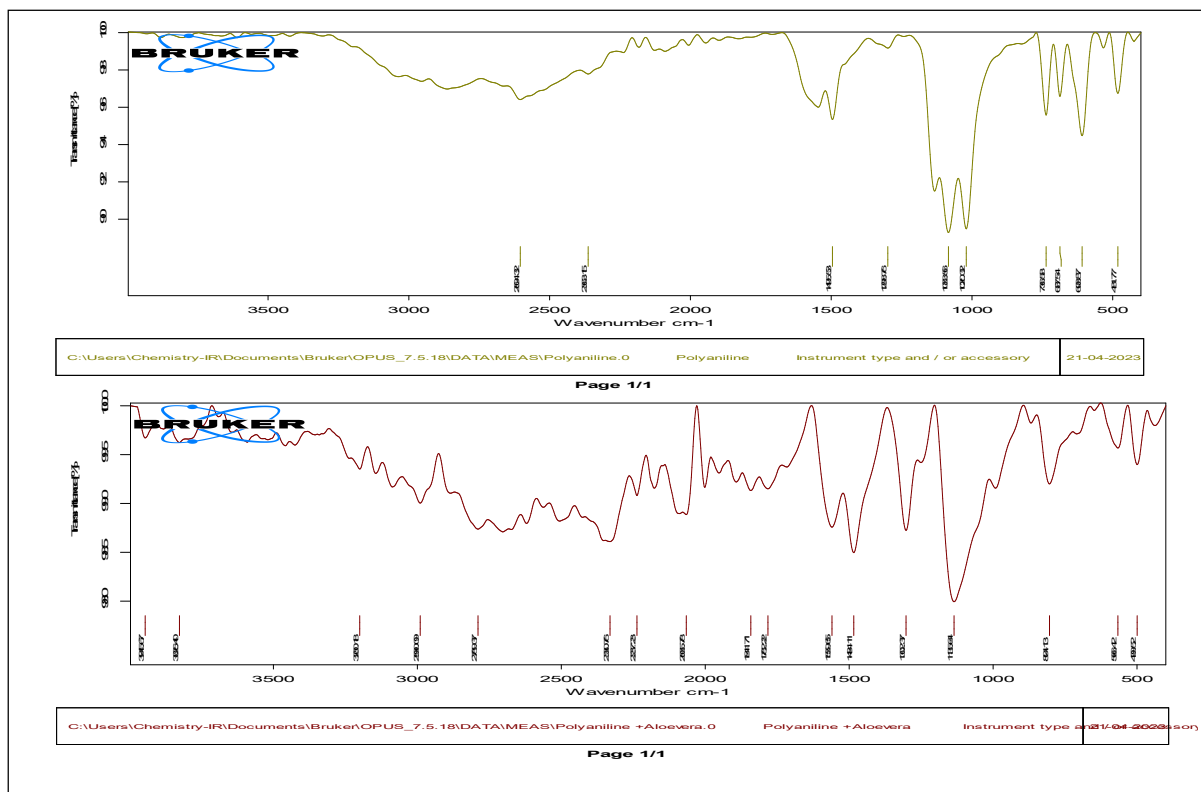

Fig 3.2.FTIR Synthesized biocomposites of PANI-SnNPs.

In Fig 3.2 the polyaniline spectra where the characteristic peaks are the broad peak at 3251 to 3310 cm^{-1} intense peak is attributable to the N–H stretching vibration, 2950 cm^{-1} is assigned to stretching vibration of the aromatic C-H bond. The two bands appearing at ~1525–1558 cm−1 and ~1437–1467 cm^{-1} correspond to the stretching vibration of quinoid and benzenoid rings, respectively. The peak at ~1296 cm^{-1} is attributed to the C–N= stretching vibration between benzenoid and quinoid units. The band at ~1246 cm^{-1} can be assigned to the π-electron delocalization induced in the polymer through protonation or C-N-C stretching vibration, while the peak at ~1246 cm^{-1} is due to the C-N^{+} stretching vibration in the polaron structure. The band at 1183–1161cm^{-1} is assigned to the plane bending vibration of C–H (modes of N=Q=N, Q=NH+–B. The peak at ~1105 cm^{-1} is attributed to the aromatic C-H bending in the plane. The second FTIR peak was observed between 3600 cm^{-1} to 3200 cm^{-1} due to the presence of aromatic Hydroxyl O-H Stretching and the peak appeared at 1657 cm^{-1} attributed to amino group and Poly alcoholic group present in Aleovera NPs Synthesis of PANI-Sn –Aleovera extract of Secondary metabolites. The instance peaks appeared at 1135

to 980 cm^{-1} due to the presence of tin metal composites in Pani-Sn –Aleovera Biocomposites. The result from FTIR analysis suggests that the biological molecules may have a double function in the SnO formation and stability in the medium. The FTIR study above peak or various instance peaks clear idea about formation Nano synthesis Biocomposites Pani-SnNPs -Aleovera.

3.3 XRD of PANI-SnNPs.

XRD analysis is used to identify the crystalline structure of the biosynthesized SnO$_2$ particle. The X-ray diffraction (XRD) patterns were recorded with a Bruker Advance diffractometer using CuKα (λ = 1.5418 Å) radiation in 2θ ranging from 200to 800 at a scanning rate of 0.02∘/s. The peak at 2θ ¼ 26.299, 34.580, 37.512, 41.324,46.572,56.342,62.223, 70.231,73.523, and 76.342, are assigned to the (110), (101), (111), (201), (211), (310), (0301), (0), (311), and (410) reflection lines the polycrystalline nature of the sample of SnO, which could be well- diffractions from the (110), (101) and (211) planes of the tetragonal rutile structure SnO, respectively. The calculated average crystallite size was 0.322 nm XRD patterns. The FWHM image clearly reveals the lattice planes with a d-spacing of about 0.34 nm, which corresponds to the (110) planes of SnO$_2$. Hence, the interplanar distances measured from the FWHM image agree well with the data obtained from the XRD pattern; the particles were quite small due to the biological synthesis adopted to prepare the NP. The XRD analysis confirms the SnO. The XRD peaks tubulate in table 2θ FWHM relative intensity and crystalline size, θ is the Bragg's angle, d-spacing represents the interplanar distance and (hkl) refers to the miller indices. The crystallite size was calculated by employing the well-knownScherrer formula as in-equation

$$D = (k\lambda / \beta cos\theta)$$

 where D stands for the mean crystallite size, K is a particle size dependent constant whose value is 0.9, β represents the full width at half of the peak maximum (FWHM) and θ is the Bragg's angle. The crystallite size was calculated to be approximately 33.83nm and 24.22nm.
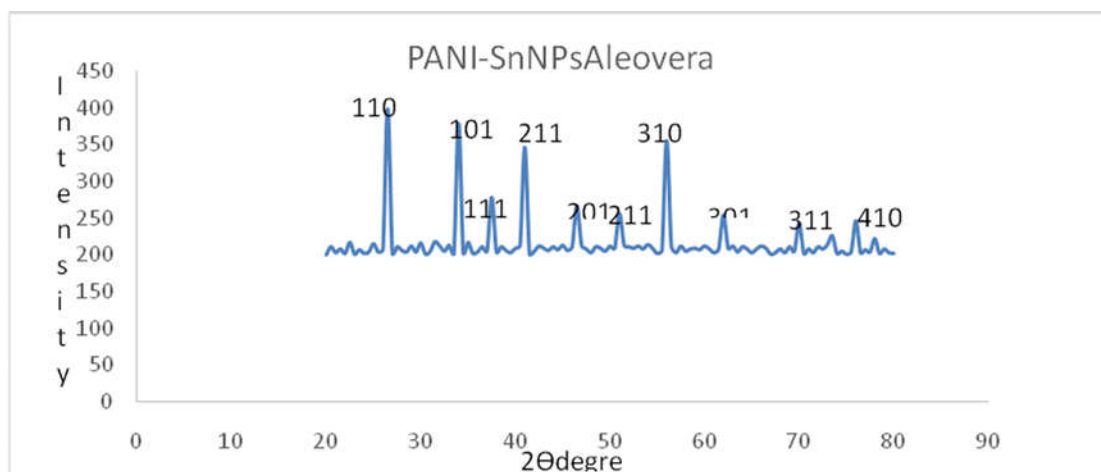
Fig 3.3.1. XRDof PANI-SnNPs. Spectra

Table 3.3.1 .It given the crystalline size of SnO_2 metal exists in Biocomposites having Nano sizeSynthesised.

Properties	Plane(hkl)	Method
2Θdgree	110	26.299,
	101	34.580,
	111	37.512,
FWHM(degree)	110	0.2523
	101	0.3312
	111	0.3617
D spacing nm	110	0.3443nm
	101	0.2697nm
	111	0.2423nm
Relative Intensity	110	398.12
	101	378.24
	111	278.37
Crystalline Size nm	110	33.83nm
	101	26.32nm
	111	24.24nm

3.4 **Morholpolgy of PANI-SnNPs.**

The PANI-SnNPs of Aloe-Vera composites were synthesized on a glass substrate and recorded the image of high-power Electron Microscopy instruments. The morphology of synthesized film is also observed under Scanning Electron microscopy. The morphology of Synthesised films showed that uniform film granular SnO_2 metal oxides biocomposites of PANI-SnNPs observed the sensing and current -voltage characteristics using four probe instruments. The dopant metal having 20-40 nm in average size granular size is shown in fig

3.4. The micrograph shows the presence of surface holes that correspond to the pores present in the material. These pores are responsible for the adsorption of the metal Fig. 3.4 These images revealed a porous and irregular surface (different heterogeneous surface structures) with deep pores such as granules and tubulars.
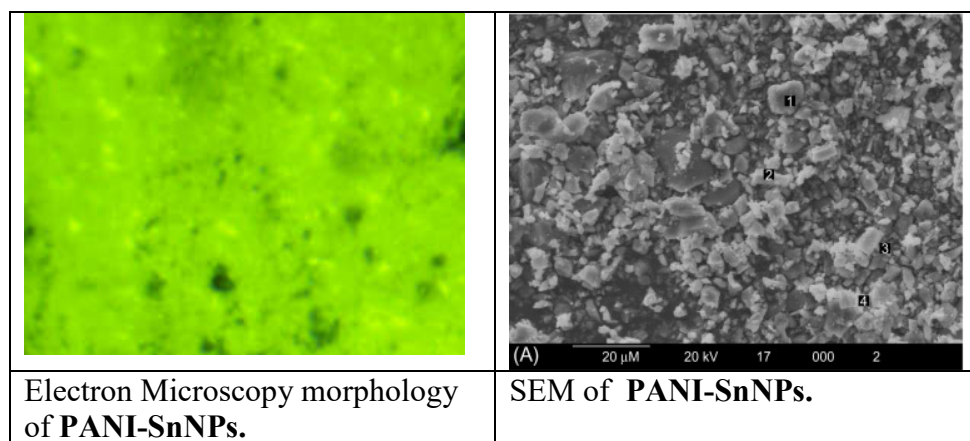

| Electron Microscopy morphology of **PANI-SnNPs**. | SEM of **PANI-SnNPs.** |

Fig 3.4.**Morholpolgy of PANI-SnNPs.**

3.5 Photocatalytic degradation of methylene blue of PANI-SnNPs.

The methylene blue is organic dye it can be degraded either oxidative or reductive degradation.The degradation of MB is not a consequence of a direct redox reaction between the conducting polymer and the dye molecules but results from the interaction of the dye molecules with radicals of metal free radicals. During photo-enhanced degradation, the electrons generated in the SnO_2, under the irradiation of visible light, would either recombine with the holes of the valence band or react with the adsorbed oxygen on the surface of Conducting composites. The activation of $SnO_2$of PANI-SnNPsby incident light (hυ) generates excitations (electron–hole pairs), which are powerful oxidizing and reducing agents, respectively (8). The photodegradation efficiency of the synthesized Pani-SnNPs, was observed, MB solutions were determined, by a UV–vis spectrophotometer at 10 min time interval and over a 150 minutesperiod. The Figures showed pronounced reduction with time in the absorption peaks of the MB solutions at 664 nm in the presence of the nanoparticles, due to an oxidative degradation process. The photocatalytic activity of Pani-SnNPs photocatalysts for MB photodegradation was calculated using the equation:

$$Degradation \% = \left(\frac{A_c - A_t}{A_c}\right) * 100$$

where Ac is the initial solution of dye concentration and At is the final solution of dye concentration after treating with the photocatalyst. The photocatalytic degradation activity is enhanced by the doped Sn, in comparison, the efficiency of Sn metal doped than non-metal doped polyaniline.
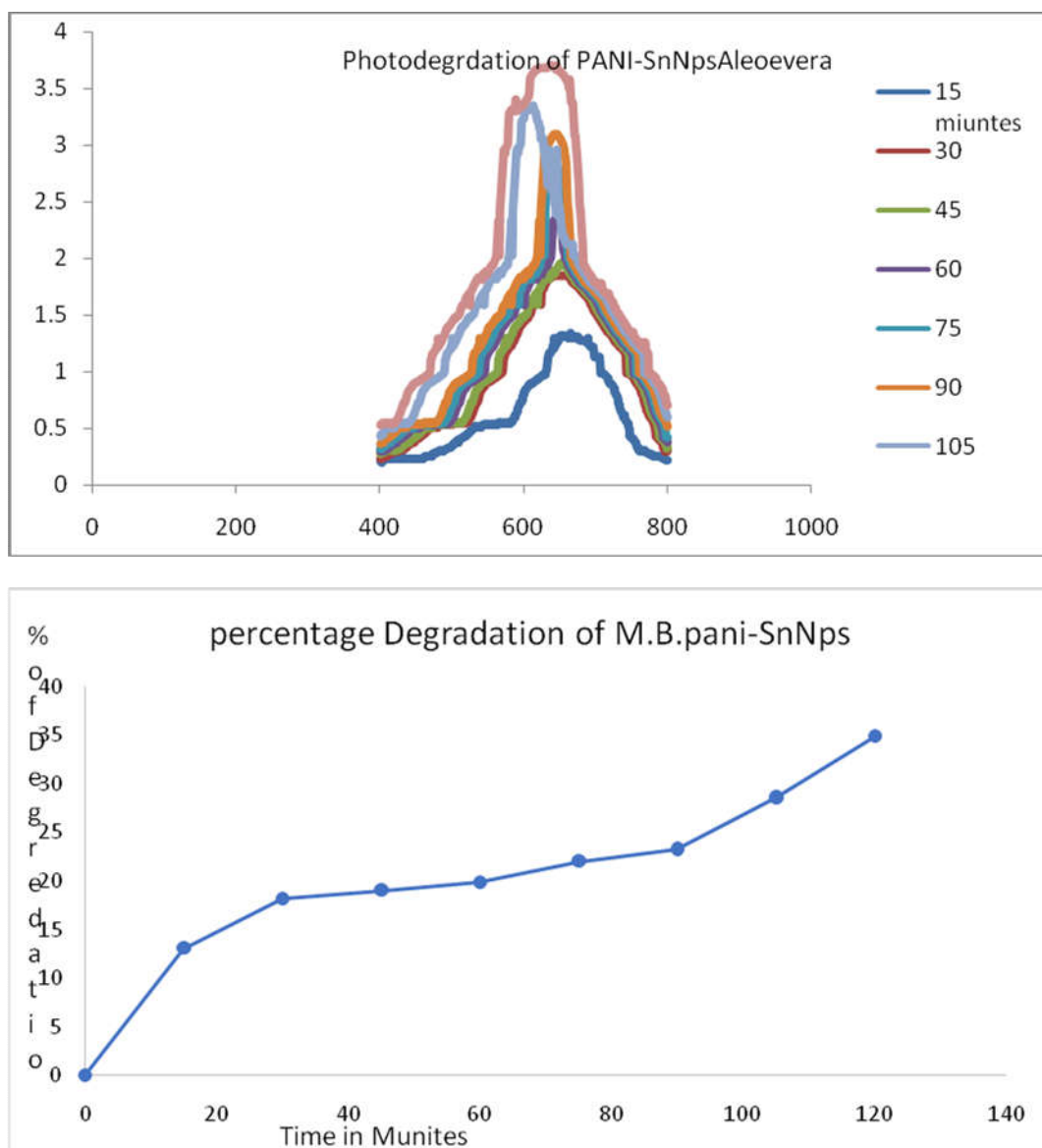

Fig 3.5a) Absorption spectra of aqueous MB at different time intervals and

Fig 3.5b) percentage degradation of MB using Pani-SnNPs.

3.6 I-V Charterers of Pani-SnNPs Film.

The I–V Charterers observed for this Pani-Sn-NPs composites thin film on glass substrate is included in this Fig. 3.6, The I –V behaviors of the film were carefully checked foreffects of current voltage vernation using the doped PANI-Sn NPs composites films. The effects were seen for voltagesincrease between 0.5 to 10 V, consistent with metallic liner behavior at 8V then after it shown nonlinear behavior at room temperature 300k. The observation that the average resistivity (4.2×10^5 Ὼ) lies in between that and perpendicular to the basal plane. Composites have a positive temperature coefficient of resistance up to 4.2×10^5 Ὼ in the temperature range of 300k to 315k. It is shown that the temperature coefficient of resistance is positive and increases with increasing electric field strength. The decrease in the electrical conductivity of composites with increasing temperature is explained by the expansion of the polymer matrix and the rupture of the current-conducting channels between the conducting grains.it was noticed that at 300 K to 315k current was decreased from $\sim$94.4μA to 44.8μA at versatile voltage applied from 300k to 315k temperature. The behavior of these curves also slightly shifted from ohmic to non-ohmic as voltage applied more toPani-SnNPs composites film.
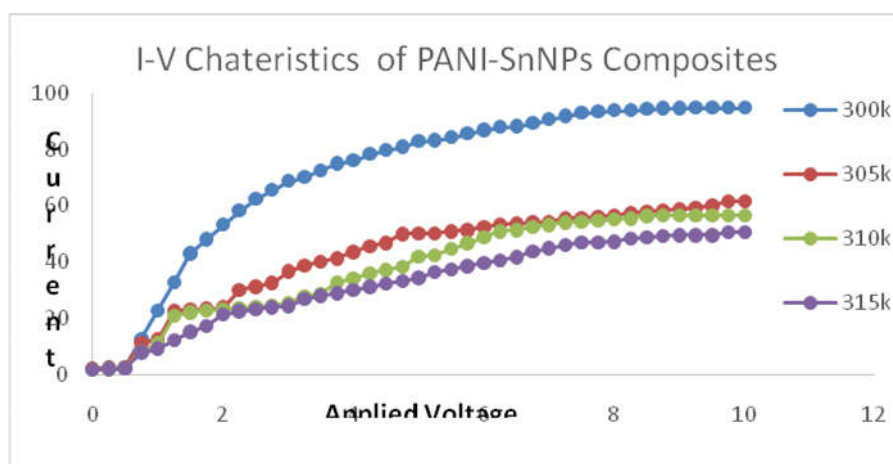
Fig. 3.6, I-V Charterers of Pani-SnNPs Film.

3.7 Amine gas sensor.

The sensor applicability of synthetic filmsPANISn-Nps was observed for ammonia gas at 10ppm to 50 ppm level. The computer control four probe instrumentation were used to record the change in resistivity of film to exposed and de-exposed of gases that is response time and recovery time are find in second. The minimum response time is kept constant that is 300

seconds the observed the recovery time in second for both gases. The instrumentation chamber has limits it does not response to below 10ppm gas.
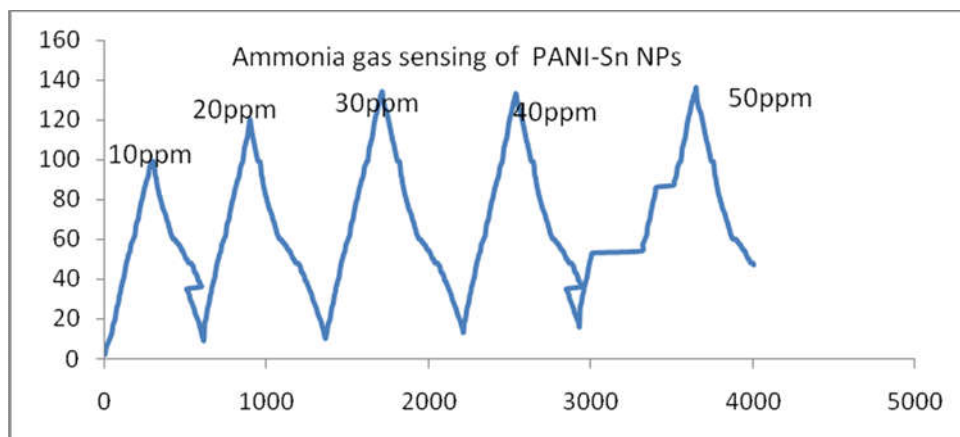
Fig 3.7 the ammonia gas sensing

4. Conclusion:

We Synthesised the PANI Sn-NPs /Aloe-Vera films composite by using biomaterial as a Aleovera plant extract as capping and stabilizing agents. The Synthesised PANI Sn-NPs composites material confirms the composition by techniques such as U.V, FTIR and EM, SEM and XRD.   It confirmed that the biocomposites have Stannous metal with Aloevera were successfully incorporated into the PANI matrix. FTIR analysis showed good intermolecular interaction between the PANI /Sn-NPs / Aloe-Vera matrix. The surface morphology of PANI /Sn-NPs / Aloe-Vera composite films was examined using EM analysis and the results confirm that Sn-NPs are homogeneously dispersed in the PANI matrix. The synthesis composite films with Sn-NPs / Aloe-Vera doping showed the highest conductivity with a value of 1.305×10^{-4} Scm^{-1}. The results obtained in the present study for PANI and PANI /Sn-NPs / Aloe-Vera composite films observed electrochemical behavior which is linear. The synthesized material observed for photo degradation efficiency of the synthesized Pani-SnNPs, was observed as well as Ammonia gas sensing applicabilitypropertiesobserved which is toxic at more than 30ppm ammonia gas for human being.

References:

1. George Soupions, Pantelitsa Georgiou and LoukasZoumpoulakis"Polymer Composite Materials Fiber-Reinforced for the Reinforcement/Repair of Concrete Structures"Polymers 2020, 12(9), 2058 pp 1-14; https://doi.org/10.3390/polym12092058.

2. L S faeq "Thermal and Mechanical Properties of Polymer/Nickel Composites" 3rd International Conference on Sustainable Engineering Techniques (ICSET 2020) IOP Conf. Series: Materials Science and Engineering 881 (2020) 012092 IOP Publishing pp 1-8 doi:10.1088/1757-899X/881/1/012092.

3. EwelinaMackiewicz, Tomasz Wejrzanowski , BogusławaAdamczyk-Cie´slak and Graeme J. Oliver "Polymer–Nickel Composite Filaments for 3D Printing of Open Porous Materials"Materials 2022, 15(4), 1360 pp 1-15; https://doi.org/10.3390/ma15041360.

4. Hind Ahmed, Bahaa H. Rabee, Hussein Hakim, Ahmed Hashimand Saba R. Salman "Preparation and Study of Optical Properties of (Polymer-Nickel Nitrate) Composite"Advances in Physics Theories and Applications ,ISSN 2225-0638,Vol.20, 2013 pp 152-157.

5. R. K. Goyal, R. Sulakhe"Study on poly(vinylidene fluoride)/nickel composites with low percolation"Adv. Mater. Lett. 2015, 6(4), 309-317DOI: 10.5185/amlett.2015.5627.

6. M. Lahelin a, I. Aaltio b, O. Heczko b, O. Söderberg b, Y. Ge b, B. Löfgren a, S.-P. Hannula b, J. Seppälä a "DMA testing of Ni–Mn–Ga/polymer composites"omposites Part A: Applied Science and Manufacturing publishes Volume 40, Issue 2, February 2009, Pages 125-129 https://doi.org/10.1016/j.compositesa.2008.10.011.

7. HafizaVaneezaHussain, Mateeb Ahmad, Muhammad TamoorAnsar , Ghulam M. Mustafa , SairaIshaq , ShahzadNaseem , GhulamMurtaza , Farah Kanwal and ShahidAtiq "Polymer based nickel ferrite as dielectric composite for energy storage applications"Synthetic Metals, Volume 268, October 2020, 116507 https://doi.org/10.1016/j.synthmet.2020.

8. MohdMohsinNizam Ansari, Shakeel Khan and Naseem Ahmad "A comprehensive investigation of structural, thermal and electrical properties of $T_{0.35}$ $Zn_{0.55}$ $Cu_{0.1}Fe_2O_4$ (T = Mn, Ni) nanoferrites"Physica B: Condensed Matter,Volume 566, 1 August 2019, Pages 86-95.https://doi.org/10.1016/j.physb.2019.05.003.

9. A. Suhasinia and K. P. Vinod Kumar "Solubility and swelling studies of polymer hybrid-nickel oxide nanocomposite"J. Indian Chem. Soc., Vol. 96, January 2019, pp. 7-8

10. Wangping Wu, DingkaiXie, JiaqiHuang,Qinqin Wang and Junjun Huang "Adhesion enhancement for nickel layer deposited on carbon fiber reinforced polymer (CFRP) composites by pretreatment processes for lightning strike" https://doi.org/10.1080/00218464.2022.2082870.

11. Yesappa L, Niranjana M, Ashokkumar SP, Vijeth H, Sharanappa C, Raghu S and Devendrappa H, "Synthesis, Characterization and Absorption Study of Aloe Vera doped Polyaniline Bio-Composite"Materials Today: Proceedings 5 (2018) 21076–21081.

12. Annu, ShakeelAhmed,Ranjeet Kumar, Nirala, Ravi Kumar, and SaiqaIkram "Green synthesis of chitosan/nanosilver hybrid bionanocomposites with promising antimicrobial, antioxidant and anticervical cancer activity"Polymers and Polymer Composites, Vol. 29, Issue 9 November 2021, Pages S199-S210.

Comparative Study of Electrochemical properties of Synthesized PANI and PANI/Ni-NPs / Aloe-Vera thin films Biocomposite.

Dr. D. B. Dupare@ *

1*@ Department of Chemistry, Shri R.G. Rathod Arts and Science College, Murtizapur, Di.Akola.

Abstract:

This study deal with comparative observation of synthesized polyaniline films on glass subtract by chemically oxidative polymerization technique and synthesized polydisperse nickel nano particles(NiNPs) Stabilized on Aloe Vera Leaf Extract. The secondary phytochemical of plant extract polyphenols stabilizing and capping agentsfor the more stability and conductivity enhancement property.We synthesized PANI-Ni-NPs. Aloe Vera leaf extract and metal salt nickel chlorides dopant for the thin film composite formation on the glass substrate and studied their U.V. FTIR and Electronic microscopy Characterizationfor their comparative study of Electrochemical Behavior and current voltage Characteristics. The four-probe instrumentation indicate that the PANI-NiNPs modified electrode was good conductivity and stability on glass substrate (Resistivity = $1.305 \times 10^4 \Omega$) compared to that of the PANI thin films electrode (Resistivity = 1.024×10^5 Ω)

Key word: Polyaniline, Conductivity, I-R Characterization, Thin film and PANI-Ni-NPs, Biocomposites

Introduction:

The polyaniline exhibits excellent characteristic such as good electrical conductivity also environmental stability and aneasy synthetic route. This characteristics property polyaniline applied in several area such as sensor, actuator, battery storage, electronic application has been reported [1-2]. Recent development in this field that nano-sized PANi/metal composites/hybrids exhibit even better characteristics as compared to the single homopolymer.There are numbers of different technique to Synthesized hybrids polymers composites like chemical oxidative polymerization, Electrochemical polymerization, spraying technique, coating systems,one-pot synthesis techniques, thin films coatingto Synthesis such conducting polymer/metal nanocomposites [3-4].

In this study we reported the synthesis PANI-Ni-NPs -Aloe Vera hybrids thin films composites on glass substrate via simple chemical oxidative polymerization technique by using ultra sonicator. The Ni-NPs are first synthesized through the reduction of Nickel chlorides salts with Aloe -Vera leaf extracts of polyphenol. How ever the Aloe-Vera polyphenol has not reported yet to, its utility as a nanoparticle fabrication precursor hybrid. The Aloe-Vera plant has large antioxidation property are due to the fact that it contains largequantities of polyphenols.It is believed that these polyols can play a vital role as stabilizers/capping agents in the production of the Nickle nanoparticles. The Novelty of this works is that plant extract polyols as well as flavonoids are used to stabilize the nano particle in formation of thin films on glass substrate and their utility for electrochemical characterizations in different application as sensor or biosensors.

68

2. Materials and Methods

2.1 Materials and chemical

Aniline and Ammonium oxysulphides from Sd -Fine chemical are used. Aniline distilled prior to used, The Nickel (II) chloride hexahydrate ($NiCl_2.6H_2O$, >98%) was from Sd-Fine chemicals.Aloe-Vera was bought from a local college medicinal garden. Double Distilled deionized water (DDW) was from the analytical laboratory, Chemistry Department, was used for all aqueous preparations.

2.2 Extraction of Aloe-Vera gel and Ni -NPs synthesis

We are collected the one fresh leaves of Aloe-Vera was bought from a local college medicinal garden and remove the hard green coat from leave by using knife, the after near about 10 g semi liquid parts gel and 10 ml of doble distilled water are mixed in 100ml beaker by using ultra sonicator for 20 minutes. The resultant supernatant was collected, filtered and stored at 10 °C before use. The NiNPs were prepared by adding 0.1 M Nickel II chloride solution to the Aloe-Vera extract (supernatant at ambient temperature) in a series of 1:1,1:2,1:3 and also 4:1,3:1, 2:1 volume ratio. The mixture was hand shaken for 1 min and allowed to stand at room temperature for 30 minutes in ultra sonicator at 40 to 90 °C to prepare the nanoparticles.

2.3 Synthesis of PANI films.

The aniline was double distilled prior to used then in 100ml, we have taken glass substrate andoptimize the stoichiometric ratio of both chemicals that is 2ml of aniline and 0.5 M ammonium peroxydisulphate under continuous stirring at room temperature and kept in ultrasonicates for 20 minutes then cool it below -10 °C freezers for 12 hours to obtained homogenous stable thin film formation.

2.4 Synthesis of PANI-Ni NPs of Aloe-Vera films.

The optimize stoichiometric concentration of 2ml aniline and 0.01, 0.02, 0.03, 0.04 upto 0.1 M Concentration of Ni-NPs of Aloe-Vera extract solution added to in series of 100 ml beaker with glass substrate to oxidized with 0.5 M ammonium peroxydisulphate under continuous stirring at room temperature and kept in ultrasonicates for 20 minutes then cool it below -10 °C freezers for 12 hours to obtained homogenous stable thin film formation. The thin films substrates wash with deionized water kept to dry at room temperature with drier. The Figure shown in Fig 1.1 and 1.2 is that Synthesis of PANI-Ni NPs of Aloe-Vera films before oxidation and after oxidation the formation Biocomposites films of PANI-Ni NPs. Fig 1.3 indicate the formation of thin films of PANI-Ni NPs on Glass substrate.

Fig 1.1 and 1.2 before oxidation and after oxidation the formation Biocomposites films of PANI-Ni NPs.
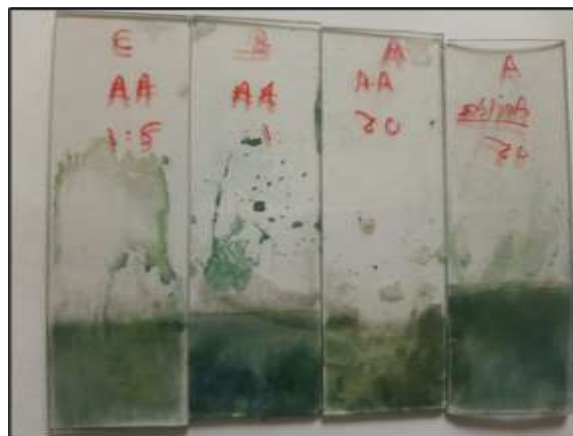
69

Fig 1.3. Optimization PANI-Ni NPs of Aloe-Vera films

2.5 Electrochemical Characterization of the PANI-Ni NPs of Aloe-Vera films

The PANI-Ni NPs of Aloe-Vera films were prepared by Chemical oxidative polymerization method are Characterized by U.V.-Visible spectroscopy was recorded on UV- VIS Spectrophotometer Carry Agilent Tech at Department of chemistry SGBAU, Amravati. In case of UV- VIS Spectroscopy transition that results in the absorption of electromagnetic radiation in UV-VIS Absorption Region are Spectrum of transition between electronic levels.

Infrared spectroscopy is the analysis of infrared light interacting with molecule. This can be analyzed in three ways by measuring abortion, Emission and reflection. It is used to determine functional group in molecule FTIR Spectroscopy measure the vibration atoms and based in this it is possible to determine functional groups. The following IR spectra were recorded on Bunker Alpha-T FT IR Spectrometerat Department of chemistry SGBAU, Amravati.

Olympus electron microscope is used for thin and observation of stability as well as granular or tubular size nanoparticles of PANI/Ni-NPs /Aloe-Veragranules at Department of Botany. The conductivity and Current -Voltage characterization was carried out by using four probe Instrumentation.

3. Result and Discussion.

3.1. U. V. Visible of PANI and PANI/Ni-NPs / Aloe-Verafilms.

The U.V.-Visible spectroscopy was studied in range between 200nm to 700nm after dissolution of PANI and PANI/Ni-NPs / Aloe-Verathin films in DMSO solvents. The spectrum shows a prominent peak at absorption maxima of 292 nm which has been assigned to the $\pi \rightarrow \pi*$ transitions of the Aloe-Vera polyols. The high absorbance value of 1.5 obtained indicates a high concentration ofthe polyols in solution.A broad peak extending from 260-380 nm with absorption maxima at 298 nm was seen. Such observationis characteristic of transition metal elements where the observed broad peaks are due to transitions within the filled and unfilled d-orbitals of metal salts by influence from other external factors.

The new peak formed was slightly shifted bathochromically compared to the 292 nm peak of the Aloe-Vera extracts. This peak at 290 nm and the smaller hub at around 350 nm have been shown to be due to the presence of the Ni-NPs nanoparticles in the Ni (II) state. It means the reluctant polyols within the matrices successfully reduced the Ni (II) ions to the Ni zero states also indicating the formation of theNi-NPs/polyols hybrid. The reduction of the prominent extract peak at 292 nm indicates the polyols were actually involved in the reduction process and the consequent formation of a new compound the PANI/Ni-NPs / Aloe-Vera film composite as shown in figure 3.1.
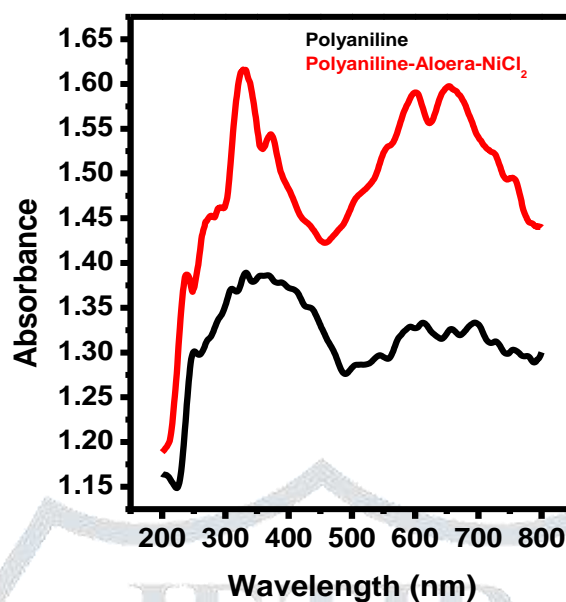
70

Figure 3.1. U. V. Visible of PANI and PANI/Ni-NPs / Aloe-Vera film

3.2.FT-IR spectra of PANIand PANI/Ni-NPs / Aloe-Vera films.

FT-IR spectra of PANI solid exhibited the characteristicabsorption bands of emeraldine salt at 1518 and 1616 cm^{-1}, whichcorrespond to the C- C stretching vibration of benzenoid (N -B-N)and quinonoid (N =Q= N) ring, respectively [5]. The peaks in therange of 1300–1400 cm^{-1} as arise from C-N stretching vibrationsof the secondary aromatic amines, while the intense absorptionpeak at 1193 cm^{-1} is associated to the B- NH -B and protonatedQ =NH^+-B stretching modes of PANI chains [6]. The vibrationalfeatures at 519, 593 and 838 cm^{-1} correspond to the aromaticring deformation (C-C stretching modes) and C- H out-of-planebending mode of 1,4-disubstituted benzene ring, respectively [7].

Compared with the pure PANI in figure 3.2.1 and figure 3.2.2 of the hybrid PANI/Ni-NPs / Aloe-Vera composite materials indicated a considerable red shift ($\sim$15–20 cm^{-1}) of theN-B-N and N =Q=N vibrational bands at $\sim$1501 and $\sim$1600 cm^{-1}respectively, suggesting interaction of PANI chains with anionic heteropolyacids. The IR spectra of the hybrid samples indicate thepresence of Ni-Od (terminal bonds) and Ni-Ob -Ni (bridge bonds between the corner-sharing NiCl octahedra; M = Ni) stretchingvibrations at $\sim$972–988 and $\sim$879–890 cm^{-1} respectively [8,9]. However, these absorption bands are considerably red-shifted ($\sim$10 cm^{-1}) compared with theNi-Nps -Aleo vera, suggesting strong binding of Ni-Nps –Aleovera units to the polymer network. The intense absorption bands at$\sim$1140 and $\sim$1080 cm^{-1} observed in the samples of Ni-Nps –Aleovera and PANI–Ni-Nps -Aleovera are ascribed to the clusters, respectively. The PANI–Ni-Nps sample exhibits the corresponding Ni-Clvibration band of cluster at $\sim$804 cm^{-1}.

71
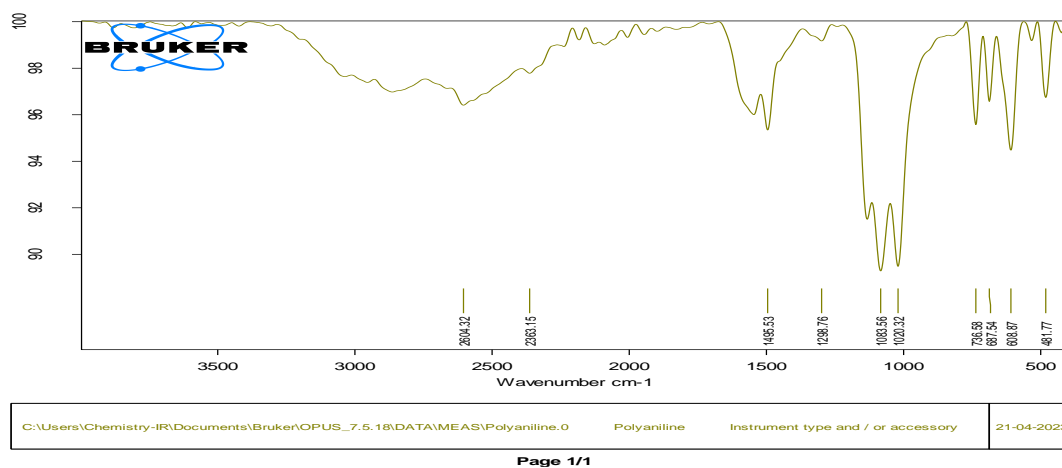
Fig 3.2.1 FTIR Spectrum of Polyaniline
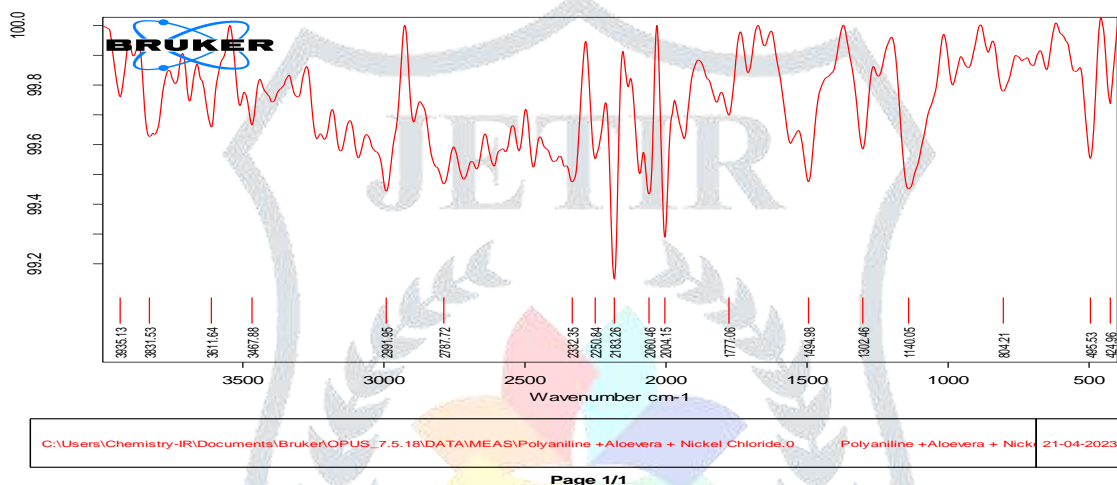
Figure 3.2.2 FTIR Spectrum of PANI-NiNps AloeVera

Sr.	Assignments	PANI-NiNpsAloeVera Observed Value (cm^{-1})	PANI Observed Value (cm^{-1})	Literature value (cm^{-1})
1	O-H Stretching Aromatic Polyol ring	3631, 3611		~3560
2	N-H Stretching Aromatic ring	3467,	3300	~3400
3	C-H stretching vibration aliphatic	2991	2968.	~2930
4	diazonium salts	2787	2604	~2740
5	asymmetric NH+=)	2332,2183	2363,	~2156
6	N-B-N and N =Q=N vibrational bands at ~1501 and ~1600 cm−1 benzenoid unitsC=C	1777, 1494	1496, 1296	~1600, ~1300
7	Intense absorption Ni-Nps	1140,1080.	1083,1020	~1080 cm−1
8	Ni -Od (terminal bonds) and Ni -Ob -Ni (bridge bonds between (M = Ni)	804,		~972–988 and ~879–890 cm−1
9	Para, ortho substituted aromatic rings	495	736,608	519, 593

72

3.3. **Electron microscopy of PANI and PANI /Ni-NPs / Aloe-Vera films.**

The actual integration and the structurization effect of the Aloe-Vera polyphenols/flavanoids were observed in the Electron microscopy images obtained. .The rod or fiber like morphologies are obtained by suppressing secondary growth. It has been shown that PANI first forms fibers in figure 3.3.1; however, with the progress of the polymerization, the formed fibers serve as the scaffolds for the further growth of PANI and finally develop to a particle form. The average particle sizes with variation in polymerization can be seen that for polymerization time, rod-like particles are present. With increase in polymerisation duration, rod-like particle become less abundant and more spherical/globular particles are seen due to the presence of Aleo-Vera polyol that is polyphenol immersed with or coagulant of Nickel metal atoms are presen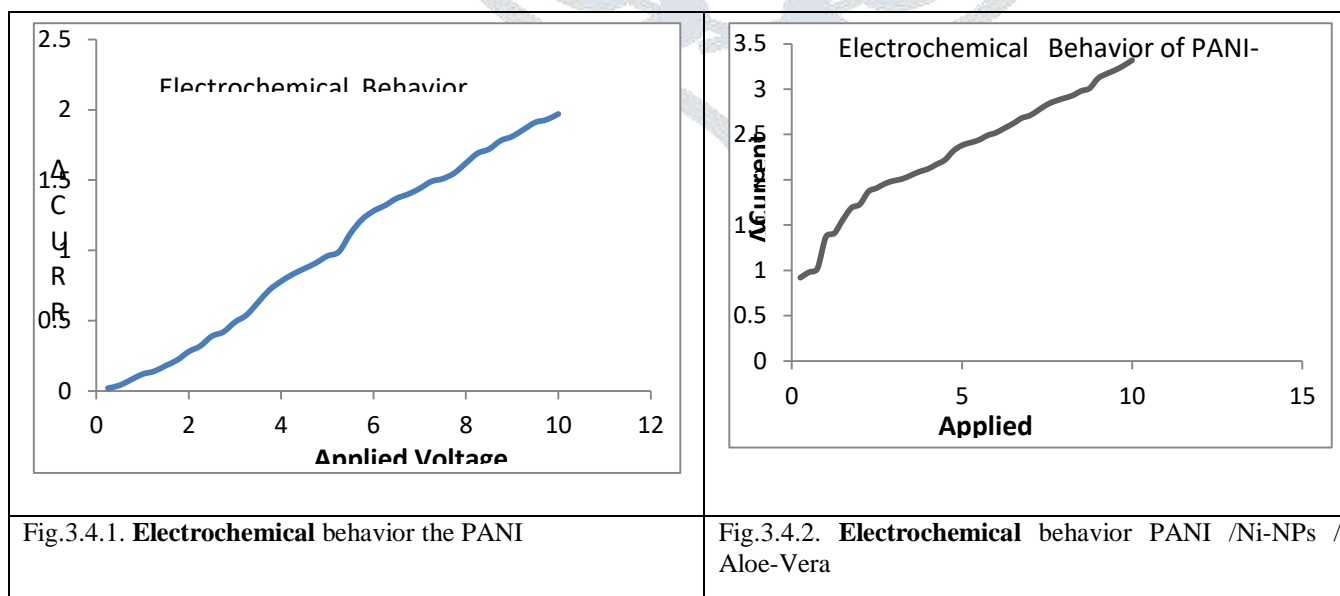t in formation of Polymeric thin of PANI /Ni-NPs / Aloe-Vera films in figure 3.2.2 .The nickel metal morphology in figure 3.2.3. favors the formation globular particles.

Figure 3.3.1.Electron microscopy morphology PANI	Figure 3.3.2 Electron microscopy morphology PANI /Ni-NPs / Aloe-Vera.	Figure 3.3.3 Electron microscopy Image Nickel metal.
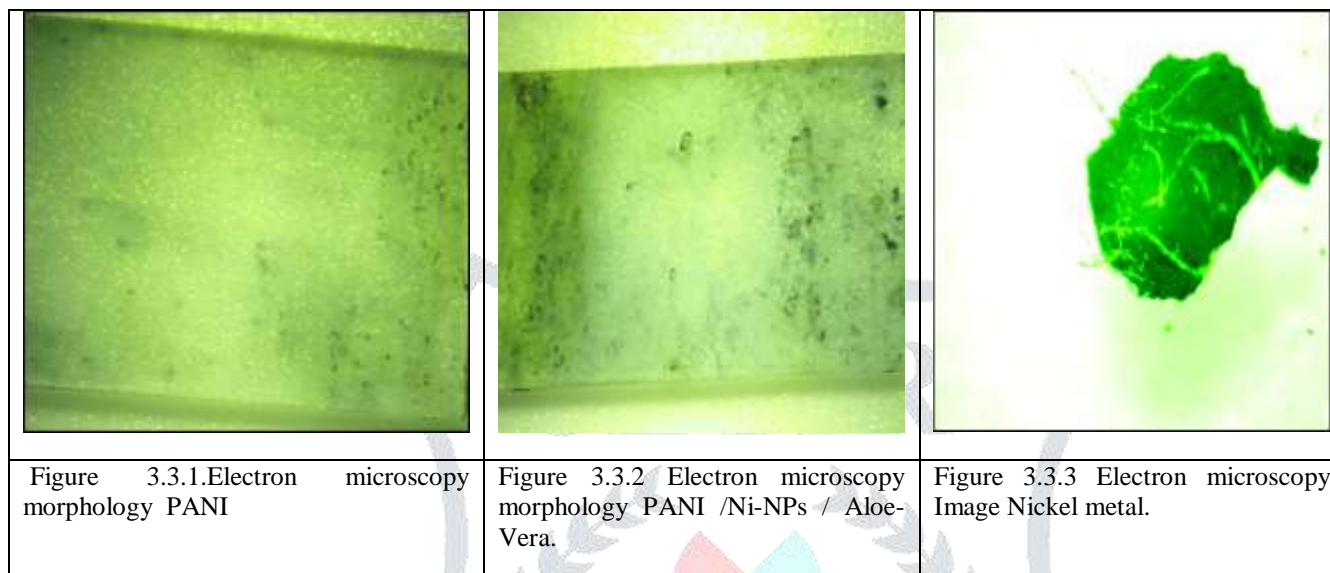
3.4. Electrochemical Characterization

The I-V characterization measurement of the PANI and PANI /Ni-NPs / Aloe-Vera films was recorded by an indigenously developed computer controlled using four- probe method at room temperature. The current–voltage (I-V) characteristics of the synthesized PANI and PANI /Ni-NPs / Aloe-Vera thin films were studied to ensure an ohmic behavior of the films. A linear relationship of the I-V characteristics shown in Fig.3.4.1. reveals that the PANI and Fig.3.4.2. PANI /Ni-NPs / Aloe-Vera composites film has an ohmic behavior at room temperature. The four-probe instrumentation indicate that the PANI-Ni-NPs modified electrode was good conductivity and stability on glass substrate (Resistivity = 1.305×104 Ω) compared to that of the PANI thin films electrode (Resistivity = 1.024×105 Ω) at room temperature.

Fig.3.4.1. **Electrochemical** behavior the PANI	Fig.3.4.2. **Electrochemical** behavior PANI /Ni-NPs / Aloe-Vera

73

Conclusion:

This study comparesthe synthesis the PANI and PANI /Ni-NPs / Aloe-Vera films composite. The characterization techniques such as U.V, FTIR and EM analysis confirmed that Nickel chloride with Aleo Vera was successfully incorporated into the PANI matrix. Effect of different concentration of Nickel chloride with Aleo vera on structural, electrical and properties of PANI /Ni-NPs / Aloe-Vera films composite were studied. FTIR analysis showed good intermolecular interaction between PANI /Ni-NPs / Aloe-Vera matrix. The surface morphology of PANI /Ni-NPs / Aloe-Vera composite films was examined using EM analysis and the results confirm that Ni-NPs are homogeneously dispersed in PANI matrix. The synthesis composite films with Ni-NPs / Aloe-Vera doping showed highest conductivity with a value of $1.305 \times 10^{-4} Scm^{-1}$. The results obtained in the present study for PANI and PANI /Ni-NPs / Aloe-Vera composite films observed electrochemical behavior which is linear.

References

1. George Soupions, Pantelitsa Georgiou and Loukas Zoumpoulakis "Polymer Composite Materials Fiber-Reinforced for the Reinforcement/Repair of Concrete Structures"Polymers 2020, 12(9), 2058 pp 1-14; https://doi.org/10.3390/polym12092058.

2. L S faeq "Thermal and Mechanical Properties of Polymer/Nickel Composites" 3rd International Conference on Sustainable Engineering Techniques (ICSET 2020) IOP Conf. Series: Materials Science and Engineering 881 (2020) 012092 IOP Publishing pp 1-8 doi:10.1088/1757-899X/881/1/012092.

3. Ewelina Mackiewicz, Tomasz Wejrzanowski , Bogusława Adamczyk-Cie´slak and Graeme J. Oliver "Polymer–Nickel Composite Filaments for 3D Printing of Open Porous Materials"Materials 2022, 15(4), 1360 pp 1-15; https://doi.org/10.3390/ma15041360.

4. Hind Ahmed, Bahaa H. Rabee, Hussein Hakim, Ahmed Hashim and Saba R. Salman "Preparation and Study of Optical Properties of (Polymer-Nickel Nitrate) Composite"Advances in Physics Theories and Applications ,ISSN 2225-0638,Vol.20, 2013 pp 152-157.

5. R. K. Goyal, R. Sulakhe"Study on poly(vinylidene fluoride)/nickel composites with low percolation"Adv. Mater. Lett. 2015, 6(4), 309-317DOI: 10.5185/amlett.2015.5627.

6. M. Lahelin a, I. Aaltio b, O. Heczko b, O. Söderberg b, Y. Ge b, B. Löfgren a, S.-P. Hannula b, J. Seppälä a "DMA testing of Ni–Mn–Ga/polymer composites"omposites Part A: Applied Science and Manufacturing publishes Volume 40, Issue 2, February 2009, Pages 125-129 https://doi.org/10.1016/j.compositesa.2008.10.011.

7. Hafiza Vaneeza Hussain,MateebAhmad, Muhammad Tamoor Ansar , Ghulam M. Mustafa , Saira Ishaq , Shahzad Naseem , Ghulam Murtaza , Farah Kanwal and Shahid Atiq "Polymer based nickel ferrite as dielectric composite for energy storage applications"Synthetic Metals, Volume 268, October 2020, 116507 https://doi.org/10.1016/j.synthmet.2020.

8. Mohd Mohsin Nizam Ansari, Shakeel Khan and Naseem Ahmad "A comprehensive investigation of structural, thermal and electrical properties of $T_{0.35}Zn_{0.55}Cu_{0.1}Fe_2O_4$ (T = Mn, Ni) nano ferrites"Physica B: Condensed Matter,Volume 566, 1 August 2019, Pages 86-95.https://doi.org/10.1016/j.physb.2019.05.003.

9. A. Suhasiniaand K. P. Vinod Kumar "Solubility and swelling studies of polymer hybrid-nickel oxide nanocomposite"J. Indian Chem. Soc.,Vol. 96, January 2019, pp. 7-8

10. Wangping Wu, Dingkai Xie, Jiaqi Huang,Qinqin Wang and Junjun Huang "Adhesion enhancement for nickel layer deposited on carbon fiber reinforced polymer (CFRP) composites by pretreatment processes for lightning strike"https://doi.org/10.1080/00218464.2022.2082870.

74

IDEAL

ENGLISH PART - V

Peer Reviewed Referred and
UGC Listed Journal No. 47026

Single Blind Review/Double Blind Review

ज्ञान-विज्ञान विमुक्तये

❖ EDITOR ❖

Assit. Prof. Vinay Shankarrao Hatole
M.Sc (Math's), M.B.A. (Mkt), M.B.A (H.R),
M.Drama (Acting), M.Drama (Prod & Dirt), M.Ed.

7. Effect of Different Metal Salts Dopant on Electrochemical behavior of on PANI-Aloe-Vera Biocomposites

Mohan Wasankar
Department of Chemistry, Shri R. G. Rathod Arts and Science College,
Murtizapur, District Akola.
Dr. D. B. Dupare
Department of Chemistry, Shri R. G. Rathod Arts and Science College,
Murtizapur, District Akola.

Abstract

This study deal with comparative effect of different metal salts on electrochemical behavior synthesized polyaniline- Aloe Vera leaf extract films by oxidative polymerization technique. The metal salts are selected for this which increases the electrochemical potential of films like $ZnSO_4$ and $MnSO_4$. The dopant composite Characterized by using U.V. FTIR and Electronic microscopy Characterization for formation of Composites and confirmation for their comparative study of Electrochemical Behavior and current voltage Characteristics. Electronic microscopy Characterization observed that, this thin film competitive have uniform surface for various application. The size and morphology of the doped composites are important parameters that affect their major applicable properties. The biomaterial gel of Aloe Vera leaf plant extract used to stabilizer for polyaniline on glass substrate. The four-probe instrumentation technique is used for observed the conductivity of synthesized electrode material. The conductivity of $ZnSO_4$ and $MnSO_4$ at room temperature (5.3×10^4 S·cm^{-1} and 6.4×10^4 S·cm^{-1}), with the achievement of such high conductivity, became a promising material for electronic applications.

Key word: Polyaniline, Conductivity, I-R Characterization, Thin film and metal salt dopant.

1. Introduction

Conducting polymer focuses attention on past several decades due strong potential as alternatives to their inorganic counterparts, leading to significant fundamental and practical research. Conducting polymer has distinguishable properties that are chemical diversity, low density, flexibility, corrosion resistance, easy-to-control shape and morphology, and tunable

conductivity.(1-2) Conducting polymer have been hybridized with other heterogeneous material components like metal salt dopant biomaterial, plant extract to overcome their limitations in terms of solubility, conductivity, and long-term stability. Conducting polymer mixed with other materials can result attractive properties and new application (3-4). Researchers have done number of efforts in this field to obtained a variety Conducting polymer -based composites and hybrids with novel structures and improved properties such material is more attractive ness like carbon Nano-species such as grapheme, carbon Nano fibers (4). The research to achieve the overcome in ranging from insulating to metalloid and conductive (5).

Our research group to focus on the most important factor for progress in such fields is achieving to control of the electrical or electrochemical properties of conducting polymer. Consequently, this work related a discussion of the electrochemical properties of Conducting Polymer with biomaterial varies with doped with metal salts to identify the variable range to achieve the conductance of conducting polymers at their highest range for latest trends of applications.

2. Materials and Methods

2.1 Materials and Chemical

Aniline and Ammonium peroxydisulphides from Sd -Fine chemical are used. Aniline was distilled prior to used, The $MnSO_4$ and $ZnSO_4$ Dihydrate metal salts was from Sd-Fine chemicals. Aloe-Vera was bought from a local college medicinal garden. Deionized water (DDW) was from the analytical laboratory, Chemistry Department, was used for all aqueous preparations.

2.2 Synthesis of $MnSO_4$ and $ZnSO_4$ Doped Films

The fresh leaves of Aloe-Vera were bought from a local college medicinal garden and remove the hard green coat from leave by using knife, the after near about 10 g semi liquid parts gel and mixed 20 ml distilled water by using ultra sonicator for 20 minutes. The $MnSO_4$ and $ZnSO_4$ metal salt doped in Aloe vera extract with in the ratio of 0.1 M to 0 .01M of both salt and kept this baker in ultrasonication for 30 minutes.

The double distilled aniline 0.05M to 0.01M added in the corresponding system of metal salt solution then glass substrate added to developed thin films the APS(Ammonium peroxydisulphides) to oxides the aniline to developed polyaniline composites doped with metal oxides kept it 10° C. at refrigerator to developed uniform morphology of thin film composites.

77

2.3 Characterization of Synthesis Metal doped Film

The synthesized films composites Characterized by various instrumentation technique U.V.-Visible spectroscopy was recorded on UV- VIS Spectrophotometer. Infrared spectroscopy is the analysis of infrared light interacting with molecule. It is used to determine functional group in molecule FTIR Spectroscopy measure the vibration atoms and based in this it is possible to determine functional groups. Olympus electros films. Electron microscope is used for thin and observation of stability as well as granular or tubular size of metal are present in these composites. The conductivity and Current -Voltage characterization was carried out by using four probe Instrumentation.

3. Result and Discussion

3.1. U. V. Visible of $MnSO_4$ and $ZnSO_4$ doped Films

The U. V.-Visible spectroscopy was studied in range between 200nm to 700nm after dissolution composites films in DMSO solvents. The spectrum shows a prominent peak at absorption maxima of 292 nm which has been assigned to the $\pi \rightarrow \pi^*$ transitions of the Aloe-Vera polyols. A broad peak extending from 260-380 nm with absorption maxima at 298 nm was seen. Such observations characteristic of transition metal elements where the observed broad peaks are due to transitions within the filled and unfilled d-orbitals of metal salts by influence from other external factors.

The new peak formed was slightly shifted bathochromically compared to the 292 nm peak of the Polyaniline. This peak at 290 nm and the smaller hub at around 350 nm have been shown to be due to the presence of the Mn and Zn metal salts. The reduction of the prominent extract peak at 292 nm indicates the polyols were actually involved in the reduction process and the consequent formation of a new compound the PANI//Aloe-Vera film with metal salt dopant composite as shown in figure 3.1. The conducting state of the optical absorbance properties of the as-synthesized material. The metal salt Mn and Zn with polyaniline heterostructure's absorption edge was observed at 670 nm, as illustrated in figure. A broad and significant absorbance was detected in the PANI-Alvera doped with metal salt heterostructure.

78
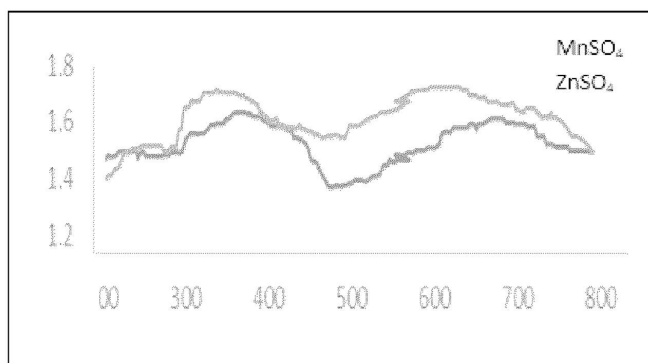
Figure 3.1. PANI//Aloe-Vera film with metal salt

3.1. FTIR of MnSO4 and ZnSO4 doped Films

The FTIR spectra of polyaniline Aloe-Vera doped MnSO4 and ZnSO4 metal salt observed to dissolving the sample in DMSO solvent. FT-IR spectra of PANI doped Mn and Zn exhibited the characteristic absorption bands of emeraldine salt at 1518 and 1616 cm^{-1}, which correspond to the C- C stretching vibration of benzenoid (N -B-N) and quinonoid (N =Q= N) ring, respectively [5]. The peaks in the range of 1300–1400 cm^{-1} as arise from C-N stretching vibrations of the secondary aromatic amines, while the intense absorption peak at 1193 cm^{-1} is associated to the B- NH -B and protonated =NH^{+}-B stretching modes of PANI chains [6]. The vibrational features at 519, 593 and 838 cm^{-1} correspond to the aromatic ring deformation (C-C stretching modes) and C- H out-of-plane bending mode of 1,4-disubstituted benzene ring, respectively [7]. The FTIR Spectra of both metal dopant are observer the similar pattern of FIIR Spectrum but Slightly change in metal to metal from Mn to Zn dopant.

Fig 3.2 FTIR of MnSO4 and ZnSO4 doped films

79

3. 3. Electron microscopy of MnSO₄ and ZnSO₄ doped Films
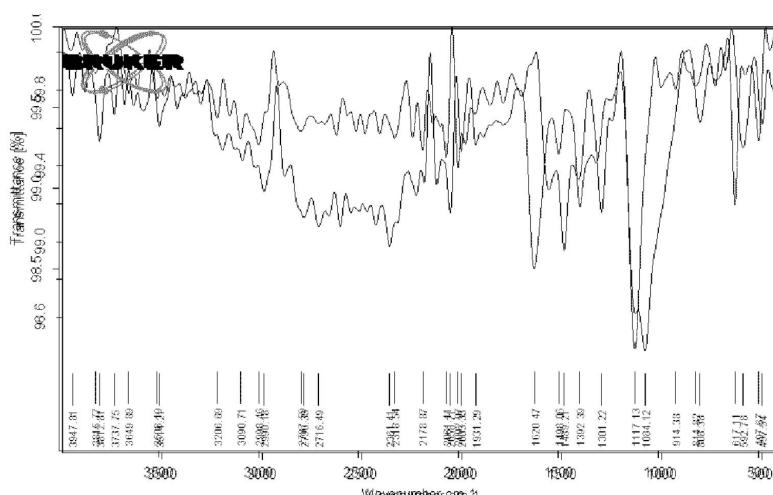
Electron microscopy images observed under high density electron microscopy, morphologies are obtained for both metal salt dopant in polyaniline and Aleovera figure 3.3.1 and 3.3.2 however, with the progress of the polymerization, the formed fibers serve as the scaffolds for the further growth of PANI and finally develop to a particle form. The average particle sizes with variation in polymerization can be seen that for polymerization time, rod-like particles are present. With increase in polymerization duration, rod-like particle become less abundant and more spherical/globular particles are seen due to the presence of Aleo-Vera polyol that is polyphenol immersed with or coagulant of metal atoms are present in formation of Polymeric thin film shown in fig 3.3.1 and 3.3.2. The morphology observed that thin film have uniform in nature having porous which porosity is applicable for gas sensing property as well as electrical store capacitance.

Fig 3.3.1 Electron microscopy morphology PANI-Aleovera Mn SO₄
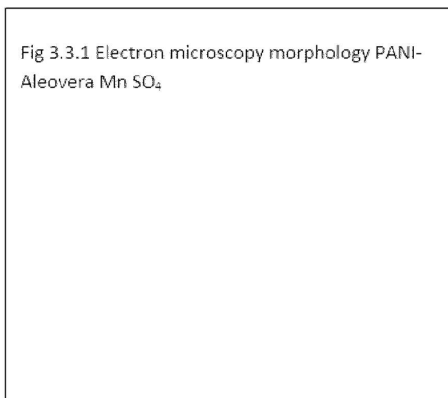
Fig 3.3.2 PANI-Aleovera Zn SO₄
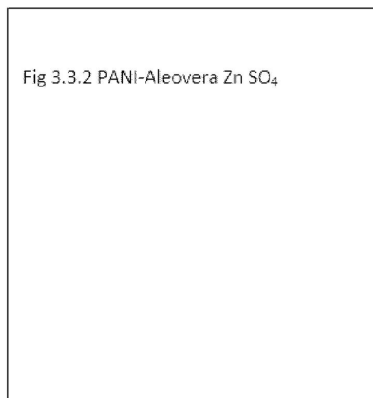
3.4. Electrochemical behavior

The electrical conductivity measurements or the synthesized Mn and Zn doped metal salt thin films were calculated by four probe methods by wejood. Figure 3.4 shows the electrical conductivity as a function of polymerization period and applied potential for PANI metal doped at 4 PH. The electrical conductivity increase as the applied potential is increase is for MnSO₄ metal doped and ZnSO₄. The value of conductivity at different temperature range to appled voltage 1volt to 10volt 300 k to 315 k Range Fig 3.4.1 indicate it varies 55.3×10^4 S·cm^{-1} for PANI Aleovera doped MnSO₄ metal salt and 6.4×10^4 S·cm^{-1} PANI Aleovera doped ZnSO₄ metal salt at 300k.
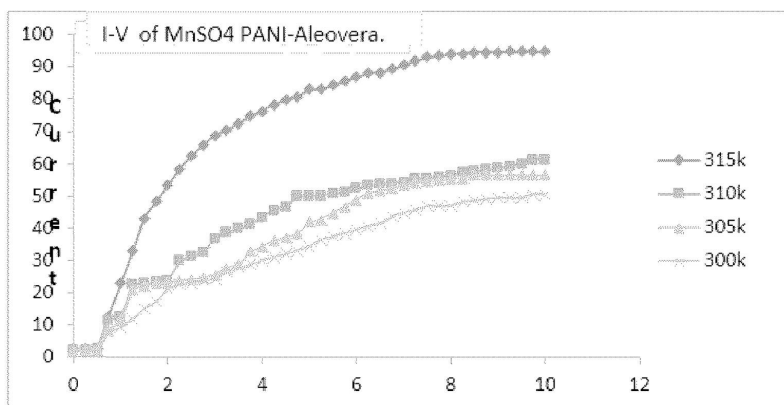
Fig 3.4.1 I-V behaviors of PANI Aleovera MnSO$_4$
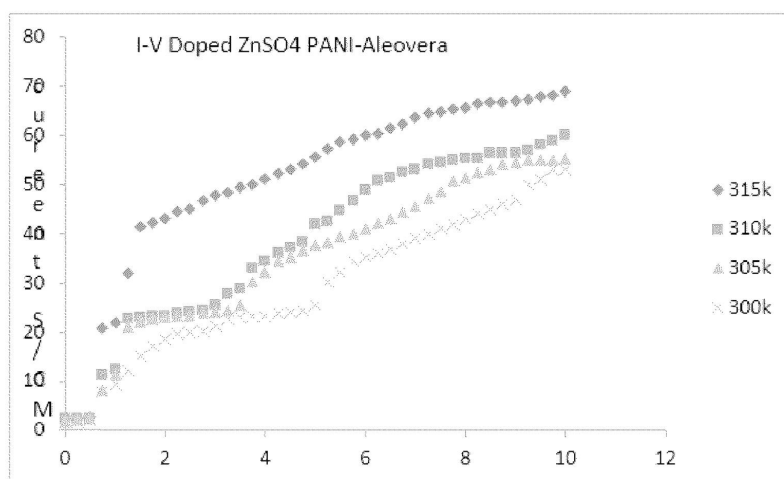
Fig 3.4.2 I-V behaviors of PANI Aleovera ZnSO$_4$

The electrical behavior was observed MnSO$_4$ doped PANI Aleovera film at 1 volt to 10 volt at different temperature from 300k to 315k. it observed that as temperature increase at that range then it shows that temperature increase then current also increase for both films but at 300k electrical DC conductivity is 55.3×10^4 S·cm^{-1} and 6.4×10^4 S·cm^{-1}.

Conclusion

This study related to successfully synthesized MnSO$_4$ doped PANI Aleovera film and ZnSO$_4$ doped PANI Aleovera film and confirm the synthesized films have metal like MnSO$_4$ and Zn SO$_4$ and polyaniline -Aleover confirms with help of chaterization technique like U.V, FTIR and Electron Microscopy. The DC electrical conductivity observed at different at variable temperature for both metal salts as the temperature is increase the conductivity is increases. From

300k to 315k. the stable conductivity also at 300k is electrical DC conductivity is 55.3×10^4 $S \cdot cm^{-1}$ and 6.4×10^4 $S \cdot cm^{-1}$.

References

1. George Soupions, Pantelitsa Georgiou and Loukas Zoumpoulakis "Polymer Composite Materials Fiber-Reinforced for the Reinforcement/Repair of Concrete Structures" Polymers 2020, 12(9), 2058 pp 1-14; https://doi.org/10.3390/polym12092058.

2. L S faeq "Thermal and Mechanical Properties of Polymer/Nickel Composites" 3rd International Conference on Sustainable Engineering Techniques (ICSET 2020) IOP Conf. Series: Materials Science and Engineering 881 (2020) 012092 IOP Publishing pp 1-8 doi:10.1088/1757-899X/881/1/012092.

3. Ewelina Mackiewicz, Tomasz Wejrzanowski , Bogusława Adamczyk-Cie′slak and Graeme J. Oliver "Polymer–Nickel Composite Filaments for 3D Printing of Open Porous Materials"Materials 2022, 15(4), 1360 pp 1-15; https://doi.org/10.3390/ma15041360.

4. Hind Ahmed, Bahaa H. Rabee, Hussein Hakim, Ahmed Hashim and Saba R. Salman "Preparation and Study of Optical Properties of (Polymer-Nickel Nitrate) Composite"Advances in Physics Theories and Applications, ISSN 2225-0638,Vol.20, 2013 pp 152-157.

5. R. K. Goyal, R. Sulakhe"Study on poly (vinylidene fluoride)/nickel composites with low percolation"Adv. Mater. Lett. 2015, 6(4), 309-317DOI: 10.5185/amlett.2015.5627.

6. M. Lahelin a, I. Aaltio b, O. Heczko b, O. Söderberg b, Y. Ge b, B. Löfgren a, S.-P. Hannula b, J. Seppälä a "DMA testing of Ni–Mn–Ga/polymer composites"omposites Part A: Applied Science and Manufacturing publishes Volume 40, Issue 2, February 2009, Pages 125-129 https://doi.org/10.1016/j.compositesa.2008.10.011.

7. Hafiza Vaneeza Hussain,MateebAhmad, Muhammad Tamoor Ansar , Ghulam M. Mustafa , Saira Ishaq , Shahzad Naseem , Ghulam Murtaza , Farah Kanwal and Shahid Atiq "Polymer based nickel ferrite as dielectric composite for energy storage applications"Synthetic Metals, Volume 268, October 2020, 116507 https://doi.org/10.1016/j.synthmet.2020.

8. Mohd Mohsin Nizam Ansari, Shakeel Khan and Naseem Ahmad "A comprehensive investigation of structural, thermal and electrical properties of $T_{0.35}Zn_{0.55}Cu_{0.1}Fe_2O_4$ (T

82

= Mn, Ni) nano ferrites"Physica B: Condensed Matter,Volume 566, 1 August 2019, Pages 86-95.https://doi.org/10.1016/j.physb.2019.05.003.

A. Suhasiniaand K. P. Vinod Kumar "Solubility and swelling studies of polymer hybrid-nickel oxide nanocomposite"J. Indian Chem. Soc.,Vol. 96, January 2019, pp. 7-8

9. Wangping Wu, Dingkai Xie, Jiaqi Huang,Qinqin Wang and Junjun Huang "Adhesion enhancement for nickel layer deposited on carbon fiber reinforced polymer (CFRP) composites by pretreatment processes for lightning strike"https://doi.org/10.1080/00218464.2022.2082870.

10. Thanh-Hai Le Yukyung Kim, and Hyeonseok Yoo "Electrical and Electrochemical Properties of Conducting Polymers" Polymers (Basel). 2017 Apr; 9(4): 150.

11. Imene Bekari-Abbes and Ezzeddine srasra "Electrical and Dielectric properties of polyaniline and Polyaniline montmormorillonite nanocomposites prepared by solid reaction using spectroscopy impendence." Journal of nanomaterials vol 2015 page 1-8.

SYNTHESIS OF 2-AMINO-4H-CHROMENE DERIVATIVES VIA THREE COMPONENT REACTION USING SODIUM BENZOATE AS A GREEN CATALYST

B. J. Yeotikar[a], N. H. Deore[a], R. Patil[a], S. S. Katkar[b], S. V. Deshmukh[c] and A. H. Kategaonkar[d]*

[a]*Department of Chemistry, K.S.K.W. Arts, Science and Commerce College CIDCO Nashik-422 008, Maharashtra, India*
[b]*Department of Chemistry, MSS'S Arts, Science and Commerce College, Ambad, Dist. Jalna-431 204, Maharashtra, India*
[c]*Department of Chemistry, Shri Dr. R. G. Rathod Arts and Science College, Murtizapur, Dist-Akola-444 107, Maharashtra, India*
[d]*Department of Chemistry, G.M.D. Arts, B.W. Commerce and Science College, Sinnar, Dist. Nashik-422 103, Maharashtra, India*
[*]*Corresponding Author Email: amol.kategaonkar@gmail.com*

ABSTRACT: To synthesize the chromene and benzochromene derivatives with the use of salt catalyst i.e sodium benzoate. This is multicomponent reaction This is carried out by using reactants benzaldehyde , malanonitrile and activated phenols like resorcinol, 1-naphthol and 2-naphthol, mixture of ethanol and water is used as a solvent. The synthesis takes place by taking care of environment and use of hazardous solvents, catalysts and chemicals is reduced.

KEYWORD: Chromene, Benzochromene, activated Phenol, Malanonitrile, Multicomponent reaction

INTRODUCTION:
In the heterocyclic compounds amino chromenes and chromenes are important as structural precursors that have gained tremendous value in organic and medicinal chemistry. Chromenes are exploited for synthesis of cosmetics, pigments [I] and potentially biodegradable agrochemicals [II]. Pharmacologically active compounds [III] are made by utilising chromene as an important precursor [III]. In the medicinal chemistry and chemical biology Chromene skeleton plays important structural part. Antimicrobial, mutagenicity, antiviral, anti-proliferative, antitumor, central nervous system activities (CNS) activities [III] are some of the important activities that are shown by Chromene skeleton. 2*H*-chromenes are utilised in synthesis of natural products. Chromene compound are used as photochromic materials. Chromenes proves to provide important biological activities such as antimicrobial [IV], antibacterial [IV], anticancer, anticoagulant, antioxidant, anti-inflammatory, anti-

797

tubercular, antiviral [V], anti-fungicidal, anti- anaphylactic activity [VI]. We are practicing to taking care of inexpensive and less hazardous catalysts and reagents. It is important from the industrial point of view and also should be less hazardous for environment. The increasing attention during the last decades for environmental protection has led modern academic and industrial groups to develop chemical processes with maximum yield and minimum cost whilst using nontoxic reagents, solvents and catalysts [VII]. MCRs reaction allows us to synthesize complex molecules from simple reactants and one step reaction. This is beneficial because it reduces expenses and energy and minimises the production of waste and toxic Chemicals that are hazardous for environment. It is important to carry out the synthesis of 2-amino-4*H*chromene by using energy efficient procedure. By using environment friendly catalysts and solvents and using reactants such as aldehydes, malanonitrile and activated phenols [VIII] (MCR) reaction includes two or more than two steps and isolation of intermediate do not takes place in this process, it is profitable strategy for industrial synthesis and saving time also good for environmental point of view. It helps to reduce time, energy and cost of the process [IX]. 2-amino-4*H* chromene with cyano-functionality is used as antitherapeutic effect to cure rheumatoid, psoriasis, and cancer. It also acts as pigments, laser dyes, optical brighteners, fluorescence markers, and also biodegradable agro chemicals [X]. Various methods have been performed for synthesis of chromene using catalyst such as silica nanoparticles [XI]. Because of the reasons such as to produce the desired products with the easily obtainable reactants with the help of single step without isolation of intermediate One-pot multicomponent reaction gets recognition in industrial synthesis using energy efficient way[XII] and also by taking care of principles of green chemistry. With the help of reactants such as malanonitrile, aldehyde and activated phenols or naphthol by using reflux condition and acetonitrile or DMF is used as solvent by using basic ionic liquid catalysts such as [bmim] OH amino-chromenes have been synthesized[XIII]. Various methods for preparation of heterocycles have been reported [XIV-XX]. We are trying to work on the procedure to synthesize aminochromene derivatives with the help of green solvents and green reusable salt catalyst by MCR in the organic synthesis; this gives us idea to use sodium benzoate as a green catalyst by performing condensation reaction between aldehydes, active methylene reagents and activated phenols. Sodium benzoate is the sodium salt of benzoic acid, widely used as a food preservative and a pickling agent. It appears as a white crystalline chemical compound.

EXPERIMENTAL:
All the melting points were determined in open capillaries in a paraffin bath and are uncorrected. The progress of the reactions was monitored by TLC.
General Procedure for synthesis of 2-amino-4-aryl-7-hydroxy 4*H*-chromene-3 Carbonitrile 1a
Method A
A mixture of appropriate benzaldehyde (1mole), malanonitrile (1mole), resorcinol (1mole) and sodium benzoate as a catalyst is added (1mole) to this mixture (1:1) ratio of ethanol and water is added as a solvent. The reaction mixture is stirred for 150 minutes. The progress of reaction is monitored by TLC. When the product obtained it is extracted with ethyl acetate, then 4 ml water is added remove the water layer. Catalyst is removed with aqueous layer as catalyst is soluble in water. the organic layer is dried by adding sodium sulphate. the dried material is then recrystallized with ethanol. Pale yellow crystals are obtained. (MP:-209-215 ºC)
**Method B**
A mixture of appropriate benzaldehyde (1mole), malanonitrile (1mole), resorcinol (1mole) and sodium benzoate as a catalyst is added (1mole) to this mixture (1:1) ratio of ethanol and

798

water is added as a solvent. The reaction mixture is stirred for 150 minutes. The progress of reaction is monitored by TLC. The precipitate obtained is filtered and washed with water. Catalyst is removed with water. Dry and crude product is recrystallized with ethanol. Pale yellow crystals are obtained. (M.P-208-218 ºC)

RESULT AND DISCUSSION: We have performed the synthesis of 2-amino-4*H*-derivative by three component efficient reaction between aromatic aldehydes, malanonitrile and resorcinol, α-naphthol and β-naphthol by using ethanol and water as a solvent by using sodium benzoate as an efficient catalyst at room temperature. The method gives efficient and improved pathway for the synthesis of chromenes in terms of short reaction time and reusable and green catalyst. The catalyst is soluble in water and easy to recover or remove and reaction proceeds in short period of time.
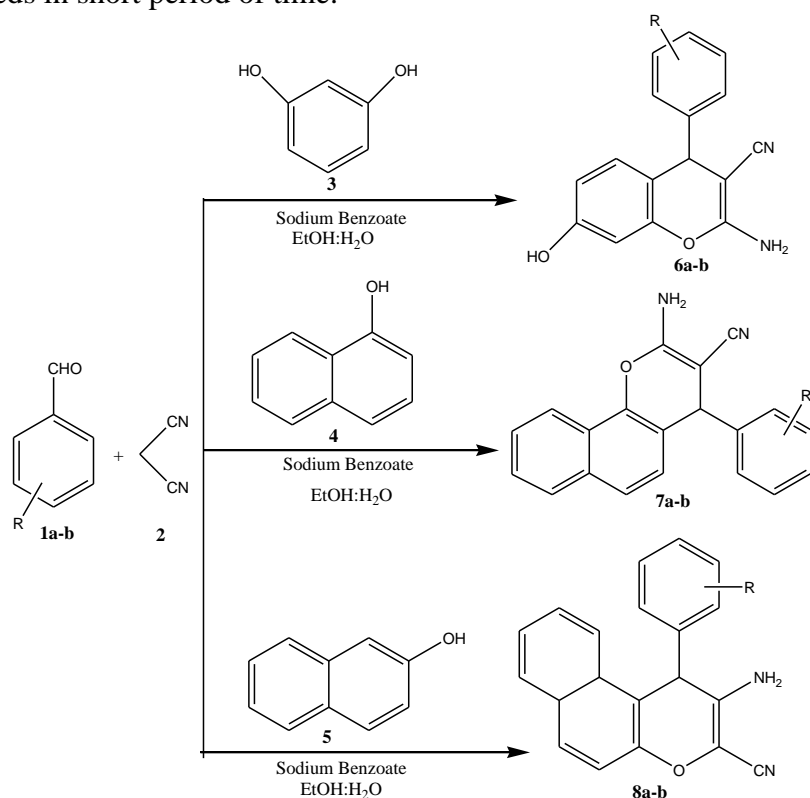
Our interest is to synthesize the substituted chromenes and benzochromenes by using sodium benzoate as a green catalyst and green solvents like ethanol and water. When the solvent is not used reaction takes more time to proceed by using energy efficient procedure. We started the synthesis by allowing reaction of a mixture of aromatic aldehydes, malanonitrile and resorcinol in equimolar amount (mole ratio 1:1:1) by using stirring condition at room temperature containing catalytic amount of sodium benzoate and the solvents used in this reaction is the mixture of ethanol and water in the ratio (1:1) to give 2-amino-4aryl-7 hydroxy-4*H* Chromene-3-carbonitriles.2-naphthol give the above one-pot three-component reactions for extended periods. When solvent is not used in above reaction takes more time to proceed even if we provide the temperature and gives minimum yield when, a mixture of ethanol and water was used as a solvent in the previous reactions, the three phenols gave the desired products in good yields at room temperature. Some of the products were sticky solids but after recrystallization it appeared as crystals. We can remove or recover catalyst by filtration/washing process with water or extraction process because catalyst we have used is soluble in water. All known compounds were identical in all physical and spectroscopic

799

aspects with the others which are the structures of the isolated products were confirmed on the basis of their elemental analysis and spectral data.

The structure of the isolated product **6a** was confirmed on the basis of LCMS data shows that a sharp broad peak is obtained. at the retention time 1.54. at this retention time mass obtained is 265.14 (m+2). and the reported mass of the product is 264. Furthermore in the ^{1}H NMR the presence of aromatic protons shows value in between 7.2-7.4 ppm protons adjacent to the OH group shows value 6.8 ppm and 6.9 ppm. The presence of NH_2 group is confirmed with value 4.8 ppm, OH proton give signal at 9.7ppm. Aromatic protons adjacent to the OH group shows value 6.8ppm and 6.5ppm. Aromatic protons that are adjacent to the CN group show the value 6.4ppm due to de-shielding effect.

Table No 1- Synthesis of substituted 2 amino chromenes by using sodium benzoate

Sr. no	R	Substrate	Products	time(minutes)	M.P[3] (^{o}C)	Yield (%)[a]
1	H	Resorcinol	6a	150	220-222	90
2	H	1-naphthol	7a	150	208-210	82
3	H	2-naphthol	8a	180	278-280	80
4	4-Cl	Resorcinol	6b	150	164-169	92
5	4-Cl	1-naphthol	7b	180	232-234	85
6	4-Cl	2-naphthol	8b	180	188-191	82

[a]Isolated Yields.

SPECTRAL ANALYSIS:
All known compounds were identical in all physical and spectroscopic properties with the structure of isolated product on the basis of their elemental analysis and spectral data.
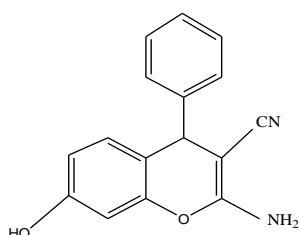
2-amino-4phenyl-4H-benzo(h)chromene-3-carbonitrile

^{1}H NMR (DMSO-d6, 400 MHz ppm): 4.6 (s, 2H, NH$_2$), 6.4 (s, 1H, H-Ar), 6.5 (d, 1H, H-Ar), 6.8 (d, 1H, H-OH), 6.9 (d, 2H, H-Ar), 7.2 (t,3H, Ar-H),7.3(dd, 2H, Ar-H), 9.7 (s, 1H, O-H)
LCMS: m/z 265.14(m+2)

CONCLUSION:
We have found a new way of synthesizing amino chromenes of expected biological and chemical characteristics using energy efficient, green, and environment friendly procedure by using salt catalyst i.e. sodium benzoate, as an green, reusable and efficient catalyst for this reaction by taking care of 12 principles of green chemistry.

REFERENCES:

I.	G.P. Ellis, A Weiss-berger and E.C Taylor *EDS* chapter 2,pp 11-139 John Wiley, New York, NY, USA**, 1977**
II.	Kai Gong, Hua-Lan Wang, Jun Luo, and zu-Liang Liu, *Wiley Interscience,* **2009**
III.	Awatef Mohammad El- Maghraby ,A. M. *Org Chemistry international* **2014**
IV.	M. M Khafagy A. H. F. A. El-Wahab, F. A. Eid, and A.M. EAgrody, *Farmaco*, Vol, no 9, pp. 715-722, **2002**
V.	Mohammad G. Dekamin, Mohammad Eslami, Ali MalekiTetrahedron 69(2013) 1074-1085 **2012**
VI.	Javad Safari Zohre Zarnegar, *Journal of Molecular Structure* volume 1072, pages 53-60 **2014**
VII.	Musa M. MusaJay M. Pateland Robert S. Phillips, *ACS Catal.* **2015**
VIII.	Martinez-Grau and J.L. Macro, friendlander *Letters*, vol 7, no 24 pp 3165-3170,**1997**
IX.	Bita Baghernejad, Samaneh Koosha , Payame Noor, *journal of Applied Chemical research* 14, 3, 19-25 **2020**
X.	H. Eshghi S. Damavand & G. H. Zohuriages, *synth React Inorg Met,* **2011**
XI.	a)Abdolmohammadia, S; Balalaie, S *Tetrahedron Lett* **2007**, 48, 3299; (b) Balalaie, S; Bararjanian, M; Sheikh-Ahmandi M. *Synthetic commun* **2007**, 37, 1097
XII.	a) Foye, W.O. Prinicipidi Chemico Farmaceutica; Piccin; Padova, Italy, **1991**, P 416; (b) Bonsignore,L ; Loy, G; Secci, D; Calignano, A *Eur J Med chem.* **1993**, 28, 517
XIII.	Ishmael B Masesane & Shetonde O Mihigo *Synthetic communication* **2015**
XIV.	Sara Hosseinzadeh-Baghan, MasoudMirrzari, Hossein Eshtiagh-Hosseini,Vahideh Zadsirjan, Majid M. Heravi, Joel T. Mague *John Wiley & sons* **2020**
XV.	Ishmael B Masesane & Shetonde O Mihigo *Synthetic communication* **2015**
XVI.	a) Bloxham, J; Dell, C. P; Smith C. W. Heterocycles Yu, H. Z. *Synthetic Common* **2004,** 34, 509; (b) Jiang H.;Tu, S, J ; Fang, F; Wang, X. S.. Chin *J Org Chem*, **2004**, 24, 1458 (c) Zhou, J F; Tu,S. J.; Gao, Y chin *J Org Chem*, **2001**, 21,742
XVII.	Y Sarrafi, E Mehrasbi, A Vahid, M Tajbakhsh Chinese *journal of Catalysis*, **2012**
XVIII.	C. J. Li and T.H. Chan, Organic Reactions in aquous media, Wiley, New York, NY, USA,**1997**.

XIX. Jafari-Moghaddam, S. A. Beyramabadi, M. Khashi, A. Morsali, *J. Mol. Struct.* **2018**, 1153, 149.

XX. Mostafa Habibi-Khorassani, M. Shahraki, E. Mollashahi,S.Shadfar Pourpanah, S. Keshavarz Majdabadi, **2016,** 19, 865

Received on February 23, 2023.

KANTOWSKI SACHS MACROSCOPIC BODY COSMOLOGICAL MODELS IN SCALAR TENSOR THEORIES OF GRAVITATION

A.S. NIMKAR[1], S.R. HADOLE[2] AND S.C. WANKHADE[3]

DEPARTMENT OF MATHEMATICS, SHRI DR. R. G. RATHOD ARTS AND SCIENCE
COLLEGE, MURTIZAPUR, DIST.AKOLA, MAHARASHTRA (INDIA)
E-MAILS: [1]ANILNIMKAR@GMAIL.COM, [1]SANGITA.HADOLE2000@GMAIL.COM AND
[3]SHARVARIWANKHADE006@GMAIL.COM

ABSTRACT. In this paper, we have obtained the field equations in scalar-tensor theories of gravitation proposed by Brans-Dicke [5] and Saez-Ballester [28] with the aid of Kantowski Sachs Space time in the presence of macroscopic body. Both theories' field equations can be solved definitively by using transformation.The present discussion explores into the expression involving energy density, energy flow vector, stress tensor, and specific physical features of both of these models.

AMS Classification: 54H20.

Keywords: Kantowski-Sachs model; Brans-Dicke; Saez-Ballester theory; Macro-scopicbody.

1. INTRODUCTION

Scalar-tensor theories are considered essential in explaining gravitational interactions in the range of the Plank scale. Many theories, such as string theory, higher order theories in the Ricci scalar, extended inflation and others demand the presence of a scalar field. Scalar-tensor theories of gravity are widely regarded as the most natural extensions of general relativity. These theories propose that the force of gravity is expressed not only by the metric of space-time, but also by a scalar field. The gravitational constant is a dynamical variable that is determined by the

Stability of Axially Symmetric Cosmological Model in Lyra Geometry

A. S. Nimkar[*], J. S. Wath

Department of Mathematics, Shri. Dr. R. G. Rathod Arts & Science College, Murtizapur, Dist. Akola (M.S.) India

Abstract

The present study concerns an examination of a cosmological model that exhibits axially symmetric and incorporates perfect fluid within the context of Lyra geometry. The field equations are solved by utilising the relation between the metric coefficients and the equation of state for a stiff fluid. The physical and kinematic properties, namely the Hubble parameter, the deceleration parameter, the energy density, and the pressure, have been examined, and their graphical behaviour has been analysed. Furthermore, we examined several additional parameters, including the redshift and the Om(z) diagnostic, and verified the stability of the model by utilising the sound speed ratio and perturbation technique.

Keywords: Axially symmetric space-time; Lyra Geometry; Perfect fluid.

1. Introduction

Since the introduction of Einstein's theory of gravitation, attempts have been made to unify the field theories; such a theory would be required to generalize the usual Riemannian space-time. Weyl [1] made one of the best attempts in this direction. He proposed a more general theory in which electromagnetism is also described geometrically. Later, Lyra [2] suggested a modification of Riemannian geometry, which may also be considered a modification of Weyl's geometry, by introducing a gauge function into the structure less manifold, which removes the non-integrability condition of the length of a vector under parallel transport and a cosmological constant is naturally introduced from the geometry. In the subsequent investigations, Sen [3], Dunn *et al.* [4] formulated a new scalar-tensor theory of gravitation and constructed an analog of Einstein's field equations based on Lyra's geometry.

Halford [5] says that the current theory predicts the same effects within the limits of what can be seen when it comes to the classic tests of the solar system. Soleng [6] has pointed out that the constant displacement field in Lyra's geometry will either include a creation field and be equal to Hoyle's creation field in cosmology [7-9] or contain a

---

[*] *Corresponding author*: anilnimkar@gmail.com

special vacuum field, which together with the gauge vector term may be considered a cosmological term.

The field equations (in geometrized units for which $c = 1$, $G = 1$), in normal gauge for Lyra's manifold, obtained by Sen [3] as

$$R_{ij} - \frac{1}{2}R g_{ij} + \frac{3}{2}\varphi_i\varphi_j - \frac{3}{4}g_{ij}\varphi^k\varphi_k = -8\pi T_{ij} \qquad (1)$$

where φ_i is the displacement vector field and defined as $\varphi_i = (\beta(t),0,0,0)$ and Conservation law $T_{ij} = 0$ \qquad (2)

Agrawal *et al.* [10] studied vacuum solutions of *FRW* and axially symmetric space-time in *f(R)* theory of gravity, Mete *et al.* [11] investigated an axially symmetric non-static space-time in the presence of bulk stress in the scalar-tensor theory formulated by Saez and Ballester, Sahoo *et al.* [12] studied an axially symmetric cosmological model in *f(R, T)* gravity in the presence of perfect fluid. Vinutha *et al.* [13] studied the Kantowski–Sachs perfect fluid cosmological model in R2-Gravity. Hadole *et al.* [14] studied Bianchi type VI_0 string cosmological model in Lyra's manifold. Pradhan *et al.* [15] examined some exact Bianchi type-V cosmological models in scalar tensor theory : kinematic tests. Reddy *et al.* [16] studied axially symmetric cosmic strings and domain walls in Lyra geometry. Adhau *et al.* [17] investigated an axially symmetric non-static space-time in the presence of thick domain walls with scalar-tensor theories formulated by Brans and Dicke. Sharma *et al.* [18] presented a comparative study of transit FRW and axially symmetric cosmological models in the framework of domain walls in *f(R, T)* modified theory of gravity considering the time-dependent deceleration parameter. Hegazy *et al.* [19] studied Bianchi's type VI_0 model in Lyra geometry. Yadav *et al.* [20] investigated a model of the quintessence universe with the dominance of dark energy in Lyra geometry. Aditya *et al.* [21] studied the Bianchi type-IX model in the presence of anisotropic dark energy and a massive scalar meson field in Lyra geometry. Mollah *et al.* [22] investigated the behavior of viscous fluid in string cosmological models within the framework of Lyra geometry. Reddy [23] static and non-static plane-symmetric string cosmological models are obtained in the Lyra manifold.

Many authors have studied the stability of cosmological models using various techniques, some of them are Nimkar *et al.* [24], Geovanny *et al.* [25], Katore *et al.* [26, 27], Shah *et al.* [28], Ahmed *et al.* [29], Sharif *et al.* [30], Knutsen [31,32], and Wanas *et al.* [33], Vinutha *et al.* [34], Koussour *et al.* [35], Yadav *et al.* [36], Chiang-Mei Chen *et al.* [37], and Saha *et al.* [38]. Also, Santhi *et al.* [39], Thakur [40], Zhai *et al.* [41], and Debnath *et al.* [42] proposed a new parameter called the $Om(z)$ diagnostic.

Drawing inspiration from the previously mentioned works, this research investigates an axially symmetric cosmological model with perfect fluid in the presence of Lyra geometry. The work is organised as follows: after the introduction, Section 2 provides a description of the metric and field equations. Section 3 is devoted to the solution of the field equations. Section 4 is dedicated to the examination of the physical and kinematical properties of the model. Section 5, Stability Analysis, and the last section contain some conclusions.

2. Metric and Field Equations

Consider the axially symmetric space-time given by Bhattacharya and Karade [43] in the form

$$ds^2 = dt^2 - A^2(t)(d\chi^2 + f^2(\chi)d\varphi^2) - B^2(t)dz^2 \tag{3}$$

Where A, B are functions of the proper time t alone while f is a function of co-ordinate χ alone.

The energy-momentum tensor for perfect fluid is given by

$$T^{ik} = (p + \rho)u^i u^k - pg^{ik} \tag{4}$$

Here p is the pressure, ρ is the energy density, and u_i is the four-velocity vectors of the distribution, respectively.

From Eq. (4), we have

$$T_1^1 = T_2^2 = T_3^3 = -p \text{ and } T_4^4 = \rho \tag{5}$$

The trace of energy-momentum tensor is given by

$$T = T_1^1 + T_2^2 + T_3^3 + T_4^4 = -3p + \rho$$

Using the equations (1), (2), (4), and (5), the field equations of metric (3) are

$$\frac{A_{44}}{A} + \frac{B_{44}}{B} + \frac{A_4}{A}\frac{B_4}{B} + \frac{3}{4}\beta^2 = -8\pi p \tag{6}$$

$$\frac{2A_{44}}{A} + \left(\frac{A_4}{A}\right)^2 - \left(\frac{f_{11}}{f}\right)\frac{1}{A^2} + \frac{3}{4}\beta^2 = -8\pi p \tag{7}$$

$$\frac{2A_4}{A}\frac{B_4}{B} + \left(\frac{A_4}{A}\right)^2 - \left(\frac{f_{11}}{f}\right)\frac{1}{A^2} - \frac{3}{4}\beta^2 = 8\pi\rho \tag{8}$$

$$\rho_4 + (p + \rho)\frac{B_4}{B} = 0 \tag{9}$$

Where the subscript '4' denote ordinary differentiation with respect to t. Together with equations (7) and (8), the functional dependency of the metric provides

$$\frac{f_{11}}{f} = k^2, k^2 = \text{Constant}$$

If $k = 0$, then $f(\chi) = (\text{constant} f)\chi$, $0 < \chi < \alpha$

By selecting the appropriate units for φ, it is possible to set this constant to 1. Thus, equations (7) and (8) will be transformed into the following as $f(\chi) = \chi$ results in the flat model of the universe [16].

$$\frac{2A_{44}}{A} + \left(\frac{A_4}{A}\right)^2 + \frac{3}{4}\beta^2 = -8\pi p \tag{10}$$

$$\frac{2A_4}{A}\frac{B_4}{B} + \left(\frac{A_4}{A}\right)^2 - \frac{3}{4}\beta^2 = 8\pi\rho \tag{11}$$

93

3. Solutions of Feld Equations

The field equations (6), (10), and (11) are three equations in five unknowns $A, B, \beta, p \& \rho$. Hence to get a determinate solution, one has to assume the relation between metric coefficients, i.e., $A = B^n$ and the condition of stiff fluid $\rho = p$ gives,

$$\frac{B_{44}}{B} + 2n\frac{B_4}{B} = 0 \tag{12}$$

The above equation admits an exact solution given by

$$A = N^n \{k_1 t + k_2\}^{n/2n+1} \tag{13}$$

$$B = N \{k_1 t + k_2\}^{1/2n+1} \tag{14}$$

Also,

$$p = -\frac{(3n+1)}{32\pi} \left[\frac{2nk_3{}^2 + k_4}{\{k_1 t + k_2\}^2} \right] \tag{15}$$

$$\rho = \frac{1}{8\pi} \left[\frac{(n+3)k_4 - n^2 k_3{}^2}{\{k_1 t + k_2\}^2} \right] \tag{16}$$

and $\beta^2 = \frac{4}{3} \left\{ \frac{2n(n+1)k_3{}^2 - (n+3)k_4}{\{k_1 t + k_2\}^2} \right\}$ $\tag{17}$

The axially symmetric cosmological model in equation (3) takes the form

$$ds^2 = dt^2 - N^{2n}(k_1 t + k_2)^{2n/2n+1}[d\chi^2 + f^2(\chi)d\varphi^2] - N^2(k_1 t + k_2)^{2/2n+1}dz^2$$

4. Physical and Kinematical Properties of the Model

In this section, some of the important physical parameters are given. Expansion Scalar, Hubble parameter, spatial Volume, Shear Scalar, and deceleration parameter are given by

Expansion Scalar: $\quad \theta = \frac{k_1}{3(k_1 t + k_2)}$ $\tag{18}$

Hubble Parameter: $H = \frac{k_1}{(k_1 t + k_2)}$ $\tag{19}$

Spatial Volume: $V = \sqrt{-g} = N^{2n+1}(k_1 t + k_2)\chi$ $\tag{20}$

Shear Scalar : $\sigma^2 = \frac{1}{2}\sigma^{ij}\sigma_{ij} = \frac{k_1{}^2}{54(k_1 t + k_2)^2}$ $\tag{21}$

Deceleration Parameter: $q = \frac{-3}{\theta^2}\left[\theta_{;\alpha}u^\alpha + \frac{1}{3}\theta^2\right] = 2$ $\tag{22}$

Average Scale factor $a(t) = V^{1/3} = (N^{2n+1}(k_1 t + k_2)\chi)^{\frac{1}{3}}$ $\tag{23}$

Graphs are plotted for particular values of the physical parameters and other integration constants.
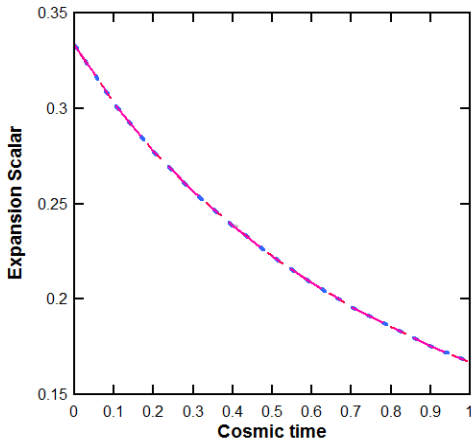
Fig. 1. Plot of Expansion Scalar Vs. Cosmic time for $k_1 = k_2 = 1,2,3$.
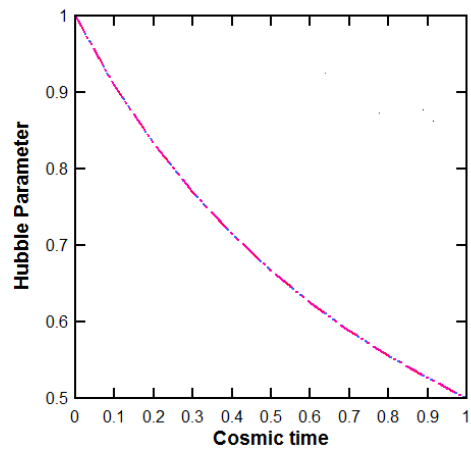
Fig. 2. Plot of Hubble Parameter Vs. Cosmic time for $k_1 = k_2 = 1,2,3$
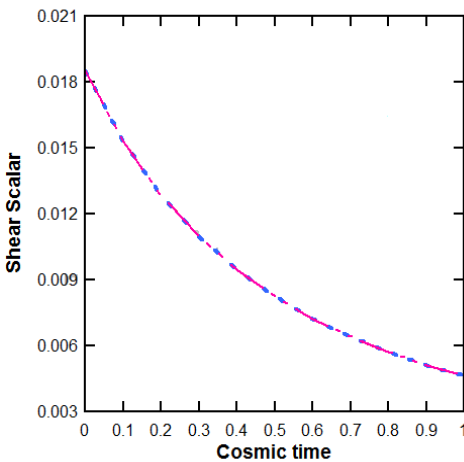
Fig. 3. Plot of Shear Scalar Vs. Cosmic time for $k_1 = k_2 = 1,2,3$.
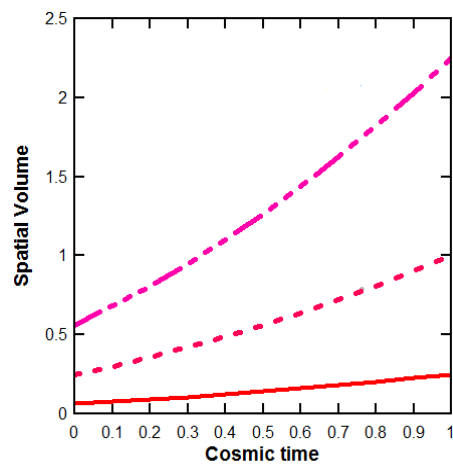
Fig. 4. Plot of Spatial Volume Cosmic time for $n = 0.5$ and $k_1 = k_2 = 1,2,3$.

The decomposition of a time-like tidal tensor is

$$u_{a;b} = N^{2n}\left(\frac{n}{2n+1}\right)k_1(k_1 t + k_2)^{\frac{-1}{2n+1}} + N^{2n}f^2\left(\frac{n}{2n+1}\right)(k_1 t + k_2)^{\frac{-1}{2n+1}} -$$

$$N^2\left(\frac{1}{2n+1}\right)k_1(k_1 t + k_2)^{\frac{1-2n}{2n+1}} \tag{24}$$

and, Vorticity $\omega_{11} = \omega_{22} = \omega_{33} = \omega_{44} = 0$ (25)

The vorticity of the model along *x, y, z,* and *t*-axes is zero. So, the obtained model is non-rotating. Whereas Vorticity is nonzero, the model is rotating.

4.1. *Redshift*

The scale factor a and redshift z are connected through the relation

$$1 + z = \frac{a_0(t)}{a(t)} \tag{26}$$

Where $a_0(t)$ is the present value of the scale factor, take $a_0(t) = 1$.

Using equation (23) and the relation $a(t) = \frac{1}{1+z}$, with z being the redshift, gives us the following relation

$$t = \frac{(1+z)^{-3} - k_2 N^{2n+1}\chi}{k_1 N^{2n+1}\chi} \tag{27}$$

From equation (19) and (27), gives

$$H(z) = k_1 N^{2n+1}\chi(1+z)^3 \tag{28}$$

4.2. *Om (z)* **diagnostics**

The starting point for Om(z) diagnostics is the Hubble parameter, and it is defined as

$$Om(z) = \frac{\left(\frac{H_z}{H_0}\right)^2 - 1}{(1+z)^3 - 1}$$

Thus, *Om(z)* involves only the first derivative of the scale factor through the Hubble parameter and is easier to reconstruct from observational data, gives

$$Om(z) = \frac{\left[k_1 N^{2n+1}\chi(1+z)^3\right]^2 - H_0^2}{H_0^2[(1+z)^3 - 1]} \tag{29}$$

From equation (29), it is observed that $Om(z)$ increases as z decreases, so $Om(z)$ increases due to the evolution of the universe.

5. Stability Analysis

In this section, check the stability of obtained model using the ratio of sound speed and perturbation technique.

Firstly, discuss the stability of the model by observing the ratio of sound speed given by $\frac{dp}{d\rho} = c_s^2$, A positive value of this ratio i.e., $c_s^2 > 0$, indicates a stable model, while a negative value i.e., $c_s^2 < 0$ indicates an unstable model.

In the present model,

$$c_s^2 = \frac{dp}{d\rho} = \frac{(3n+1)(2nk_3^2 + k_4)}{4(n^2 k_3^2 - (n+3)k_4)} \tag{30}$$

From Fig. 5, it is observed that for $k_3 = k_4 = 1$ and $n \geq 2.5$, the ratio of sound speed c_s^2 is positive, it gives the present cosmological model is a stable. Whereas for $n < 2.5$, the

ratio of sound speed $c_s{}^2$ is negative, so the present cosmological model is unstable. The stability condition of the model also depends on values of constant.
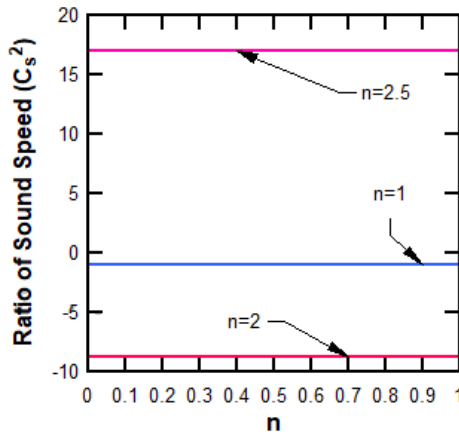
Fig. 5. Plot of ratio of sound speed Vs. constant n for $k_3 = k_4 = 1$.

Now, check the stability of the solution with respect to the perturbation of the metric. By using a perturbative technique, a through investigation of the stability of the relevant solutions may be performed. To ensure the stability of the precise or approximative background solution, perturbations of a gravitational system's fields should be compared to the background evolutionary solution [33-37]. Then investigate the stability of the background solution concerning metric perturbations. Here, the solutions' metric perturbation stability is as follows:

$$a_i \to a_{\boldsymbol{B}i} + \delta a_i = a_{\boldsymbol{B}i}\left(1 + \frac{\delta a_i}{a_{\boldsymbol{B}i}}\right) = a_{\boldsymbol{B}i}(1 + \delta b_i)$$

where $\delta b_i = \frac{\delta a_i}{a_{\boldsymbol{B}i}}$

Similarly, represent the perturbation in the spatial Volume as $V = \prod_{i=1}^{3} a_i$, directional Hubble parameter $H_i = \frac{\dot{a}_i}{a_i}$ and mean Hubble parameter $H_i = \frac{1}{3}\sum_{i=1}^{3} H_i$ as follows

$$V \to V_{\boldsymbol{B}} + V_B \sum_i \delta b_i,$$

$$H_i \to H_{\boldsymbol{B}i} + \sum_i \delta b_i,$$

$$H \to H_{\boldsymbol{B}} + \frac{1}{3}\sum_i \delta b_i$$

The following equations can be used to demonstrate how the metric perturbations δb_i, to the linear order in δb_i, obey them.

$$\sum_i \ddot{\delta b_i} + 2\sum_i H_{Bi}\dot{\delta b_i} = 0 \tag{31}$$

97

$$\ddot{\delta b_i} + \frac{\dot{V_B}}{V_B} \dot{\delta b_i} + \sum_j H_{Bi} \dot{\delta b_j} = 0 \tag{32}$$

$$\sum_i \dot{\delta b_i} = 0 \tag{33}$$

Solving equations (31)-(33), it gives

$$\ddot{\delta b_i} + \frac{\dot{V_B}}{V_B} \dot{\delta b_i} = 0 \tag{34}$$

For our model, background spatial volumes V_B is given by

$$V_B = N^{2n+1}(k_1 t + k_2)\chi \tag{35}$$

From above equations (31)-(35), obtain

$$\delta b_i = \frac{C}{N^{2n+1}\chi k_1} log(k_1 t + k_2) + C_1$$

Where C and C_1 are integrating constants. Therefore, the "actual" fluctuations for each expansion factor $\delta a_i = \delta b_i a_{Bi}$ is given by

$$\delta a_i = \left[\frac{C}{N^{2n+1}\chi k_1} log(k_1 t + k_2) + C_1 \right] N^{-(2n+1)}\chi^{-1}(k_1 t + k_2)^{-1} \tag{36}$$

The behavior of actual fluctuations δa_i as a function of time can be seen in equation (36), which also demonstrates that δa_i begins with a slightly positive value and rapidly decreases to zero as the universe expands. So, even when the gravitational field is perturbed, the background solution remains stable.

Conclusion

The present study examines a cosmological model that is axially symmetric and features Lyra geometry within a perfect fluid. In order to solve the field equations, we use the relation $A = B^n$ and the condition of the stiff fluid. In the present study, negative pressure and positive energy density were found. The concept of repulsive gravity is associated with the negative pressure that is present on a cosmological scale or within spherical entities like planets. Graphically, it can be observed that the spatial volume of the universe exhibits an increase as time progresses. This suggests that the universe's expansion originated from a finite volume and continues to expand as time elapses. Also, it is interesting to note that as t gradually increases, the scalar expansion θ, Hubble parameter H, and shear scalar. σ^2 decreases, which means all the physical parameters are well-behaved. In the present model $Om(z)$ increases as z decreases, so $Om(z)$ increases due to the evolution of the universe. For the values of $k_3 = k_4 = 1$ and $n \geq 2.5$, the ratio of sound speed c_s^2 is positive, This positive ratio leads to the stability of the current cosmological model. While for $n < 2.5$, the ratio of sound speed c_s^2 is negative, the present cosmological model is unstable. The values of the constants also have a role in determining the stability condition of the model. As the universe continues to expand, the value of the actual fluctuations δa_i starts out with a little positive sign and quickly

approaches zero. As a result, the background solution is stable against the perturbation of the metric.

References

1. H. Weyl, Sber Preuss Acad. Wiss. Berlin **465** (1918).
2. G. Lyra, Math. Z **54**, 52 (1951). https://doi.org/10.1007/BF01175135
3. D. K. Sen, Z. Physik **149**, 311 (1957). https://doi.org/10.1007/BF01333146
4. D. K. Sen and K. A. Dunn, J. Math. Phys. **12**, 578 (1971). https://doi.org/10.1063/1.1665623
5. W. D. Halford, Australian J. Phys. **23**, 863 (1970). https://doi.org/10.1071/PH700863
6. H. H. Soleng, Gen. Relat. Gravit. **19**, 1213 (1987). https://doi.org/10.1007/BF00759100
7. F. Hoyle, Monthly Notices of the Royal Astronomical Soc. **108**, 372 (1948). https://doi.org/10.1093/mnras/108.5.372
8. F. Hoyle and J. V. Narlikar - *Proc. of the Royal Society of London. Series A, Mathematical and Phys. Sci.* **273**, 1352 (1963). https://doi.org/10.1098/rspa.1963.0072
9. F. Hoyle and J. V. Narlikar, Proc. R. Soc. Lond. A **282**, 191 (1964). https://doi.org/10.1098/rspa.1964.0227
10. P. K. Agrawal and D. D. Pawar, Iran J Sci Technol Trans Sci **42**, 1639 (2017).
11. V. G. Mete, A. S. Nimkar, and V. D. Elkar, Int. J. Theor. Phys. **55**, 412 (2016). https://doi.org/10.1007/s10773-015-2675-2
12. P. K. Sahoo, B. Mishra, and G. C. Reddy, Eur. Phys. J. Plus **129**, 4 (2014). https://doi.org/10.1140/epjp/i2014-14049-7
13. T. Vinutha, K. V. Vasavi, K Niharika, and G. Satyanarayana, Indian J. Phys. **97**, 1621 (2023). https://doi.org/10.1007/s12648-022-02470-5
14. S. R. Hadole, A. S. Nimkar, A. M. Pund, South East Asian J. Math. Mathematical Sci. **18**, 379 (2022).
15. A. Pradhan, S. K. Singh, Electronic J. Theor. Phys. **7**, 407 (2010).
16. D. R. K. Reddy and M. V. S. Rao, Astrophys. Space Sci. **302**, 157 (2006). https://doi.org/10.1007/s10509-005-9022-7
17. K. S. Adhav, A. S. Nimkar, and R. L. Naidu, Astrophys. Space Sci. **312**, 165 (2007). https://doi.org/10.1007/s10509-007-9670-x
18. U. K. Sharma, A. K. Mishra, and A. Pradhan, Canadian J. Phys. **99**, 5 (2021).
19. E. A. Hegazy, M. Abdel-Megied, and A. A. Gedamy, Sohag J. Sci. **8**, 7 (2023). https://doi.org/10.21608/sjsci.2022.164780.1035
20. A. K. Yadav, G. K. Goswami, A. Pradhan, and S. K. Srivastava, Indian J. Phys. **96**, 1569 (2022).
21. Y. Aditya and U. Y. D. Prasanthi, Int. J. Modern Phys. A **37**, ID 2250107 (2022). https://doi.org/10.1142/S0217751X2250107X
22. M. R. Mollah and K. P. Singh, New Astronomy **88**, ID 101611 (2021). https://doi.org/10.1016/j.newast.2021.101611
23. D. R. K. Reddy, Astrophys. Space Sci. **300**, 381 (2005). https://doi.org/10.1007/s10509-005-4716-4
24. A. S. Nimkar and S. R. Hadole, J. Sci. Res. **15**, 55 (2023). http://dx.doi.org/10.3329/jsr.v15i1.59676
25. G. A. R. Franco, Eur. Phys. J. C. **80**, 677 (2020).
26. S. D. Katore and R. J. Baxi, Int. J. Phys. (2019).
27. S. D. Katore and S. P. Hatwar, Prog. Theor. Exp. Phys. ID 033E01 (2016). https://doi.org/10.1093/ptep/ptw009
28. P. Shah and G. C. Samanta, Eur. Phys. J. C **79**, 414 (2019). https://doi.org/10.1140/epjc/s10052-019-6934-x
29. N. Ahmed and Sultan Z. Alamri, Res. Astrono. Astrophys. **18**, 123 (2018).

30. M. Sharif and Saadia Mumtaz, EPJ Web Conf. **168**, ID 08006 (2018). https://doi.org/10.1051/epjconf/201816808006
31. H. Knutsen, Astrophys. Space Sci. **140**, 385 (1988). https://doi.org/10.1007/BF00638992
32. H. Knutsen, Astrophys. Space Sci. **232**,163 (1988). https://doi.org/10.1093/mnras/232.1.163
33. M. I. Wanas and M. A. Bakry, Astrophys. Space Sci. **228**, 239 (1995). https://doi.org/10.1007/BF00984978
34. T. Vinutha, K. Niharika, and K. S. Kavya, Astrophysics **66**, 64 (2023).
35. M. Koussour and M. Bennai, Class. Quantum Gravity (2022).
36. A. K. Yadav, P. K. Sahoo, and V. Bhardwaj, Mod. Phys. Lett. A **34,** ID 1950145 (2019). https://doi.org/10.1142/S0217751X19501458
37. C.-M. Chen and W. F. Kao, Phys. Rev. D **64**, 124019 (2001).
38. B. Saha, H. Amirhashchi, and A. Pradhan, Astrophys. Space Sci. **342**, 257 (2012). https://doi.org/10.1007/s10509-012-1155-x
39. M. V. Santhi and Y. Sobhanbabu, Indian J. Phys. **96**, 1867 (2022). https://doi.org/10.1007/s12648-021-02121-1
40. P. Thakur, Indian J. Phys. **96**, 981 (2022). https://doi.org/10.1007/s12648-021-02018-z
41. Z. -X. Zhai, M. -J. Zhang, Z. -S. Zhang, X. -M. Liu, and T. -J. Zhang, Phys. Lett. B **727**, 8 (2013).
42. U. Debnath and S. Chattopadhyay, Int. J. Theor. Phys. **52**, 1250 (2013). https://doi.org/10.1007/s10773-012-1440-z
43. S. Bhattacharya and T. M. Karade, Astrophys. Space Sci. **202**, 69 (1993). https://doi.org/10.1007/BF00626917

ORIGINAL PAPER

Anisotropic dark matter distribution in Saez–Ballester theory of gravitation

J S Wath* and A S Nimkar

Department of Mathematics, Shri. Dr. R. G. Rathod Arts & Science College, Akola District, Murtizapur, MS, India

Abstract: In this paper, Kantowski–Sach's cosmological model is investigated in presence of Saez–Ballester scalar tensor theory of gravitation and an anisotropic dark matter distribution the energy momentum tensor. Exact solutions of field equations are obtained by the law of Hubble parameter. An anisotropic stellar object's stability is discussed with the help of sound speed, Aberu's stability condition, and causality condition. In addition to this, we studied the physical aspects of the derived cosmological model, such as transverse and radial pressure, energy density, and anisotropy factor etc.

Keywords: Kantowski–Sach; Saez–Ballester; An anisotropic DM matter distribution the energy momentum tensor

1. Introduction

Einstein came up with the general theory of relativity (GR), which is a geometric theory of gravity [1]. GR says that things bend reality around them. Bodies that are gravitating are affected by gravity. The expanding of space–time shows how things move through it. Einstein's theory is based on the principle of relativity, the principle of general covariance, and the principle of equivalence. Gravitational waves (GR) can explain weak fields, but not strong field eras. Based on what we know about the world right now, we need new theories of gravity. In the past few years, cosmology, astrophysics, and high-energy physics have contributed to changes in gravity models.

There are various physical explanations for gravitation that explain some physical features of the phenomenon more fully. Numerous studies have been conducted on alternative theories of gravity and how they can be used in the study of the universe. We add a scalar field ϕ to the general theory of relativity to make all versions of the scalar tensor theories work. This scalar field, along with the metric tensor field, makes up the gravitational field. It is now possible to measure how gravitational interactions work with the help of alternative theories. These theories should also help us learn more about strong field times, like when we are close to black hole singularities or at the

Planck scales. The latest data from the cosmic microwave background, supernovae type Ia, and the Planck orbiter show that 95% of the energy budget of the universe comes from hidden matter, which is made up of dark matter and dark energy. This is causing the universe to expand faster than before. Both dark matter and dark energy are required in order for the picture we have of the universe to be accurate. In this regard, different theories of gravity have attracted a lot of attention and consideration. In many different versions of the GRT, compact stellar structures including quark stars, dark stars, gravastars, neutron stars, and black holes were taken into careful consideration. The explosion of massive stars known as supernovae can result in the production of odd compact stars such as neutron stars and quark stars (SN).

It is important to note that over the course of the past decades, numerous models of astrophysical objects such as stars and galaxies, among others, have been investigated in a variety of ways. This is in addition to the investigation of the cosmic evolution of the Universe in the scalar tensor theory, which makes a significant contribution to the discovery and understanding of a variety of relativistic phenomena. One of the most significant scalar tensor theories is Saez–Ballester theory. Recently, it has been shown that Saez–Ballester theory (SBT) is flexible enough to deal with the problem of dark energy and to allow for reconstruction scenarios [2–4]. In this theory, the metric potentials are linked to a scalar field, which is well-known for being an important part of gravity and cosmology [5–7]. In a broader sense, SBT has been talked about in Bianchi Cosmology

*Corresponding author, E-mail: jotsnawath@gmail.com

STABILITY OF MACROSCOPIC BODY COSMOLOGICAL MODEL IN RUBAN'S BACKGROUND

By

J. S. Wath and A. S. Nimkar

Shri Dr. R. G. Rathod Arts and Science College, Murtizapur, Dist. Akola, Maharastra, India-444107

Email: jotsnawath@gmail.com, anilnimkar@gmail.com

Abstract

In this paper, the Barber Self-Creation theory of gravitation is used to examine the stability of the cosmological model in the Ruban's background in the presence of macroscopic body. Exact solution is obtained by considering the relation between metric coefficients and radiation. The physical, kinematical, and thermodynamical aspects of the derived cosmological model have been examined. The relationship between sound speed, causality, and adiabatic index are used to discuss the stability of these models. Also, the discussion includes different energy conditions.

1 Introduction

Einstein's general theory of relativity *(GR)* has been used as a basis for many different alternative theories. In 1982, Barber [4] put up two hypotheses that would later be referred to as self-creation theories. His first theory is a modification of the Brans and Dicke theory (1961), while his second theory is a modification of general relativity. Both of these modifications were made independently. Brans [5] pointed out that Barber's first theory of self-creation is inconsistent with experiment as well as in general due to the fact that it violates the equivalence principle. Barber's second hypothesis, on the other hand, fixes earlier abnormalities while maintaining the first theory's appealing qualities. Einstein's field equations' gravitational coupling can be a variable scalar on the space-time manifold, according to Barber's second theory. In this theory the scalar field does not directly gravitate but simply divides the matter tensor with the scalar acting as a reciprocal gravitational constant.

In recent years, self-creation theory has been the focus of many authors, who have used different space-time models with different energy-momentum tensors. Katore *et al.* [15] have investigated phantomic behaviour of generalized ghost pilgrim dark energy models in self-creation theory. Wankhade *et al.* [36] have studied Bianchi type *VIII* cosmological model with wet dark fluid in Barber self-creation theory of gravitation. Nimkar *et al.* [24] have investgated Bianchi Type *IX* cosmological model in self-creation theory of gravitation. Vinutha *et al.* [35] have studied dynamics of *FRW* type Kaluza-Klein *MHRDE* cosmological model in self-creation theory. Pawar *et al.* [27] have investigated Bianchi type *IX* cosmological model with magnetized anisotropic dark energy by using Barbers self-creation theory are some of the researchers who have investigated the various aspects of Barbers second self-creation theory. The Barber field equation in second self-creation theory (Barber [4]) can be expressed as

$$R_{ij} - \frac{1}{2}Rg_{ij} = -8\pi\phi^{-1}T_{ij}, \tag{1.1}$$

and

$$\Box\phi = \phi^{'k}_{;k} = \frac{8\pi\lambda}{3}T, \tag{1.2}$$

where ϕ is the Barbers scalar,T_{ij} is the energy momentum tensor,
$\Box\phi$ is the invariant DAlembertian, T is the trace of energy momentum tensor T_{ij} , λ is a coupling constant to be determined from experiment and $0 <| \lambda |< \frac{1}{10}$.

1

In the limit $\lambda \to 0$, this theory approaches the Einsteins theory in every respect. Due to the nature of the space time Barbers scalar ϕ is a function of t.

There are a few studies in the literature about Ruban universe model. Lima *et al.* [18] have investigated the solutions of Ruban universe model with electromagnetic field. Lima *et al.* [19,20] have researched thermodynamics of Ruban universe model and they have studied inhomogeneous two cosmological models. Tomimura *et al.* [32] have obtained exact solutions of Ruban spacetime with dust, radiation and electromagnetic field. Recently, Aktas [1] studied energy momentum distributions of Ruban universe in general relativity and teleparallel gravity. Mete *et al.* [22] have investigated Rubans cosmological model in presence of bulk stress source in the framework of general theory of relativity.

In addition to this, Sarkar *et al.* [30], Bhar *et al.* [6,7], Nimkar *et al.* [25], Thirukkanesh *et al.* [33], Herrera [12], Ahmed *et al.* [2], Franco *et al.* [11], Knutsen [16,17], Wanas *et al.* [37] have analyzed stability of cosmological models using various methods. Hegazy [13], Hawking *et al.* [14], Santos *et al.* [31], Ayala *et al.* [3], Maity *et al.* [23], Prigogine *et al.* [28], Nojiri *et al.* [26] are some of the authors who have investigated different aspects of thermodynamics.

Based on the above research, we proposed to study the stability of Ruban's cosmological model in the presence of an energy momentum tensor for a macroscopic body. Our paper is organized as follows. In section 2, Metric and field Equations. Section 3, Solutions of field Equations. Section 4, The Physical and Kinematical Properties of the model. Section 5, Thermodynamics of the model, Section 6, Stability solution of the model, Section 7, Energy conditions, and the last section contains some conclusion.

2 Metric and field Equations

As everyone knows, models of the universe like the inhomogeneous and anisotropic Szekeres metrics are very important for explaining how the universe began. The Ruban universe model is also a special kind of the Szekeres universe [18]. It is not homogeneous and is not the same everywhere. Ruban's model of space- time is given by [29]

$$ds^2 = dt^2 - Q^2\left(x,t\right) dx^2 - R^2(t)\left(dy^2 + h^2 dz^2\right), \tag{2.1}$$

where

$$h(y) = \frac{sin\sqrt{k}y}{\sqrt{k}} = \begin{array}{ccc} siny & if & k = 1 \\ y & if & k = 0 \\ sinhy & if & k = -1 \end{array},$$

and k is the curvature parameter of the homogeneous 2-spaces t and x constants. The functions Q and R are free and will be determined.

The energy momentum-tensor for a macroscopic body (Landue and Lifshitz [21]) is given by

$$T^{ik} = \left(p + \varepsilon\right) u^i u^k - pg^{ik}. \tag{2.2}$$

Here p is the pressure, ε is the energy density and u_i is the four velocity vector of the distribution respectively.

From Eq. (2.2), we have

$$T_1^1 = T_2^2 = T_3^3 = -p, \quad T_4^4 = \varepsilon. \tag{2.3}$$

The trace of energy-momentum tensor is given by

$$T = T_1^1 + T_2^2 + T_3^3 + T_4^4 = -3p + \varepsilon. \tag{2.4}$$

Using the equations (1.1), (1.2) and (2.2) - (2.4), the field equations of metric (2.1) are

$$\frac{2R_{44}}{R} + \left(\frac{R_4}{R}\right)^2 + \frac{k}{R^2} = -8\pi\phi^{-1}p, \tag{2.5}$$

$$\frac{R_4 Q_4}{RQ} + \frac{R_{44}}{R} + \frac{Q_{44}}{Q} = -8\pi\phi^{-1}p, \tag{2.6}$$

$$\frac{R_4 Q_4}{RQ} + \left(\frac{R_4}{R}\right)^2 + \frac{k}{R^2} = 8\pi\phi^{-1}\varepsilon, \tag{2.7}$$

$$\left(\frac{2R_4}{R} + \frac{Q_4}{Q}\right)\phi_4 + \phi_{44} + = \frac{8\pi\lambda}{3}(-3p + \varepsilon), \tag{2.8}$$

where the subscript 4 after R, Q, ϕ denote partial differentiation with respect to t.

2

3 Solutions of field Equations

The above system of the equations (2.5) to (2.8) are four equations and five unknown R, Q, ϕ, p and ε. In order to solve this undermined system one additional constraints are required.

Hence to find a determinate solution we assume the relation between metric coefficients i.e. $Q = x^n R^n$ and radiation universe

$$\varepsilon = 3p, \tag{3.1}$$

$$(n+2)\frac{R_{44}}{R} + (n^2+n+1)\left(\frac{R_4}{R}\right)^2 + \frac{k}{R^2} = 0. \tag{3.2}$$

The above equation admits an exact solution given by

$$R = N_1(k_3 t + k_4)^{\frac{1}{N+1}}, \tag{3.3}$$

$$Q = N_2(k_3 t + k_4)^{\frac{n}{N+1}}, \tag{3.4}$$

and

$$\phi = -k_7(k_3 t + k_4)^{-\frac{(n+1)}{N+1}} + k_6, \tag{3.5}$$

where $N = \frac{(n^2+n+1)}{(n+2)}$, $N_1 = (N+1)^{\frac{1}{N+1}}$, $N_2 = x^n N_1^n$,
where k_3, k_4, k_6, k_7 are constants of integration.

Using equation (3.3) and (3.4), the Rubans cosmological model in equation (2.1) takes the form

$$ds^2 = dt^2 - N_2^2(k_3 t + k_4)^{\frac{2n}{N+1}} dx^2 - N_1^2(k_3 t + k_4)^{\frac{2}{N+1}}(dy^2 + h^2 dz^2). \tag{3.6}$$

Also, the pressure and density of obtained cosmological model is

$$p = \frac{1}{8\pi}\left[k_6 - \frac{k_7}{(k_3 t + k_4)^{\frac{n+1}{N+1}}}\right]\left[\frac{L + k_{10}(k_3 t + k_4)^{\frac{2N}{N+1}}}{(k_3 t + k_4)^2}\right], \tag{3.7}$$

and

$$\varepsilon = \frac{3}{8\pi}\left[k_6 - \frac{k_7}{(k_3 t + k_4)^{\frac{n+1}{N+1}}}\right]\left[\frac{L + k_{10}(k_3 t + k_4)^{\frac{2N}{N+1}}}{(k_3 t + k_4)^2}\right]. \tag{3.8}$$
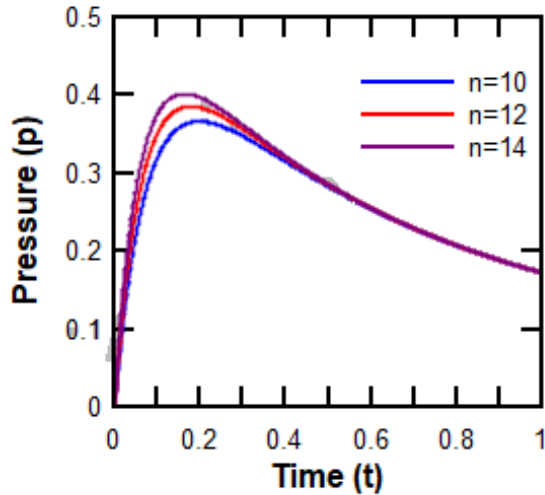

Figure 3.1: Plot of pressure Vs. time for $k_3 = k_4 = k_6 = k_7 = k_{10} = 1$ and $L = 0.5$, $N = 0.2$
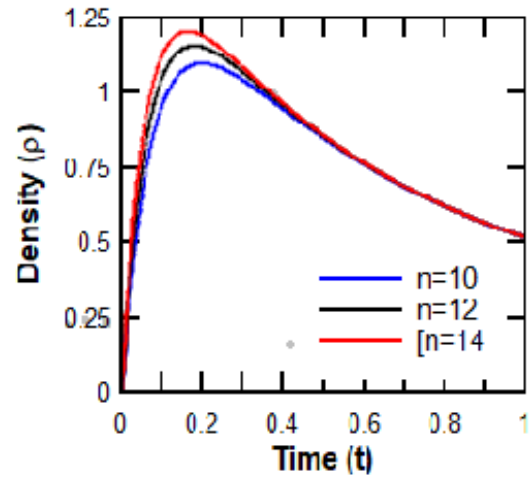
Figure 3.2: Plot of density Vs. time for $k_3 = k_4 = k_6 = k_7 = k_{10} = 1$ and $L = 0.5$, $N = 0.2$

From Fig. 3.1 and Fig. 3.2, it is clear that, pressure and density is positive throughout the evolution of universe.

3

4   The Physical and Kinematical Properties of the model

Some physical parameters of model spatial volume, shear scalar, Hubble parameter and expansion scalar are given by

Spatial Volume:
$$V = \sqrt{-g} = h N_1^2 N_2 (k_3 t + k_4)^{\frac{n+2}{N+1}}. \tag{4.1}$$

Shear Scalar:
$$\sigma^2 = \frac{1}{2}\sigma^{ij}\sigma^{ij} = \frac{k_3^2}{6(k_3 t + k_4)^2}\left(\frac{n+2}{N+1}\right)^2. \tag{4.2}$$

Hubble Parameter:
$$H = \frac{k_3}{3}\left(\frac{n+2}{N+1}\right)\frac{1}{(k_3 t + k_4)}. \tag{4.3}$$

Expansion Scalar:
$$\theta = k_3\left(\frac{n+2}{N+1}\right)\frac{1}{(k_3 t + k_4)}. \tag{4.4}$$

The graphs are plotted for particular values of physical parameters and other integration constants. Here the following graphs are plotted for $N_1 = N_2 = h = 2$ and $N = 0.2$.
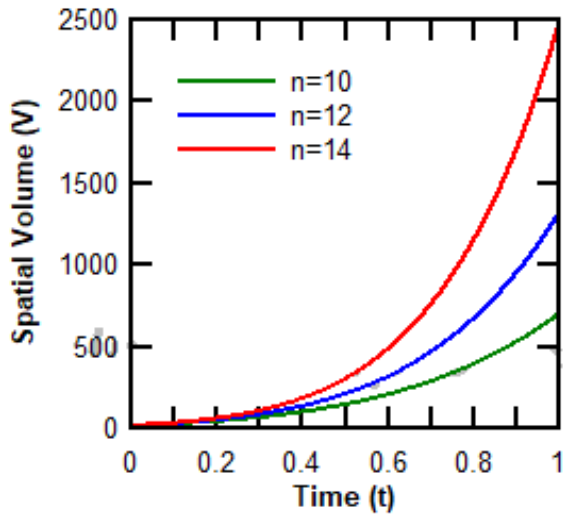

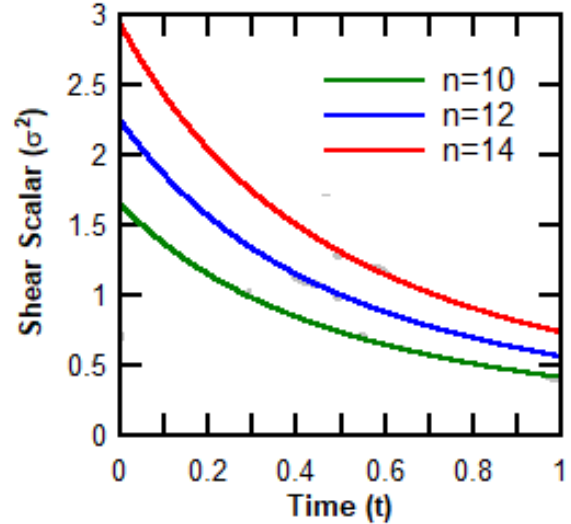**Figure 4.1:** Plot of spatial volume Vs. time for $k_3 = k_4 = 1$

Figure 4.2: Plot of shear scalar Vs. time for $k_3 = k_4 = 1$

From Fig. 4.1 and Fig. 4.2, it is observed that time (t) gradually increases, spatial volume increases and goes to infinity but shear scalar decreases and finally vanish at $t \to \infty$.
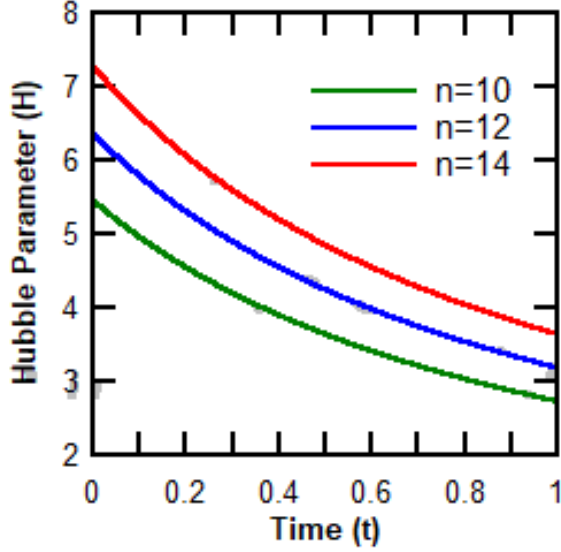
4

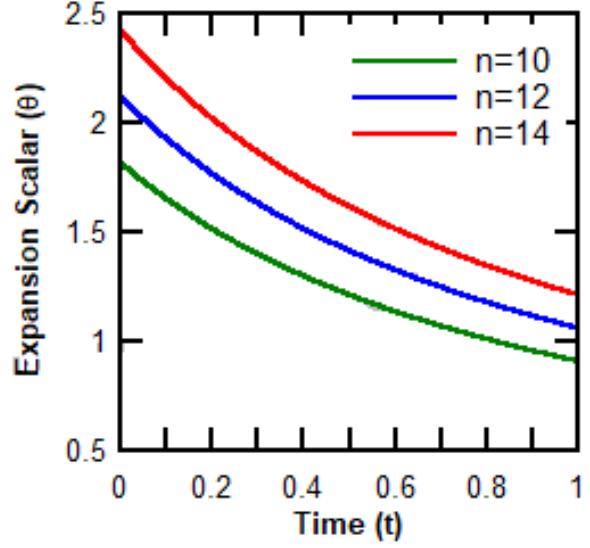**Figure 4.3:** Plot of Hubble parameter Vs. time for $k_3 = k_4 = 1$

Figure 4.4: Plot of expansion scalar Vs. time for $k_3 = k_4 = 1$

From Fig. 4.3 and Fig. 4.4, it is observed that time (t) gradually increases, Hubble parameter and expansion scalar decreases.

Also, in this model spatial volume, Hubble parameter, expansion scalar and shear scalar are the function of time throughout the universe. All the above parameters vanish when time is infinite except spatial volume increases as time increases, whereas when time is zero all the above parameters are finite except spatial volume is zero when time is zero.

Now, the expression for the energy density W, energy flow vector S and stress tensor $\sigma_\alpha\beta$ are

$$W = \frac{\left(3 + \frac{\nu^2}{c^2}\right)}{8\pi\left(1 - \frac{\nu^2}{c^2}\right)}\left[k_6 - \frac{k_7}{(k_3 t + k_4)^{\frac{n+1}{N+1}}}\right]\left[\frac{L + k_{10}(k_3 t + k_4)^{\frac{2N}{N+1}}}{(k_3 t + k_4)^2}\right], \tag{4.5}$$

$$S = \frac{4\nu}{8\pi\left(1 - \frac{\nu^2}{c^2}\right)}\left[k_6 - \frac{k_7}{(k_3 t + k_4)^{\frac{n+1}{N+1}}}\right]\left[\frac{L + k_{10}(k_3 t + k_4)^{\frac{2N}{N+1}}}{(k_3 t + k_4)^2}\right], \tag{4.6}$$

$$\sigma_{\alpha\beta} = \frac{1}{8\pi}\left[\frac{4\nu_\alpha\nu_\beta}{c^2\left(1 - \frac{\nu^2}{c^2}\right)} + \delta_{\alpha\beta}\right]\left[k_6 - \frac{k_7}{(k_3 t + k_4)^{\frac{n+1}{N+1}}}\right]\left[\frac{L + k_{10}(k_3 t + k_4)^{\frac{2N}{N+1}}}{(k_3 t + k_4)^2}\right]. \tag{4.7}$$

If the velocity v of the macroscopic motion is small compared with the velocity of the light, then we have approximately $S = (p + \varepsilon)\nu$.

Since $\frac{S}{c^2}$ is the momentum density and $\frac{(p+\varepsilon)}{c^2}$ plays the role of the mass density of the body.

From the expression (2.2), we get

$$T_i^i = \varepsilon - 3p, \tag{4.8}$$

but,

$$T_i^i = \sum_a m_a c^2 \sqrt{1 - \frac{\nu_a^2}{c^2}} \delta(r - r_a). \tag{4.9}$$

Compare the relation (4.8) with the general formula (4.9) which we saw was valid for an arbitrary system. Since we are at present considering a macroscopic body, the expression (4.9) must be averaged over all the values of r in unit volume. We obtain the result $\varepsilon - 3p = \Sigma_a m_a c^2 \sqrt{1 - \frac{\nu_a^2}{c^2}}$.

Here the summation extends over all particles in unit volume. The right side of this equation tends to zero in the ultra-relativistic limit,so in this limit the equation of state of matter is $p = \frac{\varepsilon}{3}$.

Also, the decomposition of time-like tidal tensor is

5

$$u_{a;b} = \frac{-k_3}{(N+1)(k_3t+k_4)} \left\{ nN_2^2 (k_3t+k_4)^{\frac{2n}{N+1}} + N_1^2 (k_3t+k_4)^{\frac{2}{N+1}} + h^2 N_1^2 (k_3t+k_4)^{\frac{2}{N+1}} \right\}, \quad (4.10)$$

and

Vorticity $\qquad \omega_{11} = \omega_{22} = \omega_{33} = \omega_{44} = 0.$

Vorticity of model along x, y, z and t- axes is zero. So, the obtained model is non-rotating. Whereas vorticity is nonzero, model is rotating.

5 Thermodynamics of the model

According to the second law of thermodynamics, the universe's entropy will always rise through time and can never decrease. Entropy is a way to measure how random something is. The entropy changes because of internal and external dissipative effects, and these changes are always positive, so $dS > 0$. The enthalpy **(H)** is a way to measure how much heat a system has (universe). The greatest amount of work that can be drained out of a universe is known as the Gibbs energy **(G)**. Helmholtz's energy **(F)** is a way to measure the work that can be done in the universe.

The entropy **(S)** is reads as

$$S = \frac{A}{4G} = \frac{\pi (k_3t+k_4)^2 (N+1)^2}{Gk_3^2(n+2)^2}, \quad (5.1)$$

where $A = 4\pi R_H^2$, $R_H = \frac{1}{H}$ indicates as Hubble horizon and H is the Hubble parameter.

Considering the universe's internal energy $U = \varepsilon V$ and the temperature **(T)**

$T = \frac{H(mean\, hubble\, Parameter)}{2\pi}$ [9],

$$T = \frac{k_3(n+2)}{2\pi (N+1)(k_3t+k_4)}. \quad (5.2)$$

The values for enthalpy **(H)**, Helmholtz energy **(F)**, and Gibbs energy **(G)** are as follows:

$$H = U + pV = (\varepsilon + p) V$$
$$= \frac{hN_1^2 N_2 (k_3t+k_4)^{\frac{n+2}{N+1}}}{2\pi} \left[k_6 - \frac{k_7}{(k_3t+k_4)^{\frac{n+1}{N+1}}} \right] \left[\frac{L + k_{10}(k_3t+k_4)^{\frac{2N}{N+1}}}{(k_3t+k_4)^2} \right] \quad (5.3)$$

$$F = U - TS$$
$$= \frac{3hN_1^2 N_2 (k_3t+k_4)^{\frac{n+2}{N+1}}}{8\pi} \left[k_6 - \frac{k_7}{(k_3t+k_4)^{\frac{n+1}{N+1}}} \right] \left[\frac{L + k_{10}(k_3t+k_4)^{\frac{2N}{N+1}}}{(k_3t+k_4)^2} \right] - \frac{k_3(N+1)(k_3t+k_4)}{2G(n+2)}. \quad (5.4)$$

$$G = H - TS$$
$$= \frac{hN_1^2 N_2 (k_3t+k_4)^{\frac{n+2}{N+1}}}{2\pi} \left[k_6 - \frac{k_7}{(k_3t+k_4)^{\frac{n+1}{N+1}}} \right] \left[\frac{L + k_{10}(k_3t+k_4)^{\frac{2N}{N+1}}}{(k_3t+k_4)^2} \right] - \frac{k_3(N+1)(k_3t+k_4)}{2G(n+2)}. \quad (5.5)$$

6 Stability solutions of the model

In this section, we will concentrate on the stability analysis of our model using the ratio of sound speed, causality condition, and adiabatic index.

(i) Ratio of sound speed. The stability of the model by observing the ratio of sound speed given by $\frac{dp}{d\varepsilon} = c_s^2$ when the ratio $\frac{dp}{d\varepsilon}$ is positive i.e. $c_s^2 > 0$, we have a stable model whereas when the ratio $\frac{dp}{d\varepsilon}$ is negative i.e. $c_s^2 < 0$, we have an unstable model.

For the current model,

$$c_s^2 = \frac{dp}{d\varepsilon} = \frac{1}{3} = constant. \quad (6.1)$$

Based on the results of equation (6.1), it can be seen that the ratio of sound speed is positive. So, the model of the universe that was found is stable.

(ii) Causality condition. According to the causality condition, the value of sound speed belongs to the interval $0 \leq c_s = \sqrt{\frac{dp}{d\varepsilon}} < 1$ for physical matter distribution.

As a result of the solution, we get $0 \leq 0.5773 < 1$. When compared to the needed interval, the value of

6

the speed of sound is found to be acceptable. As a result, we are able to reach the conclusion that the requirement of causality has been met by our solution.

(iii) Adiabatic index. The adiabatic index is another essential metric that plays a role in determining the stability of any given object. The relativistic adiabatic index is defined as follows

$$\gamma = \frac{p + \varepsilon}{p} \frac{dp}{d\varepsilon} = \frac{4}{3}. \tag{6.2}$$

According to the Newtonian approximation, the Newtonian sphere is stable if $\gamma > \frac{4}{3}$. If $\gamma = \frac{4}{3}$, that means equilibrium and stability must be present [8, 34]. As a result, equilibrium and stability must be present in an obtained model.

7 Energy Conditions

Several theories try to explain how the universe changed over time and describe the properties of matter in the universe by using a set of rules called "energy conditions". The role of energy conditions is to show that the universe is expanding faster, and looking at the model's energy conditions is one way to see if it is physically correct. There are many different kinds of energy conditions, such as a null energy condition (NEC), a weak energy condition (WEC), and a strong energy condition (SEC). All of these energy conditions can be presented as

(i) Null energy condition (NEC) :$\varepsilon - p \geq 0$.
(ii) Weak energy condition (WEC) : $\varepsilon > 0$,$\varepsilon - p \geq 0$.
(iii) Strong energy condition (SEC) :$\varepsilon - p \geq 0$.
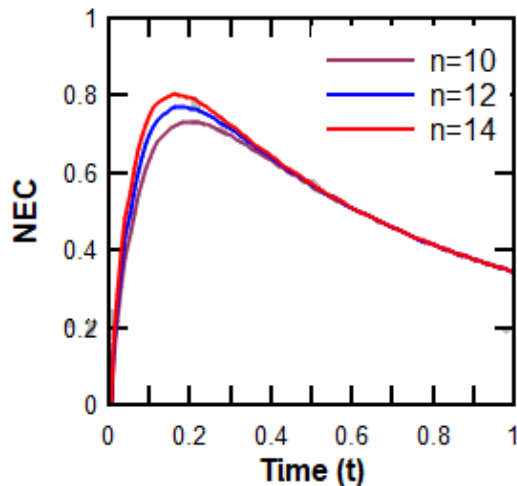
Figure 7.1: Plot of NEC Vs. time for $k_3 = k_4 = k_6 = k_7 = k_{10} = 1$ and $L = 0.5, N = 0.2$
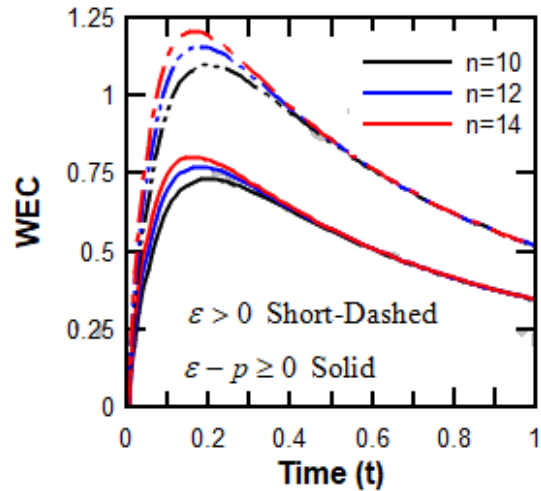
Figure 7.2: Plot of WEC Vs. time for $k_3 = k_4 = k_6 = k_7 = k_{10} = 1$ and $L = 0.5, N = 0.2$

Figures 7.1 and 7.2 show how the weak and null energy conditions of our model changed over time. From the above figures, we can see that the WEC and NEC are well met throughout the evolution of the universe. On the other hand, the derived model consistently violates SEC. Hence, the acceleration of the universe is due to the violation of the SEC.

8 Conclusion

In this paper, we have studied the stability of the cosmological model in Ruban's background in the presence of macroscopic body. In order to solve the field equations, we use the relation between metric coefficients and radiation. The parameters of metric potential, pressure, and density were discussed. From Figs. 3.1 and 3.2, it is observed that pressure and density are positives throughout the evolution of the universe. Some important physical parameters for the solutions, such as spatial volume (V), shear scalar (σ^2), Hubble parameter (H), and expansion scalar (θ), are evaluated. As we can see graphically, the universe has been expanding from a finite starting volume over an ever-increasing period of time. The smooth decay

of the expansion scalar, the Hubble parameter, and the shear scalar over time shows that all physical parameters are behaving as they should. Several thermodynamic properties are examined, including entropy (S), temperature (T), enthalpy (H), Helmholtz energy (F), and Gibbs energy (G). We have performed an investigation into the aspect of stability by calculating the ratio of sound speed, causality condition, and adiabatic index. From equation (6.1), it can be seen that the ratio of sound speed is positive. So, the model of the universe that was found is stable. In our model value of causality condition is lies between 0 to 1 i.e. $0 \leq 0.5773 < 1$. As a result, we are able to reach the conclusion that the requirement of causality has been met by our solution. Here,$\gamma = \frac{4}{3}$ that means equilibrium and stability must be present in the obtained model. Also, it's important to remember that the adiabatic index is greater than one. This means that the temperature decreases as you move away from the centre of the star. From equations (6.1) and (7.1) we get $\frac{dp}{d\varepsilon} = 0.3333 < 1$. So that in the obtained cosmological model entropy is the same everywhere, which means that the fluid sphere is isentropic. From Figures 7.1 and 7.2, we observed that the *WEC* and *NEC* are well met throughout the evolution of the universe, but the *SEC* is consistently violated. Hence, the acceleration of the universe is due to the violation of the *SEC*.

Conflict of Interest The authors declares no conflict of interests.

References

[1] C. Aktas, Energymomentum distributions of Ruban universe in general relativity and teleparallel gravity, *International Journal of Modern Physics A*, **34** (2019), 1-12. 1950011, DOI: 10.1142/S0217751X19500118.

[2] N. Ahmed and S. Z. Alamri, A stable flat universe with variable Cosmological constant in *f(R, T)*, *Res. Astron. and Astrophys.*, **18** (2018), 123-1 –123-10.

[3] J. G. Ayala, J. P. Oregon, R. Cordero and F. A. Brown, A Possible Cosmological Application of Some Thermodynamic Properties of the Black Body Radiation in n-Dimensional Euclidean Spaces, *Entropy*, **17** (2015), 4563-4581. doi:10.3390/e17074563.

[4] G.A. Barber, On two self-creation cosmologies, *General Relativity and Gravitation*,**14** (1982), 117-136.

[5] C. Brans, Consistency of field equations in Self-Creation cosmologies, *General Relativity and Gravitation*, **19** (1987), 949–952.

[6] P. Bhar, K. N. Singh, N. Sarkar and F. Rahaman, A comparative study on generalized model of anisotropic compact star satisfying the Karmarkar condition, *Eur. Phys. J. C*, **77** (2017), article number 596. DOI 10.1140/epjc/s10052-017-5149-2.

[7] P. Bhar and P. Rej, Compact stellar model in the presence of pressure anisotropy in modified Finch Skea spacetime, *J. Astrophys. Astr.*, **42** (2021), article number 74. https://doi.org/10.1007/s12036-021-09739-x.

[8] H. Bondi, The Contraction of Gravitating Spheres, *Proc. R. Soc. Lond. A*, **281** (1964), 39-48. doi: 10.1098/rspa.1964.0167

[9] R. G. Cai and S. P. Kim,First Law of Thermodynamics and Friedmann Equations of Friedmann-Robertson-Walker Universe, *J. High Energy Phys.,* **02** (2005), 050. https://doi.org/10.1088/1126-6708/2005/02/050.

[10] A. R. Curtis, The velocity of sound in general relativity, with a discussion of the problem of the fluid sphere with constant velocity of sound, *Proc. Roy. Soc.(London) A*, **200** (1950) 248-261.

[11] G. A. R. Franco, C. Escamilla-Rivera and J. L. Said, Stability analysis for cosmological models in *f(T, B)* gravity, *Eur. Phys. J. C.*, **80** (2020), article number 677. https://doi.org/10.1140/epjc/s10052-020-8253-7.

[12] L. Herrera, Stability of the isotropic pressure condition,*Physical Review D*,**101** (2020), 104024 (10pp).

[13] E. A. Hagazy, Bulk viscous Bianchi type I cosmological model in Lyra geometry and in the general theory of relativity, *Astrophys Space Sci.*, **365** (2020), article number 119.

[14] S. W. Hawking and D. N. Page, Thermodynamics of Black Holes in Anti-de Sitter Space, *Commun. Math. Phys.*, **87** (1983), 577-588.

8

[15] S.D. Katore and D.V. Kapse, Phantomic Behaviour of Generalized Ghost Pilgrim Dark Energy Models in Self Creation Theory, *Bulgarian Journal of Physics*, **49** (2022), 297313.

[16] H. Knutsen, Some Physical Properties And Stability of An Exact Model of A Relativistic Star, *Astrophysics and Space science*, **140** (1988), 385-401.

[17] H. Knutsen, On the stability and physical properties of an exact relativistic model for a superdense star, *Mon. Not. R. astr. Soc.* , **232** (1988), 163-174.

[18] J. A. S. Lima and M. A. S. Nobre, Inhomogeneous two-fluid cosmologies with electromagnetic field, *Class. Quantum Grav.* , **7** (1990), 399-409.

[19] J. A. S. Lima and J. Tiomno, On the thermodynamics of one-fluid Szekeres-like cosmologies, *Class. Quantum Grav.*, **6** (1989), L93-L98.

[20] J. A. S. Lima and J. Tiomno, Inhomogeneous two-fluid cosmologies, *Gen. Relativ. Gravit.*, **20** (1988), 10191035.

[21] L. D. Landau and E. M. Lifshitz, *The classical Theory of Fields*, Fourth Revised English Edition, Pergamon Press, 1994.

[22] V. G. Mete, V. D. Elkar and A. S. Nimkar, Rubans Cosmological Model with Bulk Stress In General Theory of Relativity, *IOSR Journal of Mathematics*, **11** (2015), 25-33.

[23] S. Maity, P. Bhandari and S. Chakraborty, Universe consisting of diffusive dark fluids: thermodynamics and stability analysis, *The European Physical Journal C*, **79** (2019), article number 82.

[24] A. S. Nimkar, J. S. Wath and V. M. Wankhade, Bianchi Type-IX Cosmological Model in Self-Creation Theory of Gravitation, *Journal of Dynamical Systems and Geometric Theories*, **19** (2021), 25-34.

[25] A. S. Nimkar, S. R. Hadole and J. S. Wath, Cosmological model in BransDicke theory of gravitation, *Indian Journal of Physics*, **97** (2022), 1633-1640.

[26] S. Nojiri, S. D. Odintsov and E. N. Saridakis, Modified cosmology from extended entropy with varying exponent, *The European Physical Journal C* , **79** (2019),article number 242.

[27] D. D. Pawar and Y. S. Solanke, Magnetized Anisotropic Dark Energy Models in Barbers Second Self-Creation Theory, *Advances in High Energy Physics*, Article ID 859638, 9 pages, 2014. https://doi.org/10.1155/2014/859638.

[28] I. Prigogine, J. Geheniau, E. Gunzig and P. Nardone, Thermodynamics of cosmological matter creation, *Proc. Natl. Acad. Sci. USA*, **85** (1988),7428-7432.

[29] V. A. Ruban, Spherically Symmetric T-Models In The General Theory of Relativity, *JETP*, **29** (1969), 1027-1034.

[30] N. Sarkar, S. Sarkar, K. N. Singh and F. Rahaman, Relativistic compact stars with dark matter density profile, *The European Physical Journal C*, **80** (2020), article number 255.

[31] F. C. Santos, M. L. Bedran and V. Soares, On the thermodynamic stability of the generalized Chaplygin gas, *Physics Letters B*, **636** (2006) 86-90.

[32] N. Tomimura and I. Waga, Inhomogeneous cosmological models-New exact solutions with dust, isotropic radiation, and electromagnetic field, *Astrophysical Journal*, **317** (1987), 52-61.

[33] S. Thirukkanesh, Robert S. Bogadi, Megandhren Govender and Sibusiso Moyo, Stability and improved physical characteristics of relativistic compact objects arising from the quadratic term in $p_r = \alpha \rho^2 + \beta \rho - \gamma$, *The European Physical Journal C*, **81** (2021).

[34] R. Tamta, P. Fuloria and P, Tamta, Models of Super Dense Structures using a New Form of the Mass Function, *A journal of physical sciences, Engg. and Tech.*, **14** (2022), 1-8.

[35] T. Vinutha and K. S. Kavya, Dynamics Of *FRW* Type Kaluza-Klein Mhrde Cosmological Model In Self-Creation Theory, *Journal of Dynamical System and Geometric Theories*, **18** (2020), 111-129.

[36] S. C. Wankhade, A. S. Nimkar and A. M. Pund, Bianchi type *VIII* cosmological model with wet dark fluid in Barber self-creation theory of gravitation, *J. Sci. Res.*, **13** (2021), 869-878.

[37] M. I. Wanas and M. A. Bakry, Stability of cosmological models, *Astrophysics and Space science*, **228** (1995), 239-253.

Current Scenario of Wild Edible Plants (WEPs), their Importance, Possible Threats, and Conservation: A Mini Review

Rupali Shirsat [a], Tripty Jagtap [b], Ashwini Sirsat [b], Shubham Rathod [b] and Dipak Koche [b*]

[a] *Department of Botany, Shri Dr. R. G. Rathod College of Arts and Science, Murtizapur, District- Akola, M.S.-444107, India.*
[b] *Department of Botany, Shri Shivaji College of Arts, Commerce and Science, Akola, District- Akola, M.S.-444003, India.*

Mini-review Article

ABSTRACT

The knowledge of Wild Edible Plants (WEPs) is as old as human civilization and still, they are playing a supplementary role in global food security. WEPs are an integral part of their traditional food systems and have nutritional and cultural values in their routine livelihood. WEPs are increasingly considered a potential source of a naturally healthy diet. But in many cases, the available WEPs resources are under threat of various kinds like overexploitation, overgrazing, forest fires, agricultural encroachment, etc.; the changing climate also negatively impacts on WEPs. Therefore, there is an urgent need for the conservation of the diversity of WEPs and their

Corresponding author: E-mail: kochedeepak77@gmail.com;

sustainable management. The present mini-review is an attempt to present the current scenario of WEPs, their importance, and a potential source of nutrients for future food security, ethnic knowledge associated with them, threats encountered by WEPs, and their possible sustainable management scheme.

1. INTRODUCTION

Since early civilization, humans use to consume wild edible plants (WEPs) which later became an integral part of their routine food. During their early evolutionary period, humans use to obtain their food by gathering eatable items from plants or plant parts (like roots, stems, leaves, flowers, seeds, etc.) and hunting animals. When the humans started settling by making huts and shades, they also started the domestication of some plants and animals [1]. Still, such types of traditions could be observed in different tribal communities across the globe [2].

It is now a clear fact that all the cultivated crop plants of today's era were ones known as wild edible plants (WEPs). After thousands of years of regular practice of cultivation by humans following the strategy of selecting more favorable traits of plants, some of them have reached the status of domesticated crop plants. With the emergence of domesticated crops, another term 'weed' comes into the picture. Weeds are the undesired plants growing along with crop plants. It was noted that most of the weed species are found to be the relatives of domesticated crop plants.

As per literature, the term "Wild", commonly indicates those species that grow spontaneously in self-sustaining populations outside cultivated areas, along the field margins, hedges, grasslands, and forest woodlands [3]. However, the distinction between "wild" and "domesticated" or "cultivated" is not so clear, and many WFPs fall somewhere in between these extremes depending on the degree of human intervention [4]. There are several plant species that are not domesticated to that extent but play prominent roles as good sources of food and nutrition by various local as well as tribal communities globally. There are a few examples that farmers use to grow a few wild species to meet their food and nutrition needs [5,6]. Under the WEPs, various communities across the globe consume leaves, flowers, fruits, nuts, legumes, pods, fruiting bodies of mushrooms, and other non-timber forest products [7].

The knowledge of WEPs is as old as human civilization and still, they are playing a supplementary role in global food security. But in many cases, the available WEPs resources are under threat of various kinds like overexploitation, overgrazing, forest fires, agricultural encroachment etc. Recent studies suggest that there are more than 7000 wild edible plant species that are being used for their multiple uses as food, nutrition, medicine, or environmental cause [8] and about 11% of them are under the threatened category of IUCN.

In this review, the authors tried to explain the term wild edible plants (WEPs) considering all possible dimensions [9] and elaborate on their importance to human beings and will also focus on the possible threats.

2. MATERIALS AND METHODS

For the present work, all the work related to wild edible plants (WEPs), their food values and nutrition, traditional knowledge associated with WEPs, and probable threats to the existing biodiversity of WEPs was collected from different online and offline journals included in various reputed databases like Scopus, WOS, Springer, Elsevier, etc. Later, the collected resource material was analyzed and interpreted critically and thematically presented in this mini-review. The related articles published in different databases were selected on the basis of their titles, abstracts, and text focusing on the reasons to include the reference in the present article and later screened by reading the full text and removing the references or part of it which do not meet the criteria of inclusion.

3. RESULTS AND DISCUSSION

3.1 The Importance of WEPs as a Source of Food and Nutrition

Since ancient days, wild edible plants (WEPs) continue to play a vital role as the principal provider of food and nutrition to sizable human populations particularly under the scarcity and

unavailability of main food crops. Further, many tribals and poor villagers residing in the vicinity of the forest depend on WEPs for their food, nutrition, and medicine [8–13].

The studies on various indigenous communities confirm the fact that wild edible plants (WEPs) are an integral part of their traditional food systems and have nutritional and cultural values in their routine livelihood [14]. Indigenous community peoples about 5% of the global population, are deeply connected to their land. Today these indigenous peoples are considered the sole custodians of rich and diverse traditional knowledge about how to use different plants, traditional food systems, and local biodiversity within the ecosystem range [15].

Indigenous communities also have a better ecological understanding of local environments and thus they could use the available food resources as per their requirement [16]. However, it was noted that the caloric contribution of WEPs is a little low compared to conventional staple foods [17]. But, these wild species contribute to diet diversification in many geographical regions which usually have different types of monotonous food systems, unique to that region [18-19].

The foods obtained from wild edible plants and plant parts usually contain a significant amount of mineral nutrients (Calcium, copper, iron, manganese, potash, sulfur, zinc, etc.) and different vitamins [17] required to support proper growth and development. These wild edible plants are otherwise neglected biological resources as the work in this field is comparatively less, but available reports indicate that these contain a significant amount of nutrients compared to available regional commercial crops [20,21]. If the nutritional potential of wild edible plants is properly assessed and managed, could be introduced as one of the main-stream foods; it might be a step towards food and nutrition security with nutrient adequacy. WEPs are increasingly considered a potential source of natural health products, therefore it is necessary to foster biochemical research on them and document their nutritional properties and main bioactive products [22,23].

If managed properly, Wild edible plants (WEPs) could also boost to empower the local market in turn local communities as it will reduce the distance between the producers and consumers. Further, it will also reduce the complete reliance of the local market on the global market. Some major pieces of evidence indicate that the local trade and markets where the local minor crops, traditional varieties, and wild edible plants are traded, have the potential to empower communities and increase livelihoods in rural areas, particularly of women and youth [24-26].

The current global crisis of the Covid-19 pandemic reveals the importance of local markets and locally available wild edible plants as most of the global food systems and supply chains were affected adversely due to pandemic lockdowns [27-29]. Several workers reported that such a situation opens up opportunities for a new type of food system that supports the local traditional market [30,31]. If such situations create food shortages, peoples turn towards traditional foods and wild edible plants as an important available source of minerals and vitamins, and herbal ingredients [7-8,32,33].

3.2 Traditional Knowledge Associated with WEPs

If we knew and understand the nutritional importance of WEPs and the traditional knowledge associated with them, it might be useful that assist in the prioritization process. The availability of nutrient content and health-promoting properties of WEPs could help in developing local guidelines in different geographical patches. The collection of nutritional data from earlier references is daunting work [34]. The documentation and protection of traditional knowledge related to consumption and recipe preparation of WFPs are available largely to the local users, i.e., rural, indigenous, and forest-dependent communities, including local farmers and elder peoples. The national floras, herbaria, and ethnological studies of local ethnic groups also provide additional botanical, culinary, nutritional, and cultural information needed for research requirements to fill this knowledge gap.

Biological knowledge of individual species is also frequently lacking but particularly essential for conservation. One of the most recent and comprehensive attempts to fill the evidence gap in food composition data is provided by the GEF-supported Biodiversity for Food and Nutrition Project (BFN). Led by Brazil, Kenya, Sri Lanka, and Turkey, and implemented by Biodiversity International with support from the UN Environment Programme (UNEP) and the Food and Agriculture Organization of the United

Nations (FAO), the project has generated food composition data for 185 plant species, many of them wild, particularly in Brazil and Turkey [34,35]. Considering the significance and role of WEPs, they are considered as food for the future [36].

In a case study of Central India, authors have demonstrated that WEPs supplements significantly higher quantities of nutrients in the core zone compared to other zones. These are currently underutilized especially in buffer and transition zones and complement the local staple foods and partially supplement the essential macro- and micro-nutrients [7]. However, most of these WEPs have the potential to fulfill dietary needs and ensure balanced nutrition. Peduruhewa et. al. explained the potential of underutilized WEPs to cope with malnutrition and food insecurity, which are burning issues that need immediate attention [36]. About 71 wild edible plants (WEPs) belonging to 57 genera and 27 families from the semi-arid zone of Punjab, Pakistan were reported by Waheed et al. [35]. They further stated that most of these WEPs are also being used as ethnomedicinal plants for long and as seasonal wild vegetables that have high amounts of nutrition.

3.3 Threats to Wild Edible Plants (WEPs)

The researchers in recent past indicate that Wild edible plants (WEPs) are an integral part of local biodiversity and play a vital role in food security at the local level. Despite its importance, it was found that the diversity of WEPs is declining rapidly. To combat this issue, in 2019, the Food and Agricultural Organization (FAO) constituted "The State of World Biodiversity for Food and Agriculture (SOWBFA), an independent body to take care of and assess the diversity of food and agriculture [37].

According to the reports of FAO [37] and Royal Botanical Garden [38] changes in land use and management like conversion of forest-covered land area to agriculture, for industry and infrastructure development, habitat destruction due to grazing, forest fires, and overharvesting of forest products are some of the major causes of depletion in plant diversity including WEPs. These reasons account for about 62% of threats to WEPs which are growing beyond the range of protected forests [7]. Some workers also reported a decline in the abundance and diversity of WEPs from different areas [39,40]. Many

WEPs found to grow in agricultural lands as weeds, in hedges, as wild trees in agroforestry systems, and in some small forest patches [17]. The change in agricultural practices, including intensification, use of more pesticides, and removal of existing flora can negatively impact the existence of these biological resources [41,42].

The SOWBFA used the Sampled Red List Index for Plants prepared by the International Union for Conservation on Nature (IUCN) [41]. Under this project, a total of 822 WEPs species were considered across 7 different classes of which 73% are currently at low risk of extinction but some classes are highly threatened in the wild. However, the IUCN Red List Index for Plants includes global conservation assessments for only one-third (31%) of known WFPs. Furthermore, International Center for Tropical Agriculture (CIAT) as part of a larger study to identify conservation gaps for useful plants, an assessment of the comprehensiveness of conservation of 1587 WFP taxa was carried that showed only 3.3% of WFPs are sufficiently conserved ex-situ, while 89.1% require urgent off-site conservation measures [42]. Of the WFP taxa analyzed 42.1% are sufficiently conserved, 46.7% deserve medium priority and 11.1% require stepping up conservation measures [42]. Rapidly increasing temperatures and habitat destruction can alter the species' geographic distribution, driving them across the artificially designated boundaries of many protected areas in pursuit of favorable growing conditions.

3.4 Priorities and Integrated Approach for Conservation of WEPs

The conservation and sustainable management strategies of WFPs must include close collaboration with indigenous and local communities and tribes who are the main users and custodians of WEPs local diversity. It must have participatory research approaches that integrate traditional and scientific knowledge about WEPs; it will be most appropriate to maximize benefits for those communities or community peoples who are involved in the process. Before starting such work, the local community people should be made aware and they should agree on every aspect of the research process including methodology, analysis, and purpose of research or data collection [43].
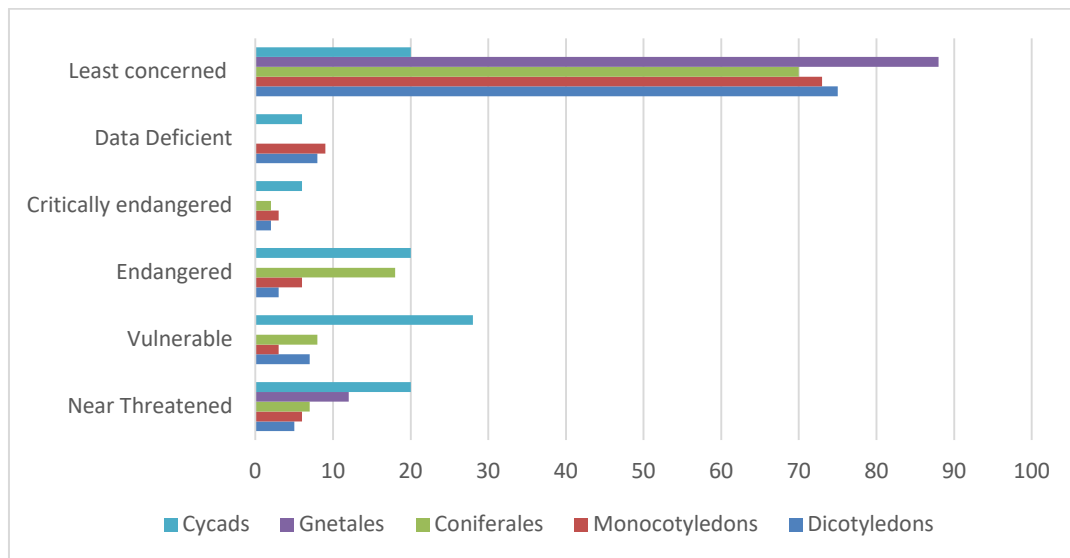
Fig. 1. Major plant groups and their IUCN status (2019)
(Note: All values are in percentage. Adopted from FAO (2019))

There are several reports on declining of WEPs from their habitats, local markets, and even from regular diets of different local communities. Therefore, their conservation and sustainable management for future food security is one of the very difficult tasks for the entire human community. For the sustainable management of WEPs, Borelli [35] proposed a highly appreciable scheme. It includes the challenges in environmental conditions, information, and infrastructure, and the practices to be conducted for sustainable management of WEPs. Reportedly there are over 20,000 species of WEPs across the globe; some of which are enlisted in the form of their respective references in Table 1 as per the literature available [51]. Currently, we are utilizing less than 10% of these WEPs, others are declining due to mere negligence and less awareness of these species worldwide. For future food security, and to maintain the ecological balance these species must have to conserved. It is very urgent to conserve the diversity of WEPs using both in-situ and ex-situ conservation methods. For maximum utilization, we need to develop a specific knowledge system for WEPs and provide the required infrastructure and support (Fig. 2) to strengthen the developing system for the conservation and management of WEPs across the globe.

Fig. 2. Integrated approach to conserving WEPs

Table 1. Literature available on wild edible plants (WEPs) from different countries

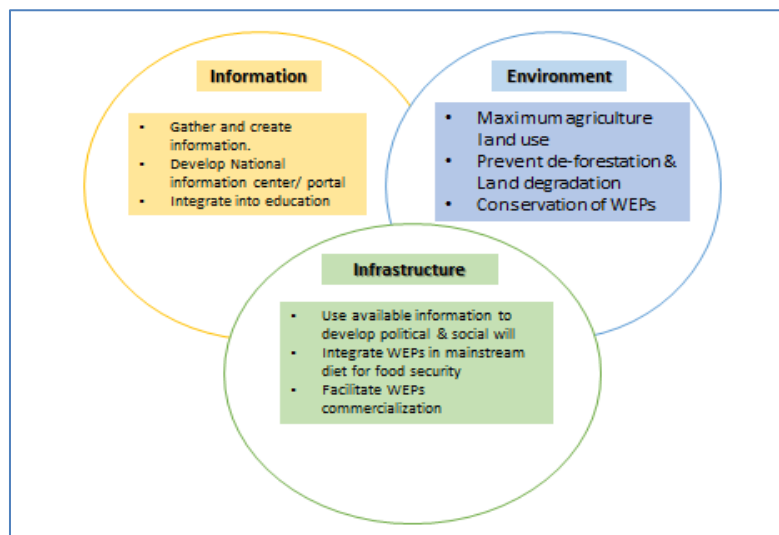| Sr. No.	Country	Work done by
1	African countries (South Africa, Ethiopia, Kenya, Tanzania, Zambia)	[44,45,46,47,48,49,50,52]
2	America (USA)	[5,80]
3	China	[56,57,58,59,60]
4	European Countries	[61,62,63,64,65]
5	Asian Countries excluding China (India, Pakistan, Bhutan, Nepal, Srilanka, Thailand, etc.)	[53,54,55,66,67,68,69,70,71,72,73,74,75, 76,77,78,79]
6	Australia	[81,82]

4. CONCLUSION

At the local level, Wild edible plants (WFPs) contribute significantly to the diets and livelihoods of millions of people worldwide. Several workers reported the importance of WEPs at the local level, but their national scenario and conservation assessment are not recorded, and thus it fails to convey the full utility of WEPs in food security and as a bioresource. As we do not explore the WEPs fully, their role in mankind is not fully appreciated and they remain neglected. There are limited cases that clearly demonstrate that the contribution of WFPs to food security, nutrition, and livelihoods is significant. Now it becomes a challenge to apply useful strategies for the conservation and sustainable management of WEPs. Further, we are unaware of how the changing climate impacts the WEPs now and in the future. For sustainable management of WEPs, we have to follow the integrated conservation approach. For the same, apart from their nutritional potential, medicinal values, and pharmacological importance must have to be considered to bridge the knowledge gap while strategic planning WEP's sustainable management. Further, it is essential to involve local communities in the conservation process of WEPs so that they could cooperate and will get the maximum benefit out of it.

COMPETING INTERESTS

Authors have declared that no competing interests exist.

REFERENCES

1. Sowunmi MA. The beginnings of agriculture in West Africa: botanical evidence. Curr Anthropol. 1985;26(1):127-9.
2. Johnson A, Behrens CA. Nutritional criteria in Machiguenga food production decisions: A linear- programming analysis. Hum Ecol. 1982;10(2):167-89.
3. Heywood VH. Use and potential of wild plants in farm households; FAO farm system management series. Rome, Italy: Food and Agriculture Organization. 2010;1999. Bharucha Z, Pretty J. The roles and values of wild foods in agricultural systems. Philos Trans R Soc Lond B Biol Sci. 2010;365(1554):2913-26.
4. Bharucha Z, Pretty J. The role and importance of wild foods in agricultural systems. Phil Trans R Soc B. 2010;365 (1554):2913-26.
5. Casas A, Otero-Arnaiz A, Pérez-Negrón E, Valiente-Banuet A. In situ management and domestication of plants in Mesoamerica. Ann Bot. 2007;100(5): 1101-15.
6. Cruz-Garcia GS. Management and motivations to manage "wild" food plants. A case study in a mestizo village in the amazon deforestation frontier. Front Ecol Evol. 2017;5:127.
7. Mishra A, Swamy SL, Thakur TK, Bhat R, Bijalwan A, Kumar A. Use of wild edible plants: can they meet the dietary and nutritional needs of indigenous communities in central India. Foods. 2021; 10(7):1453.
8. Ulian T, Diazgranados M, Pironon S, Padulosi S, Liu U, Davies L, et al. Unlocking plant resources to support food security and promote sustainable agriculture. Plants People Planet. 2020; 2(5):421-45.
9. Asprilla-Perea J, Díaz-Puente JM. Importance of wild foods to household food security in tropical forest areas. Food Sec. 2019;11(1):15-22.
10. Broegaard RB, Rasmussen LV, Dawson N, Mertz O, Vongvisouk T, Grogan K. Wild food collection and nutrition under commercial agriculture expansion in

agriculture-forest landscapes. For Policy Econ. 2017;84:92-101.

11. Ickowitz A, Powell B, Rowland D, Jones A, Sunderland T. Agricultural intensification, dietary diversity, and markets in the global food security narrative. Glob Food Sec. 2019;20:9-16.

12. Ojelel S, Mucunguzi P, Katuura E, Kakudidi EK, Namaganda M, Kalema J. Wild edible plants used by communities in and around selected forest reserves of Teso-Karamoja Region, Uganda. J Ethnobiol Ethnomed. 2019;15(1):3.

13. Rowland D, Ickowitz A, Powell B, Nasi R, Sunderland T. Forest foods and healthy diets: Quantifying the contributions. Environ Conserv. 2017;44(2):102-14.

14. Kuhnlein HV, Erasmus B, Spigelski D. Indigenous peoples' food systems: the many dimensions of culture, diversity and environment for nutrition and health. Rome, Italy: food and agriculture organization of the United Nations; 2009.

15. Kuhnlein HV. Holding on to agrobiodiversity: human nutrition and health of indigenous peoples. In: Hunter D, Guarino L, Spillane C, McKeown PC, editors. Routledge handbook of agricultural biodiversity. London, UK: Routledge. 2017;692.

16. Angelsen A. Policies for reduced deforestation and their impact on agricultural production. Proc Natl Acad Sci U S A. 2010;107(46):19639-44.

17. Powell B, Thilsted SH, Ickowitz A, Termote C, Sunderland T, Herforth A. Improving diets with wild and cultivated biodiversity from across the landscape. Food Sec. 2015;7(3):535-54. .

18. Aryal KP, Poudel S, Chaudhary RP, Chettri N, Chaudhary P, Ning W et al. Diversity and use of wild and non-cultivated edible plants in the western Himalayas. J Ethnobiol Ethnomed. 2018;14(1):10.

19. Smith E, Ahmed S, Dupuis V, Running Crane M, Eggers M, Pierre M et al. Contribution of wild foods to diet, food security, and cultural values amidst climate change. J Agric Food Syst Community Dev. 2019;9;Suppl 2:1-24.

20. Fernández-Ruiz V, Morales P, Ruiz-Rodríguez BM, Isasa ET. Nutrients and bioactive compounds in wild fruits through different continents. In: Wild plants, mushrooms and nuts. Chichester, UK: John Wiley & Sons, Ltd. 2016; 263-314.

21. Hunter D, Borelli T, Beltrame DMO, Oliveira CNS, Coradin L, Wasike VW, et al. The potential of neglected and underutilized species for improving diets and nutrition. Planta. 2019;250(3):709-29.

22. Alwafa RA, Mudalal S, Mauriello G. *Origanum syriacum* L. (Za'atar), from raw to go: A review. Plants (Basel). 2021;10(5):1001.

23. Sibiya NP, Kayitesi E, Moteetee AN. Proximate analyses and amino acid composition of selected wild indigenous fruits of Southern Africa. Plants (Basel). 2021;10(4):721.

24. Kinnunen P, Guillaume JHA, Taka M, D'Odorico P, Siebert S, Puma MJ et al. Local food crop production can fulfill the demand for less than one-third of the population. Nat Food. 2020;1:229-37.

25. Padulosi S, Mal B, King O, Gotor E. Minor millets as a central element for sustainably enhanced incomes, empowerment, and nutrition in rural India. Sustainability. 2015;7(7):8904-33.

26. Shackleton S, Paumgarten F, Kassa H, Husselman M, Zida M. Opportunities for enhancing poor women's socioeconomic empowerment in the value chains of three African Non-Timber Forest Products (NTFPs). Int For Rev. 2011;13(2):136-51.

27. Béné C. Resilience of local food systems and links to food security—A review of some important concepts in the context of COVID-19 and other shocks. Food Secur. 2020;12(4):805-22.

28. Fernandes N. Economic effects of coronavirus outbreak (COVID-19) on the world economy. SSRN Electron J; 2020.

29. Torero M. Without food, there can be no exit from the pandemic. Nature. 2020;580(7805):588-9.

30. Cappelli A, Cini E. Will the COVID-19 pandemic make us reconsider the relevance of short food supply chains and local productions? Trends Food Sci Technol. 2020;99:566-7.

31. Vandebroek I, Pieroni A, Stepp JR, Hanazaki N, Ladio A, Alves RRN, et al. Reshaping the future of ethnobiology research after the COVID-19 pandemic. Nat Plants. 2020;6(7):723-30..

32. Kitessa GB, Tokuma UG. Edible woody plants diversity and potential contribution to food security in Ethiopia. Int J Ecotoxicol Ecobiol. 2022;7(3):37-48.

33. Waheed M, Haq SM, Arshad F, Bussmann RW, Pieroni A, Mahmoud EA et al.

Traditional wild food plants gathered by ethnic groups living in semi-arid region of Punjab, Pakistan. Biology. 2023;12(2):269.

34. Gee E, Borelli T, Beltrame DMO, Oliveira CNS, Coradin L, Wasike V, et al. The ABC of mainstreaming biodiversity for food and nutrition. Concepts, theory and practice. In: Hunter D, Borelli T, Gee E, editors. Biodiversity food and nutrition. A new agenda for sustainable food systems. Abingdon, UK: Routledge; 2020.

35. Borrelli P, Robinson DA, Panagos P, Lugato E, Yang JE, Alewell C et al. Land use and climate change impacts on global soil erosion by water (2015-2070). Proc Natl Acad Sci U S A. 2020;117(36): 21994-2001.

36. Peduruhewa PS, Jayathunge KGLR, Liyanage R. Potential of Underutilized Wild Edible Plants as the Food for the Future – a review. J Food Sec. 2021;9(4):136-47.

37. FAO. The state of the World's biodiversity for food and agriculture. Rome, Italy: Food and Agriculture Organization; 2019.

38. Royal Botanic Gardens, Kew. State of the World's plants. London, UK: Royal Botanic Gardens, Kew; 2016.

39. Díaz S, Settele J, Eduardo B, Ngo HT, Guèze M, Agard J, et al. The global assessment report on biodiversity and ecosystem services. Summary for policymakers. Bonn, Germany: IPBES; 2019.

40. Masson-Delmotte V, Zhai P, Pörtner H-O, Roberts D, Skea J, Calvo E, et al. Climate change and land [IPCC report]. Geneva, Switzerland: IPCC; 2019.

41. Kew. Plants under pressure—A global assessment. London, UK: Royal Botanic Gardens, Kew, UK and Natural History Museum; 2016.

42. Khoury CK, Amariles D, Soto JS, Diaz MV, Sotelo S, Sosa CC, et al. Comprehensiveness of conservation of useful wild plants: an operational indicator for biodiversity and sustainable development targets. Ecol Indic. 2019; 98:420-9.

43. SCBD. Report of the AHTEG on indicators for the Strategic Plan for biodiversity 2011-2020. Montreal: Secretariat of the Convention on Biological Diversity; 2011.

44. Boedecker J, Termote C, Assogbadjo AE, Van Damme P, Lachat C. Dietary contribution of Wild Edible Plants to women's diets in the buffer zone around the Lama forest, Benin-an underutilized potential. Food Sec. 2014;6(6):833-49.

45. Shackleton C, Shackleton S. The importance of non-timber forest products in rural livelihood security and as safety nets: A review of evidence from South Africa. S Afr J Chem. 2004;100:658-64.

46. Ogoye-Ndegwa C. Traditional gathering of wild vegetables among the luo of Western Kenya-a nutritional anthropology project1. Ecol Food Nutr. 2003;42(1):69-89.

47. Shumsky SA, Hickey GM, Pelletier B, Johns T. Understanding the contribution of wild edible plants to rural social-ecological resilience in semi-arid Kenya. Ecol Soc. 2014;19(4).

48. Mulenga BP, Richardson RB, Tembo G. Non-timber forest products and rural poverty alleviation in Zambia. Zambia: Indaba Agricultural Policy Research Institute; 2012.

49. Maundu P. Utilization and conservation status of wild food plants in Kenya. In: The biodiversity of African plants. Springer. 1996; 678-83.

50. Keller GB, Mndiga H, Maass BL. Diversity and genetic erosion of traditional vegetables in Tanzania from the farmer's point of view. Plant Genet Resour. 2005; 3(3):400-13.

51. Tinsae Bahru ZA, Sebsebe D. Wild edible plants: sustainable use and management by in and the buffer area of awash national park, Ethiopia. Ethiopian J Sci. 2013;3:93-108.

52. Tahir M, Abrahim A, Beyene T, Dinsa G, Guluma T, Alemneh Y et al. The traditional use of wild edible plants in pastoral and agro-pastoral communities of Mieso District, eastern Ethiopia. Trop Med Health. 2023;51(1):10.

53. Ugyen J, Gurung T. Assessment of yam (*Dioscorea spp.*) diversity at community level in Nangkor gewog under Zhemgang dzongkhag. J Bhutan Stud. 2015;33.

54. Chhoeda Yangchen U. Wild vegetable diversity and their contribution to household income at Patshaling gewog, Tsirang. Bhutan J Nat Resour Dev. 2017;4(1):30-8.

55. FAO, editor. Non-wood forest products of Bhutan Bangkok, Thailand RAP publication; 1996.

56. Ju Y, Zhuo J, Liu B, Long C. Eating from the wild: diversity of wild edible plants used by Tibetans in Shangri-la region, Yunnan,

China. J Ethnobiol Ethnomed. 2013;9 (1):28.

57. Kang Y, Łuczaj Ł, Kang J, Zhang S. Wild food plants and wild edible fungi in two valleys of the Qinling Mountains (Shaanxi, central China). J Ethnobiol Ethnomed. 2013;9(1):26.

58. Baranov AI. Wild vegetables of the Chinese in Manchuria. Econ Bot. 1967;21(2):140-55.

59. Cheng Z, Lu X, Lin F, Naeem A, Long C. Ethnobotanical study on wild edible plants used by Dulong people in northwestern Yunnan, China. J Ethnobiol Ethnomed. 2022;18(1):3.

60. Sachula G, Zhang, Zhang YY, Zhao H, Khasbagan. *et al.* Wild edible plants collected and consumed by the locals in Daqinggou, Inner Mongolia, China. J Ethnobiol Ethnomed. 2020;16(1):60.

61. Radina K, editor. Booklet. Common useful wild plants in Central Europe. Promoting traditional collection and use of wild plants to reduce social and economic disparities in Central Europe. Budapest, Hungary: TRAFFIC and WWF Verlagsgesellschaft; 2013.

62. Pardo De Santayana M, Pieroni A, Puri RK. Ethnobotany in the new Europe: people, health, and wild plant resources. New York: Berghahn Books; 2010.

63. Tardío J, Pascual H, Morales R. Wild food plants traditionally used in the province of Madrid, Central Spain. Econ Bot. 2005;59(2):122-36.

64. Benítez G, Molero-Mesa J, González-Tejero MR. Wild edible plants of Andalusia: Traditional uses and potential of eating wild in a highly diverse region. Plants (Basel). 2023;12(6):12-8.

65. Łuczaj Ł, Pieroni A, Tardío J, Pardo-de-Santayana M, Sõukand R, Svanberg I et al. Wild food plant use in 21st century Europe: the disappearance of old traditions and the search for new cuisines involving wild edibles. Acta Soc Bot Pol. 2012;81(4):359-70.

66. Barua U, Hore D, Sarma R. Wild edible plants of Majuli island and Darrang districts of Assam. Indian J Trad Knowl. 2007;6(1):191-4.

67. Yesodharan Y, Sujana KA. Wild edible plants traditionally used by the tribes in the Parambikulam wildlife sanctuary, Kerala, India. Nat Prod Radiance. 2007;6(1):7.

68. Tiwari J, Ballabha R, Tiwari P. Some promising wild edible plants of Srinagar

and its adjacent area in Alaknanda valley of Garhwal Himalaya, India. J Am Sci. 2010;6(4):167-74.

69. Sundriyal M, Sundriyal RC, Sharma E. Dietary use of wild plant resources in the Sikkim Himalaya, India. Econ Bot. 2004;58(4):626-38.

70. Arora RK, Pandey A. Indian Council of Agricultural Research. National Bureau of Plant Genetic Resources: wild edible plants of India: diversity, conservation, and use. New Delhi: Indian Council of Agricultural Research. National Bureau of Plant Genetic Resources; 1996.

71. Ray A, Ray R, Sreevidya EA. How many wild edible plants do we eat—their diversity, use, and implications for sustainable food system: an exploratory analysis in India. Front Sustain Food Syst. 2020;4:56.

72. Abbasi AM, Khan MA, Shah MH, Shah MM, Pervez A, Ahmad M. Ethnobotanical appraisal and cultural values of medicinally important wild edible vegetables of Lesser Himalayas-Pakistan. J Ethnobiol Ethnomed. 2013;9(1):66.

73. Shaheen S, Ahmad M, Haroon N. Status of edible wild plants in Pakistan: Case studies. In: Edible Wild Plants: An alternative approach to food security. Springer. 2017;65-125.

74. Gajurel PR, Singh B, Kashung S, Adhikary P, Nopi S, Barman R et al. Foods from the wild: a review on the diversity and use pattern of wild edible plants of Arunachal Himalaya for sustainable management. Plant Sci. Today. 2023;10(1):80-9.

75. Talang H, Yanthan A, Rathi RS, Pradheep K, Longkumer S, Imsong B et al. Nutritional evaluation of some potential wild edible plantsof North Eastern region of India. Front Nutr. 2023;10: 1052086.

76. Aryal K, Berg Å, Ogle BM. Uncultivated plants and livelihood support: A case study from the Chepang people of Nepal. Ethnobot Res Appl. 2009;7:409-22.

77. Nirmala J, Siwakoti M, Kehlenbeck K. Developing a Domestication Priority Setting Approach for Wild Vegetable to improve food security in Makanwar District, Central Nepal. Stuttgart-Hohenheim Tropentag. 2013;3.

78. Bhattarai S, Chaudhary RP, Taylor RS. Wild edible plants used by the people of Manang district, Central Nepal. Ecol Food Nutr. 2009;48(1):1-20.

79. Panyadee P, Wangpakapattanawong P, Inta A, Balslev H. Very high food plant diversity among ethnic groups in Northern Thailand. Diversity. 2023;15(1):120.

80. Available:https://www.kuhl.com/borninthemountains/edible-plants-on-the-trails-in-usa.

81. Canning AD. Rediscovering wild food to diversify production across Australia's agricultural landscapes. Front Sustain Food Syst. 2022;6:865580.

82. Fyfe S, Smyth HE, Schirra HJ, Rychlik M, Sultanbawa Y. The framework for responsible research with Australian native plant foods: A food chemist's perspective. Front Nutr. 2021;8: 738627.

Fluorescent study, preliminary phytochemistry and HPTLC profiling of *Salvinia molesta* D. S. mitchell

Rupali P Shirsat
Department of Botany, Shri Dr. R. G. Rathod College of Arts and Science, Murtizapur, Akola, Maharashtra, India

Abstract
Salvinia molesta D. S. Mitchell is one of the most invasive alien aquatic plant species commonly known as giant salvinia or Kariba weed. The present study is focused on fluorescent study, preliminary phytochemistry, and HPTLC profiling of ethanolic leaf extract of *S. molesta*, so that some possible out-way could be drawn to use this weed for the benefit of mankind. In the fluorescent pharmacognostic study, the leaf extract showed distinct colors with routine chemicals and reagents of the laboratory under normal sunlight and under UV light; it could be used as a marker test for powder to identify adulteration. Further, the preliminary phytochemistry revealed that the plant is rich in major phytochemicals. The HPTLC profile showed that the ethanolic extract showed the presence of some phenolic compounds like ferulic acid, vanillic acid, caffeic acid and flavonoids which are possible compounds that provide specific bioactivities to the plant and the plant could be further explored for related drug formulation.

Keywords: Fluorescence study, phytochemistry, HPTLC, *Salvinia molesta*

Introduction
The plant under study, *Salvinia molesta* D. S. Mitchell, has been identified as a troublesome invasive aquatic plant and known as the world's most invasive alien species in the Global Invasive Species Database since 2013. *Salvinia molesta*, commonly known as giant *Salvinia* or Kariba weed, is a floating fern belonging to the family of Salviniaceae. It was native of Southern Africa and spread across the globe through various types of introduction patterns and established itself as an alien invasive aquatic plant species.

Some biologists did a comprehensive study to explore the phytochemical composition, antioxidant potential, and antibacterial properties of *S. molesta*. Salleh *et al.*, (2023) [14] reported that the plant is rich in phenolics, flavonoids, tannins, alkaloids, and saponins. Earlier similar report was given by Gaya *et al.*, (2016) [5] and Al-Maliki *et al.*, (2017). In their study, Gini and Jothi, 2018 [6], isolated the active fraction of the leaf extracts of *S. molesta* using column chromatography, showed the presence of phenolic compounds, and also demonstrated that the plant possesses significant pharmacological activities (Gini and Jothi, 2018) [6].

Though *S. molesta* is a troublesome invasive plant, the ability of *Salvinia* species to bioaccumulate certain metals makes it potentially useful for waste management and effluent treatment. The phytochemical investigation of its allied species, the *S. natans* showed that it consists of 96% of amino compounds, such as γ-amino butyric acid, asparginine, and glutamine (Lahdesmaki, 1968) [11]. Few scientists have explored the utility of *S. molesta* in phytoremediation and wastewater treatment (Israa *et al.*, 2011 and Hauwa *et al.*, 2021) [9, 8]. An understanding of the phytochemistry of *Salvinia* plants can help control their invasive growth, and promote their utilization for useful purposes. Therefore, the present study was planned to investigate the preliminary phytochemistry and HPTLC profile of *S. molesta* to understand which bioactive chemicals are present in this plant.

Material and Methods
The plant *Salvinia molesta* D. S. Mitchell was collected from the small perennial lakes of Akola regions (MS) India in December 2022. The plant was taxonomically identified using the flora of Maharashtra State (Karthikeyan and Singh, 2000). Further, the plant specimen was submitted to the herbarium of the Department of Botany, Shri Dr. R. G. Rathod Arts and Science College, Murtizapur District-Akola (MS). Later, the leaves were shade-dried and made into powder. The powdered material was processed further for fluorescent analysis, preliminary phytochemical analysis and HPTLC profiling. The fluorescent analysis was done using the protocol of (Gandhi *et al.*, 2022) [4], the preliminary phytochemistry was done using the standard protocols (Harborne, 1998 and Jasutkar *et al.*, 2018) [7, 10]. The powdered material was sent to the Qualichem Laboratory Nagpur (MS) for HPTLC profiling.

Results and Discussion
The plant *Salvinia molesta* D. S. Mitchell was selected for the study. The plant material is preserved for the pharmacognostic study of the leaf. The powdered sample of plant material was subjected for the preliminary phytochemical analysis using three solvents, distilled water, ethanol, and chloroform. Also, the powder sample is use for the HPTLC test. The various observations done and results obtained are as follows.

Fluorescent analysis of leaf powder of *S. molesta*
Pharmacognostic and fluorescent analysis was done to authenticate the crude powder. This was done using routine laboratory chemical reactions with powdered material and its appearance under normal sunlight and UV- light. In the present investigation, the powder as such appeared light green under normal sunlight, while under UV- light is showed dark green coloration. With concentrated HCL, it appeared light green but after exposing UV light, it turned light yellow. With 50% HCL, the powder appeared colorless in normal sunlight, while showing a light yellow color under

UV. When mixed with H_2SO_4, the powder gives brown coloration but when observed under UV light, the color changes to blackish brown. But with 50% H2SO4, it turns dull green in normal sunlight and when observed under UV-light, it showed a light brown color. In the case of NaOH solution, when mixed with powder, it appeared light yellow under normal sunlight but the same in UV -light was colorless. With 5% ferric chloride, the mixture appeared pale yellow and turned light yellow under UV. With nitric acid, the powder showed a light yellow color under sunlight but the color changed to blackish green when observed under UV- light (Table 1).

Table 1: Fluorescent analysis of leave powder of *S. molesta*

Sr. No.	Test (Powder)	Sunlight	UV-light
1	Powder such as	Light green	Dark green
2	Powder + HCL	Light green	Light yellow
3	Powder + 50% HCL	Colourless	Light yellow
4	Powder + H2SO4	Brown	Blackish brown
5	Powder + 50% H2SO4	Dull green	Light brown
6	Powder + NaOH solution	Light yellow	Colourless
7	Powder + Ferric Chloride5%	Pale yellow	Light yellow
8	Powder + Nitric acid 50%	Light yellow	Blackish green

Preliminary Phytochemical Analysis

The preliminary phytochemical analysis of *Salvinia molesta* leaves is presented in Table 2. The qualitative tests were carried out for 09 major phytochemicals including alkaloids, phenolics, flavonoids, steroids, quinones, glycosides, saponins, and tannins. It was noted that most phytoconstituents are present in chloroform extracts. The extract of distilled water showed the presence of phenolics and tannins. The qualitative tests of ethanolic extract for terpenoids, phenolics, flavonoids, steroids and Tannins. In the chloroform extract, only flavonoids, phenolics, saponin, and tannin (Table 2). Thus, it indicates that among the selected solvents, chloroform is the most suitable solvent to obtain the most number of phytochemicals from the crude plant powder. The experimental proof is given in photoplate-1.

Table 2: Preliminary phytochemical tests of *Salvinia molesta*

Sr. No.	Test	Distilled water	Ethanol	Chloroform
1	Alkaloids	-	-	-
2	Flavonoids	-	+	+
3	Terpenoids	-	+	-
4	Quinones	-	-	-
5	Steroids	-	+	-
6	Phenol	+	+	+
7	Glycosides	-	-	-
8	Saponin	-	-	+
9	Tannin	+	+	+

Note: the results are average of triplicate analysis

HPTLC Profiling of *Salvinia molesta* Chloroform leaf extract

The HPTLC analysis facility was availed from Qualichem Laboratories Pvt. Ltd. Nagpur. The analysis of done using a glass tank chamber (10 x 10 cm) with a solvent system Toluene: Ethyl Acetate: Formic acid (5:4:0.2). The solvent front position 70.00 mm, dryer used- Oven with temperature 60oC and time 5 minutes. The detector used was CAMAG TLC Scanner "Scanner_171005" S/N 171005 (2.01.02) with a scanning speed of 20mm/S and data resolution of 100mm/step. The analysis was done on two wavelengths 254 nm and 366 nm.

HPTLC analysis of ethanolic *S. molesta* leaf extract on 254 nm

At 254 nm, the HPTLC chromatogram showed 15 different peaks (Fig. 1) and visualized the same number of bands on the TLC visualizer (Fig. 2). The details of different peaks are presented in table-3 that includes, including peak number, start rf, maximum rf, the height of peak and peak area, etc. This information is necessary to identify the respective compounds giving that peak or band.

Fig 1: HPTLC chromatogram of *S. molesta* leaf extract at 254 nm

Fig 2: HPTLC Bands for *S. molesta* leaf extract at 254 nm

Table 3: Details of HPTLC chromatogram of ethanolic leaf extract of *S. molesta* at 254 nm

Peak	Start Rf	Start Height	Max Rf	Max Height	Max %	End Rf	End Height	Area	Area %	Assigned substance
1	-0.02	7.4	0.01	606.1	59.66	0.08	19.5	12680.8	44.75	Un-identified
2	0.23	19.8	0.28	30.5	3.00	0.30	27.7	1088.5	3.84	Flavonoid
3	0.30	28.1	0.33	39.2	3.86	0.35	35.1	1135.2	4.01	Un-identified
4	0.54	38.2	0.58	50.8	5.00	0.61	43.4	1875.7	6.62	Caffeic Acid
5	0.64	47.9	0.69	68.4	6.74	0.73	57.6	3364.7	11.87	Un-identified

6	0.73	57.4	0.74	58.8	5.79	0.77	46.9	1433.3	5.06	Vanillic acid
7	0.78	47.9	0.82	74.6	7.35	0.86	41.8	3104.7	10.96	Un-identified
8	0.87	42.2	0.91	87.5	8.61	1.03	4.9	3653.8	12.89	Ferulic acid

From the chromatogram of leaf extract of *S. molesta*, which showed 8 peaks at 254 nm, 04 peaks were identified. These were peak numbers 2 4, 6, and 8 having maximum Rf values 0.28, 0.58, 0.74 and 0.91. These compounds were identified as flavonoid, caffeic acid, vanillic acid and Ferulic acid.

HPTLC analysis of P. guajava leaf extract on 366 nm
At 366 nm, the HPTLC chromatogram showed 5 different peaks (Fig. 4) and visualized same number of bands on the TLC visualizer (Fig. 5). The details of different peaks are presented in table-4 that includes, including peak number, start Rf, maximum Rf, height of peak and peak area etc. This information is necessary to identify the respective compounds giving that peak or band.
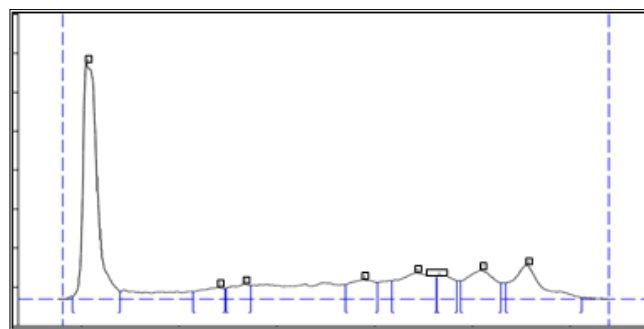

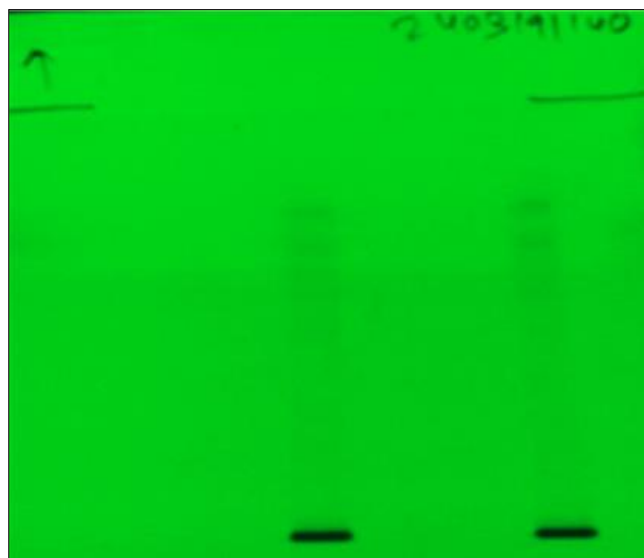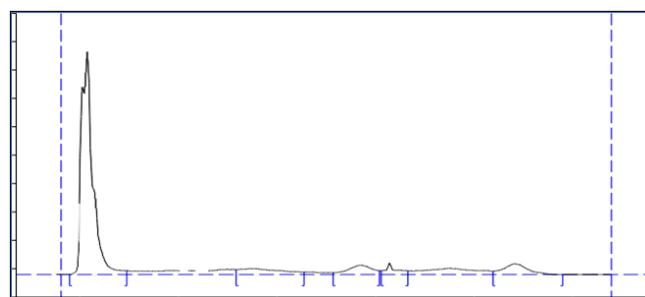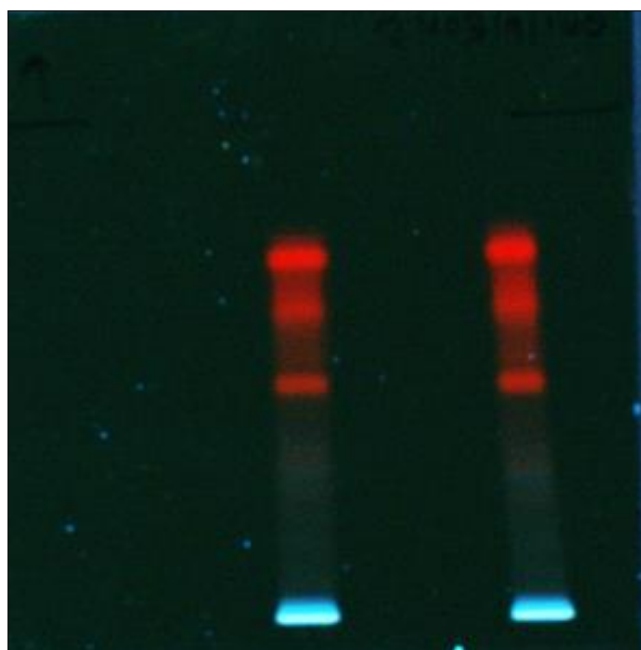**Fig 3:** HPTLC chromatogram of *S. molesta* leaf extract at 366 nm

Fig 4: HPTLC band visualization of *S. molesta* leaf extract at 366

Table 4: Details of HPTLC chromatogram of *S. molesta* leaf extract at 366 nm

Peak	Start Rf	Start Height	Max Rf	Max Height	Max %	End Rf	End Height	Area	Area %	Assigned substance
1	-0.02	0.1	0.02	760.7	72.02	0.10	12.7	13403.7	51.75	unknown
2	0.40	20.5	0.41	21.3	2.01	0.46	12.8	639.3	2.47	unknown
3	0.51	11.1	0.58	56.1	5.31	0.61	25.3	2034.5	7.86	Caffeic acid
4	0.67	26.8	0.75	59.2	5.60	0.82	44.5	4010.5	15.48	Vanillic acid
5	0.82	44.7	0.88	159.0	15.05	0.97	1.8	5811.6	22.44	Flavonoid

From the chromatogram of leaf extract of *S. molesta*, which showed 5 peaks at 366 nm, 05 peaks were identified. These were peak numbers 3, 4and 5 having maximum Rf values 0.58, 0.75, and 0.88. These compounds were identified as caffeic acid, vanillic acid and flavonoid.

A major study conducted in *S. molesta* by Li *et al*. (2013) using bioactivity-guided fractionation of ethanol extract yielded 50 compounds, including 17 abietane diterpenes nine phenolics (Chaudhary *et al*., 2008) [3], five fatty acids, five triterpenes, four apocarotenoids, two acyclic sesquiterpenoids, two monoterpenes, two jasmonates, two steroids and two coumarins. Another study has shown that naringenin was the major phenolic compound present in acetone: methanol (1:1) extract of *S. molesta* which was identified and quantified by HPLC followed by myricetin along with rutin, epicatechin, catechin, quercetin, kaempferol, and vanillin. These compounds were also found to have free radical scavenging potential (Panda *et al*., 2014 and Gini and Jyoti, 2018) [13, 6]. Salleh *et al*., (2023) [14] reported that the plant is rich in phenolics, flavonoids, tannins, alkaloids, and saponins. Santhosh *et al*., (2022) [15] and Al-Knani *et al*., (2023) showed that allied species *S. cucullata* and *S. natans* have potential antimicrobial and antioxidant activities. These are some reports which supports the present study.

The present study showed the plant is very rich in phytochemicals and has various phenolic compounds like ferulic acid, vanillic acid, and other flavonoids. Therefore, it can be concluded that this plant is one of the plausible natural antioxidants the phenolic compounds could be used

as a lead candidate for synthesizing antioxidant drugs which can be useful for the treatment of many oxidative stress-related diseases.

Acknowledgment

References
1. Al Knani ZMI, Al Ashoor AS, Hussein AN. Antioxidant activities of some *Salvinia natans* L., extract and a study of their efficacy against isolated bacteria from diabetic foot ulcers. Journal of Survey in Fisheries Sciences,2023:10(1):1954-1968.
2. Al Maliki GM, Al Khafaji K Kh, Karim RM. Antibacterial activity of two water plants, *Nymphaea alba* and *Salvinia natans* leaves against pathogenic bacteria. International Journal of Fisheries and Aquatic Studies,2017:5(5):353-355.
3. Chaudhary MI, Naheed N, Abbaskhan A, Musharraf SG, Siddiqui H, Atta Ur Raheman. Phenolics and other constituents freshwater fern *Salvia molesta*. Phytochemistry,2008:69(4):1018-1023.
4. Gandhi RR, Kopare NP, Rathod SA, Shirsat RP, Koche DK. Physico-chemical, fluorescent and phytochemical analysis of *Anisochillus carnosus* (L.f.) Wall: a Lamiaceae herb from Maharashtra, India. Indian Journal of Applied and Pure Biology,2022:37(1):1-12.
5. Gaya KS, Ramesh Babu MV, Lizzy M. Preliminary phytochemical study of *Salvinia molesta* from North Paravur, Ernakulam, Kerala, India,2016:5:3437-3441.
6. Gini TG, Jothi GJ. Column chromatography and HPLC analysis of phenolic compounds in the fractions of *Salvinia molesta* Mitchell. Egyptian Journal of Basic and Applied Sciences,2018:5(3):197-203. DOI: 10.1016/j.ejbas.2018.05.010.
7. Harborne AJ. Phytochemical methods a guide to modern techniques of plant analysis. Springer Science and Business Media, 1998.
8. Hauwa MM, Gasim Hayder. Performance of *Salvinia molesta* plants in tertiary treatment of Domestic wastewater. Helyon,2021:7(1):E06040.
9. Israa AA, Suja F, Abdullah SRS, Idris M. Preliminary test of Hydrocarbon exposure on *Salvinia molesta* in phytoremediation process,2011:1(2):52-56.
10. Jasutkar JM, Shirsat RP, Koche DK. Pharmacognostic Study, Chemical Analysis and Antioxidant Potential of Leuca indica L. (R. Br.). Herbal Drugs,2018:9(1):1-5.
11. Lahdesmaki P. Free amino acids in the leaves of *Salvinia natans* and *Azolla fliliculoides* grown in light and dark. Physiology Plantarum,1968:21(5):1097-1103.
12. Li S, Wang P, Deng G, Yuan W, Su Z. Cytotoxic compounds from invasive giant salvinia (*Salvinia molesta*) against human tumor cells. Bioorganic and Medicinal Chemistry letter,2013:23(24):6682-6687.
13. Panda SS, Sahoo K, Rana M, Rout NC, Dhal NK. Antimicrobial activities and phytochemical investigation of some native Pteridophytes. Asian Journal of Pharmaceutical and Clinical Research,2014:7(1):43-45.
14. Salleh NAM, Pa'ee F, Manan MA, Sabran SF, Bakar FIA, Muhammad N, *et al*. Evaluation of Salvinia molesta Mitch (Salviniaceae) for antioxidant and antimicrobial properties, 2023, 7(11). http://www.doi.org/10.26538/tjnpr/v7i11.13
15. Santhosh P, Nithya S, Lakshmi G, Marino GLS, Balvaishnavi M, Kamraj M. Assessment of phytochemicals, antioxidant, antibacterial activity, and Profiling of functional molecules in novel freshwater fern *Salvinia Cucullata* Roxb. South African Journal of Botany, 2022. DOI: 10.1016/j.sajb.2022.02.030.

STUDY OF LOCAL FISH AVAILABILITY AND FISH MARKETING SYSTEM OF MURTIJAPUR, AKOLA DISTRICT (MAHARASHTRA)

S.S. **Dhande**

Department of Zoology, Shri. Dr. R. G. Rathod Arts and Science College Murtijapur, Dist- Akola, M.H., India
satyavijaydhande@gmail.com

Abstract
This study was conducted on the local fish availability and fish marketing system of Murtijapur. The 13 different fish species belongs to freshwater were available in this market for sold. The most commonly available fish species for selling are Catla, Rohu, Mrigal, Murral, Poshti, Suwa, Katarna, Pankaj, Gobi, Chala Chanda etc. The most important fish species including Murral, Catla and Rohu. The demand of Mrigal fish is more as compared other local fishes in this market. Most of the fish seller catches the local fishes from the different resources like Purna river, and small water reservoir nearby Murtijapur and they sell the fishes in this market. The cost of fishes was exceptionally high as a result of the unsure of catch and sort run supply. Fish seller in this fish market do not have appropriate refrigeration and freezing facilities and they depend on ice for fish storage. Hygiene conditions at this fish market was very poor. Fish are made available for purchase on plastic sheets, plastic sacks, and open flour. Cutting blades and platforms are not as expected put away and frequently expose on ground loaded with soil, mud and residue.
Keywords: fish market, fish seller, water reservoir, hygiene, cutting blades.

Introduction
Murtijapur is a taluka place situated in Akola district. This is the main market place for all the surrounding villages. So, all the people of the villages are dependent on this market. The local fish market is famous and people come to buy local fish. A weekly market is held here on Tuesdays and Fridays and people flock here for it. Some local fishes are available in the market throughout the year. The main source of fish is rivers, small ponds and reservoirs near Murtijapur. The fisherman goes to various water sources nearby to catch fish and sell them in this market.This fish market is very popular among the nearby villages as fish are timely available as per the need of buyers. The very important thing of this market is that the local fish like Katarna, Chanda, Pankaj, Gobi, Chala, Kolshi are made available for the buyers. Making fish available to consumers at the right time and place requires an effective marketing system. According to Adrika (1977), marketing performs so many functions in an economic system, as it connects buyers and sellers, enabling an exchange relationship. It improves the way of life and aggressive marketing has been largely responsible for the high standard of living of most advanced countries. The growth of fish production and the economic and infrastructural development of the fisheries sector are highly dependent on an efficient fish marketing system (Chourey *et al*., 2014). In India most of the fish production and capture sold in local markets. Most of the markets are still in development stage and only few having facilities. Major hindrance in fish marketing includes perish ability and large quantities, storage, transportation, quality and quantity of commodity, low demand elasticity and high price spread (Ravindranath *et al*., 2008).

Material and Methods
The data used in this study came from primary sources. With the aid of direct observation, an interviewing approach, and a questionnaire, the primary data are gathered through a study of the fish market. The information gathered through a field trip, individual interviews, and market observations in the study area.

Observation and Results
The fish sellers in this area bring their own nets to catch fish from the nearby rivers and streams. To catch fish, a net is placed in the water the day before and the flies caught in the net are collected the next day. Before catching, fish sellers in this area throw thorn branches into the water to stop the night-time fishes from coming there. In the morning the fishes are catches by using net. Fishermen go to different waters resources nearby to catch fish and sell them in the market. The price fluctuation of fish is very high due to uncertain catch production and sort run supply. (Vala *et, al* 2020).
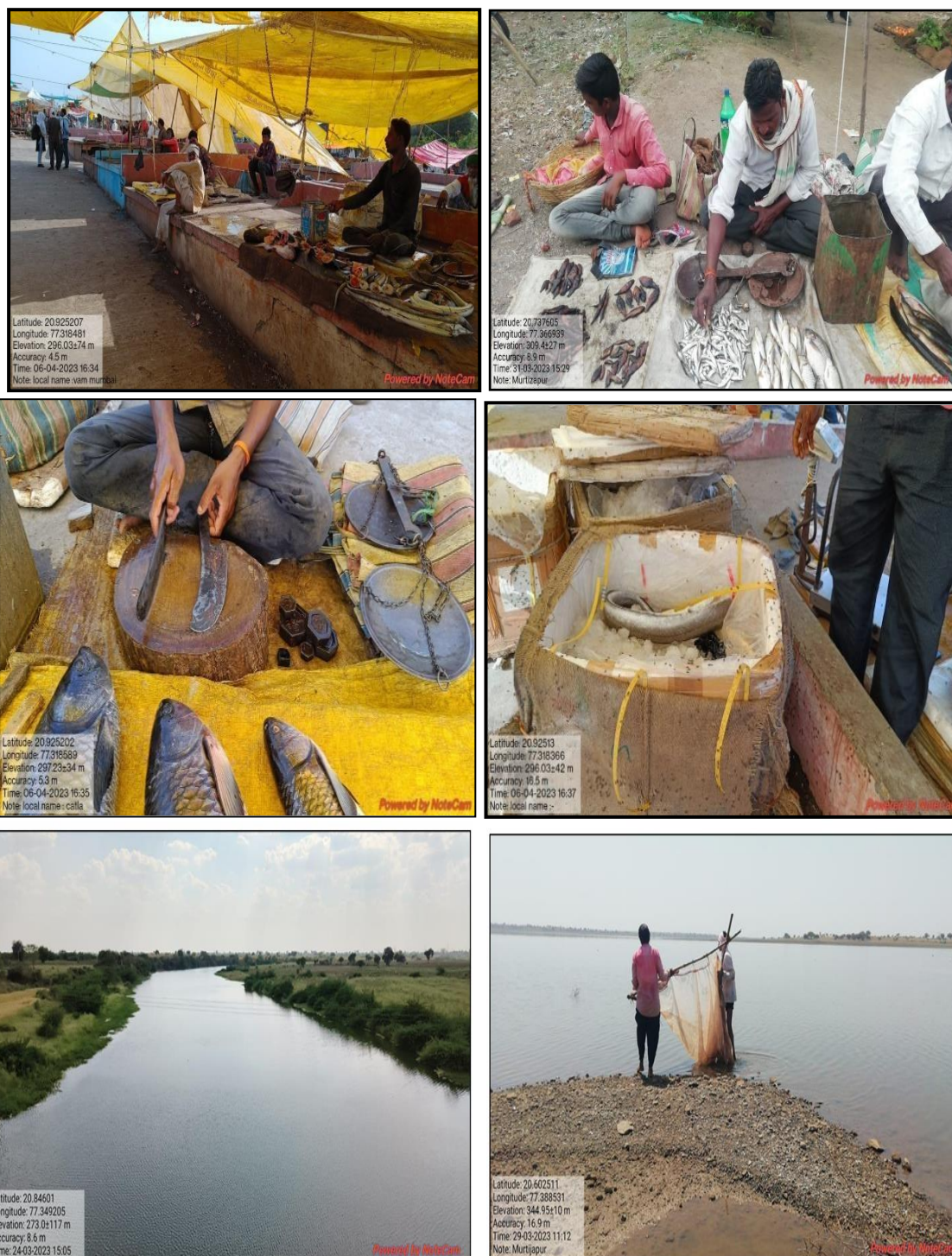
Fig: fish market showing hygiene condition, water resources, equipment used by fish sellers and storage facility.

On days when fishes are available in abundance, the price of local fishes goes down. On other days the price of the same fish is kept higher by the fish seller. The fish that are not sold at the market are stored in ice and sold again at low prices on the next market day. Alam *et al*., (2010) also reported influence of market structure, species quality, size and weight in price of fish. The fish sellers of Murtijapur have no special facility to sell their fish. The local fish seller covers their fish selling platform with temporary roofs of green nets to protect from the sunlight.

126

Sr. No.	Local name	Scientific name	Size of Fish	Price/Kg	Availability
1	Catla	*Catla catla* (Ham.)	**Medium**	160-200	High
2	Chanda	*Chandanama* (Ham.)	**Small**	100-120	Medium
3	Murral	*Channa marulius* (Ham.)	**Medium**	240-360	High
4	Mrigal	*Cirrhinus mrigala* (Ham.)	**Medium**	120-140	High
5	Gobi	*Glossogobius giuri* (Ham.)	**Small**	80-120	Medium
6	Rohu	*Labeo rohita* (Ham.)	**Medium**	160-200	High
7	Bam	*Mustocembelus pancalus* (Ham.)	**Medium**	150-180	High
8	Katarna	*Myctus cavasius* (Ham.)	**Small**	160-180	High
9	Pankaj	*Pangasius pangasius* (Ham.)	**Medium**	100-120	Medium
10	Kolshi	*Puntius Kolus* (Sykes.)	**small**	100-120	Medium
11	Poshti	*Puntius sarana* (Ham.)	**Small**	60-80	Medium
12	Chala	*Salmostoma phulo*(Ham.)	**Small**	100-120	Medium
13	Suwa	*Xenetodon cancila* (Ham.)	**Small**	60-80	Medium

Table.1 Average Selling Price (kg) and Demand of available Fishes in Murtijapur market.

They store fishes in plastic baskets and plastic sacks to safeguard them. The principal devices utilized by fish sellers are blades, scrubbers and wooden stages to cut the fish. There is no facility to store fish in this fish market. They depend on ice for fish storage. So, the fish sellers here store the remaining fish in the refrigerator at their homes and the next day the same fish are brought to the market and sold. Since it is a perishable commodity, cold chain is an essential part of fish marketing (Markad et. al 2019). The most regularly sold species are Catla, Rohu, Rigal, Murral, Poshti, Suwa, Ktarna, Pankaj, Gobi, Chala Chanda, etc.

The main fish during this study including Catla, Rohu, Murral, Mrigal were sold in enormous amount. Cleanliness conditions of this fish market, which was the subject of the review, were exceptionally poor. The same findings were supported by Uddin *et al.* (2018) and Kumar *et al.* (2008) who reported that infrastructure facilities drainage system and sanitation conditions of fish markets were found grossly inadequate and maintained poorly. Fish were made available for purchase on plastic sheets, plastic sacks, and open flour. Cutting blades and stages were not as expected clean.

Summary and Suggestions

In this paper local fish availability and fish marketing system in Murtijapur market was studied. The marketing system of fish market was found to be simple one. This fish market is important as local fish is available to the people of all the surrounding villages. This market has different types of fish available as well as the fish sellers in and around Murtijapur have a good business. This is a traditional profession of many families and their children are also seen doing this profession. It became the main income

source of these people. Fish seller catches different fishes from the river with help of fishing net and brought to the market and sold it at specific price.

Mostly fishes caught in morning time and were brought to the market by evening time. Most of the fisherman tries to sell their whole catches on the same day due to unavailability of proper cold storage facilities. Most of the fishermen were found working in individually for fishing. There is a need of cold storage and preservation facilities. There is need of improvement of existing fish market, Improvement of sanitation, hygienic condition, drainage and washing facilities. In conclusion, condition of Murtijapur fish market is poor facilities. Need tohave some development of this fish market.

References

1. Adrika, O.B. (1977). Principle and practice of market. 1 and 11 Jamoe Enterprise Publisher, 36p.
2. Alam, M.J., Yasmin, R., Rahman, A Nahar, N., Islam, N. and Hasan. M. (2010). A Study on Fish Marketing System in Swarighat, Dhaka, Bangladesh. Nature and Science. 8(12): pp. 96-103.
3. Chourey, P., Meena, D.,Varma., A and Saxena. G. (2014). Fish marketing system in bhopal (M.P.). Biological Forum –An International Journal 6 (1): pp.19-21.
4. Markad, S.S., Gaikwad, J. M., Patil, D. W. and Shinde, V. D. (2019). Marketing system and state of fish markets in Hingoli district, Maharashtra. Advances in Fisheries, Biological & Allied Research; 1 (2): pp.105-110.
5. Ravindranath, K. (2008). In National Workshop on Development of Strategies for

Domestic Marketing of Fish and Fishery Products, College of Fisheries Science, Nellore, India. pp. 43-48

6. Kumar, B.G., Datta, K.K., Joshi, P.K., Katiha, P.K., Suresh, R. and Ravisankar, T. (2008). Domestic fish marketing in India-changing structure, conduct, performance and policies. Agricultural Economics Research Review, 21: 345-354.

7. Uddin M.H., Sirazunnesa, M.S. Haq, Z.F. Ahmed, Fatema, J. and Fatema, M.K. (2018). Structural performance of fish market in Bogura district, Bangladesh. Research in Agriculture Livestock and Fisheries, 5 (3): 399-410.

8. Vala, S. R., Lende, S. R., Jora, 6. K., Dhimmar, H., Mevada, J., Fofandi D. and Dhimmar S. (2020). A study of fish marketing system in Himmatnagar, Sabarkantha, Gujarat Int. J. Curr. Microbiol. App. Sci 9(1): 1pp. 1054.

STUDY OF SOME SPIDERS FROM FAMILY ARANEIDAE IN AND AROUND DARYAPUR TEHSIL, DISTRICT AMRAVATI.

Entomology

Dr. Satyavijay S. Dhande
Assistant Professor, Dept. Of Zoology, Shri. Dr. R. G. Rathod Arts And Science College Murtizapur, Dist- Akola

ABSTRACT

Study of some spider species from family Araneidae were conducted in and around Daryapur tehsil. Total 5 species were described from genus Cyclosa, Eriovixia, and Neoscona from family Araneidae. The spider species were studied mainly in the fence around the farm and along the road leading to the farm. The spiders from genus Cyclosa and Neoscona found abundant and widely distributed in study area during August to the month of January (mid Monsoon to post Monsoon season) of the year. However, the recorded species have already been studied from other parts of the country.

INTRODUCTION:

Spiders are most common and unique invertebrate predator found on entire land of the world. Spiders have dominated all possible ecological niches on land (Turnbull 1973; Riechert 1984; Wise 1993). The spiders from family Araneidae are orb web weavers and construct a beautiful web with unique pattern in different habitat. The different spider species of family Araneidae shows their own pattern of web designing. Despite of ecological importance in many ecosystems, high diversity and documented threats to some of the species, spiders have received little attention by the scientific community. This is due to the scarcity of proper acquaintance towards the biology of spiders. Spiders are important components of agricultural systems because of negative pressure exert on insect populations (Nyffeler and Benz 1987; Young and Edwards 1990). Major contributions to the Indian spider study were made by Tikader (1980-1987), he has high lightened spider studies to the notice of another researcher.

Spiders can be easily distinguished from insects, since insects have six legs. However, spiders are adapted with appendages for feeding purpose, defence, and sensory function. The first pair of the chelicerae used for feeding purpose and help in defence mechanism. The next pair of appendages, the pedipalp, used for locomotion, feeding and in reproduction. The underside and head of a female spiders, unlike insects, have only two main body parts (tagmata) instead of three: a fused head and thorax are called as cephalothorax or prosoma and an abdomen (also called an opisthosoma). The abdomen and cephalothorax both are connected by a thin structure called pedicel. Tikader (1987) provided the pioneering list of Indian spiders. As the common name implies these spiders occur in the veil among grasses and bushes, (Hippargi, *et al.,* 2011 and Keswani *et al* 2012).

MATERIAL AND METHODS:

The present study is based on material collected from September 2017 to October 2018 in and around Daryapur taluka, district-Amravati in Vidarbha region of Maharashtra, India. The few important collecting techniques used to capture spiders at selected locations were visual search, hand collection, sweep netting, and vegetation beating. All specimens were preserved in 70% ethyl alcohol. The female genitalia were dissected and epigyne was then cleared in 10% KOH aqueous solution. The specimens were identified by using a Carl-Zeiss Stemi 2000-c Stereo-Zoom microscope mounted with Axio Cam ERc5s camera (Germany). Daryapur tahsil is located in Amravati district in Maharashtra, India. It is situated 52 km away from district headquarter Amravati.

OBSERVATIONS AND RESULTS:
Cyclosa hexatuberculata (Tikader 1982)

Cephalothorax longer than wider, yellowish brown in colour, longer than wide, slightly narrow anteriorly and broader posteriorly, thoracic region is slightly higher than cephalic region, Chelicerae is stronger, yellowish brown in colour with presence of few and dense scapulae in the inner surface, fangs a stronger yellowish brown in colour, pointed at the tip and thick at base, Sternum heart shaped, yellowish brown colour, broader anteriorly and pointed at posteriorly, concave anteriorly, clothed with hairs. Endites thick larger, lightly yellow brown with paler toward labium. Female palp with all segments

slender, blackish in color, presence of hairs over

All Segments, Leg Formula: 4123, with short spines over all over the segments of legs, clothed with straight black hairs, coxa, trochanter, femur, brown colored, Trichobothria present on patella, tibia, tarsus and metatarsus, femora I with two protrolateral spine, patella with one retrolateral spine, patella II with one retroterminal spine, III with on dorsal terminal spine, tibia I with two prolateral spine one ventral terminal spine, metatarsus and tarsus provided with numerous spines.

Eriovixia excelsa (Simon, 1889) female:

Carapace dark brown in coloration with setae on cephalic region, head is lighter, cephalic higher than thoracic, anterior thorax depressed immediately behind cephalic part, anterior narrow, posterior broad, cephalic region narrowed anteriorly, 8 Eyes are arranged in two rows, anterior eye row recurved, posterior eye row straight. Clypeus lower than eye region, presence of few curved setae, no distinct chillum, Chelicerae strong, yellowish brown with setae at outside and curved dense scapulae inner surface; fangs yellowish brown, pointed at the tip, thick at base, strongly curved serrated margins, thick at base, pointed at tip, pro margin with four teeth, among which first and third are large and strong as compared with other two teeth; retro margin with three teeth in which first and second are strong teeth surrounded by fine scapulae. Labium dark brown, slightly wider crescent shaped presence of few setae over it and presence of dense scapulae at its anterior tip and inner margin. Female palp with all segment is slender, longer tarsus and metatarsus, presence of numerous setae over all segments except trochanter and femur. Leg formula- 1243.

Abdomen globular, black in color with white patches, dorsal two pairs of sigilla present, few large straight setae present at distal tip of abdomen near to pedicel, rest of the abdomen in the form of folding muscles with hairs, at posterior end bears a small tubercle. Venter side blackish brown with a pair of chalk-coloured white spots. Spinnerets small, aggregated together ventrally, surrounded by rounded fold, clothed with hair, segmented brown colored.

Neoscona nautica (Koch, 1875) female:

Cephalic region higher than thoracic, longer than wide, narrow anteriorly, depression between cephalic and thoracic, provided with longitudinal light band, covered with hairs and grey pubescence, eyes arranged in two row, anterior medians slightly larger than posterior medians, median eyes away from laterals, recurved eyes, MOQ slightly wider anteriorly, than posteriorly, each eye black bordered, presence of few curved setae. Sternum heart shaped, broader anteriorly, pointed at posteriorly, clothed with pubescence and hairs, dark brown, labium wider than long, dark brown in colour with pale margin at distal end, female palp with all segments slender and presence of hairs over it, yellowish brown. Leg formula: 1423, with short spines over segments of legs, legs strong with pale transverse band.

Abdomen: Triangular wider anteriorly and narrow posteriorly, covered with pubescence. Dorsum of abdomen with mid-longitudinal chalk white bar having 4 projections, presence of the greenish brown patches, 6 pairs of sigilla present, ventral side green brownish patches.

Epigyne is short and broad triangular scape, presence of lateral lobe without any constriction.

Neoscona theisi (Walckenaer, 1841) female:

Cephalic region higher than thoracic, depression between cephalic and thoracic, longer than wide, narrow anteriorly and broader posteriorly, provided with longitudinal groove, covered with hairs. Eyes arranged in two row, anterior medians slightly larger than posterior medians, median eyes away from laterals, recurved eyes, MOQ slightly wider anteriorly, than posteriorly, each eye black bordered, presence of few curved setae, no distinct chillum. Endites thick larger, yellowish with presence of setae, broader anteriorly than posteriorly. Sternum heart shaped, broader anteriorly, pointed at posteriorly, clothed with pubescence and hairs, dark brown. Labium is wider than longer, dark brown in color, presence of setae. Female palp with all segments slender, presence of hairs over all segments, yellowish brown, 1 tarsal claw is present. Leg formula: 1423.

Abdomen: Sub oval wider anteriorly than posteriorly covered with pubescence. Dorsum of abdomen with mid-longitudinal chalk white bar having 4 projections, presence of dark brown patches, 4 pairs of Sigilla present, ventral side light brownish, broad brown patch present, Epigyne with constriction in the middle, a pair of lateral lobes with circular opening at its side. Spinnerets at the top of abdomen toward ventral side, aggregated together, clothed with hairs.

Neoscona theisi (Walckenaer, 1841) male:

Cephalothorax yellow brown color, longer than wide, narrow anteriorly, broader posteriorly, thoracic region with longitudinal depression, clothed with the hairs. 8 eyes in two rows (4:4) AE rows more recurved than PE, lateral eye group is widely separated from median eye, MOQ is slightly wider anteriorly than posteriorly, presence of few curved setae, clypeus is small and very closer to eye region. Chelicerae small, yellowish brown with presence of hairs, fang swollen just posterior to middle, well developed tooth like projection is present, 4 promarginal teeth present in which 3 and 4 is larger, 4 retro marginal teeth present, Labium yellowish brown, wide, presence of few setae over Male palp with large curved paracymbium, medium hypophysis large with wide base, cymbium brownish reddish color and surface clothed with hairs. Sternum triangular, concave anteriorly, pointed posteriorly, dark brown in color, bathed with hairs and pubescence. Leg formula: 1423, Abdomen: elongate, covered with setae, broad at anterior end, and narrow at posterior end, brown with chalk colour white spot at anterior end, 2 pairs of sigilla present. Spinnerets: simple with aggregate silk gland spigots, surrounded by rounded fold, clothed with hair.

Neoscona nautica (Koch, 1875) Female

Neoscona theisi (Walckenaer, Male

Neoscona theisi (Walckenaer, 1841) female

- Eriovixia excelsa (Simon, 1889) Female
- Cyclosa hexatuberculata (Tikader, 1980) female
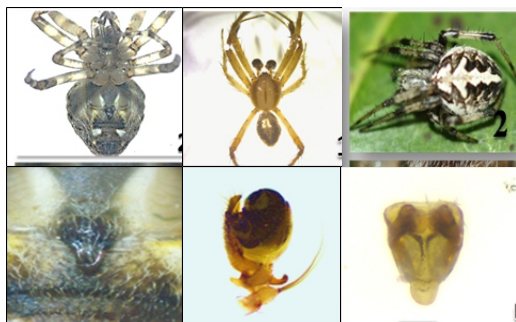
DISCUSSION:

In this study 5 species of spiders belonging to the 3 genera from family Araneidae were studied. It mainly studied spiders in fences around farms as well as roadside of agroecosystem. Elsewhere these spider species have been studied before. While conducting this study, it was found that the diversity of spiders was good. But in some places, it is declined. The reason for this was found to be deforestation as well as excessive use of pesticides in the agricultural field. Deforestation has to be stopped to increase spider population and farmers have to be made aware of it. The spider has a long way to maintain and balance the ecosystem.

CONCLUSION:

The present attempt was to study spiders from genus Cyclosa, Eriovixia, and Neoscona in and around Daryapur. This research provided the basic information on some spider in the study region. Rich diversity of Araneidae indicated that the environmental conditions, food sources and seasonal variations are suitable to them. Spiders are very sensitive to changes in the habitat arrangements and also have largely been ignored by the conservationists. Therefore, it is very essential to protect and conserve this ecosystem.
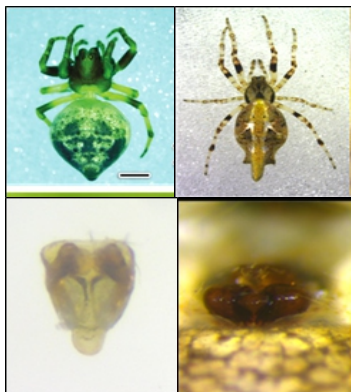
REFERENCES:
1. Turnbull, A. L. (1973) Ecology of the true spiders (Araneomorphae). *A. Rev. Ent.* 18, 305-348.
2. Reichert, S.E., and Lockley, T. (1984). Spiders as biological control agents. *Ann. Rev. Entomol, 29*, 299-320.
3. Wise, D. H. (1993). Spiders in ecological webs. *Cambridge university press,* 0-521-32

An efficient synthesis of optically active herbicide (*S*)-metolachlor *via* reductive ring opening of 2-methoxymethylaziridine

Viswanadh Nalla,[a] Mohammad Mujahid, [ab] Murugesan Sasikumar, [a] Prashant Mujumdar, [a] and Murugan Muthukrishnan [a]*

[a]*Division of Organic Chemistry, CSIR-National Chemical Laboratory (NCL), Dr. Homi Bhabha Road, Pune 411 008, India*
[b]*Department of Chemistry, Shri. Dr. R. G. Rathod Arts & Science College, Murtizapur, Dist Akola. India*
Email: m.muthukrishnan@ncl.res.in

**This manuscript is dedicated to Prof. Ahmed Kamal on the occasion of his 65th birthday**

Abstract

An efficient synthesis of a well known chiral herbicide, (*S*)-metolachlor has been described using 2-methoxymethylaziridine ring formation and reductive ring opening as key steps using commercially available (*R*)-epichlorohydrin. The present protocol delivers the required enantiomer of metolachlor in overall yield of 50.8% and high enantiopurity (>99%).
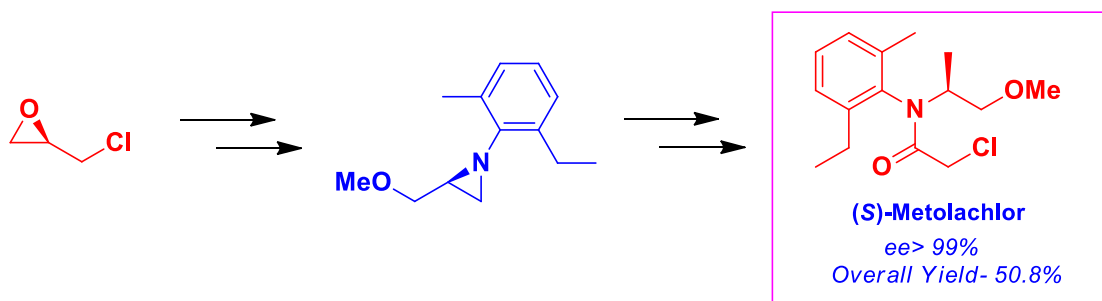
Introduction

Many pharmaceutical and agrochemical companies have limited the use of racemates which contain both the active and inactive isomers in equimolar ratio. Due to the large variations in biological activities of the two enantiomers, development of new strategies for the production of enantiopure compounds has increased remarkably.[1] Metolachlor is a widely used herbicide which comprises four stereoisomers, of which two are inactive. The stereoisomers arise from the combination of a chiral center in the side chain and a chiral axis between the aromatic ring and nitrogen atom.[2] Previously, metolachlor was applied as a racemate with a brand name Dual®, but later it was found that about 95% of the herbicidal activity of metolachlor exists in the two 1-*S* diastereomers which means that (*S*)-enantiomers possess higher herbicidal activity than the (*R*)-enantiomers. Therefore the racemate was replaced by the active (*S*)-isomer which was marketed under the trade name Dual Magnum® (Figure 1).[3]
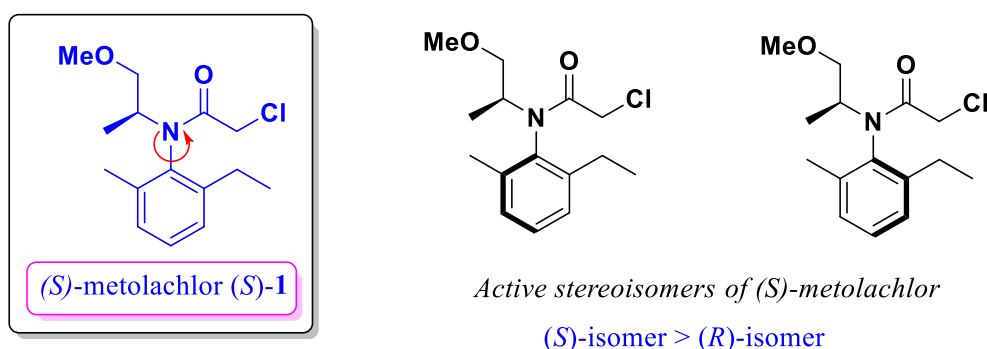

(S)-metolachlor *(S)*-**1**

Active stereoisomers of (S)-metolachlor

(S)-isomer > (R)-isomer

**Figure 1**. Active isomers of Metolachlor.

Several reports are available for the synthesis of (*S*)-metolachlor, which involves asymmetric processes: mainly hydrogenation of imines or enamides,[4] enzymatic resolution[5] and chiral pool approaches.[6] But, most of these methods suffer from at least one of the following drawbacks such as low enantioselectivity, lower overall yield, protection-deprotection sequences, expensive reagents and catalysts, drastic reaction conditions etc. Very recently, Wang and coworkers reported a new route for the synthesis of (*S*)-metolachlor. Although this method seems to be impressive, but it involves nosylation-denosylation steps that limits the superiority of the method.[7] So, still there is a scope for newer methods that can overcome these drawbacks.

Epoxides, emerged as one of the widely used functional groups in various chemical transformations because of its intrinsic strain, can be easily opened with numerous nucleophiles.[8-13] In connection with our continued interests in utilizing epoxides for the synthesis of pharmaceutically important compounds[14-18] herein, we report a new and simple synthetic strategy for the synthesis of (*S*)-metolachlor via reductive ring opening of 2-methoxymethylaziridine.[19,20]

Results and Discussion

A retrosynthetic analysis of *(S)*-**1** is depicted in Scheme 1. We envisioned that enantiomerically pure epichlorohydrin **(R)-2** can be used as a chiral starting material for the synthesis. Based on the strategies involving regioselective ring opening and Mitsunobu reaction, aziridine *(S)*-**4** could be obtained from the epoxide **(R)-2**.

This aziridine **(S)-4** intermediate can be transformed to the final product **(S)-1** via reductive ring opening and subsequent reaction.
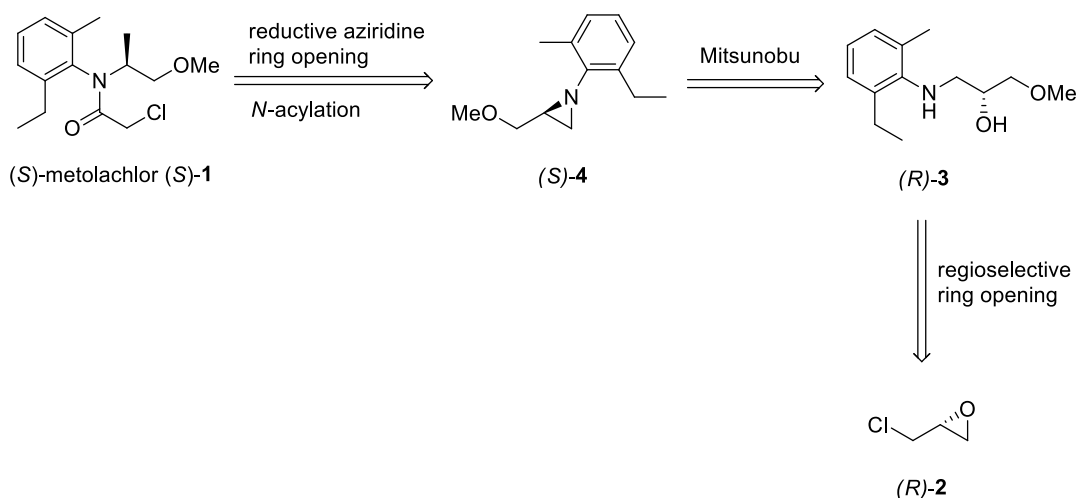
Scheme 1. Retrosynthetic analysis of (S)-metolachlor **(S)-1.**

Accordingly, epoxide **(R)-2** on treatment with 2-ethyl-6-methylaniline in refluxing methanol for 6 h afforded chlorohydrin in situ. After the complete conversion of the starting material to the corresponding chlorohydrin derivative (confirmed by TLC), powdered KOH (2.5 equiv.) was added portion wise to the reaction mixture at temperature maintained below 25°C. After stirring the reaction mixture at room temperature for 8 h the required amino alcohol **(R)-3** was obtained in high yield (Scheme 2). Subsequently, the amino alcohol **(R)-3** in hand was exposed to Mitsunobu conditions (PPh$_3$/DIAD) to afford the key intermediate aziridine **(S)-4**. Here, it is noteworthy to mention that the formation of aziridine **(S)-4** was unsuccessful at room temperature using THF as a solvent as practiced routinely, so the reaction was carried out in toluene under reflux conditions. Further, the aziridine **(S)-4** on reductive ring opening using catalytic Pd/C under H$_2$ pressure furnished the required metolachlor intermediate **(S)-5** in high enantiopurity (ee>99%). Finally, **(S)-5** was acylated using chloroacetyl chloride under basic conditions to furnish the target compound **(S)-1** in overall yield of 50.8%. The structure of **(S)-1** was confirmed by its IR, ^{1}H NMR,[7] ^{13}C NMR, [7] and mass spectroscopic analysis. The enantiomeric purity of **(S)-5** was determined by chiral HPLC analysis.
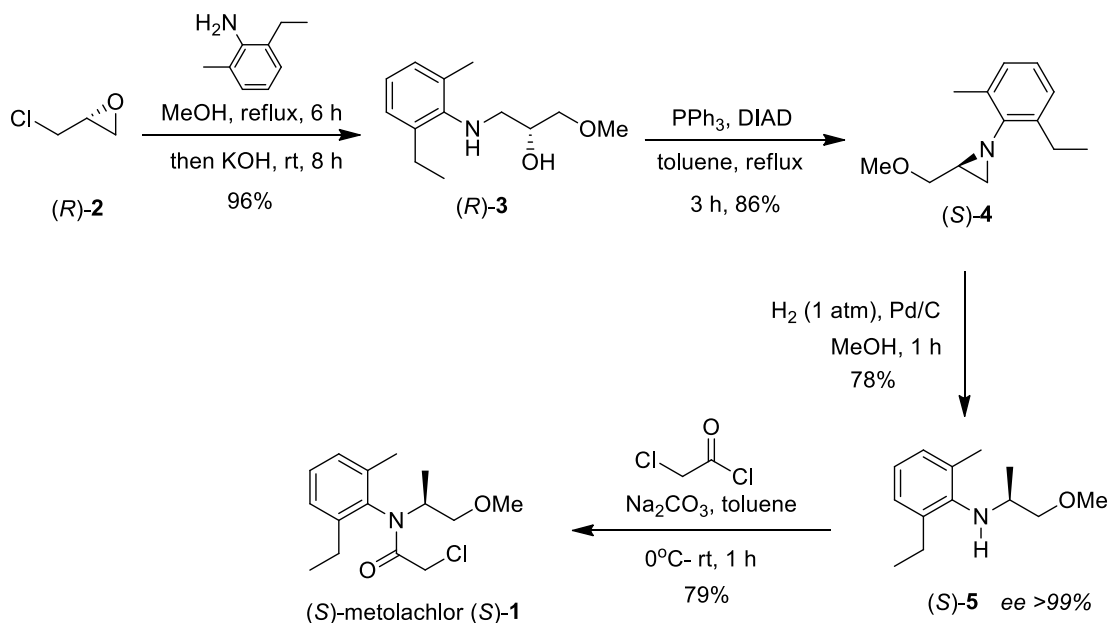
Scheme 2. Synthesis for (*S*)-metolachlor **(S)-1.**

Conclusions

In conclusion, we have developed an efficient new route for the synthesis of (*S*)-metolachlor **(S)-1** via reductive ring opening of 2-methoxymethylaziridine. The attractive features of the present protocol include readily available chiral starting material, simple chemical transformations, high enantiopurity and good overall yield (50.8%). We envisage that this simple protocol may find application in agrochemical industries for the large scale preparation of active isomer of metolachlor with high enantiopurity.

Experimental Section

General. Solvents were purified and dried by standard procedures prior to use. IR spectra were obtained from Perkin–Elmer Spectrum one spectrophotometer. ^{1}H NMR and ^{13}C NMR spectra were recorded on a Bruker AC-200 NMR spectrometer. Spectra were obtained in CDCl$_3$. Monitoring of reactions was carried out using TLC plates Merck Silica Gel 60 F254 and visualization with UV light (254 and 365 nm), I$_2$ and anisaldehyde in ethanol as development reagents. Optical rotations were measured with a JASCO P 1020 digital polarimeter. Mass spectra were recorded at ionization energy 70 eV on API Q Star Pulsar spectrometer using electrospray ionization. Enantiomeric excess was determined by chiral HPLC.

(R)-1-((2-Ethyl-6-methylphenyl)amino)-3-methoxypropan-2-ol (R)-3. To a stirred solution of (*R*)-epichlorohydrin **(R)-2** (2 g, 21.6 mmol) in methanol (15 mL) was added 2-ethyl-6-methyl aniline (3.2 g, 23.7 mmol) and the resulting mixture was refluxed for 6 h. After completion of the reaction (monitored by TLC), crushed KOH (3.0 g, 54.0 mmol) was added portion wise at temperature <25 °C. After completing the addition, the reaction mixture was stirred vigorously for 8 h at room temperature. After completion of the reaction (monitored by TLC), excess methanol was evaporated under reduced pressure. The reaction mixture was then

poured into water (20 mL) and extracted with EtOAc (2 x 15 mL). The combined organic layers were washed with brine (10 mL) and dried over Na_2SO_4. Evaporation of the solvent gave the crude residue which was purified by silica gel column chromatography using petroleum ether/EtOAc (90:10) as eluent to furnish (*R*)-1-((2-ethyl-6-methylphenyl)amino)-3-methoxypropan-2-ol **(*R*)-3** as a pale brown oil (4.6 g, 96%); $[\alpha]^{21}_D$ = +4.9 (*c* 2.09, $CHCl_3$); IR ($CHCl_3$, cm-1): ν_{max} 3421, 3009, 2966, 1593, 1466, 1377, 1216, 1129, 968, 667; ^1H NMR (500 MHz, $CDCl_3$): δ_H 1.26 (t, *J* 7.6 Hz, 3H), 2.33 (s, 3H), 2.66-2.71 (m, 2H), 2.98 (dd, *J* 12.5, 7.0 Hz, 1H), 3.10 (dd, *J* 12.5, 4.0 Hz, 1H), 3.42 (s, 3H), 3.47 (dd, *J* 9.4, 6.4 Hz, 1H), 3.51 (dd, *J* 9.7, 3.6 Hz, 1H), 3.96-4.00 (m, 1H), 6.91 (apparent t, *J* 7.2 Hz, 1H), 7.02 (d, *J* 7.3 Hz, 1H), 7.04 (d, *J* 7.6 Hz, 1H); ^{13}C NMR (50 Hz, $CDCl_3$): δ_C 145.0, 136.2, 130.6, 128.8, 126.7, 122.6, 75.3, 69.6, 59.2, 51.5, 24.2, 18.5, 14.8; MS: *m/z* 224 $[M+1]^+$, 246 $[M+Na]^+$.

(*S*)-1-(2-Ethyl-6-methylphenyl)-2-(methoxymethyl)aziridine (*S*)-4. A solution of DIAD (3.0 mL, 15.4 mmol) in dry toluene (5 mL) was added dropwise to a solution of **(*R*)-3** (2.3 g, 10.3 mmol) and triphenylphosphine (4.0 g, 15.4 mmol) in a dry toluene (25 mL) under N_2 atmosphere at 0 °C. The reaction mixture was refluxed for 3 h. After completion of reaction (monitored by TLC), the solvent was evaporated under reduced pressure and the residue was purified by silica gel column chromatography (100-200 mesh, petroleum ether/ethyl acetate, 95:5) to afford (*S*)-1-(2-ethyl-6-methylphenyl)-2-(methoxymethyl)aziridine **(*S*)-4** as a yellow oil (1.8 g, 86%); $[\alpha]^{21}_D$ = -120.5 (*c* 1.0, $CHCl_3$); IR ($CHCl_3$, cm^{-1}): ν_{max} 3419, 2967, 2875, 1915, 1745, 1592, 1460, 1378, 1355, 1276, 1217, 1188, 1108, 965, 929, 900, 666; ^1H NMR (200 MHz, $CDCl_3$): δ_H 1.28 (t, *J* 7.6 Hz, 3H), 2.04 (d, *J* 6.3 Hz, 1H), 2.39 (s, 3H), 2.41-2.50 (m, 1H), 2.80 (q, *J* 7.5 Hz, 2H), 3.46 (s, 3H), 3.49-3.54 (m, 1H), 3.93 (dd, *J* 10.4, 4.3 Hz, 1H), 6.88 (apparent t, *J* 7.3 Hz, 1H), 6.95-7.04 (m, 2H); ^{13}C NMR (50 MHz, $CDCl_3$): δ_C 149.9, 134.9, 129.1, 128.8, 126.9, 122.0, 74.0, 59.1, 39.4, 34.9, 24.3, 19.3, 14.3; MS: *m/z* 206 $[M+1]^+$, 228 $[M+Na]^+$.

(*S*)-2-eEhyl-*N*-(1-methoxypropan-2-yl)-6-methylaniline (*S*)-5. To a solution of **(*S*)-4** (1.0 g, 4.8 mmol) in methanol (10 mL) was added palladium on activated carbon (0.065 g, 10-20 wt %) and the reaction mixture was stirred under hydrogen atmosphere (balloon) for 1 h. After completion of the reaction (monitored by TLC) the catalyst was filtered over the celite bed (EtOAc eluent) and the solvent was evaporated under reduced pressure. The crude product was purified by silica gel column chromatography (100-200 mesh, petroleum ether/ethyl acetate, 98:2) to afford (*S*)-2-ethyl-*N*-(1-methoxypropan-2-yl)-6-methylaniline **(*S*)-5** (0.78 g, 78%) as a pale yellow oil; $[\alpha]^{21}_D$ = +11.7 (*c* 2.0, $CHCl_3$); ee >99% [Chiral HPLC analysis: Chiralcel OD-H (250 x 4.6 mm) column; eluent: n-hexane/isopropanol = 99.75:0.25; flow rate: 0.5mL/min; detector: 220 nm]; IR ($CHCl_3$, cm^{-1}): ν_{max} 3409, 3019, 2969, 2877, 2401, 1593, 1465, 1385, 1215, 1103, 928, 669. ^1H NMR (200 MHz, $CDCl_3$)[7]: δ_H 1.19 (d, *J* 6.4 Hz, 3H), 1.26 (t, *J* 7.5 Hz, 3H), 2.31 (s, 3H), 2.67 (q, *J* 7.6 Hz, 2H), 3.32-3.37 (m, 3H), 3.39 (s, 3H), 6.88 (apparent t, *J* 7.4 Hz, 1H), 7.00-7.06 (m, 2H); ^{13}C NMR (50 Hz, $CDCl_3$): δ_C 144.2, 135.5, 129.8, 128.7, 126.5, 121.7, 76.2, 58.9, 52.9, 24.2, 18.9, 18.5, 14.5; MS: *m/z* 208 $[M+1]^+$, 230 $[M+Na]^+$.

(*S*)-2-Chloro-*N*-(2-ethyl-6-methyl-phenyl)-*N*-(2-methoxy-1-methyl-ethyl)-acetamide ((*S*)-metolachlor (*S*)-1). To a stirred solution of **(*S*)-5** (0.1 g, 0.48 mmol) and sodium carbonate (0.102 g, 0.96 mmol) in toluene (3 mL) was added chloroacetyl chloride (0.065 g, 0.57 mmol, 46 μL) at 0 °C. The resulting mixture was stirred for 1 h at room temperature. After completion of the reaction (monitored by TLC), toluene was removed under reduced pressure and the residue was diluted with water (3 mL) and extracted with EtOAc (3 x 5 mL). The phases were separated, and the organic phase was washed with brine (2 x 5 mL), dried (Na_2SO_4) and filtered. The solvent was removed under reduced pressure and the crude residue was purified by column chromatography (silica gel, petroleum ether/ethyl acetate, 90:10) to yield **(*S*)-1** as colorless oil (0.108 g; 79%); $[\alpha]^{21}_D$ = -5.73 (*c* 2.80, n-hexane) {lit.5 $[\alpha]^{25}_D$ = -8.2 (*c* 2.1, n-hexane}; IR ($CHCl_3$, cm^{-1}): ν_{max} 3464, 3019, 1664, 1462, 1215, 1112, 765, 669; ^1H NMR (200 MHz, $CDCl_3$)[7]: δ_H 1.13-1.18 (m, 3H), 1.25 (t, *J* 7.5 Hz, 3H), 2.23 (s, 3H, major + minor), 2.48-2.69 (m, 2H), 3.28 (s, 3H, major + minor), 3.45-3.54 (m, 1H), 3.61 (s, 2H, major + minor), 3.66-3.78 (m, 1H), 4.15-4.28 (m, 1H), 7.11-7.31 (m, 3H); ^{13}C NMR (50 MHz, $CDCl_3$)[7]: δ_C 166.79, 142.56, 142.46, 137.15, 136.92, 136.81, 128.89,

126.90, 126.79, 74.54, 58.53, 55.35, 55.18, 42.87, 42.82, 23.86, 23.59, 18.89, 15.50, 15.32; 14.17, 13.92 MS: m/z 284 [M+1]$^+$, 306 [M+Na]$^+$.

Acknowledgements

Supplementary Material

Supplementary information includes copies of ^{1}H NMR, ^{13}C NMR of all the compounds & chiral HPLC chromatograph of compound (*S*)-5.

References

1. Federsel, H. J., *CHEMTECH* **1993**, *23*, 24-33.
2. Cho, B. T.; Chun, Y. S., *Tetrahedron: Asymmetry* **1992**, *3*, 337-340.
   https://doi.org/10.1016/S0957-4166(00)80268-2
3. Blaser, H.-U., *Adv. Synth. Catal.* **2002**, *344*, 17-31.
   https://doi.org/10.1002/1615-4169(200201)344:1<17::AID-ADSC17>3.0.CO;2-8
4. Brunel, J. M.; Buono, G., *Synlett* **1996**, 177-178;
   http://doi.org/10.1055/s-1996-5343
5. Zheng, L.; Zhang, S.; Wang, F.; Gao, G.; Cao, S., *Can. J. Chem.* **2006**, *84*, 1058-1063.
   https://doi.org/10.1139/v06-129
6. Zhu, H.; Li, Y.; Chen, W.; Yu, G.; Du, G.; Lv, L.; Chu, Q. *Chinese Patent* CN 101367746A, 2009.
7. Yang, P.; Wang, X.; Peng, L.; Chen, F.; Tian, F.; Tang, C.-Z.; Wang, L.-X., *Org. Process Res. Dev.* **2017**, *21*, 1682-1688.
   https://doi.org/10.1021/acs.oprd.7b00216
8. *Aziridines and Epoxides in Organic Synthesis*; Yudin, A. K., Ed.; Wiley-VCH: Weinheim, 2006.
   http://doi.org/10.1002/3527607862
9. Li, D-D.; Niu, L-F.; Ju, Z-Y.; Xu, Z.; Wu, C. *Eur. J. Org. Chem* **2016**, 3090-3096.
   https://doi.org/10.1002/ejoc.201600335
10. Hodgson, D. M.; Humphreys, P. G.; Hughes, S. P. *Pure Appl. Chem* **2007**, *79*, 269-279.
    http://dx.doi.org/10.1351/pac200779020269
11. Wong, O. A.; Shi, Y. *Chem. Rev.* **2008**, *108*, 3958-3987.
    https://doi.org/10.1021/cr068367v
12. Moschona, F.; Savvopoulou, I.; Tsitopoulou, M.; Tataraki, D.; Rassias, G. *Catalysts* **2020**, *10*, 1117-1182.
    https://doi.org/10.3390/catal10101117
13. Singh, G. S.; Mollet, K.; D'hooghe, M.; De Kimpe, N.; *Chem. Rev.* **2013**, *113*, 1441–1498.
    https://doi.org/10.1021/cr3003455
14. Mujahid, M.; Mujumdar, P.; Sasikumar, M.; Deshmukh, S. P.; Muthukrishnan, M., *Tetrahedron: Asymmetry* **2017**, *28*, 983-986.

https://doi.org/10.1016/j.tetasy.2017.06.001

15. Mujahid, M.; Subramanian, J.; Nalla, V.; Sasikumar, M.; Kunte, S. S.; Muthukrishnan, M., *New J. Chem* **2017**, *41*, 824-829.
https://doi.org/10.1039/C6NJ02928K

16. Viswanadh, N.; Mujumdar, P.; Sasikumar, M.; Kunte, S. S.; Muthukrishnan, M., *Tetrahedron Lett.* **2016**, *57*, 861-863.
https://doi.org/10.1016/j.tetlet.2016.01.032

17. Reddi, A.; Mujahid, M.; Sasikumar, M.; Muthukrishnan, M., *Synthesis* **2014**, *46*, 1751-1756
http://doi.org/10.1055/s-0033-1341104

18. Mujahid, M.; Muthukrishnan, M., *Chirality* **2013**, *25*, 965-969.
https://doi.org/10.1002/chir.22253

19. D'hooghe, M.; De Kimpe, N.; *Arkivoc*. **2008**, (ix), 6-19.
https://doi.org/10.3998/ark.5550190.0009.902

20. Stankovic, S.; D'hooghe, M.; Catak, S.; Eum, H.; Waroquier, M.; Van Speybroeck, V. V.; De Kimpe, N.; Ha, H-J.; *Chem. Soc. Rev.*, **2012**,*41*, 643-665.
https://doi.org/10.1039/C1CS15140A